THE THERMAL AND MECHANICAL PROPERTIES OF A LOW-DENSITY ELASTOMERIC ABLATION MATERIAL

by W. T. Engelke, R. W. Robertson, A. L. Bush and C. D. Pears

Prepared under Contract NAS1-11499

SOUTHERN RESEARCH INSTITUTE
BIRMINGHAM, ALABAMA

for

NATIONAL AERONAUTICS AND SPACE ADMINISTRATION

FOREWORD

This report is submitted in accordance with the statement of work of Contract NAS1-11499.

The work was conducted by the Applied Thermal Section of the Mechanical Engineering and Mechanics Division at the Southern Research Institute, Birmingham, Alabama, between April, 1972 and July, 1973. Mr. W. T. Engelke was Project Engineer and Dr. Ronald K. Clark of the Langley Research Center was the technical representative for this contract.

TABLE OF CONTENTS

TABLE OF CONTENTS - CONTINUED

LIST OF ILLUSTRATIONS

LIST OF ILLUSTRATIONS - CONTINUED

LIST OF ILLUSTRATIONS - CONTINUED

LIST OF ILLUSTRATIONS - CONTINUED

LIST OF ILLUSTRATIONS - CONTINUED

LIST OF TABLES

LIST OF TABLES - CONTINUED

LIST OF TABLES - CONTINUED

SUMMARY

Thermal and mechanical properties data were obtained for a low density elastomeric resin based ablation material with phenolic-glass honeycomb reinforcement. Data were obtained for the material in the charred and uncharred state.

The properties of the virgin material were as expected with the exception of a slight inflection in the thermal conductivity versus temperature curve. For the virgin material from approximately 100 K to 500 K the thermal conductivity ranged from 0.048 W/m K to 0.077 W/m K, and the heat capacity ranged from 0.5 J/gm K to 2.0 J/gm K. The tensile strength at room temperature averaged 267,000 N/m^2 in the "a" direction (continuous reinforcement) and 154,000 N/m^2 in the "b" direction. The average compressive strength at room temperature was 420,000 N/m^2 in the "a" direction and 552,000 N/m^2 in the "b" direction.

Ablation material specimens were charred in a laboratory furnace at temperatures in the range from 600 K to 1700 K to obtain char specimens representative of the ablation char layer formed during reentry. These specimens were then used to obtain effective thermal conductivity, heat capacity, porosity, and permeability data at the char formation temperature. This provided a "boxing" of the data which enables the prediction of the transient response of the material during ablation. Limited comparisons were made between the furnace charred specimens and specimens which had been exposed to simulated reentry conditions in one of the arc-jet test facilities at Langley Research Center.

The properties indicated that in the range of 500 K to 800 K all degradation and volatilization occurs since at 800 K the weight loss was maximum and bulk density minimum. The resulting 800 K char was unstable as observed primarily from the data scatter present for the various specimens. From 800 to 1100 K carbonization of the pyrolyzed matrix was initiated as indicated by significant increases in thermal conductivity and true density. Above 1100 K to 1700 K the thermal conductivity increased rapidly and the heat capacity decreased slightly indicating progression of carbonization to a more ordered state.

In the 1600 K to 1700 K range a firm crust is formed on both the Langley chars and the furnace chars by molten glass from the honeycomb wall, sintering and some melting of the silica spheres. This crust was not air tight but it was less permeable (10 times higher resistance to flow) than the rather open composite formed at the lower temperatures.

Of particular significance was that the structure of the Langley char contained several large gaps or separations due to the interaction of the reinforcing honeycomb and the charring filler. A major gap existed underneath the crust as well as several other cracks at random depths within each cell. In addition, the filler did shrink away from the cell wall except at the crust. This created gross anomalies in the material and allowed radiant shunting affecting the heat transfer through the composite. Some modeling was done to account for these anomalies in the measurement of effective thermal conductivity.

INTRODUCTION

This is a report to the National Aeronautics and Space Administration, Langley Research Center, for work performed under Contract NAS1-11499. This program involved the evaluation of thermal and physical properties on a low-density elastomeric ablation material in both the uncharred (virgin) and charred state.

The material evaluated is being considered as an ablative material to be used in the thermal protection system for the shuttle. Both thermal and mechanical data were measured on both the virgin and charred material to provide meaningful inputs to the design of the thermal protection system. To accomplish this, the evaluation of thermal conductivity, heat capacity, tensile strength and compressive strength for the virgin material was necessary, and for the charred material, thermal conductivity, heat capacity, permeability and porosity were examined.

The properties of the char composite were intended to provide data to predict the transient response of the material during ablation. Therefore, the "boxing" approach developed at Southern Research Institute was used. [1][1] This method involves predegrading the material at some preselected temperature; preparing specimens and performing property measurements up to the precharring temperature with steady-state devices. The locus of points of property versus precharring temperature is assumed to represent the transient behavior of the property during the first exposure. The advantages of this method are that it provides a dimensionally stable specimen and allows the use of steady-state measurement techniques. This approach seems to represent the best

---

[1]Bracketed numbers indicate reference listed at the end of the report.

state-of-the-art technique provided that the structures of the flight and laboratory chars are similar and that additional time-at-temperature during the measurements does not significantly alter the properties. Data indicate that chars are similar and that time-at-temperature does not alter the property as we control it.

The evaluation of the virgin material included the thermal conductivity and heat capacity from 150 to 500 K. Mechanical properties that were determined on the virgin material were tensile and compressive strength and modulus at room temperature. The mechanical properties were determined in the two in-plane directions and the thermal conductivity was determined in the thickness direction.

The first step in evaluating the charred material was the investigation of the methods necessary to prepare chars which would best simulate the chars formed during flight. This investigation was conducted by charring several samples in a furnace under various conditions and comparing the resultant char with several chars supplied by NASA that were formed in a ground test facility. The major criteria of the char preparation was to prepare chars suitable for evaluation as well as simulate the char formed during ablation.

The furnace chars were prepared at five temperature levels from 600 K to 1750 K. This temperature range was selected since the arc jet chars were formed over that range, which is inclusive of the temperatures predicted during flight.

Properties determined on the chars were effective thermal conductivity, heat capacity, permeability and porosity. The effective thermal conductivity was determined in the thickness direction on the various chars up to their formation temperature enabling a boxing analysis of the data. Data were measured in an environment of nitrogen at 1,333 N/m^2, 49,329 N/m^2 and 101,325 N/m^2 (10,370 and 760 torr).

The heat capacity was determined on the various chars up to the formation temperatures.

The permeability was determined on the various chars at room temperature, with a few runs being made to 800 K to assess the effect of temperature.

The porosity of the chars was determined with bulk and true density measurements at room temperature.

The philosophy of testing the chars was to provide engineering data that would assist in the prediction of the materials performance during flight. This required the determination of the effective properties of the bulk piece with some characterization of the filler alone.

In keeping with this philosophy, the permeability was determined on the crust of the arc jet char as well as the furnace chars prepared to represent the zones beneath the crust. Because of the separation between filler and the cell wall, the admittance values were very high and not precise for the furnace chars and somewhat lower for the crust. The values measured served only to predict pressure build up behind the crust during reentry rather than characterize the porous structure of the material.

The effective thermal conductivity of the total composite was determined at the three pressure levels. Some modeling was performed to enable the prediction of conductance in flight conditions.

The porosity was determined on the bulk piece, which would include filler to cell wall separation, and on the filler alone in an attempt to evaluate its porous structure.

The heat capacity was determined on a bulk piece, pulverized and packed in a drop cup to obtain maximum weight and signal for enthalpy measurements.

MATERIAL DESCRIPTION AND CUTTING PLANS

Only one material was evaluated under this program and it was designated as Material A. It is a molded, low-density, elastomeric material that is filled within a phenolic-glass honeycomb reinforcement. The elastomeric filler consists of

15% Silica spheres
10% Powdered nylon
25% Silicone elastomer resin
50% Phenolic microballoons

The silica spheres are Grade S-1 made by Emerson and Cuming, Inc., and were passed through a 32 mesh sieve. The phenolic microballoons were passed through a 20 mesh sieve. The phenolic-glass honeycomb was supplied by Hexcal Products.

A total of four panels were received which were 30.5 cm x 30.5 cm square by 1.9 cm thick. The honeycomb cell shape was similar to a hexagon and a drawing of the structure of the panels is shown in Figure 1. As seen in the figure, directions "a", "b" and "c" were identified. The "a" direction was that in-plane direction where the honeycomb ribbon was continuous and the "b" direction was also in-plane but perpendicular to the "a" direction. The "c" direction was in the thickness of the panel. The effective thermal conductivity of the virgin and charred material was determined in the "c" direction, as was the permeability of the char material. The mechanical properties of the virgin material was determined in both the "a" and "b" directions.

Cutting plans for the four panels (numbered 1 through 4) are shown in Figures 2 through 5. These cutting plans show the extraction of specimens for the evaluation of the virgin material and the extraction of blanks employed for charring. The specimen extracted from the char blanks after charring are also indicated in the figures.

A numbering system was devised that designated the type of specimen, specimen number, direction (if applicable), panel number from which it was extracted, specimen number, material and charring conditions (where applicable.)

The numbering system for the virgin specimens was as follows:

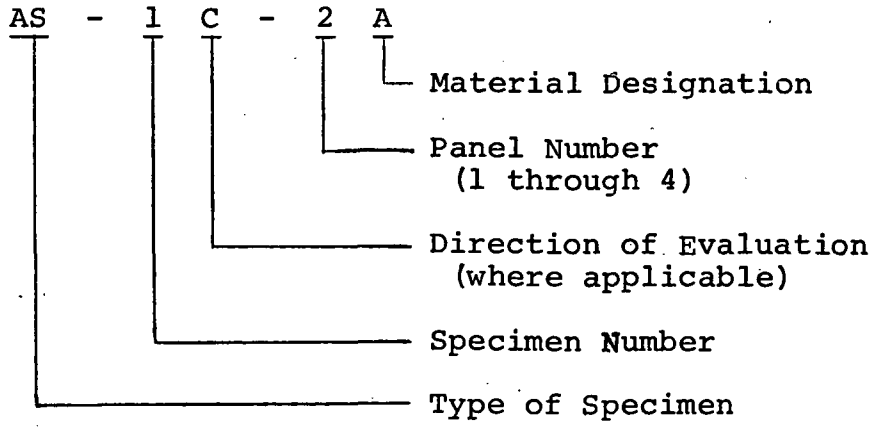

AS - Conductivity Specimen
HC - Heat Capacity Specimen
T - Tensile Specimen
C - Compressive Specimen

The numbering system for the char blanks was as follows:

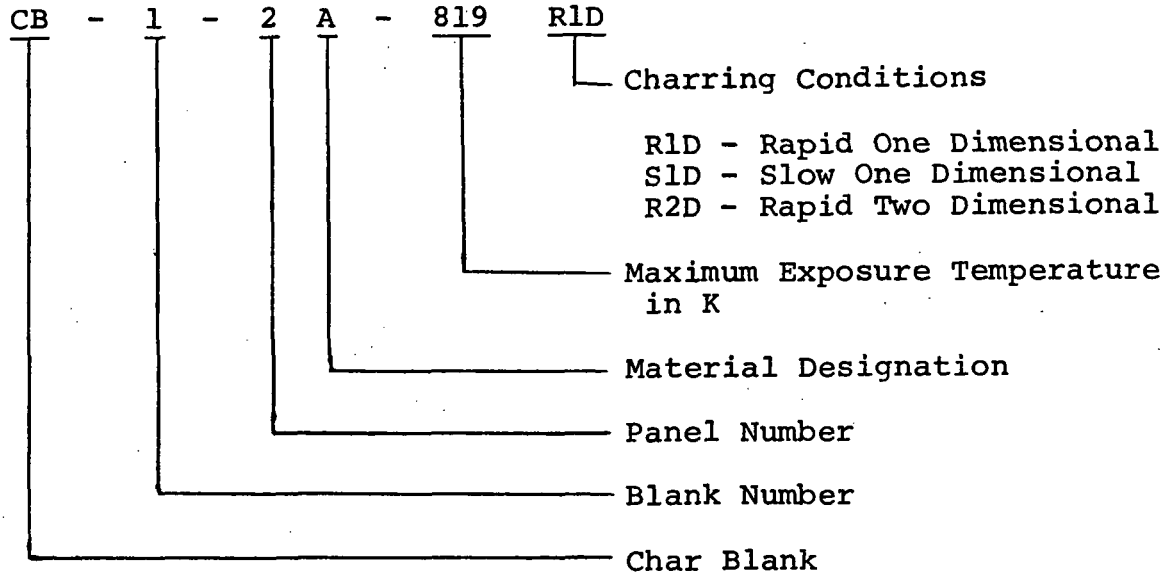

The specimens extracted from the char blanks were designated as follows:

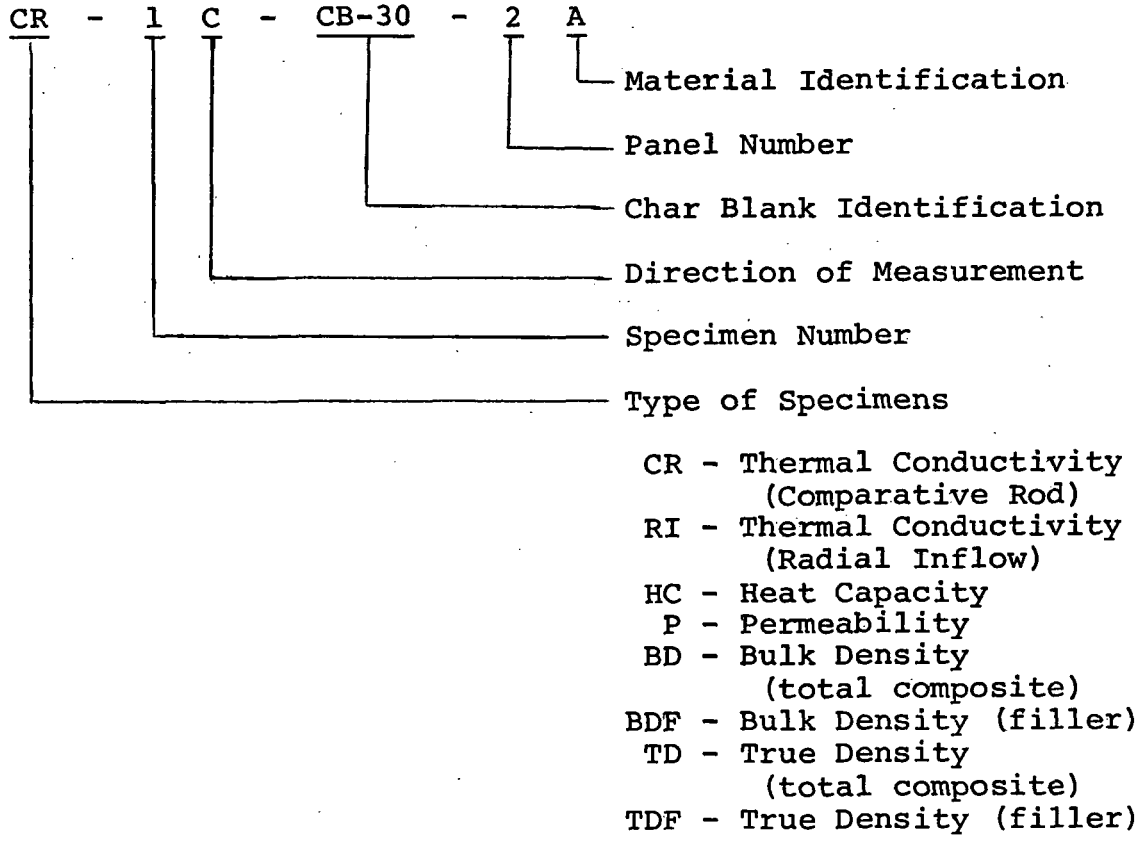

In addition to the four panels, eight blocks were received that had been exposed to the arc jet. These were necessary to provide a baseline for comparison of the furnace chars prepared at various conditions. The eight blocks were 12.7 cm by about 6.3 cm by 3.8 cm thick. Originally these blocks were 12.7 cm x 12.7 cm that were subjected to the arc jet and then sectioned in half. Some pieces and specimens were extracted from one of the blocks, the cutting plans for which are shown in Figure 6. The specimen numbers extracted from the arc-jet were as follows:

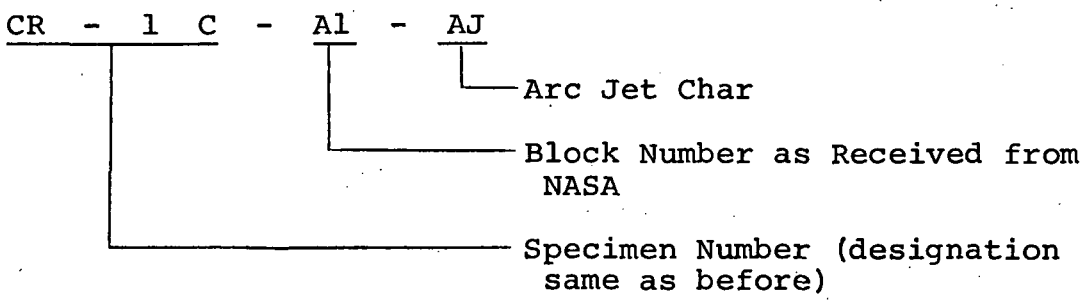

APPARATUSES AND PROCEDURES

Char Preparation

Chars were prepared in a high temperature furnace which employs an electrically heated graphite heater tube. The heater tube is cylindrical in shape. The heater tube temperature is controlled manually with a powerstat which drives a 25kw transformer.

In most cases, chars were prepared by immersion of the char blanks in the furnace after it had been preheated to a selected temperature level. The char blanks which were 3.81 cm wide x 7.62 cm long x 1.91 cm thick were supported in a holder which could be rapidly inserted or extracted from the furnace. A picture of the specimen holder is given in Figure 7. Shown in the figure is the final system decided on after the preliminary char evaluation was completed which will be discussed later. One blank was charred at a time with both faces exposed to the radiant heating from the heater tube of the furnace. The graphite felt insulation around the edges prevented lateral heating. This arrangement provided two-dimensional heating of the blanks which caused the char formation to progress from both faces to the center.

The maximum temperature was measured for each char prepared. This was done by measuring the face temperature of the char through the sight port in the furnace. Temperatures were measured either with chromel/alumel thermocouples installed at the specimen surface through the sight port or by direct readings with an optical pyrometer. When using the optical pyrometer, appropriate corrections were made for the sight window.

The specimens were cooled rapidly by withdrawing the specimen from the furnace at the end of the heating cycle and immersing it inside a cold cylinder purged with helium.

A helium purge was used in the furnace during all of the char work. A helium purge also was inserted at the bottom of the heater tube and the gas traveled from bottom to top. This was used to sweep the pyrolysis gases toward the top of the furnace.

The furnace preheat temperatures employed were approximately 600K, 800K, 1100K, 1370K and 1730K. The correlation between furnace preheat temperature and cold wall heat flux is given in Table 1. As previously reported [2], the correlation is rather good between the radiant cold wall heat flux and the convective cold-wall heat flux in a high enthalpy nitrogen gas stream.

The thermal response of the chars prepared in the laboratory were defined from measurements of temperature at the surface and in-depth. Chromel/alumel thermocouples were installed in the char centrally between the two heated surfaces. The thermocouple wires were housed in double bore alumina tubing and were inserted in holes drilled parallel to the heated surfaces. The thermocouple wires melted at the point of exit from the specimen unless special provision was made to insulate them. The wires were insulated above the specimen with phenolic-nylon tubes placed around the insulator. These tubes were made to about the same thickness as the depth of the thermocouple from the surface.

The temperature measurements were used to define the heat treatment of specimens as to the time required for the front face and the in-depth thermocouple to achieve equilibrium. This aided in defining the uniformity of the char with regard to temperature exposure. The results of the initial measurements, which established the response, were used throughout the program as being representative for all chars prepared.

Some of the chars prepared at temperature were made into specimens by careful hand sanding; however, most of these samples were extremely friable and were impregnated with polyalphamethylstyrene (Armco resin 18-210) prior to a machining operation. Then, the samples were machined to the desired dimensions. The impregnant was

removed by baking the machined sample in an inert environment for about 1 hour at 672 K. At this temperature the resin turns to a gas and leaves the specimen with essentially no residue.

Thermal Conductivity

Three apparatuses were employed to determine the thermal conductivity of both the virgin and charred material. The ASTM C-177 guarded hot plate was used to 600K for the virgin and 600K precharred material. The comparative rod apparatus was used to 1100K for the chars prepared in the arc jet and in furnace above 800K. The radial inflow apparatus was used up to 1730 K for the chars prepared at 1300 K and 1730K.

Guarded Hot Plate Apparatus. - A complete description of the ASTM C-177 guarded hot plate apparatus is included in Appendix A. For these evaluations the smaller apparatus with the 8.25 cm heater plate was employed. Due to the nature of this material, the evaluations required the following exceptions to the described procedures:

1. The specimen discs were split into a central and guard ring to minimize radial heat exchange. Figure 8 is a drawing of the specimen disc employed.

2. Temperatures on both runs were measured internally with thermocouples inserted in 0.1 cm diameter temperature wells ending within the filled cell of the honeycomb (see Figure 9). The internal thermocouple beads were potted in place with an RTV adhesive. The wires were insulated with a double bore alumina tube broken every 0.64 cm along its length to minimize thermal drain from the bead.

3. Surface temperatures were measured on the first specimen only. Here the bare but separated thermocouple wires were held in electrical contact with the Grafoil interfacial material pressed on the specimen's surface. Electrical contact was made at the central region of the Grafoil disc and the remainder of the wire was insulated from the Grafoil with Teflon tape. This provided a direct measurement of the surface temperature of the Grafoil. The surface temperature of the specimen was calculated from this measurement by adjusting for the temperature drop across the Grafoil, which was almost negligible.

4. Temperatures in the guard ring of the specimen were measured and maintained within 10 percent of the temperature gradient across the specimen.

Comparative Rod Apparatus. - The comparative rod apparatus is completely described in Appendix B. This apparatus consists basically of two cylindrical reference pieces of known thermal conductivity stacked in series with the cylindrical specimen. A small electrical heater is placed at one end of the rod, to introduce heat through the stack, and a heat sink or a second heater is employed at the opposite end of the stack to maintain the temperature drop through the specimen at the desired level. Radial losses are minimized by means of radial guard heaters surrounding the rod. The annulus between the rod and the guard heaters and surrounding the guard heater is an insulation, usually diatomaceous earth or thermatomic carbon.

Essentially, this method compares the conductivity of the specimen to that of the references and obviously requires true axial heat flow down the column with a minimum of radial heat exchange.

Modification of this apparatus was necessary for this program since the standard assembly is only accurate for measurements of conductivity above 1.4 W/mK. The reason for this is that analyses [3, 4] have shown that heat can shunt the specimen (through the insulation) when the thermal conductivity of the specimen is not an order-of-magnitude or more than that of the insulation and the guard heater is, say, twice the diameter of the specimen or more. Note that the shunting effectively gives a larger specimen area and results in an erroneously low temperature difference in the specimen relative to the reference (assuming that the references have a higher thermal conductivity than the specimen). This yields erroneously high values of thermal conductivity. With certain values for the thermal conductivities of the references, specimen and insulation, guard heater to specimen diameter ratio and guard to specimen temperature profile, these errors can easily reach 100 percent.

Analyses [3, 4, 5] have shown that the heat shunting problem can be overcome if the following conditions are satisfied:

1. The guard profile matches the specimen profile.

2. The ratio of guard diameter to specimen diameter is as near unity as possible.

These concepts were applied to the modified technique used here.

The experimental configuration used for the measurements is shown in Figure 9. The assembly consisted of a central column comprised of a 2.54 cm diameter specimen sandwiched between two references of known thermal conductivity. Guard rings made of the same materials as the specimen and references surrounded the central column. The guard rings were constructed to match the

specimen and reference lengthwise. The annulus between the central column and guard ring was 0.16 cm wide which gives a ratio guard diameter to specimen diameter of 1.125.

The references used were made from slip cast fused silica, the conductivity of which has been evaluated and well defined from several measurements made in the ASTM guarded hot plate apparatus.

Heaters made of Armco iron were placed on either end of the column to control heat flow and mean temperature. Armco iron was used because its thermal conductivity is about 200 times that of the specimen and; hence, the temperature gradient along a radial line at the top of the build-up was estimated to be no more than one or two degrees. Thus, the guard and central temperatures are matched at the ends. The entire assembly is surrounded by diatomaceous earth insulation contained inside a 10 cm diameter guard heater.

Temperatures are measured at two axial locations in each reference and in the specimen. A beaded chromel/alumel thermocouple was inserted into the drilled holes in a double bore alumina insulator. The insulator was broken about every 0.3 cm to minimize conduction losses. The thermocouples in the specimen were potted in place at the bead with Silastic RTV-731, silicone rubber.

Specimen gage lengths were determined from radiographs or X-rays. The X-rays were examined at 10x magnification to determine the gage distance relative to the overall thickness.

The idea for the assembly shown in Figure 9 was to use identical materials for a guard ring and thus create as closely as possible a matched guard condition to minimize radial heat exchange. Also, a thin specimen, 0.635 cm, is used because this also minimizes radial heat exchange and heat shunting. Further, the annulus is kept small to minimize heat shunting which occurs even with matched guarding.

In practice, perfect matching of the guard and central columns is not achieved. Hence, corrections for radial heat exchange are made to the measured data based on the measured temperature profiles. Further, corrections are made for the heat shunting through the annulus.

Details of the corrections made to the measured data are included in Appendix C. Even though two different corrections are applied to the data, the maximum value for both corrections during this program did not exceed 10 percent with the exception of two data points. Hence, sizeable uncertainties in the correction procedures do not create large uncertainties to the final data. The combined uncertainty for the several sources of uncertainty present is ±8 percent increasing to ±10 percent above 800K.

Radial Inflow Apparatus. - A complete description of the radial inflow apparatus is included in Appendix D. Due to the structure of this material, cylindrical specimens could not be employed; therefore, the strip assembly was used. A sectional view of this assembly is shown in Figure 10.

The assembly consisted of four specimen strips sandwiched between strips of ATJ graphite which contain wells for temperature measurement. The corners of the build-up were packed with thermatomic carbon to minimize extraneous heat flows. Pyrolytic graphite strips were used on the inside to aid in maintaining the isotherms normal to the directions of heat flow. The assembly was placed concentric about a calorimeter with a 1.27 cm gage section, and the annulus between the calorimeter and the pyrolytic graphite strips was packed with graphite.

Positive interfacial contact between the strips was assured in this assembly by the addition of expansion pistons to the support cylinder. These pistons were designed to counteract differential expansions that would cause a separation at the interfaces. For this program the pistons consisted of a stack of two pieces, pyrolytic graphite in "c" direction at 0.254 cm thick, and CS graphite at 0.508 cm thick.

The specimen was built up on the calorimeter tube and guards packed with thermatomic carbon were used above and below the specimen to retard longitudinal heat flow. Graphite felt insulation was used between the specimen and guards. The top guard section contained graphite sight tubes which align with the temperature wells in the specimen and provided access from outside the furnace.

During the run the procedures were similar to those detailed in the appendix.

Thermal conductivity was calculated from the measurements of temperature difference and heat flow. The equation used is:

$$k = \frac{\Delta X}{4A} \frac{Q}{\Delta T} \qquad (1)$$

where

k = thermal conductivity - W/mK

ΔX = thickness of specimen - cm

A = area of gage section of one specimen strip

Q = total measured heat flow - watt

ΔT = temperature difference across specimen strip - K

A correction to the conductivity calculated in Equation 1 is necessary for this assembly. The measured conductivity will be erroneously high due to the heat transferred through the corners packed with thermatomic carbon. The correction required has been determined analytically for the geometry of the assembly by dividing the configuration into several radial segments and assuming the temperature distribution in the thermatomic carbon is the same as in the specimen and surrounding strips. This analysis yields:

$$\frac{k_s}{k_m} = 1 - 0.19 \frac{k_p}{k_m} \qquad (2)$$

where

k_s = true thermal conductivity of the specimen

k_m = measured thermal conductivity of the specimen

k_p = thermal conductivity of the packing in the corners

As observed in Equation 2, the lower the measured conductivity the greater the bias. For these runs the maximum bias was 19 percent. The correction made on each point for the bias is shown in the table of values reported under "Data and Results."

The uncertainty of the values measured in the radial inflow apparatus can be derived from the summation of the following random uncertainties:

1. Errors associated with the basic equipment that have been set at ±7 percent. This includes the uncertainties involved in temperature measurement, heat flow measurement and other factors as discussed in the appendix.

2. Error in the analytical correction of the measured data. The error involved here is certainly no more than ±50 percent of the correction. With the maximum correction being ±19 percent the maximum error would be ±9 percent.

The combination of the above uncertainties yield a total error for the modified radial inflow system of ±12 percent.

Impregnant Removal from Conductivity Specimens. - As part of the procedures for all the conductivity runs where impregnated specimens were employed, the system with specimen was assembled and prior to the measurement of data was baked at above 670K to remove the impregnant from the specimen. After the run, photographs were taken of the "hot" and "cold" surfaces of the specimen. This was done to examine the structure of the specimens which was necessary to thermally model the specimen.

Heat Capacity

The heat capacity of both the virgin and charred materials were performed in both the adiabatic and ice calorimeter. The adiabatic calorimeter was employed to 800K and the ice calorimeter from 800K to 1730K. Both apparatuses are described fully in Appendices D and E.

A major problem with these materials, particularly that of the chars, is the very low mass times heat capacity product (mCp) due to the low density of the material. With a low mCp, the signal is, of course, very low and the measurement is subject to a lack of precision.

To minimize this problem, the chars were pulverized and packed within an aluminum container for the determinations in the adiabatic calorimeter. The pulverization increased the mCp product sufficiently and the additional mCp of the container remained a very small percentage of total signal; therefore, the correction for the mCp of the container was small. These conditions provided the precision normally obtained with this apparatus.

For the determinations using the ice calorimeter, the low density char was pulverized and packed within our normal graphite container. Unfortunately, the mCp product of the container was a significant percentage (about 50 percent) of the total signal. Since the correction for the container was significant, the heat capacity of the cups employed for the measurements were confirmed with several determinations over the temperature range of interest.

Permeability

All permeability measurements for this program were made with the high temperature permeability apparatus which is described in Appendix F. The low temperature measurements were made in this apparatus because it measures total pressure and is probably better for the high flow rates expected with these chars.

The diameter of all specimens was approximately 1 inch, but the thickness varied from 0.0438 in. to 0.3215 in. Silicone rubber (Dow Corning RTV-731 Silastic) was used as the sealant for all but one of the char specimens which were run only at room temperature. The arc jet crust and the furnace char specimens run at elevated temperatures were sealed in the fixture with Sauereisen 32 cement.

All except the two furnace chars formed at 600K were placed between two pieces of wire screen before being sealed in the fixture. This was done to prevent the specimens' destruction by the differential pressure across it. A calibration curve was obtained for the screen wire giving pressure drop as a function of gas flow rate. This correction was applied to the pressure drop measured across the permeability specimens which were backed with screen wire. The 600K char specimens were sufficiently strong that this was not necessary. Figure 11 shows a typical specimen assembly. One specimen of the chars formed at 600, 800, 1100, 1300 and 1700K and the arc jet char were run at room temperature using nitrogen as the permeating gas. Also, one room temperature run was made on the char formed at 600K using helium as the permeating gas. A second specimen of the 600K char was run at 500K using both nitrogen and helium as the permeating gases. An additional specimen of the 1100, 1300 and 1700K chars was run at 800K using nitrogen as the permeating gas. All specimens which were run at elevated temperatures were run at room temperature before and after the high-temperature measurements. This enabled us to ascertain if any physical change in the specimen occurred during the measurements at elevated temperature.

The specimens of the 1700K char and the arc jet char represented the crust of the charred honeycomb structure.

The 600K char was capable of being machined without impregnation. However, because of the fragile nature of the other chars, they were impregnated with polyalphamethylstyrene prior to machining. After the impregnated specimens were machined each one was measured, weighed and wired between two pieces of screen. This entire assembly was weighed and then heated to about 700K for about one hour to bake off the impregnant. The assembly was again weighed so the density of the specimen could be determined. Sealant was then placed around the circumference and allowed to cure to prevent pieces of the specimen from becoming dislodged. The specimen assembly was then sealed in the specimen holder and allowed to cure. Figure 12 shows a picture of one specimen sealed with Dow Corning RTV-731 Silastic and another specimen sealed with Sauereisen 32 Cement.

Porosity

The porosity of the chars were determined by calculation from measured values of bulk and true density in accordance with the following equation:

$$P = \left(1 - \frac{\rho b}{\rho t}\right) 100 \qquad (3)$$

where

P = total porosity in percent by volume

ρb = bulk density

ρt = true density

The bulk density was measured by machining a specimen to a definite geometry from which volume and weight were accurately measured. Due to the friable nature of this material, the specimen was impregnated with polyalphamethylstyrene (Armco resin 18-210) then machined. After the volume was measured, the impregnant was removed by heating to above 670K. The weight of the specimen is then measured and represents the true weight since essentially no residue remains after the heat soak.

The true density was determined using a liquid pycnometer in accordance with ASTM 135-66. The sample was pulverized and passed through a 100 mesh screen to assure that all particles were free of voids. The wetting agent used was methenol and a 25 ml pycnometer bulb was used primarily.

On some of the samples, complete wetting was not obtained as evidence by some (about 2 percent) particle floatation in the bulb. Apparently, the pulverization and passage through a 100 mesh-screen did not remove some of the porosity. It is possible that some of the smaller phenolic or silica microspheres were not crushed. The small amount of particle floatation was removed from the bulb and weighed to adjust the results to a corrected value of true density. This correction was less than 5 percent.

Early in the program water absorption measurements were made; however, for these materials where the porosity is close to 90 percent and many large voids exist, the accuracy of the measurement is very poor. The main source of error is the retention of the absorption fluid when obtaining a saturated weight. The large pores can not retain this fluid (even for the short period of time necessary) when it is removed. Due to this, the absorption measurements were merely employed for rough comparisons between the various furnace chars and the arc jet chars at the beginning of the program. The procedures for the absorption measurements are included in Appendix G.

Tension

All of the tensile evaluations were made in a Tinius-Olsen universal testing machine at 294K. Strain gage extensometers were utilized to measure strain over a 5.08 cm gage length. Two specimens were tested in each honeycomb direction (a and b).

Figure 13 shows the tensile specimen configuration. A schematic of the load train is shown in Figure 14. Strain gage extensometers were calibrated over a 0 to 0.305 cm range with 0.020 cm/cm chart calibration, and this calibration was linear within 1.0 percent over the full scale. Load was calibrated to 1 percent accuracy. The specimens had aluminum pads epoxyed to each side of each end. These pads provided load transfer to the gage section and support at the pin holes. Chain segments were used in the load train to assure uniaxial alignment.

Compression

All of the compressive evaluations were made in a Tinius-Olsen universal testing machine at 294 K. Strain gage extensometers were used to measure strain over a 5.08 cm gage length. Figure 15 shows the compressive specimen configuration. Two specimens were evaluated in each honeycomb direction (a and b) as shown in Figure 15. The extensometers were calibrated over a 0 to 0.305 cm range with 0.020 cm/cm. Chart calibration, and this calibration was linear within 1.0 percent over the full scale. Load was calibrated to 1 percent accuracy. The specimens were tested in a special loading fixture to provide uniaxial alignment and avoid specimen buckling. A schematic of the load fixture is shown in Figure 16.

RESULTS OF VIRGIN MATERIAL EVALUATION

Thermal Conductivity

The thermal conductivity from 110K to 500K in the "c" or thickness direction of the panel was measured in 1 atmosphere of nitrogen. The data are shown in Figure 17 and Table 2. As seen in the figure, the values increased from 0.048 W/m K at 120 K to 0.077 W/m K at 500 K. The data for both specimens agreed rather well except for some scatter at the temperature extremes. Also, note that the conductivity calculated across the specimen thickness agreed well with the "internal gage" measurement. Recall that the surface temperature monitors an average of the surface, whereas the internal temperature monitors a local area within the cell where the thermocouple is located. This indicates that perturbations in temperatures created by the honeycomb cell walls were negligible.

The conductivity exhibited an unusual character. An inflection in the curve occurred below room temperature (297 K) and it is unknown what caused the inflection. Apparently, a physical or structural transition occurs. A second-order transition such as that which occurs in rubber below room temperature may be responsible for this behavior.

Some comparative values are plotted in Figures 17 of a silicone phenolic in a phenolic-glass honeycomb (Material MG-45, NASA CR-111909). These data, represented with a dashed-line, were lower; however, the density was also lower, the silicone content lower, and the phenolic microballoon content higher than those for Material A.

Heat Capacity

Enthalpy and heat capacity from 120 K to 490 K were determined. The values of enthalpy and heat capacity are shown in Figure 18 and Table 3.

The heat capacity increased from 0.5 J/gm K at 120 K to 2.0 J/gm K at 490 K. These values were about 10 percent higher than the heat capacity previously measured here on the MG-45 silicone-phenolic in honeycomb measured and reported in NASA CR-111909. This is fairly close agreement considering the variation in the elastomer resin and constituents.

Attempts to determine the enthalpy at temperatures higher than 500 K resulted in values that were biased high. Observations of the thermal response of the specimen within the furnace indicated that at slightly higher temperatures an exothermic reaction initiates which would obviously alter the measurement of enthalpy.

Tension

The results of the tensile evaluations are shown in Table 4 and the stress-strain curves are included as Figures 19 through 22.

In the "a" direction, ultimate strengths for Specimens T-1a and T-2a were 348,198 N/m^2 and 186,165 N/m^2, respectively and elastic modulii were 31,372 x 10^3 N/m^2 and 30,476 x 10^3 N/m^2, respectively.

In the "b" direction, ultimate strengths for Specimens T-1b and T-2b were 138,590 N/m^2 and 168,238 N/m^2, respectively, and elastic modulii were 18,479 x 10^3 N/m^2 and 13,376 x 10^3 N/m^2, respectively. Tensile fractures did not follow the honeycomb configuration. A typical tensile fracture is shown in Figure 23.

Compression

The results of the compressive evaluations are shown in Table 5 and the stress-strain curves are included as Figures 24 through 27.

In the "a" direction, ultimate strengths for Specimens C-1a and C-2a were 372,330 N/m^2 and 468,860 N/m^2, respectively, and elastic moduli were 32,820 x 10^3 N/m^2 and 46,610 N/m^2, respectively.

In the "b" direction, ultimate strengths for Specimens C-1b and C-2b were 537,810 N/m^2 and 565,390 N/m^2, respectively, and elastic moduli were 19,582 x 10^3 N/m^2 and 21,857 x 10^3 N/m^2, respectively.

Compressive fractures followed the honeycomb configuration and were "x" shaped, crossing generally at the center of the gage section. A typical compressive fracture is shown in Figure 28.

CHAR PREPARATION IN THE LABORATORY FURNACE

Criteria

To conduct a meaningful evaluation of the thermal properties of a char formed during re-entry, one must be able to prepare suitable specimens from the char. Obviously, these specimens must be stable, compatible with the environment and other conditions of the test and be representative of the char formed during flight. In addition, to characterize a char formed at specific temperatures, the char specimen must be prepared under isothermal conditions.

Of course, the best simulation of a flight char is one that is made under a high enthalpy arc jet stream; however, the chars prepared in an arc jet are normally not practical for use as a specimen. This is due to both (1) a temperature gradient that exists during char formation and (2) gross anomolies (separations and cracks) that are present in the structure. Therefore, the chars were prepared in a furnace under this program, and the conditions of charring were selected to provide the best representation of the flight char.

To best meet the criteria of char preparation, an initial evaluation of optimum procedures was conducted, the first step of which was a study of the arc jet chars prepared by NASA.

Arc Jet Char Description

Several samples of char formed in the arc jet were received for our inspection and formed a baseline for comparison of the furnace chars at various conditions.

The arc jet specimens were prepared by mounting the block on a wedge and the hot gases impinged the surface at an angle under a constant heating rate cycle of 20 minutes. The cold wall heat flux was monitored from the leading edge to the back edge. At the midpoint, the cold wall heat flux density was 18.2×10^4 W/m^2 (16 Btu/ft^2 sec). The variation in heat flux density was linear and it ranged from 30.1×10^4 W/m^2 (26.5 Btu/ft^2 sec) at the leading edge to 7.26×10^4 W/m^2 (6.4 Btu/ft^2 sec) at the trailing edge. Assuming only radiation, heat loss from the sample and an emittance of 0.6 (probably low), the maximum equilibrium temperature of the crust on the arc jet was calculated to be 1728K or 2650F. Therefore, the temperature range for charring under this program was reduced to 1730K from the originally proposed figure of 3000K.

A photograph of a sample, as received from NASA is shown in Figure 29. Figure 30 is another photograph of a sectioned sample after impregnation. As shown in the figures, the structure of the char was quite unique. A crust was formed at the hot face of the material where a maximum temperature of about 1730K was obtained. Under the crust was a major separation or gap between the crust and the filler material. The filler within the honeycomb cells was cracked primarily in a direction parallel to the heated surface. These cracks occurred at different heights and had different widths in each honeycomb cell. The cell size remained the same as that for the virgin material since the honeycomb was rigidly attached to the virgin material at the cold face. With the exception of the crust, the charred filler shrank away from honeycomb cell wall. The formation of the gap and cracks occurred at temperature prior to cool down since gross shrinkage of the elastomer and phenolic does take place during degradation, which we have observed in previous measurements of thermal expansion.

Suitable Monitors

To properly conduct the initial evaluation of optimum char preparation in the furnace, suitable monitors and inspection procedures were necessary and a brief search was performed.

Several of the monitors and inspections techniques developed under our previous program performed under Contract NAS1-10517 [2] were considered. Unfortunately, many of the monitors that were effective under the previous program were not effective or practical for these materials. The primary reason for this is that under the previous program a phenolic-nylon composite was charred at higher temperatures and the most sensitive monitors were those that quantitized degree of graphitization or ordering of the crystallites. The lower temperatures of char formation under this

program has precluded meaningful results with monitors or graphitization. As a matter of fact, some X-ray diffraction tests were run and no ordered carbon was detected. The results of the X-ray diffraction measurements presented later merely indicated the presence of α cristobalite which would be expected from the silica spheres present in the virgin material.

A photomicrographic study was not a very sensitive inspection. To demonstrate the photomicrographs of the arc jet char and various furnace chars are shown in Figures 31 and 32 and as can be seen, the material consists of spheres bonded together with a minimum amount of matrix. For the arc jet char and various furnace chars, the structure is quite similar and any variations that may exist and be correlated to the char formation were not observed.

Some information can be extracted from the photomicrographs even though they were not sensitive monitors. During the charring process, the phenolic microballoons remained as a sphere. The sectioned spheres in the photomicrographs are most likely the charred microballoons. Figure 31 illustrates that the cohesion of the crust was obtained with a thin layer of continuous material at the surface. This layer was most likely caused by the molten glass from the honeycomb, but there appears from the photograph some evidence of the silica spheres melting and flowing to the surface layer. This would suggest some impurity in the silica spheres since pure silica melts at a higher temperature than that reached on the surface.

The best inspection procedure appeared to be the examination of the chars gross physical structure. Consideration was given to parameters such as cell size, crack probagation, shrinkage of filler from the cell wall and color. These monitors were observed sufficiently by visual inspection and side by side comparison with the arc jet char. Recall that the philosophy of testing under this program involved the determination of the effective values of a property for the bulk piece of the material. Therefore, examination of the gross physical structure was directly relatable to the effective properties desired.

The use of the 10X to 20X stereo microscope assisted in the visual inspection. The specimens were viewed in a natural state without preparation such as polishing and impregnation. This way the color of the beads and the residue formation prevelant on some of the chars could be investigated and compared.

The feel of the structure was also quite revealing. Crumbling the specimen indicated the degree of cohesiveness in the chars which varied for the various charring conditions.

The bulk density was used as a monitor. Values were obtained by both gravimetric techniques and water absorption. Due to the structure of the material, the values measured were sometimes approximate, however, important trends were detected.

Thermal conductivity was also determined on a few selected char blanks prepared in the furnace and the arc jet. Since this was an important property to be examined under this program, it was employed as a monitor in the preliminary investigation.

Preliminary Char Preparation and Study

Essentially, three methods were attempted to provide representative chars. These methods are referred to as:

1) Rapid one dimensional (R1D)

2) Slow one dimensional (S1D)

3) Rapid two dimensional (R2D)

The term rapid refers to the chars formed by a rapid heating rate which was obtained by immersion into a furnace preheated to the desired temperature. Typical temperature versus time curves for the surface and internally at a depth of 0.635 cm from the heated surface are included in Figure 33. The term slow char refers to a slower heating rate where the specimen was installed in a furnace and power to the heater tube was manually controlled and to provide the desired heating rate and temperature. The conditions for the slow heating rate were a rise rate of about 18K per hour to char temperature, held constant for 20 minutes at char temperature and allowed to cool slowly within the furnace after power shut down.

One dimensional and two dimensional indicated the application of heat to the specimen. The one dimensional chars were prepared by allowing exposure of only one surface to the radiant heat from the heater tube. This was done by using the assembly discussed under "Apparatuses and Procedures" section but two specimens were installed back to back with a piece of graphite felt inserted between them. This provided an insulated back face boundary condition and allowed one dimensional heating to occur.

The two dimensional heating allowed radiant heating to both surfaces of a specimen as discussed under the "Apparatuses and Procedures" section.

Table 6 summarizes all the char blanks prepared during the preliminary investigation. The table includes various measurements made to characterize and compare the blanks made. Some of the same measurements were made on the arc jet specimens for a basis of comparison.

The rapid one dimensional chars warped severely and exhibited significant shrinkage of the cells particularly at the back face. The cell area at the back face was 32 percent smaller than the cell area of arc jet char while the front face exhibited about 15 percent smaller area. This made it unsuitable for use as a specimen; however, the rapid chars exhibited several characteristics that were similar to the arc jet chars. Visual appearance was similar to that of the arc jet. Figure 34 shows a picture of the structure at 10X compared to the arc jet. Note the deposition of residue on the spheres of the arc jet and a similar deposition on the furnace chars was observed although to a lesser extent. A feel of both the structures was similar in that both the arc jet and the rapid one dimensional chars exhibited some cohesiveness upon crushing. The material crushed to cohesive chunks rather than a powder.

The slow one dimensional charring conditions formed a very flat specimen that was suitable for specimen preparation; however, its structure was unlike that of the arc jet char. Figure 35 shows the comparative photograph between the two chars and the significant difference was that less residue was formed on the furnace char with the surface of the beads being cleaner. Cell shrinkage was fairly high with the area of the cells being about 30 percent smaller than the cell of the arc jet.

Weight loss during slow charring was a bit higher than that for the rapid chars. The feel of the char was different than that observed for the arc jet. Crushing the slow furnace char produced a fine powder, which lacked the cohesiveness exhibited by the arc jet char.

The rapid two dimensional charring conditions produced a specimen that was flat and quite suitable for specimen preparation. Cell shrinkage was nil with the area of the cell being equivalent to that of the arc jet char. Being a rapid char, the structure was quite similar to the arc jet char. Figure 36 shows a photograph comparing the two structures at 20X. The residue formation discussed above was also apparent and similar for both.

Visual appearance of the two dimensional char was quite similar to the arc jet char. The crack network was similar, mainly due to the fact that the furnace char was formed with little cell shrinkage such as the case with the arc jet char. This condition, therefore, would generate similar stress patterns creating similar crack networks.

An examination of Table 6 clearly illustrates the contrasting as well as similar features of each char. In all cases the filler shrank more than the reinforcing cell in the thickness direction and the percentage of filler shrinkage was about the same for the various conditions attempted at each temperature.

The bulk density was the lowest for the chars prepared at 800K than that measured on the chars prepared at higher temperatures. At each temperature level, no significant systematic variation was detected between the furnace chars, S1D, R1D and R2D, except the R1D specimens did exhibit the higher densities than the others.

The bulk densities determined on the arc jet chars were running slightly higher than those of the furnace chars, but the trend of lower density in the zone just above transition (800K) was observed.

An effect of residence time (time-at-temperature) was examined with two char blanks (CB-23 and CB-24), where one was held at temperature for one second and the other for thirty minutes. Both were R2D chars. No significant difference was observed in weight loss, bulk density and visual appearance. This is in agreement with our previous work where residence time above one second is of little importance when the matrix is not graphitizable. In all cases the matrix for this composite was not graphitizable.

The conductivities exhibited a distinguishable difference with formation temperature but little sensitivity was seen for the different heating rates. The R2D did exhibit somewhat lower conductivity most likely reflecting the increased crack network in these blanks.

The important observation in the conductivity is the fair agreement observed between the values of the arc jet and furnace chars. Values measured on a specimen at a zone subjected to a temperature of 1050K to 1150K (estimated by assuming linear gradient from the crust to the transition zone) were similar to the R1D furnace char made at 1050K.

The results of the thermal conductivity evaluation did indicate that the boxing analysis for these materials will work since the furnace chars appear to be representative of the arc jet, and the values of conductivity were sensitive to formation temperature.

Selection of Charring Conditions

The rapid two dimensional (R2D) heating was selected to process the charred specimens. This selection was based on the fact that the bulk and filler structures (crack network, cell size) were most similar to those of the arc jet char. The rapid heating appeared necessary since the cohesiveness and deposition on the spheres more closely matched that of the arc jet char. Although the effective conductivity did not appear to be grossly affected by heating rate, the other properties to be determined may be correlated to heating rate.

All the chars prepared for evaluation under this program were done under the "R2D" conditions with the exception of the 600K char prepared for the specimens used for thermal conductivity. Here the 8.26 cm diameter guarded hot plate was employed for the conductivity measurement and two discs shown in the previously presented Figure 8 were employed. To accommodate this configuration, a chamber was constructed which enclosed the specimens and the chamber was purged with helium and installed within a laboratory oven. The heating cycle consisted of heating the material to 590K in 90 minutes, holding at constant temperature for 30 minutes and allowing to cool within the oven after power shut down.

The R2D chars were prepared, as discussed previously in the Apparatuses and Procedures Section, by immersing a 3.81 x 7.62 x 1.90 cm thick plate, insulated around the edges, within the preheated furnace and as stated earlier held for 50 seconds after thermal equilibrium was established. The resulting char was then impregnated with Armco resin 18-210. In most cases, the char blank was sectioned along the center plane of the thickness. Specimens were prepared from each half thickness. This procedure was adopted due to previous experience in the 2D charring of the low density phenolic-nylon chars which created a central region of low density and poor structure which was not representative of the arc jet chars. This low density region was not as obvious in these specimens as it was in the previous phenolic-nylon material, but we avoided the inclusion of this zone in our specimens where possible. Therefore, as far as the specimen was concerned, the formation of char during preparation progressed from one surface to the other rather than a progression from both surfaces into the center.

The one exception to this was the preparation of the specimens from the 1700K char. Here a crust was formed on each surface with some cracking below the surface. The area from the center of the specimen to the surface was undesirable for specimen preparation. Therefore, the conductivity specimens were taken from the core. The crust was used for permeability and the whole blank was used for porosity and heat capacity determinations.

Typical time versus temperature plots for the furnace chars employed for evaluation are shown in Figure 37. The character of the curves were quite similar to the cycles measured under the preliminary investigation and shown in Figure 33. On most of the curves a slight inflection is seen at 380K, which is about the boiling point of water. This inflection indicates that some water exists within the composite and is driven off at this point.

Table 7 is a summary of all the char blanks prepared and the specimens extracted from them. Included in the table are various physical measurements made prior to and after the cycle. The more significant parameters are shown in Figures 38 and 39. The trends were consistent with the preliminary investigation.

Figure 38 shows the weight loss versus temperature of char formation. Between 600 and 800K the highest rate of weight loss was observed which is obviously the zone of pyolysis. The maximum weight loss of 51 percent was observed at 1100K.

The shrinkage in the thickness direction is shown in Figure 39 for both the reinforcement and filler. The maximum rate of shrinkage of the filler occurred between 600K and 1100K where the value changed from 1 to 20 percent. At 1700K the shrinkage of the filler was only 14 percent and this was obviously due to the crust formation on both surfaces. The shrinkage occurred below the crust creating cracks and delaminations in the filler. The shrinkage of the reinforcement was quite different. Significant change did not initiate until above 800K and the maximum shrinkage occurred at 1730K at 11 percent.

The variation between the shrinkages of the filler and cell wall accounted for the separation between the two during charring.

Approximate bulk density and change in bulk density is shown in Table 7, however, a discussion of these results is included later under "Data and Results."

The structure of the composite after charring was consistent with that reported under the preliminary investigation. From 800K to 1370K, the filler shrank away from the cell wall leaving separations or gaps in the composite. All area remained about the same. A more detailed account of the structure is discussed under "Data and Results" on thermal conductivity since this information was necessary for the thermal model constructed.

DATA AND RESULTS

Thermal Conductivity

Model Analysis. - To provide more meaningful input to the computation of heat transfer through the flight char, a simple thermal model was prepared. This model enabled the adjustment of the measured data to values that better represent intrinsic heat transfer in this material without the radiant and gas conduction contribution provided by the major gaps and separations found in this material.

Figures 40 and 41 illustrate the typical cell structure of the specimen (furnace char) and the flight char (prepared in the arc jet). Basically, the structure of the specimen consists of the charred honeycomb cell wall, the charred elastomeric filler and a gap or separation between the filler and the cell wall. This is similar to the structure of the flight char with the exception of the large cracks and separations running perpendicular to the heat flow existing in the filler of the flight chars. Except for the gap immediately under the top surface crust of the flight char, the location of the other major cracks are random and represent gross anomalies in the structure which were not present (and would not be tolerated) in the specimen. Therefore, the purpose of the modeling done here was to enable the calculation of the effective conductivity of the "solid" (charred filler composite and cell wall) phases of the charred material. This value used in conjunction with the predicted effects of any anomalies such as the cracks running perpendicular to the heat flow can then be employed to derive the heat transfer present in the flight chars.

It is obvious from Figure 40, model of the typical furnace char cell without the cracks perpendicular to heat flow, that a parallel conduction model is present in the specimen involving three paths. Heat is transferred through the charred filler, the cell wall and the gap between the cell wall and filler. The effective conductivity of the specimen can be described by the following equation:

$$k_m = A_f\, k_f + A_h\, k_h + A_s\, k_{gs} + A_s\, k_{rs} \qquad (4)$$

where

k = effective conductivity

A = area fraction

Subscripts

m = as measured

f = charred elastomeric filler

h = honeycomb reinforcement

s = gap or separation between honeycomb and filler

gs = contribution of gas conduction in gap

rs = contribution of radiant transfer in gap

The summation of the first two terms reflects the heat transmission through the "solid" portion of the specimen.

The term solid is used in contrast to the gaps present for which the last two terms of the equation apply. Obviously, the "solid" portion, due to its porous nature in itself can be thermally modeled but was not done since it was beyond the scope of this program and was not necessary in the analysis of the data measured here. Intuitively speaking, however, we would expect little contribution by radiation in the "solid" phase particularly at the temperatures employed under this program and thus, the model would mainly include solid and gas conduction components. Since this material consists of silica and charred phenolic microballoons adhered with a small amount of charred matrix, the model would be of the type describing heat flow through powders.

The last two terms of Equation 4, describing the heat transferred along the gap, can be better defined with the following relationships. For the effect of the conductivity in the gas:

$$k_{gs} = k_g \frac{L}{L + L_g} \tag{5}$$

where

k_{gs} = contribution to thermal conductivity of the gas in the gap

k_g = thermal conductivity of the gas

L = mean free path of a molecule before collision with a bounding surface in the direction of heat flow. In this case L is the thickness of the specimen

L_g = mean free path of the gas

The conductivity of nitrogen (k_g) is given in Figure 42. Values of the mean free path L_g at various temperatures and pressures can be calculated based on a Maxwellian velocity distribution by:

$$L_g = \frac{0.707\ KT}{4\Pi\rho^2\ P} \tag{6}$$

where

K = Boltzmann's constant

T = temperature

ρ = radius of the molecule

P = pressure

For the radiant contribution

$$k_{rs} = F_{(1R2)g} \, L \, \sigma \, T_m^2 \qquad (7)$$

where

k_{rs} = contribution to thermal conductivity of the radiant heat transferred in the gap

$F_{(1R2)g}$ = radiation factor for the radiant transport through the gap. Boundary emittances assumed at 0.55

L = thickness of the specimen

σ = Stephan Boltzmann constant

T_m = mean temperature (K)

The values for the total radiation factor (F_{1R2}) were assumed equivalent to those for long slots which have been defined by Jakob [6] and were used in Equation 7 for the various gap widths present. The total radiation factor was then corrected to $F_{(1R2)g}$ for boundaries having emittances of 0.55. The values ranged from 0.13 to 0.23.

In Equation 2, the first two terms $A_f \, k_f + A_h \, k_r$ can be combined to $A_c \, k_c$ which defines the heat transfer through the "solid" phases (honeycomb cell wall plus filler). The term A_c is equivalent to $(1 - A_s)$ and k_c is the intrinsic value of conductivity we wish to define. Rearranging Equation 4 yields

$$k_c = \frac{k_m - A_s \, (k_{gs} + k_{rs})}{1 - A_s} \qquad (8)$$

In the following sections the measured conductivity k_m will be presented for the determinations on the various chars formed at the different temperature levels. In the boxing analysis k_c will be reported since it represents a more intrinsic value of the charred filler and cell wall without the effects of major cracks and separations within the composite.

Data. - The measured values of effective conductivity (k_m) and photographs illustrating the structure and condition of the specimens are included in Figures 43 through 58. Tables 8 through 14 include the effective thermal conductivity measured. The photographs provided the information tabulated in Table 15 which indicates the size and cross-sectional area of the gap present between the filler and the cell wall. This information was used to calculate the term $A_s \, (k_{gs} + k_{rs})$ of Equation 8 from which the conductivity of the "solid" phases was determined.

Before discussing the data, a brief review of the structure and condition of the specimens is in order. For the 600K char, for which a photograph is not shown, the material had essentially the same structure as the virgin material with no separations between the filler and the cell wall. Localized areas of separations were observed (see Figures 45 and 46) for the 800K char with the filler containing no visible cracks. The remaining chars (1100-1700K) shown in Figures 48, 50, 51, 52, 53, 54, 56, 57 and 58 had a uniform separation about the cell and several cracks in the filler were visible. As shown in Table 15 the cross-sectional area of the gap occupied 8 to 24 percent of the total cross-sectional area. This is probably somewhat consistent with that of the flight char.

The effective thermal conductivity of each char was determined at mean temperatures up to just below the charring value since the hot face temperature of the specimen was not allowed to exceed the prechar temperature. To determine the effective thermal conductivity at the charring temperature, the curve was extrapolated a small amount. The value of the intrinsic conductivity (k_c) was deduced from this value by use of Equation 8 and the calculation is tabulated in Table 16. The locus of k_c was then plotted against charring temperature in Figure 59. The values shown in this figure are those to be used for the effective thermal conductivity of the "solid" phases of the flight char as it is being formed.

It is interesting to note that the value of k_c deviated from k_m by less than 10 percent in most cases and was no more than 20 percent. This small deviation reduced considerably the effect of any errors involved in the modeling calculations and it is estimated that with all sources combined an uncertainty of the values shown in Figures 59 is less than ±13 percent at and above 1300K and ±10 percent at and below 1100K.

The boxing values at one atmosphere blended quite well with the values measured on the virgin material. At one atmosphere a gradual increase in conductivity from 0.045 W/m k at 100K to 0.10 W/m k at 800K was observed. Above 800K the rise in conductivity was about five times greater than that below 800K. The value at 1400K was 0.42 W/m k.

The data measured on the 1700K chars were not consistent with the other specimens. As can be seen in Figure 59, the values fell lower than the indicated trend. The measured data on the 1700K char shown in Figure 55 was widely scattered which indicated anomalies present in the specimens. In preparing the 1700K char, the resulting blanks consisted of a crust formation on both faces and a slight crack separating the crust from the core of the blank. Measurements were not attempted on the crust, which would have simulated the crust on the flight char, since the thickness after machining suitable surfaces was about 0.076 cm or too thin to

obtain a reasonable measurement. Instead a measurement was attempted on the core of the blank, the structure of which was obviously not consistent with the other specimens. We suspect that thin delaminations across the path of the heat flow were present causing the scatter and lower values in the measured data.

Due to the inconsistency of the data measured on the 1700K char, an extrapolation of the values obtained at the lower charring temperatures was made to estimate the thermal conductivity of the crust.

The character of the curve in Figure 59 was as expected. Up to 800K the increase in conductivity was gradual. At 800K the material was still unstable and in a transitional state, as can be observed with the wide divergence of the duplicate data measured on the 800K char shown in Figure 44. Above 800K the thermal conductivity increased significantly from the effects of continuing carbonization of the matrix, an increase of the radiant contribution in the porous filler and an increase in the thermal conductivity of the interstitual gas.

The variation of effective thermal conductivity with pressure is observed in Figure 59 as well as in the individual plots of conductivity for each char temperature level. There is very little difference (less than 0.01 W/m k) in the conductivity measured at 101,325 N/m^2 (760 torr) and that measured at 49,329 N/m^2 (370 torr). A larger difference is seen with the data measured at 1333 N/m^2 (10 torr), but the difference remains less than the conductivity of nitrogen.

Porosity

The porosity of the charred material was calculated from the bulk and true densities. Values were measured on the total composite and charred filler for the furnace chars. Some values were also measured on the arc jet char for comparison.

Figure 60 and Table 17 report the bulk densities measured versus char formation temperature. The values decreased from 0.262 gm/cm^3 at 300K (virgin material) to a minimum at 800K of about 0.16 gm/cm^3. Above 800K the values increased slightly and then remained about constant at 0.19 gm/cm^3 from 1100K to 1700K. The furnace chars prepared at 1700K formed a crust similar to the one formed on the arc jet char and the bulk densities were determined on both the crust and core of the charred blank. As expected, the densities of the crust were higher ranging from 0.225 to 0.265 gm/cm^3.

The bulk density measurements of the charred filler (without the honeycomb cell) are also reported in Figure 60 and Table 17. These values ran slightly lower, but due to the uncertainty of the measurement on these small pieces, one can only deduce that the bulk density of the filler is about the same as the total composite.

The increase in density from 800K to 1100K was somewhat expected from the appearance of the material (see the photographs of the thermal conductivity specimens and Table 15) where larger gaps existed in the 800K char.

This phenomenon was also observed in the bulk density values of the arc-jet char filler determined with water absorption shown in Table 6. As stated before, the absolute values of the water absorption determination were probably biased high, but the trend in increasing bulk density is definite from the transition zone to the zone adjacent to the top crust. The minimum bulk density at 800K is attributed to a high initial weight loss, (outgassing of volatiles) without full shrinkage of the bulk composite which does occur at the higher temperatures resulting in increased bulk density. This same trend was also observed and reported [7] for another elastomeric material, MG-1, previously evaluated for NASA.

The true density is shown in Figure 61 and Table 18. For the furnace chars, the measurement was made on the same specimen used in the determination of bulk density. The true density increased as expected since the polymers are carbonized from 1.4 gm/cm^3 at 600K to 2.0 gm/cm^3 at 1100K. Above 1100K a slight decrease was measured. At 1700K the crust exhibited slightly higher true density than that of the core.

The arc jet char agreed within 10 percent of the furnace chars and also showed a decrease with increasing formation temperature.

The true density of the filler alone was about 5 to 10 percent lower. Obviously, the constituents in the honeycomb reinforcement does increase the true density of the composite.

The porosity is shown in Figure 62 and the data measured was rather consistent for all the chars examined. The porosity increased from 83 percent at 600K to between 89 percent and 90 percent at 800K and remained fairly constant above that temperature. The crust of the 1700K char did reduce back to 87 percent but the core remained at 89 percent. Notice the agreement in porosity between the filler and total composite of the furnace char and the arc jet char, all being between 89 and 91 percent porosity.

Heat Capacity

The enthalpy and heat capacity data are shown in Figures 63 through 66 and Tables 20 through 26. As shown in the figures, the enthalpy did decrease in magnitude with increasing temperature of char formation. This would be expected since the degradation of the phenolic microballoons, nylon and the silicone resin would increase the weight percentage of carbon and silica in the charred composite which results in lower enthalpy values.

A boxing analysis was performed to predict the heat capacity of composite during degradation. The result of that analysis is shown in Figure 67. Below 500K the values increased with temperature in accordance with the values measured on the stable virgin material. Above 500K initial degradation occurs, and when the material reaches 811K a weight loss of about 47 percent occurs indicating the complete loss of all volatile material in the virgin composite. A slight decrease in heat capacity occurs during that initial degradation which is due to a higher weight percentage of the silica and some carbonaceous formation. From 811K to 1089K the heat capacity increases at a slope similar to that exhibited for the virgin material. The weight loss in this region is not significant and the increase in heat capacity represents a normal behavior for a stable material. Above 1089K, however, weight loss did not increase and the heat capacity decreased indicating a variation in material composition, probably the further carbonization of the charred matrix. It is suspected that if data were obtained at higher temperatures the heat capacity would have leveled out or even increased slightly with the further stabilization of the material. Note in Figure 66 the constant heat capacity above 1089K does indicate that the 1700K furnace char is becoming stable and is characteristic of a carbon-like material.

Permeability

The permeability was determined on all the furnace chars prepared at the five charring temperatures and on the crust of the arc-jet char. The values were measured at room temperature on all the chars; however, determinations at elevated temperatures of the specimen and permeating gas were obtained on the furnace chars prepared at 600K, 1100K, 1300K and 1700K (crust). The intent of the permeability measurements was to predict the pressure gradient through the thickness of the flight char as it was formed. Due to the significant separations between the filler and cell wall particularly for the furnace chars prepared at 800, 1100 and 1300K, the resistance to flow was quite low and the measurement reflects

mainly the flow through the separations rather than flow permeating the charred filler material. Even with the low permeability, significant trends were observed.

The permeability coefficients were derived from the Cornell and Katz plots shown in Figures 68 through 73. The calculations required for the Cornell and Katz plot are shown in Tables 27 through 32. A summary table is shown in Table 33 for all the coefficients including α, the viscous flow coefficient, k, Darcy's constant which is $1/\alpha$, and β, the inertial flow coefficient.

There was a significant variation in the room temperature Cornell and Katz plot between the two specimens from the 600, 800, 1100 and 1700 degree chars. There was also a bulk density variation in the duplicate specimens from these chars. In each case the specimen with the higher bulk density gave the higher value of α, the viscous flow coefficient and, therefore, the lower value of Darcy's constant, k. The value of β, the inertial flow coefficient, was also higher for the specimen with the higher bulk density, except for the 600 degree char where the value of β was not well defined.

The Cornell and Katz plots for both specimens of the 1300 degree char showed excellent agreement in the values of α and β for the room temperature runs. These specimens also had a smaller percentage difference between their bulk densities than any of the other specimens.

These same correlations with the bulk density also held generally for all the furnace chars. The 800 degree char had the lowest average bulk density and the highest average value of Darcy's constant. The 600K char, 1700K char crust and the arc jet crust had the highest bulk density values and the lowest permeability values.

Although the 600K char had about the same bulk density as the 1700 degree crust and the arc jet crust, its permeability was an order of magnitude lower. This resulted from the lack of cracking in the 600K char and its structure was still similar to the virgin material.

Both the 1700K crust and the arc jet crust had a thin layer of dense material which had condensed on the surface as a result of heating. Immediately below this the hardened coating the material was quite porous. Therefore, the gas flow rate through the crust specimens was not dependent on the thickness of the specimen, but on this thin coating of condensed material. This is subtantiated by the permeability values obtained for the 1700K and the arc jet crust specimens. Since the arc jet crust specimen was thinner than the 1700K crust specimen, its permeability should be higher since the thickness of the specimen (L) appears in the denominator of $\left(\frac{MPm\Delta P}{LRT\mu G}\right)$. Another reason for this might be that the

1700K char allowed the evolved gases to escape through the sides of the charring block as well as through the surface. Since the evolved gases of the arc jet char would be forced through the surface, this may have resulted in more holes formed in the crust of the arc jet char.

During the high temperature runs the value of α decreased by 40 to 60 percent of its room temperature value. The value of β also decreased during the high temperature runs on the 1100, 1300 and 1700K char specimens. The value of β was not well defined for the room temperature run of the 600K char specimen. Equation (2) in Appendix F shows the significance of changes in the coefficients. Note that if the coefficients α and β decrease, the flow corresponding to a given pressure drop increases, hence there is less flow resistance. Since Darcy's constant, k, is the reciprocal of the viscous flow coefficient, α, a decrease in flow resistance will be manifested by an increase in Darcy's constant. Thus, the results of the measurement show that the flow resistance becomes less as the temperature is increased. The thermal expansion of the material as it is heated probably opens up the cracks, thus decreasing the flow resistance; however, it must also be considered that some mechanical failure under the pressure drop and temperature of the material probably occurred during the high temperature runs. This was demonstrated by obtaining room temperature data after each high temperature run. The data indicated that the degree of specimen failure varied from a maximum for the 600K char to a minimum for the 1700 char. The following table shows the percent decrease in the viscous flow coefficient from the initial run at room temperature to the room temperature return.

Specimen	Percent Decrease in α
600K	44.3
1100K	33.8
1300K	11.9
1700K	8.2

The above results led us to the conclusion that except on the 1700K char the effects on the coefficients at temperature are due primarily to a physical structure change in the material during measurement and do not reflect changes in the fluid dynamics of the system. On the 1700K char the variation in values between room temperature and 800K evaluation is due to fluid considerations.

CONCLUSIONS

This study has characterized Material A in both the virgin and charred states. The data have revealed the typical progression of various thermal and physical properties that will occur during the process of ablation upon reentry.

In the virgin state the behavior was as expected with the exception of a slight inflection in thermal conductivity below room temperature, which infers the occurrence of a physical or structural transition at these temperatures. Since only the thermal conductivity appeared to be affected, and the inflection was not severe, this behavior should not greatly perturb the design or prediction of the materials performance.

The degradation of the virgin material appears to initiate at above 500K as was observed with the apparent exothermic reaction that occurred above 500K with the heat capacity specimens. To summarize and draw certain conclusions concerning the progressive change in properties of Material A during ablation, Figure 74 was included. A summary of all pertinent data measured on the chars prepared at the various temperatures up to 1700K is included in the figure and it reveals the following conclusions.

In the range of 500K to 800K all degradation and volatilization occurs. This is obvious from the weight loss history and bulk density profile with temperature since the maximum weight loss and the lowest bulk density occur at 800K. Above 800K both weight loss and bulk density remained relatively stable. At 800K the material is degraded but very unstable. Definite variations in the measured values for thermal conductivity and heat capacity on the 800K char indicated lack of specimen to specimen consistency. It was also observed that the 800K char did not remain chemically or physically stable when heat soaking at 670K was performed to remove the impregnant used. Impregnant removal from the other chars was performed without affecting the material.

With an increase in temperature from 800K to 1100K, the carbonization of the pyrolyzed matrix becomes evident as indicated by the significant increase in thermal conductivity and true density. Above 1100K and up to 1700K carbonization progresses to a more ordered state as is observed with the continued increase in thermal conductivity and slight decrease in heat capacity.

In the 1600K to 1700K range the glass and silica in the system cause the formation of the crust. This is obviously from the melting of the glass within the honeycomb reinforcement and some sintering and possibly melting (as demonstrated in the photomicrograph of Figure 31) of the silica spheres. This liquid phase

forms a thin coating at the surface and acts as the cohesive bond for the crust. Although the permeability measurements indicated a higher resistance to flow than the open structure immediately below, it was still relatively permeable indicating that liquid phase did not form an air light seal.

In conclusion, the performance of the program was successful in that the data measured can be employed toward design and performance prediction of the thermal protection system. However, precise thermal analysis will be difficult in the fact that the physical structure of the flight char contains several large gaps and separations randomly located in each cell. These anomolies do create sites for radiant shunting of heat which must be included with the reported thermal conductivity in calculating the heat transfer through the composite.

FUTURE WORK

We are continuing this program with one additional elastomeric material supplied by NASA. The performance of this new study will be in accordance with the philosophy and procedures reported herein.

ACKNOWLEDGMENTS

The mechanical properties evaluated under this program were conducted by Austin Bush, Associate Engineer, in the Solid Mechanics Section. The permeability evaluation was conducted by R. W. Robertson, Associate Engineer, in the Thermal Section. The remaining evaluations and the coordination of the entire program was performed by W. T. Engelke, Research Engineer, in the Thermal Section. Special recognition is given to Andre P. Wooten, Technical Specialist, Thermal Section, for his many long hours devoted to this program where he did much of the specimen coordination and experimental work.

Southern Research Institute
Birmingham, Alabama

June, 1973

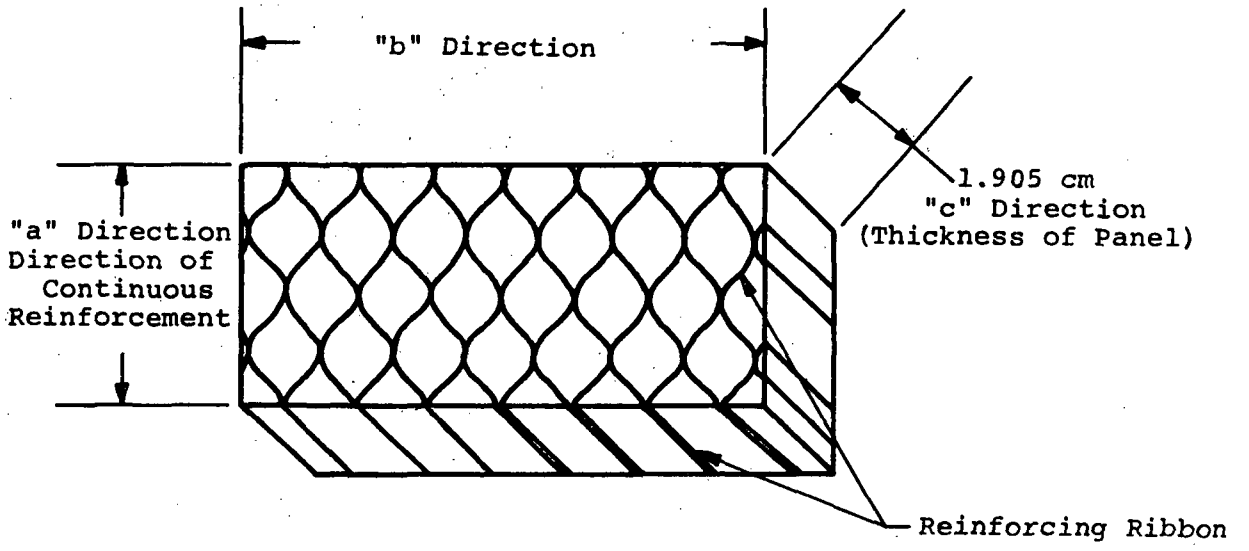

Figure 1. Drawing of Cell Structure for Material A.

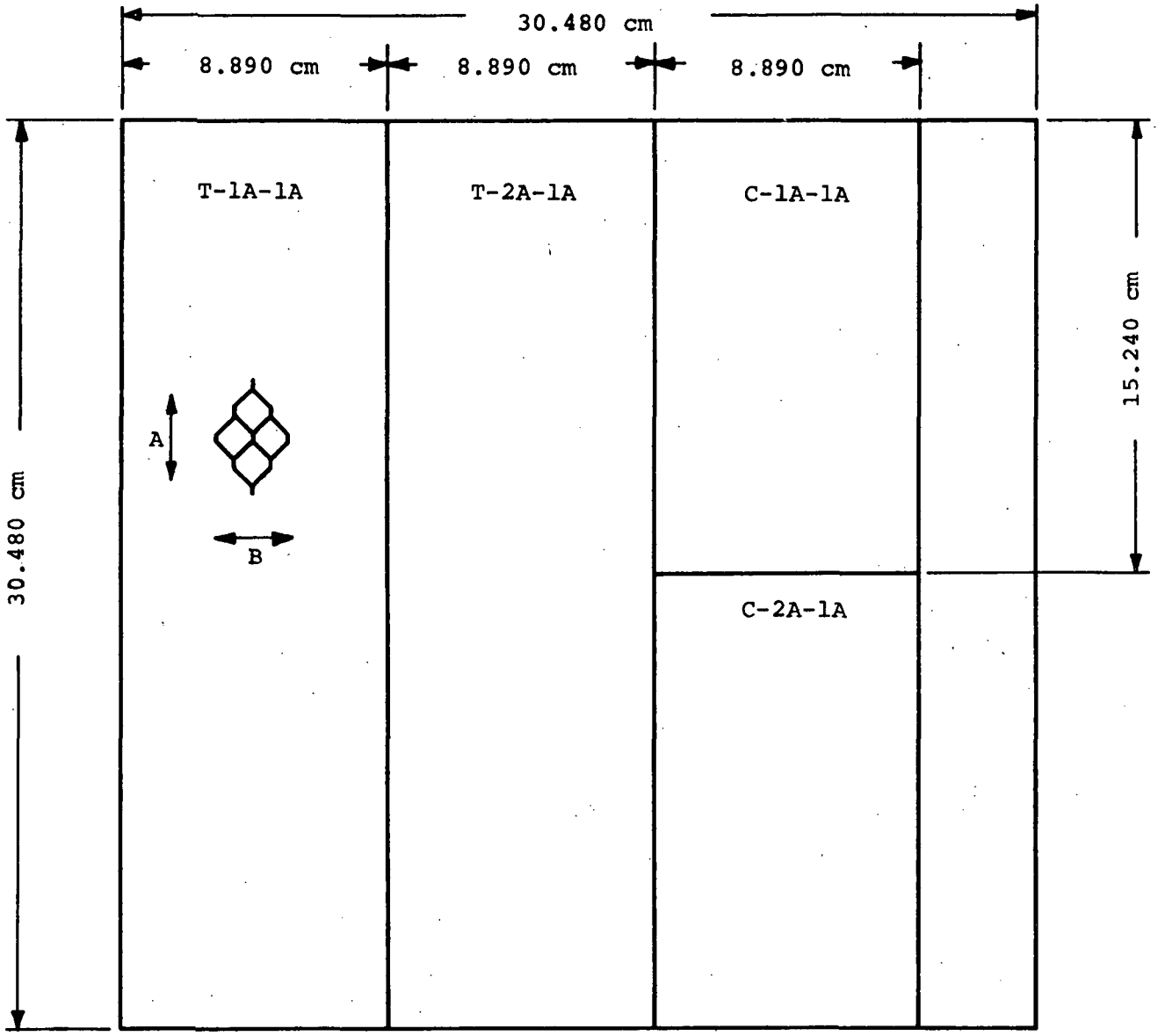

Figure 2. Cutting Plan for Panel No. 1 of Material A

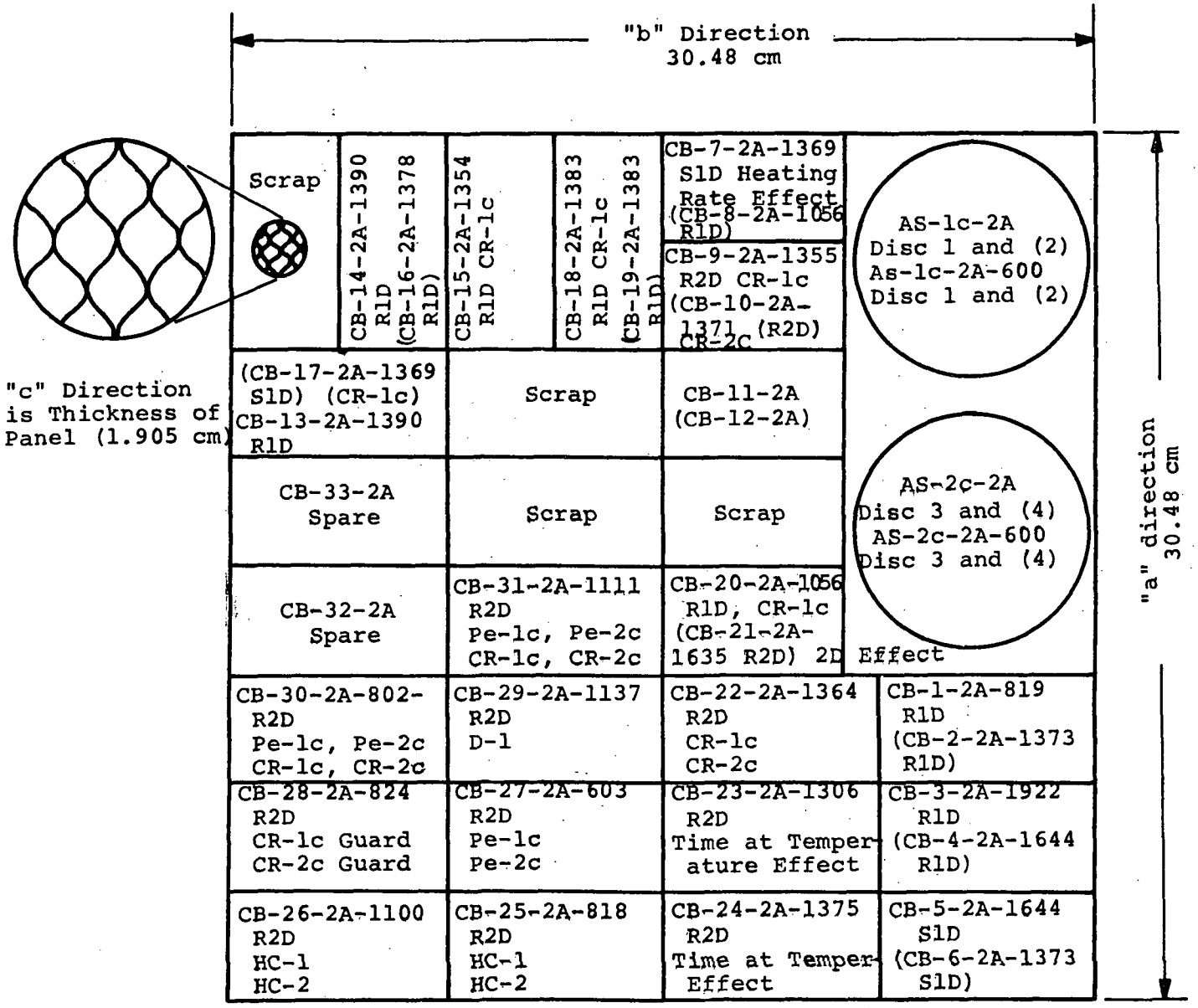

Note: Numbers in ( ) are specimens removed from lower half of panel thickness.

Figure 3. Cutting Plan for Panel 2 of Material A

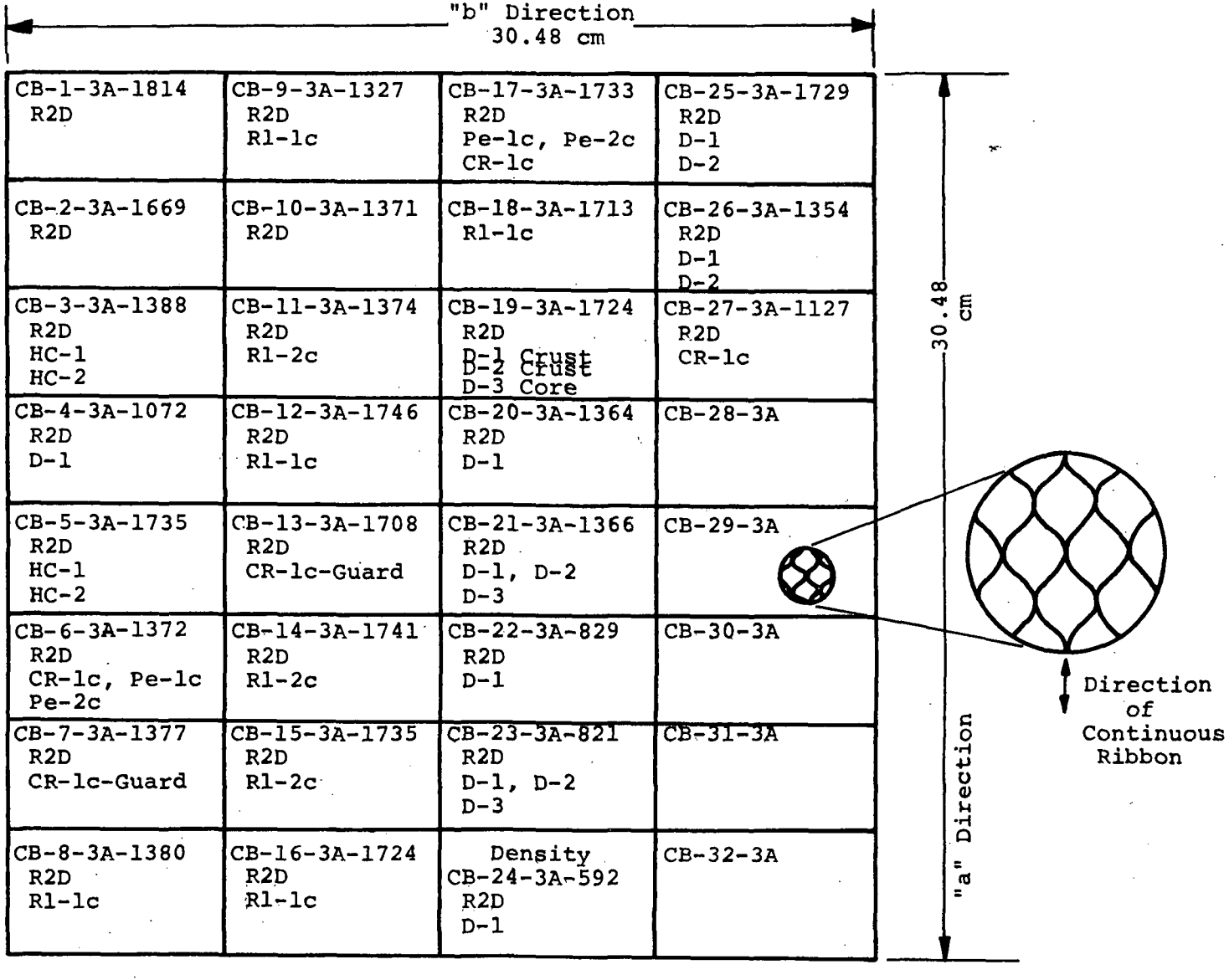

Notes: 1. "c" direction is the thickness of panel (1.905 cm)

2. Specimen numbers D-1, D-2, etc. are density specimens used for bulk and true density determinations.

Figure 4. Cutting Plan for Panel 3 of Material A

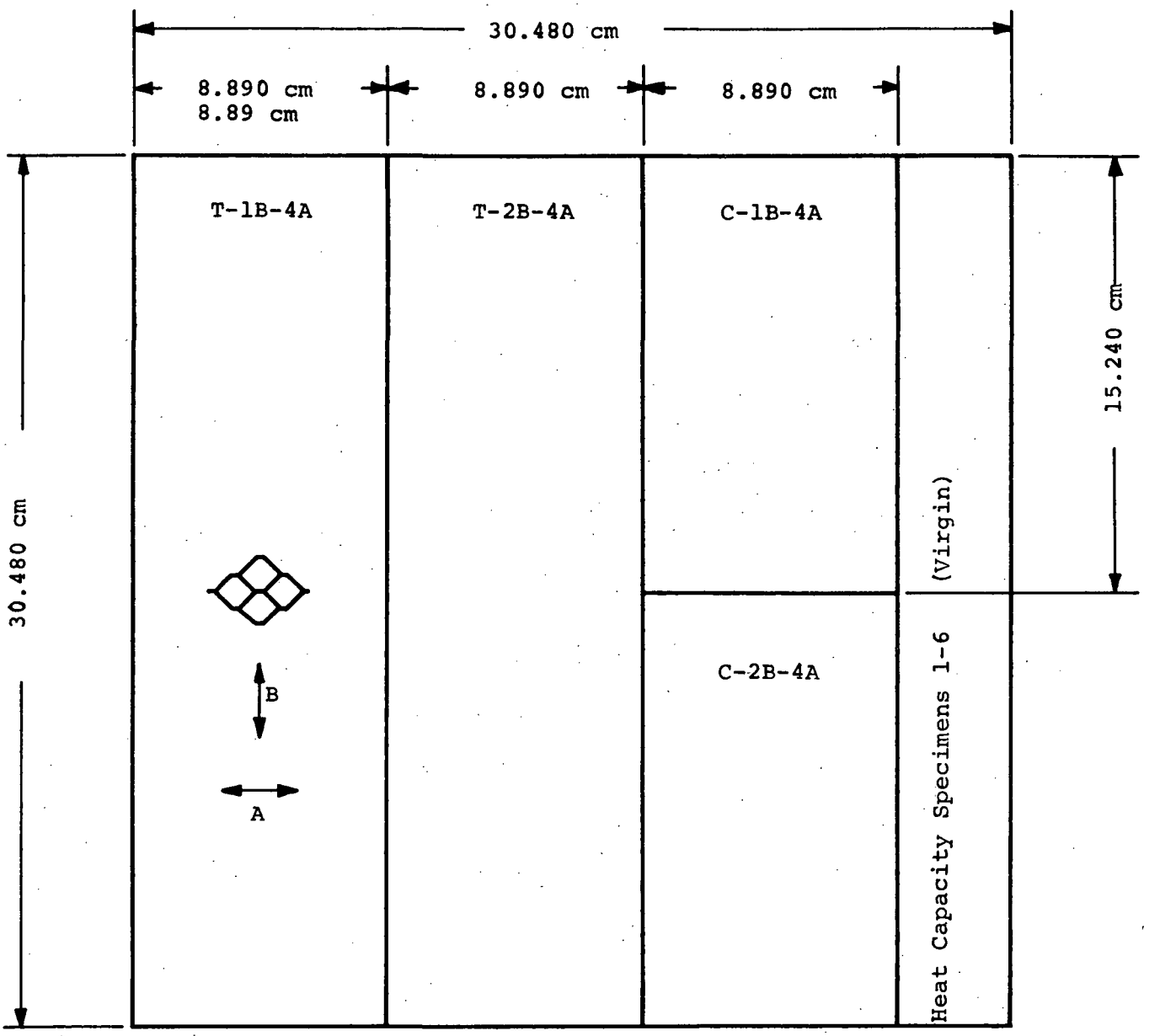

Figure 5. Cutting Plan for Panel No. 4 of Material A

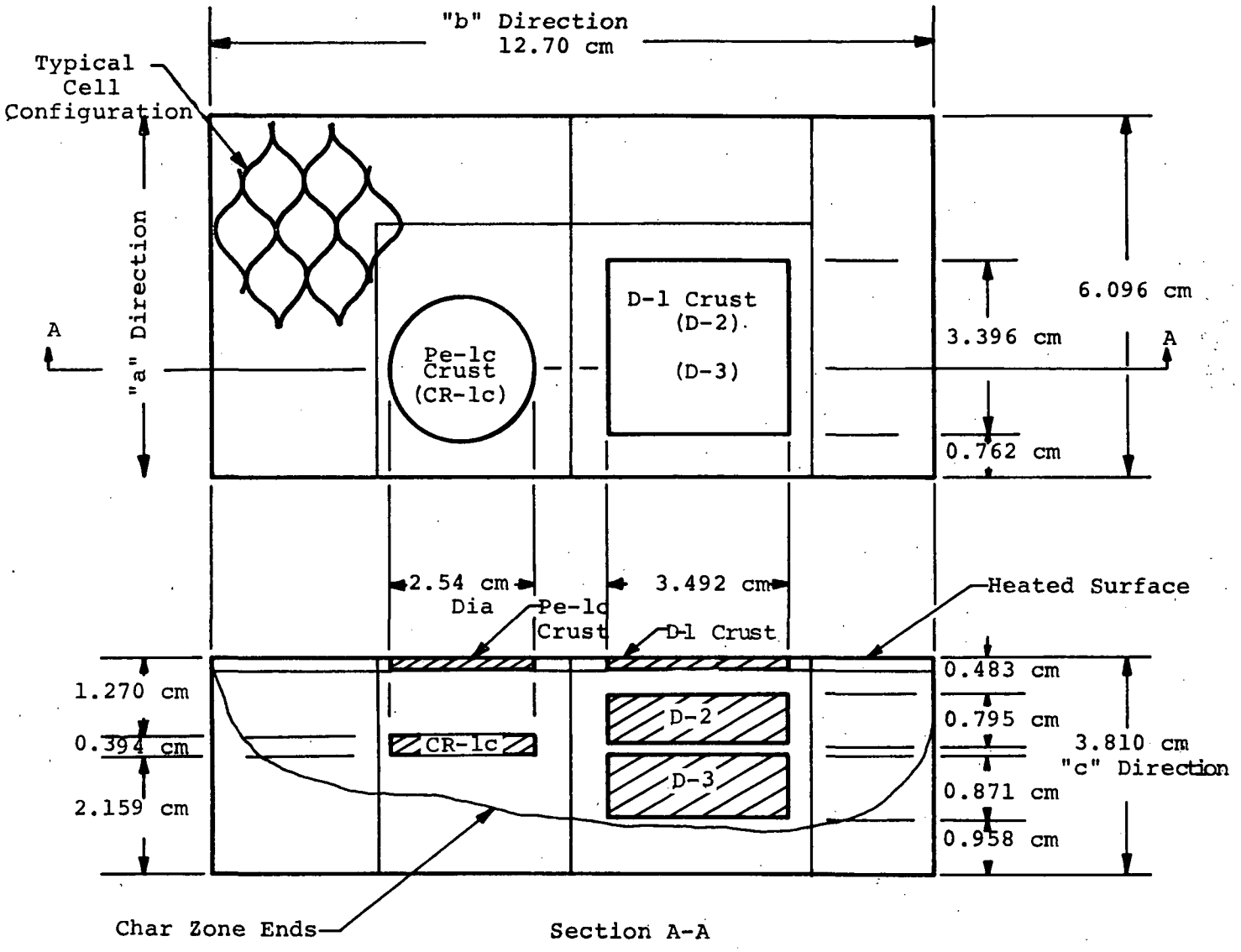

Figure 6. Cutting Plan for Arc Jet A-1

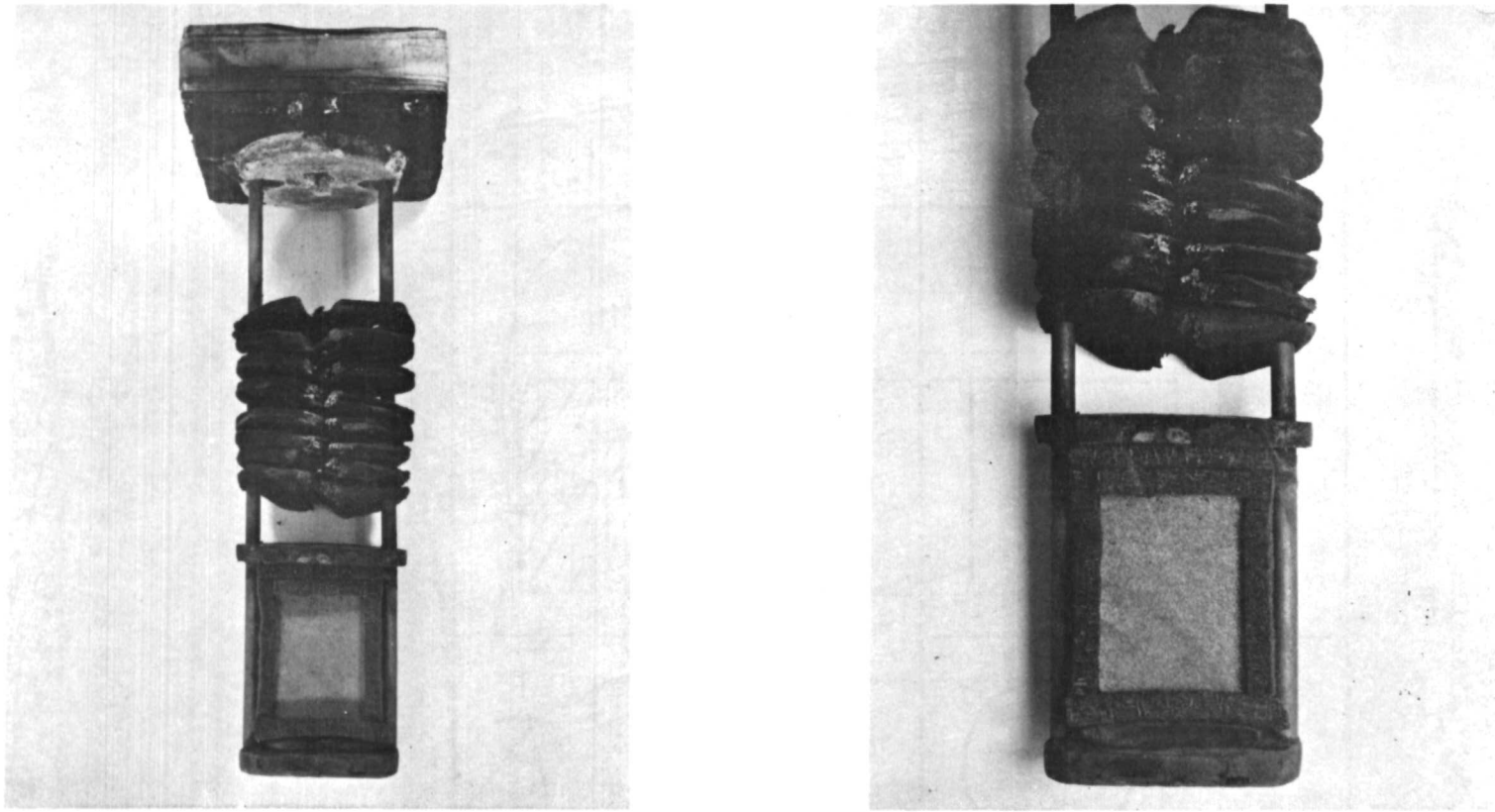

Notes:
1. One specimen 3.81 cm wide x 7.62 cm long x 1.91 cm
2. Specimen is inserted in heater tube with 7.5 cm diameter
3. Temperature measured through sight port in furnace by sighting at center of specimen.

Figure 7. Picture of Specimen Holder for Preparing Char Samples Shown With Virgin Specimen Installed.

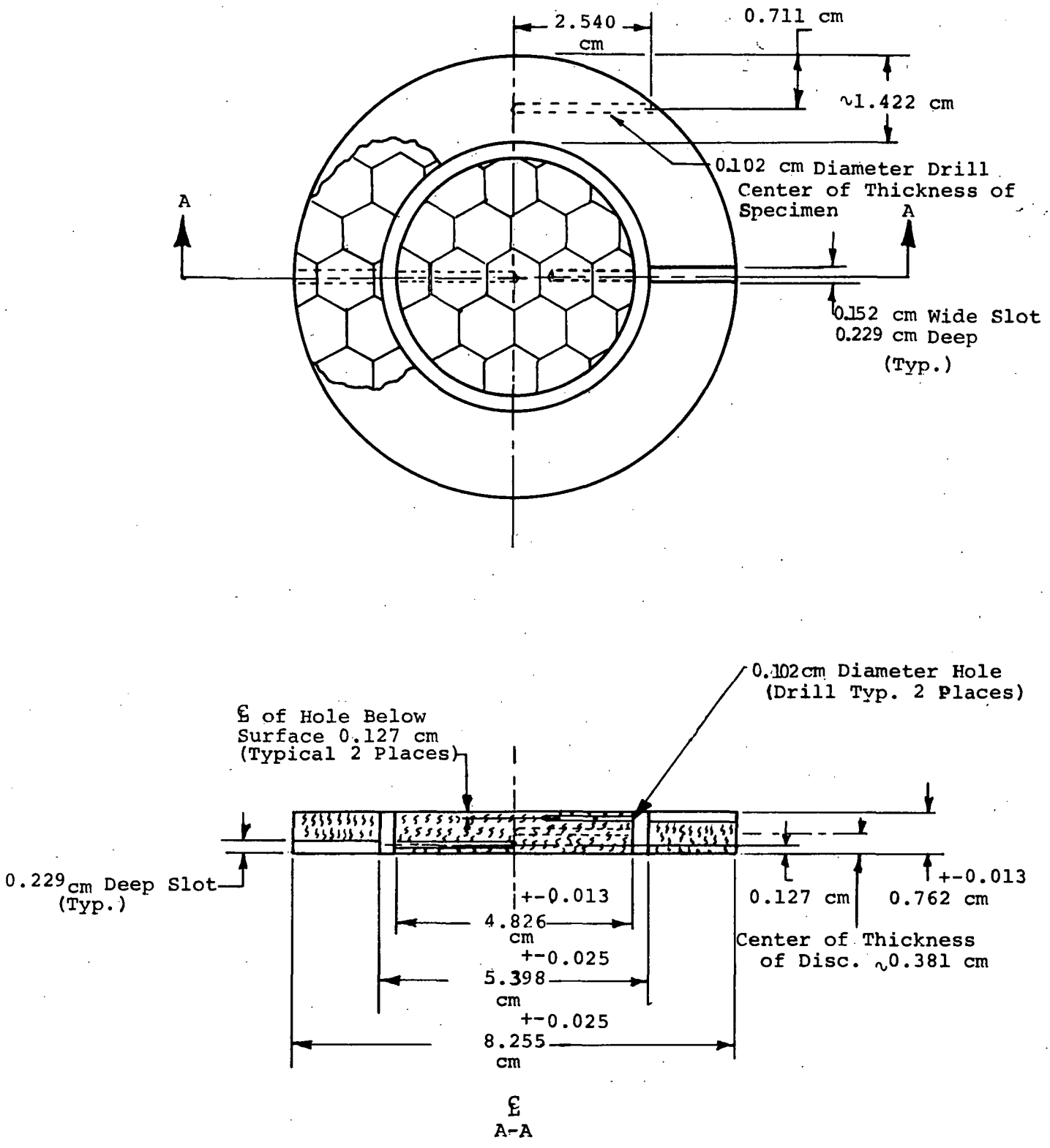

Figure 8. Thermal Conductivity Specimen for Guarded Hot Plate Apparatus

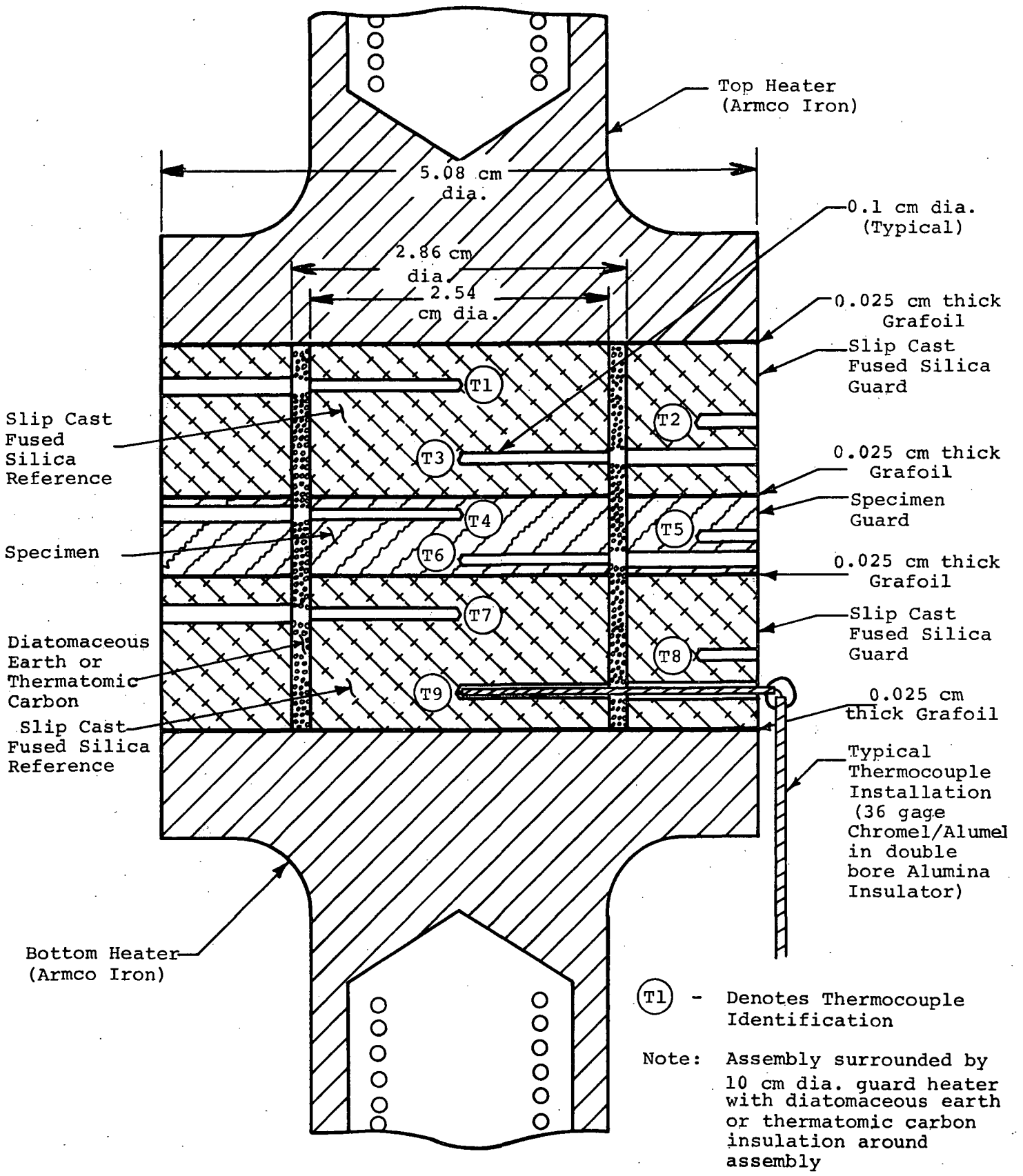

Figure 9. Assembly of Guarded Comparative Rod Apparatus

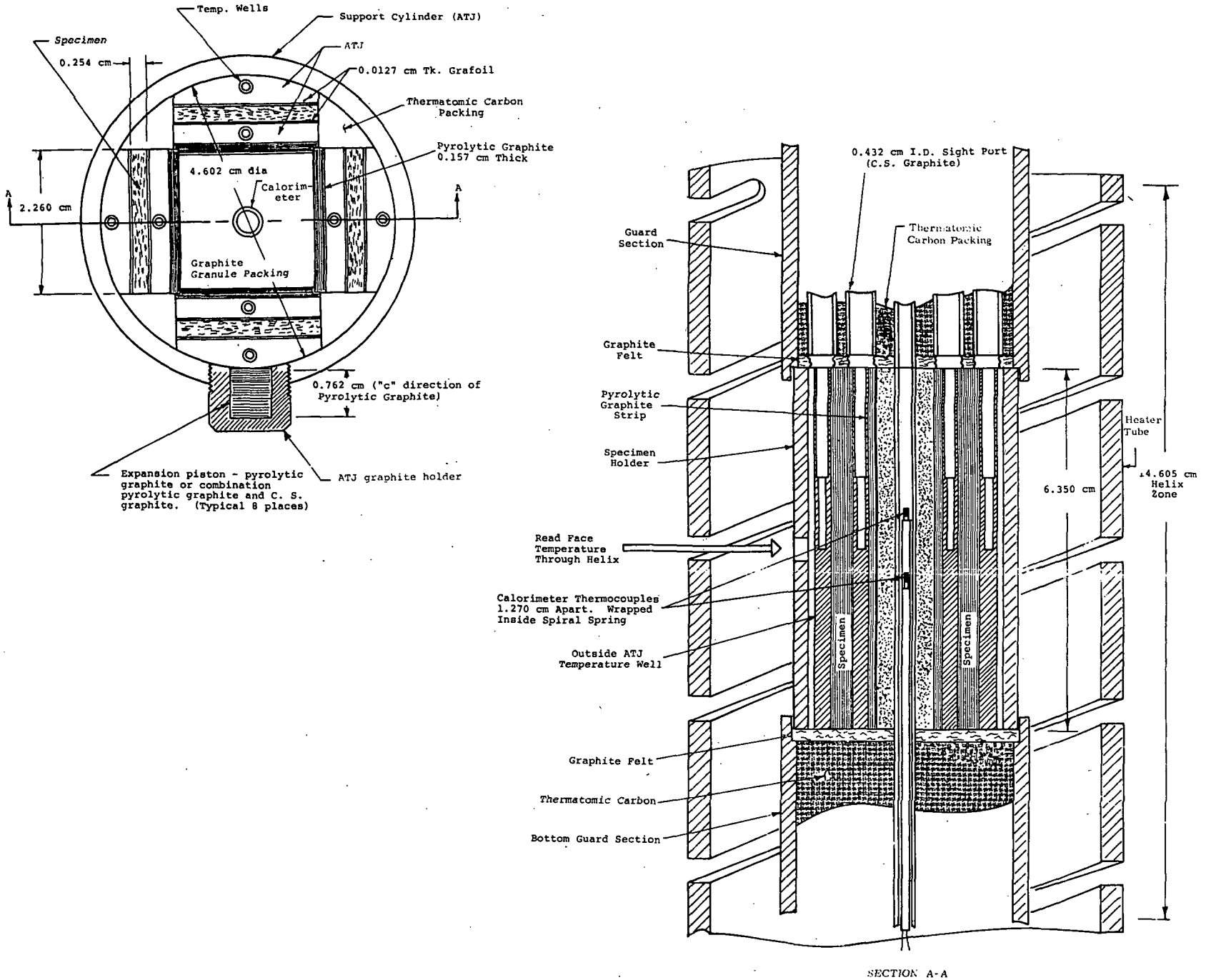

Figure 10. Schematic of Strip Specimen Configuration for Thermal Conductivity Measurements in Radial Inflow Apparatus

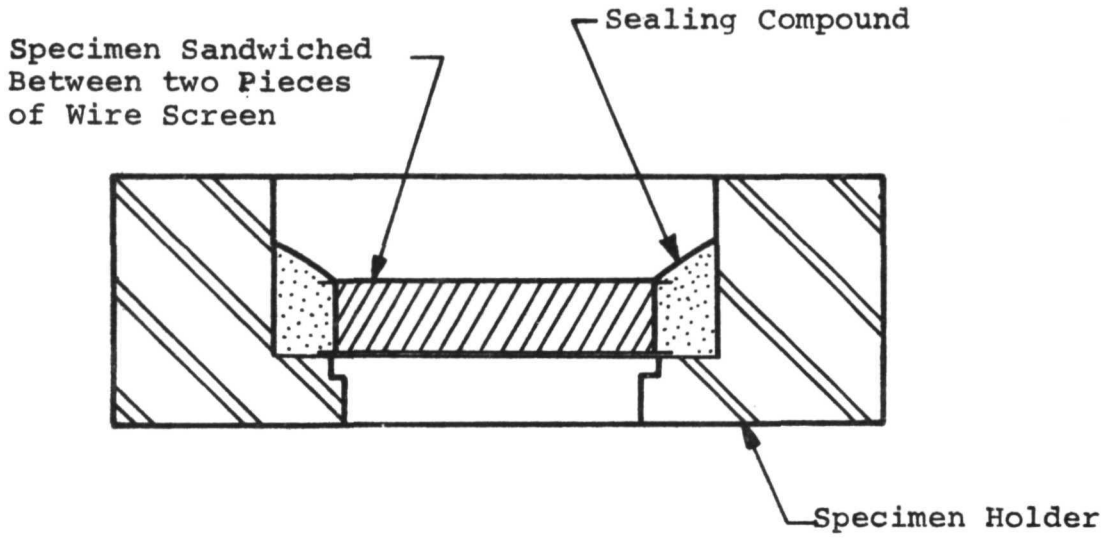

Figure 11. Typical Permeability Specimen Build-Up

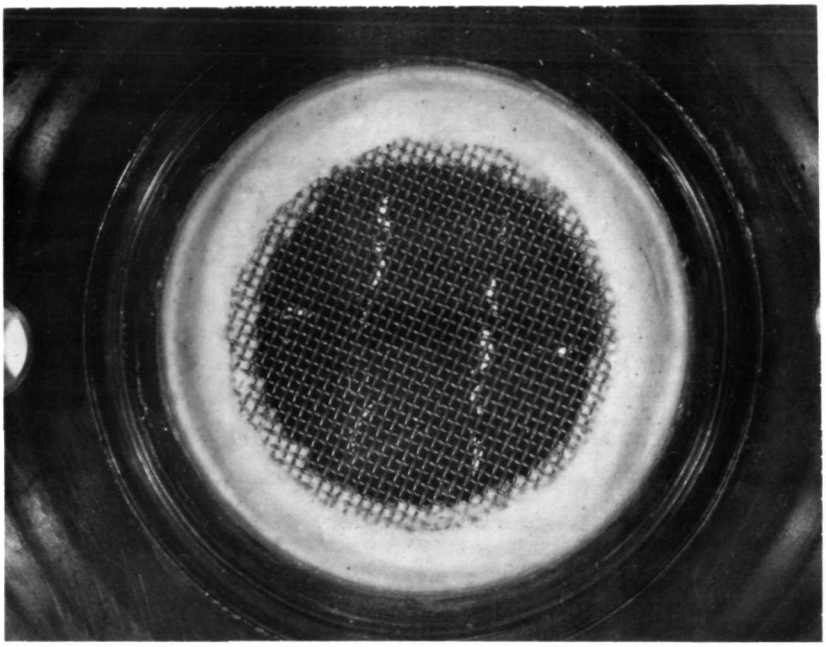

Typical Specimen Sealed in Fixture
with Sauereisen No. 32 Cement

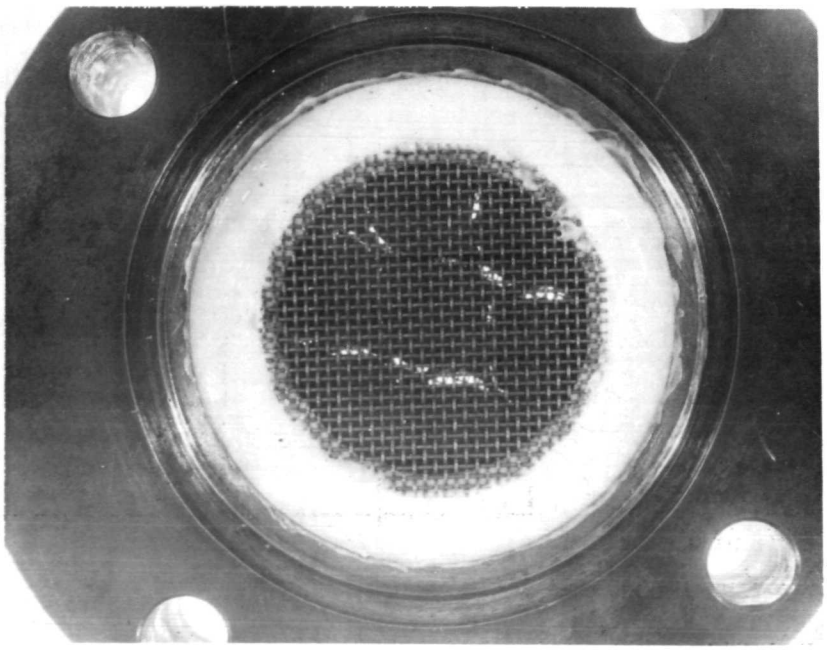

Typical Specimen Sealed in Fixture with Silicone Rubber
(Dow Corning RTV-731 Silastic)

Figure 12. An example of both methods used to seal specimens in the fixture

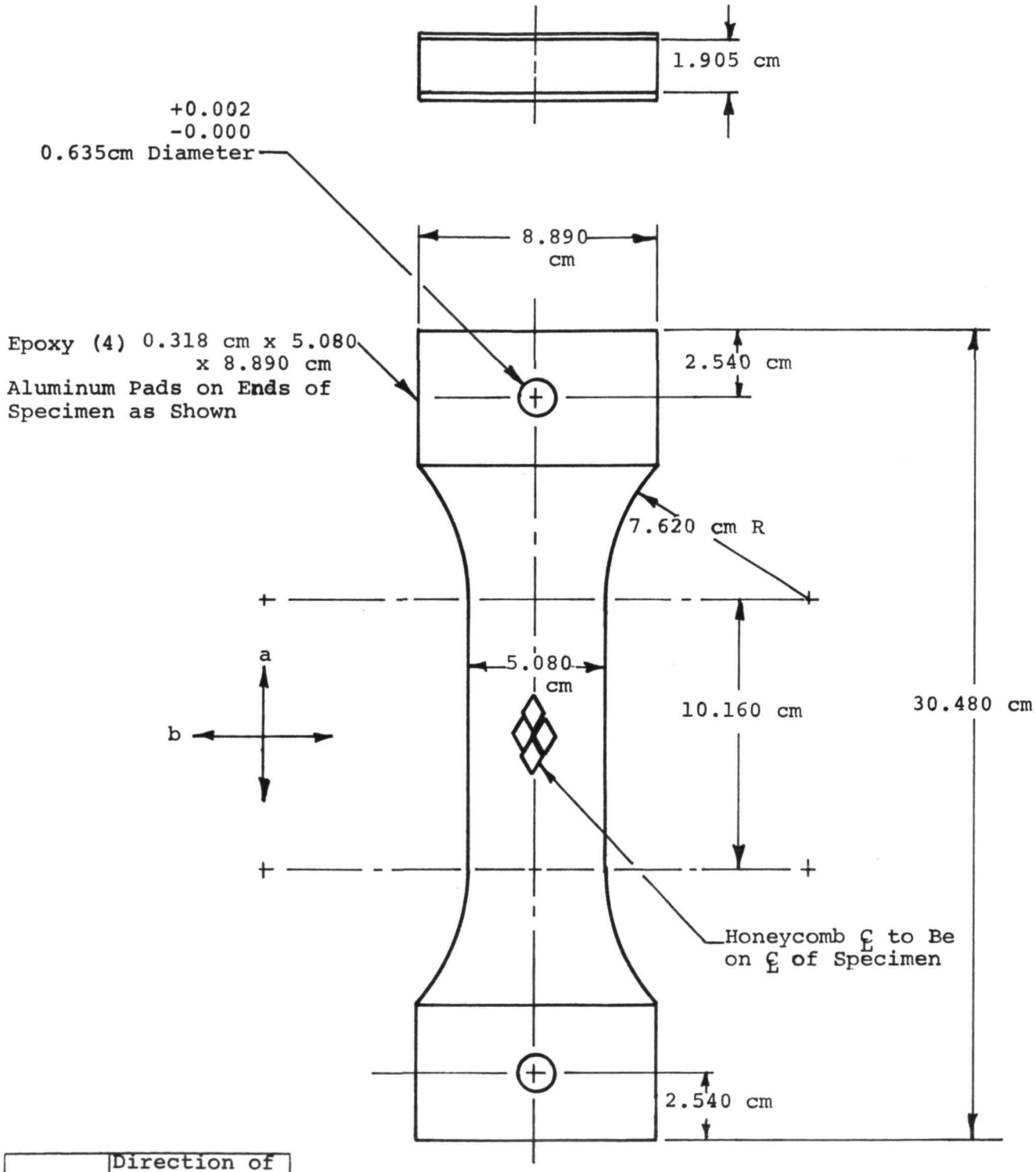

Item	Direction of Honeycomb
1	a
2	b

Figure 13. Configuration of Tensile Specimens

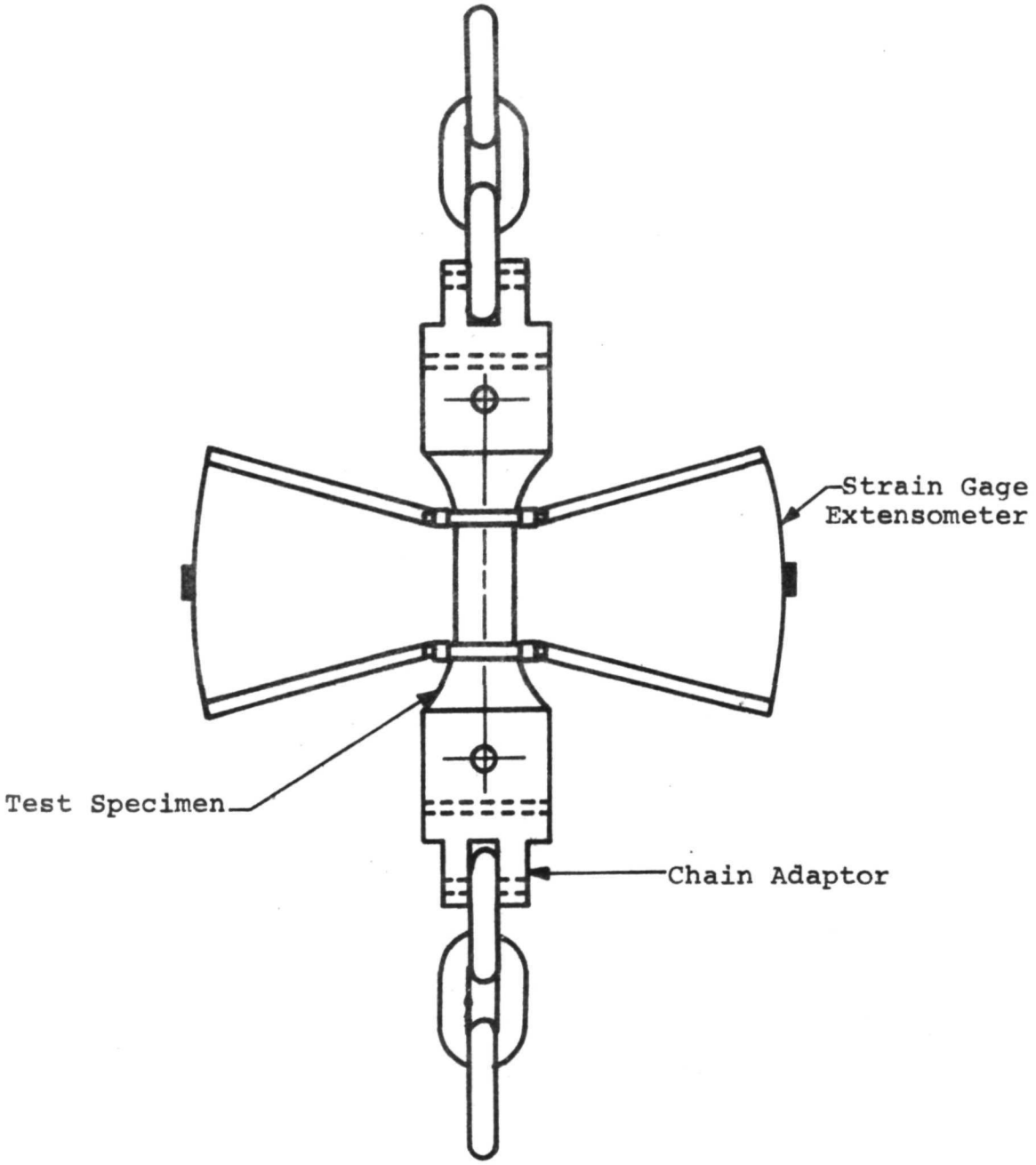

Figure 14. Schematic of Tensile Load Train Assembly.

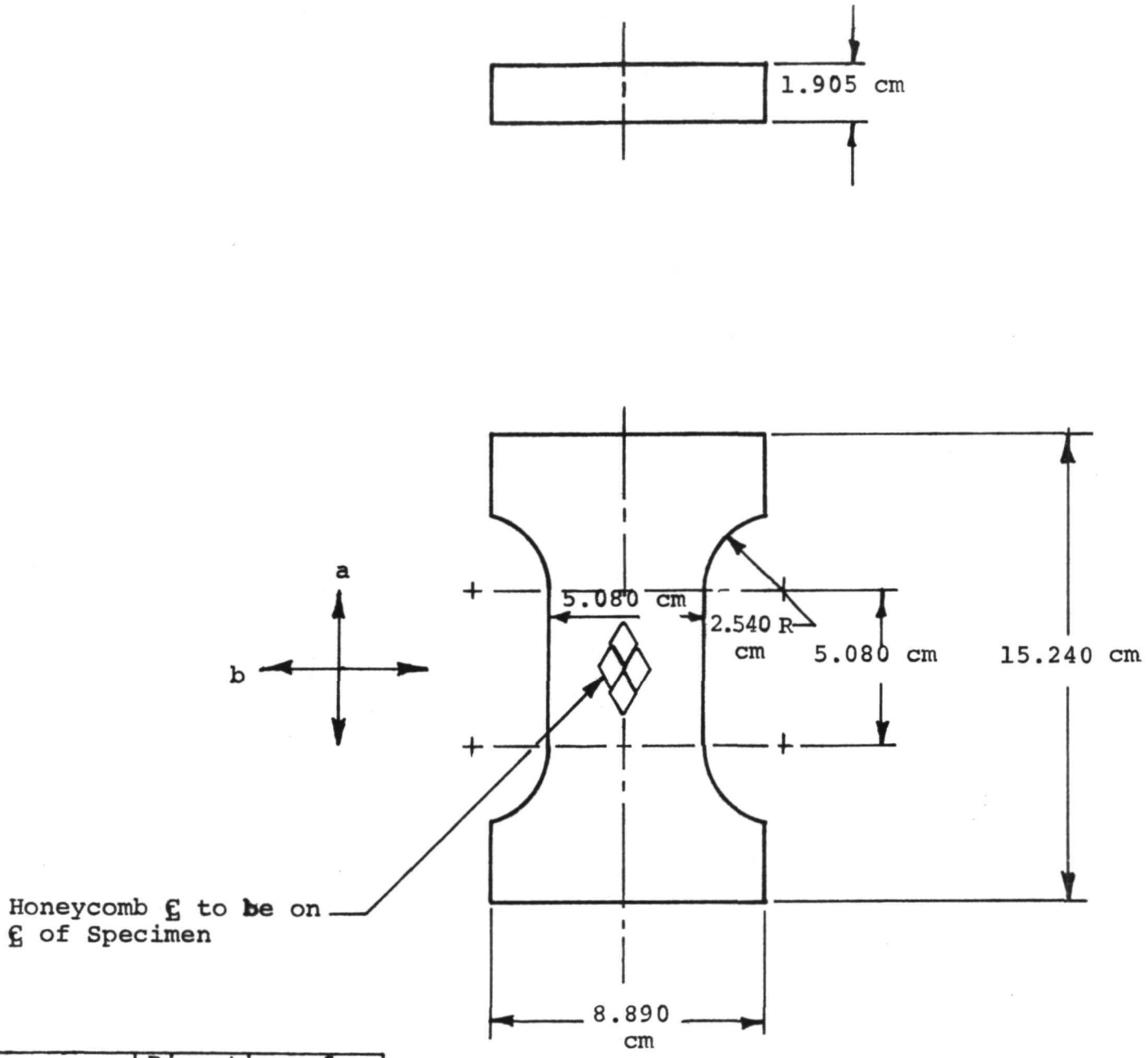

Item	Direction of Honeycomb
1	a
2	b

Figure 15. Configuration of the Compressive Specimen

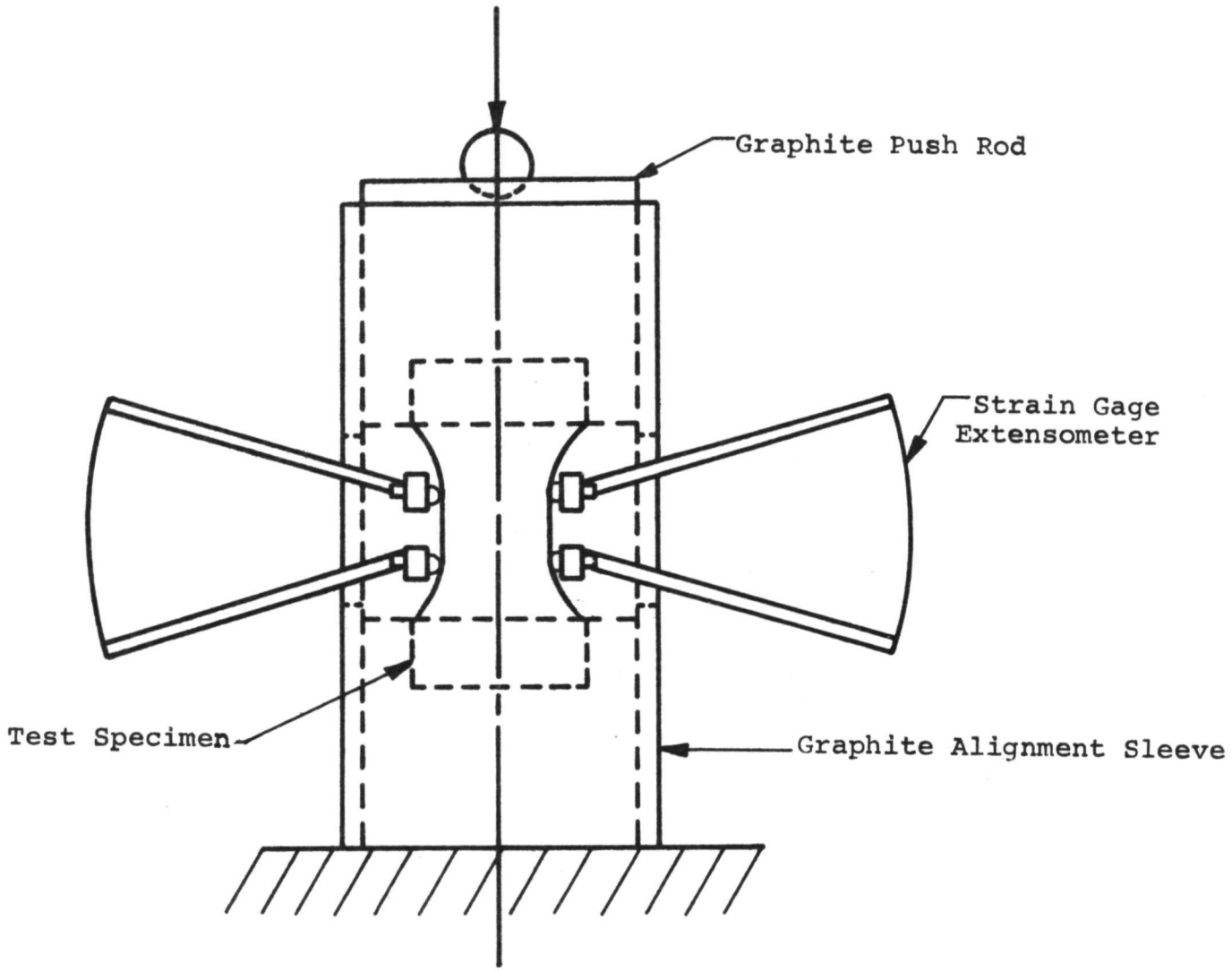

Figure 16. Schematic of Compressive Load Train Assembly

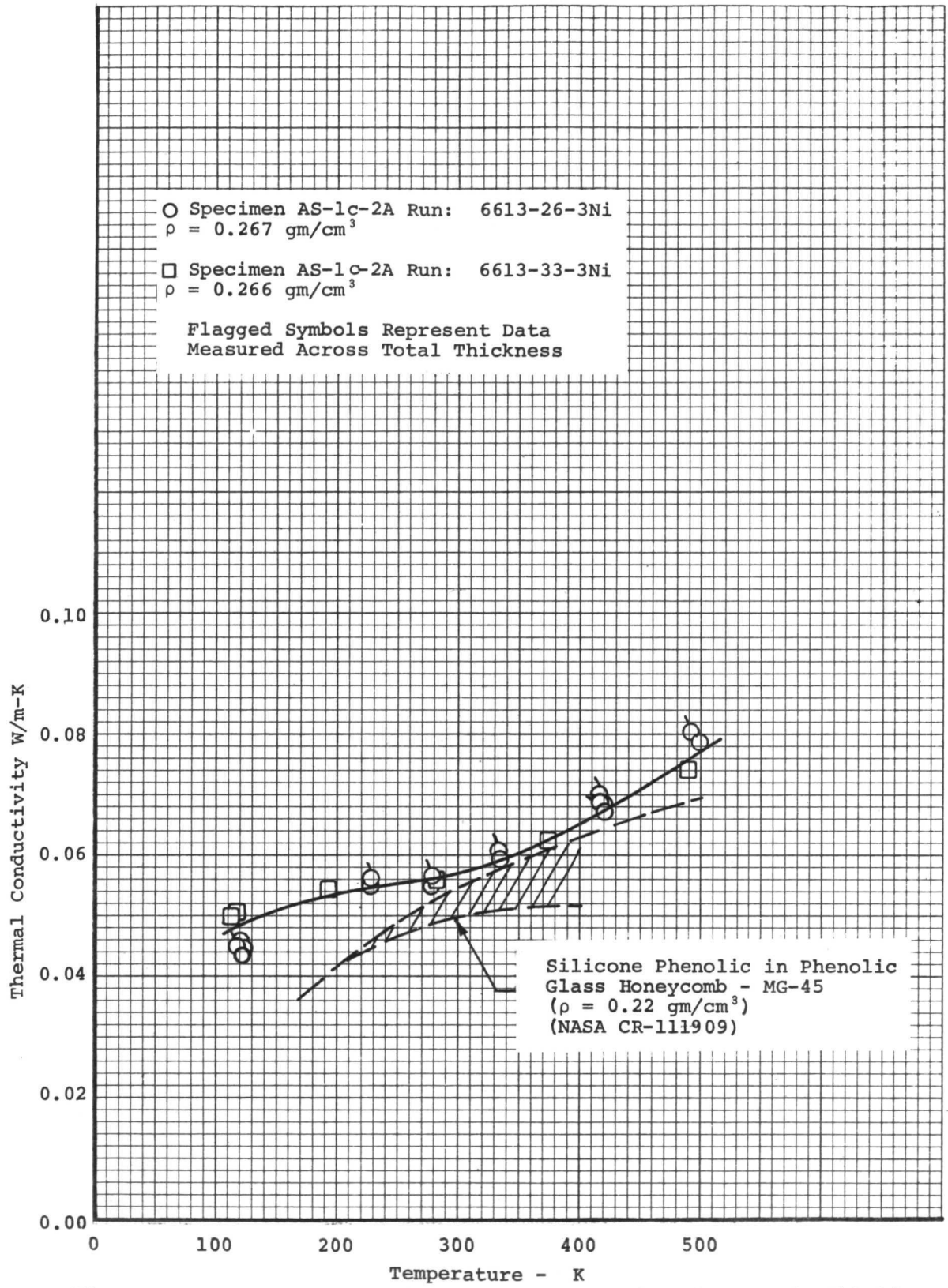

Figure 17. Thermal Conductivity of a Low-Density Elastomeric Ablation Material (Material A) in 1 Atmosphere of Dry Nitrogen

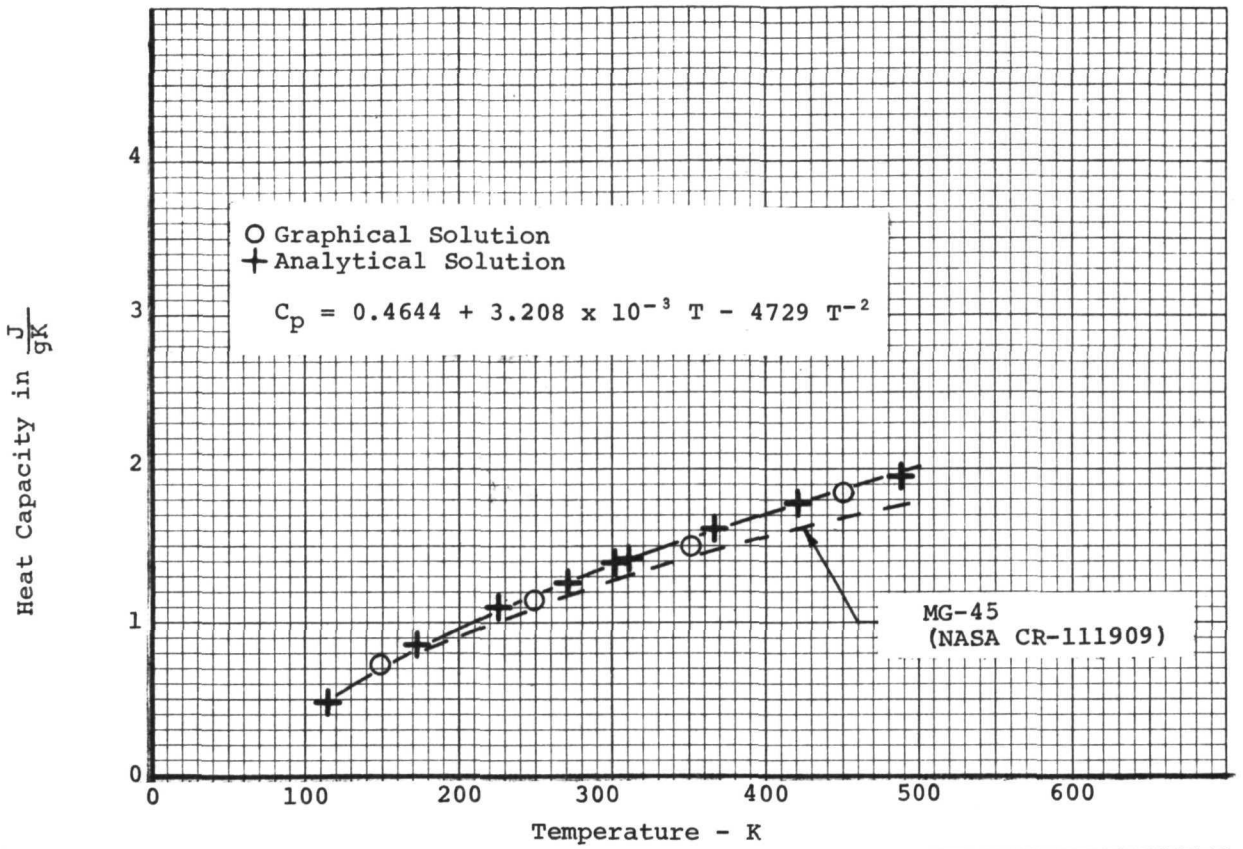

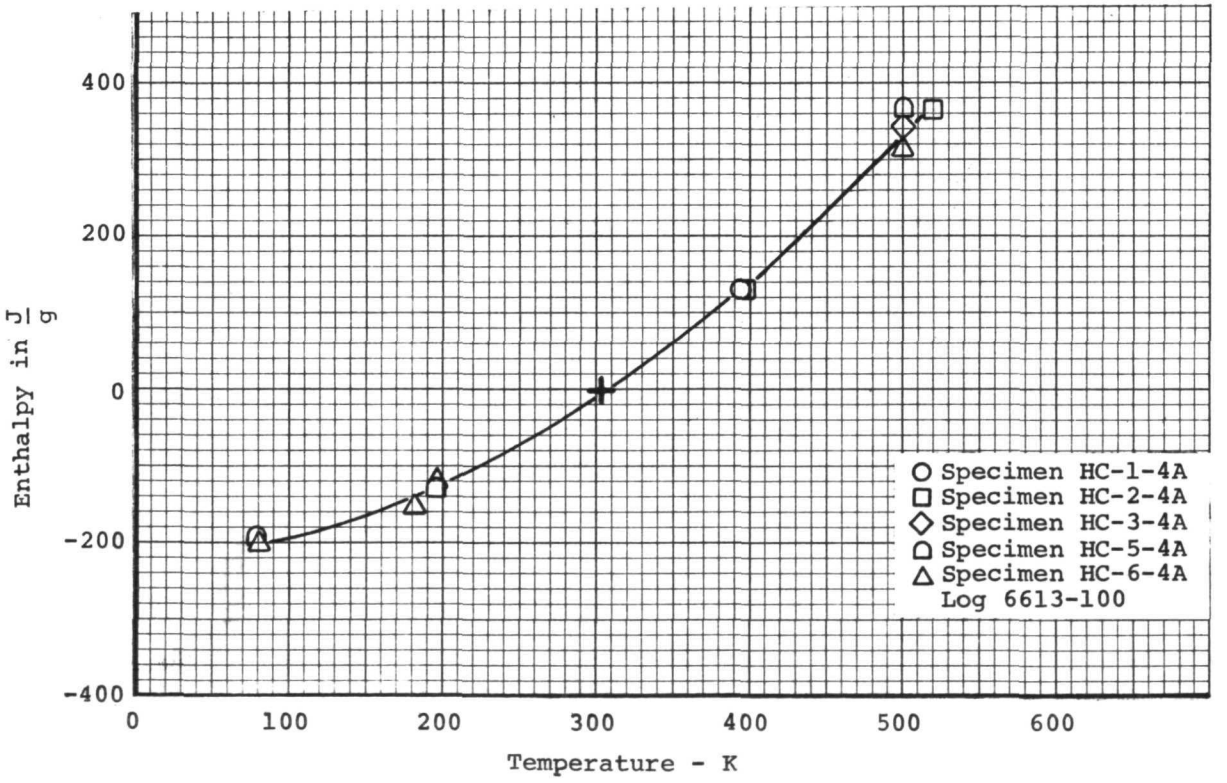

Figure 18. The Enthalpy of a Low-Density Elastomeric Ablation Material (Material A)

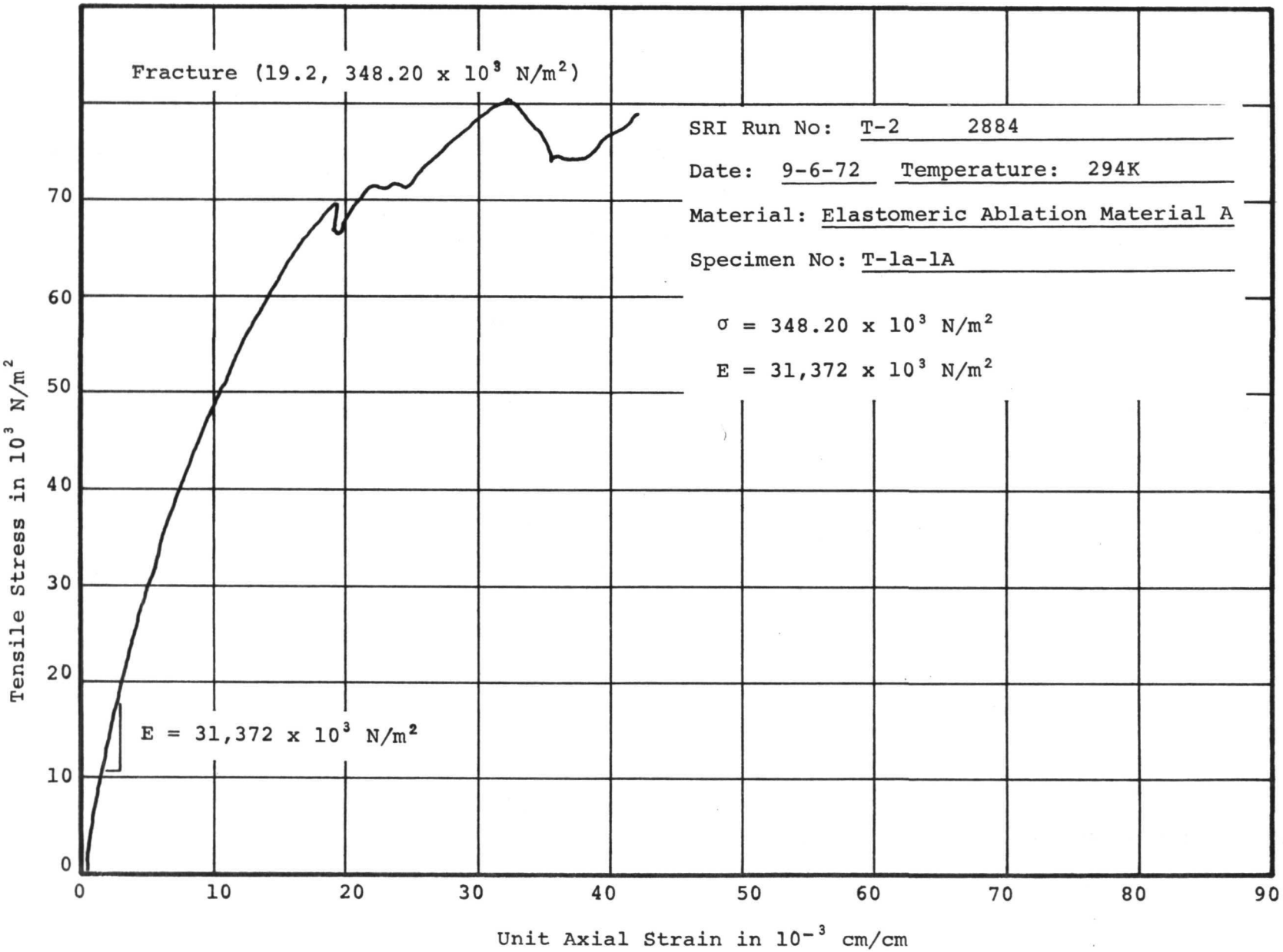

Figure 19. Tensile stress versus axial strain for specimen T-1a-1A at 294K

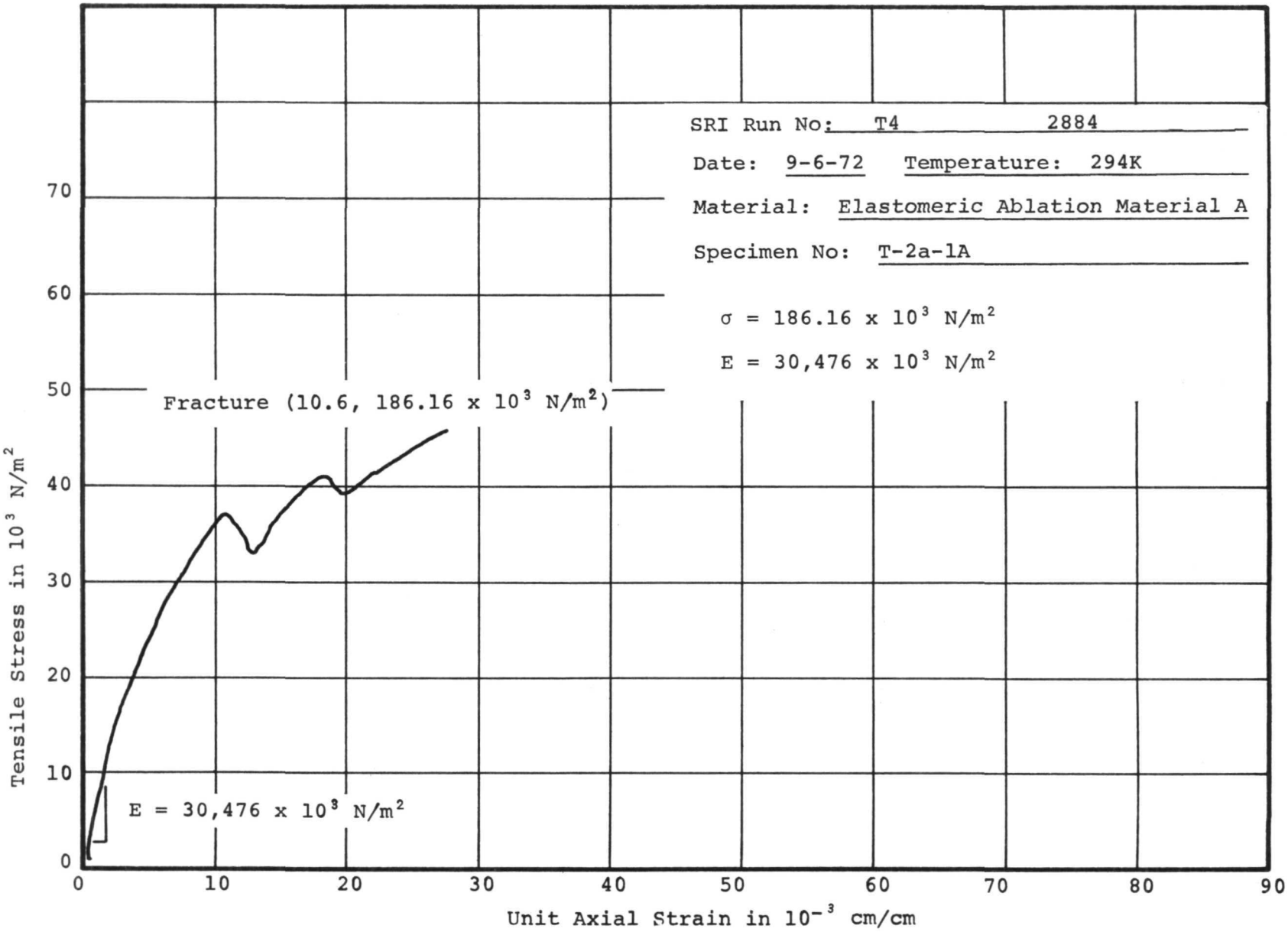

Figure 20. Tensile stress versus axial strain for specimen T-2a-1A at 294K

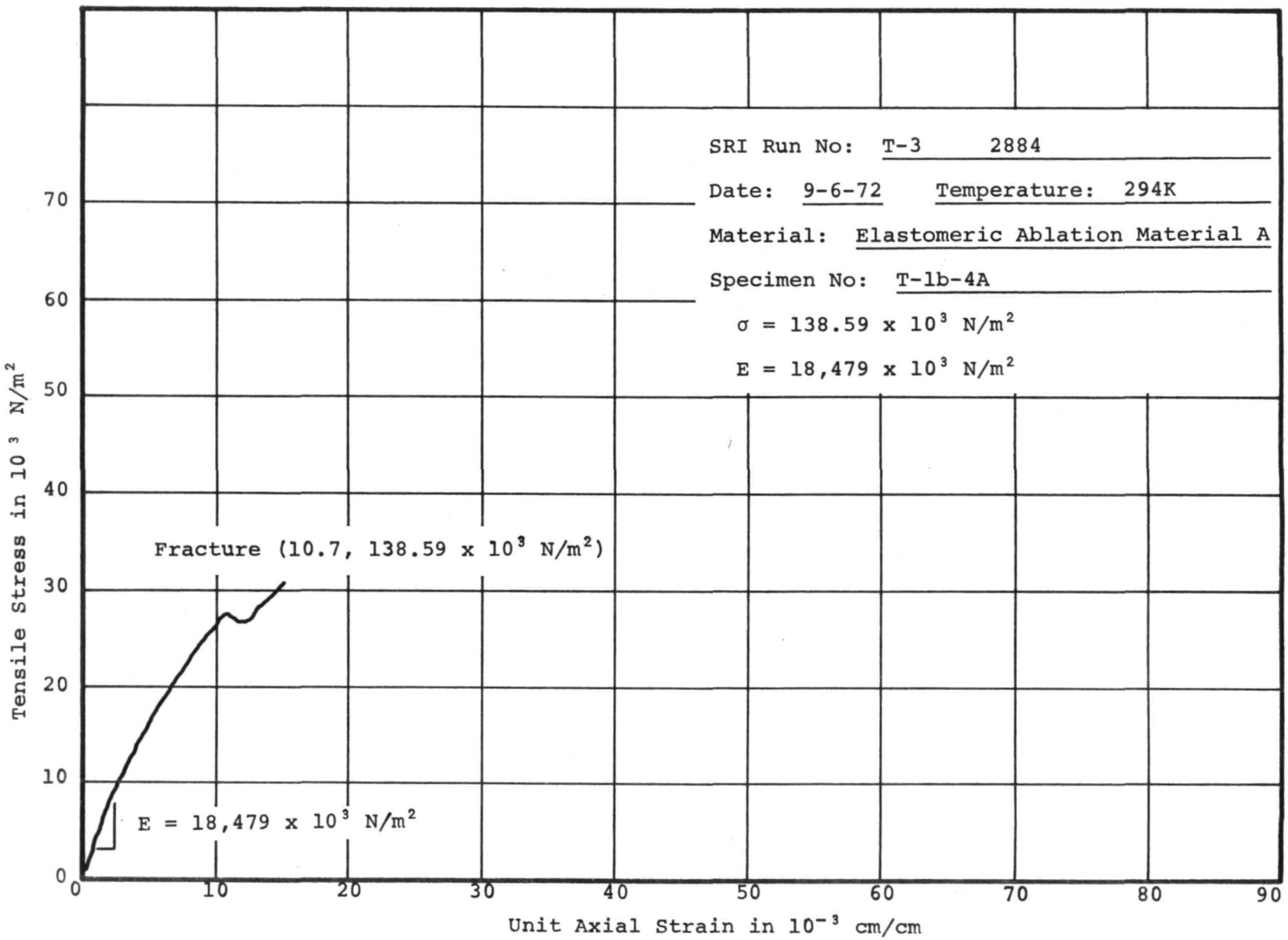

Figure 21. Tensile stress versus axial strain for specimen T-1a-4A at 294K

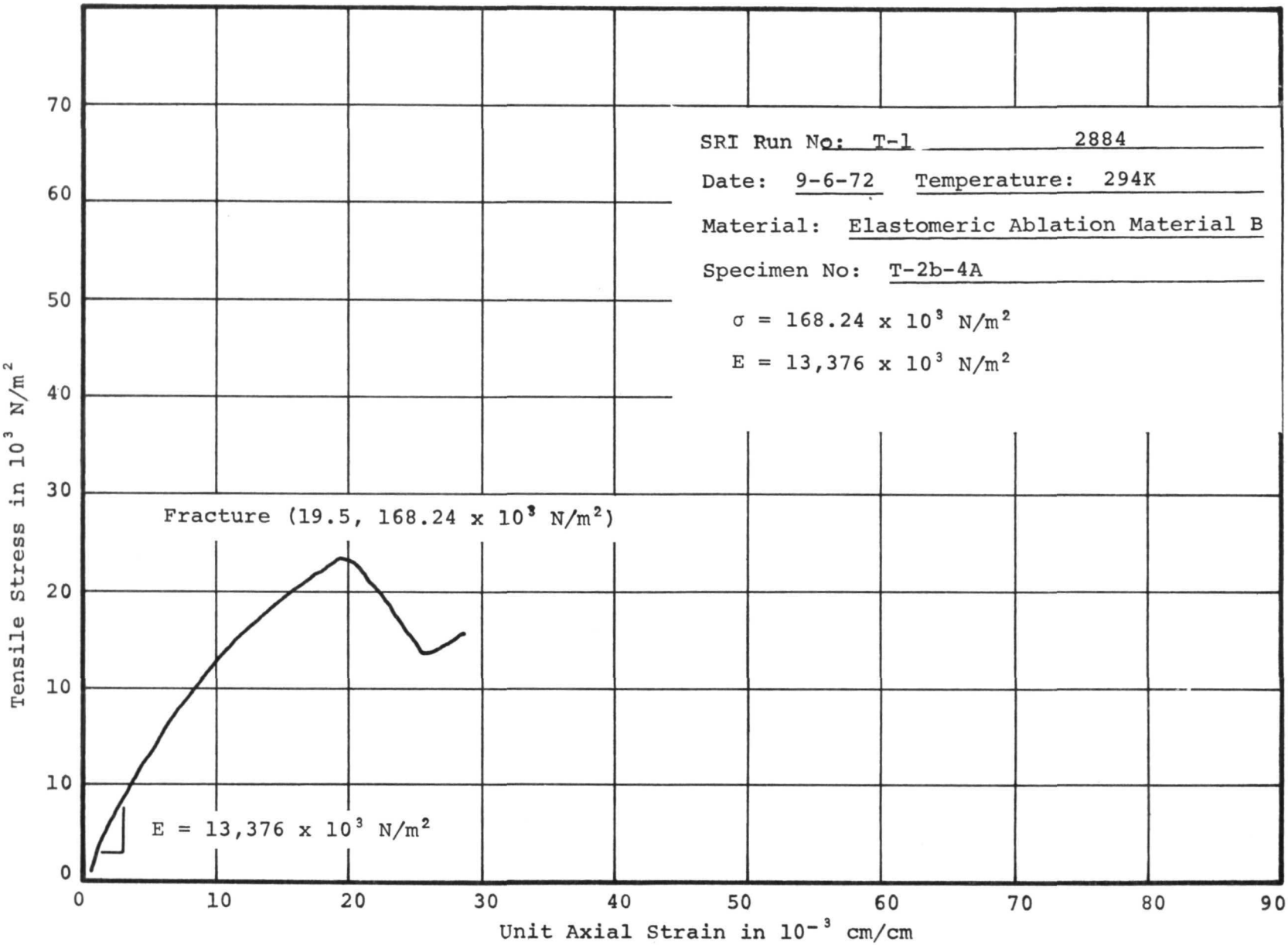

Figure 22. Tensile stress versus axial strain for specimen T-2a-4A at 294K

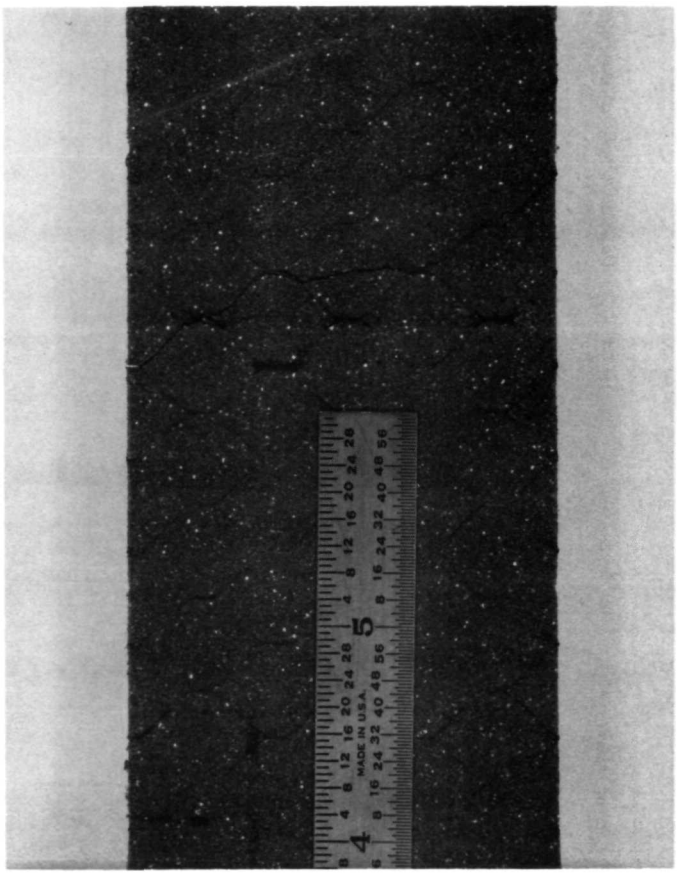

Figure 23. Typical fracture for tensile specimen

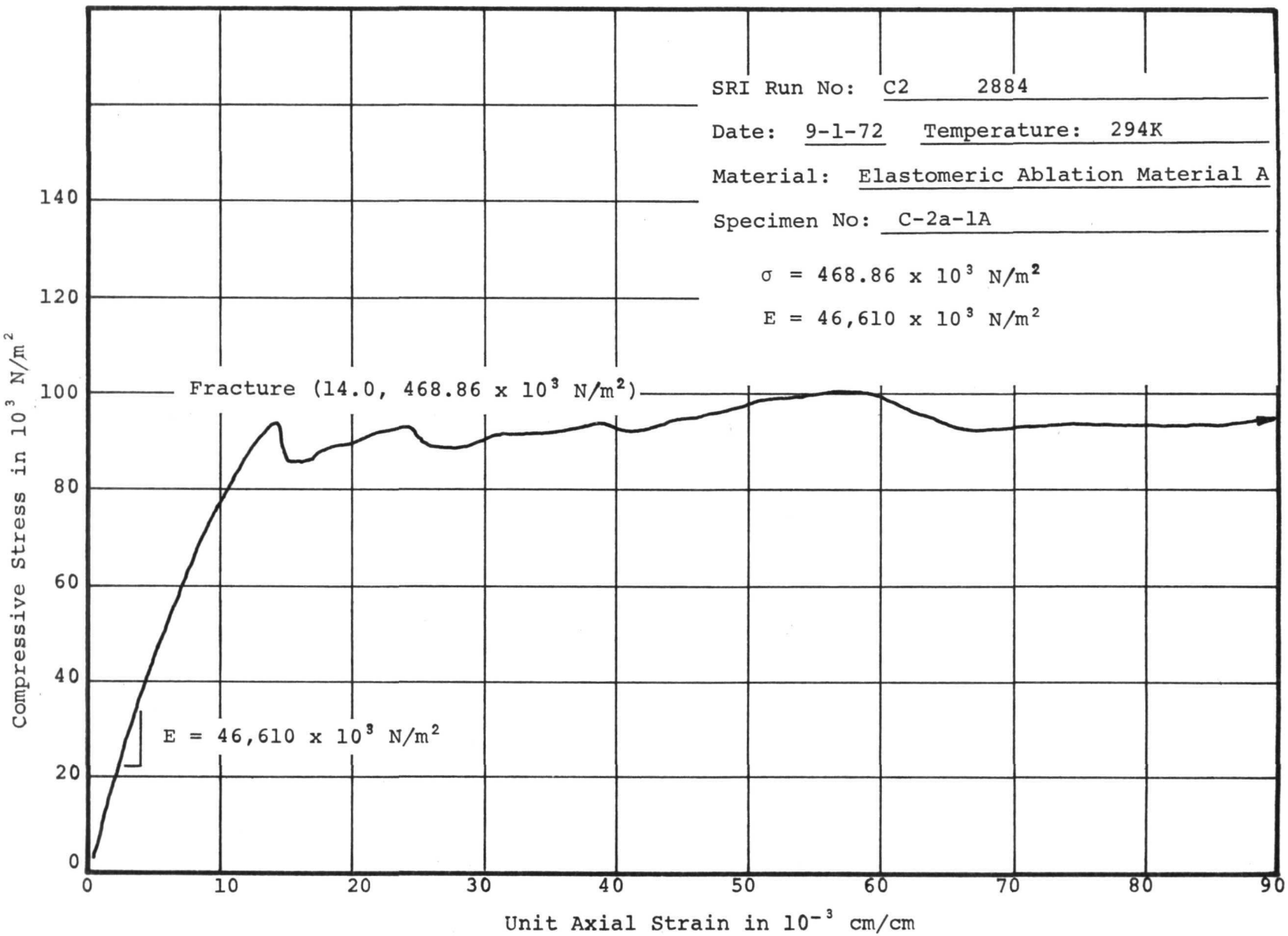

Figure 24. Compressive stress versus axial strain for specimen C-2a-1A at 294K

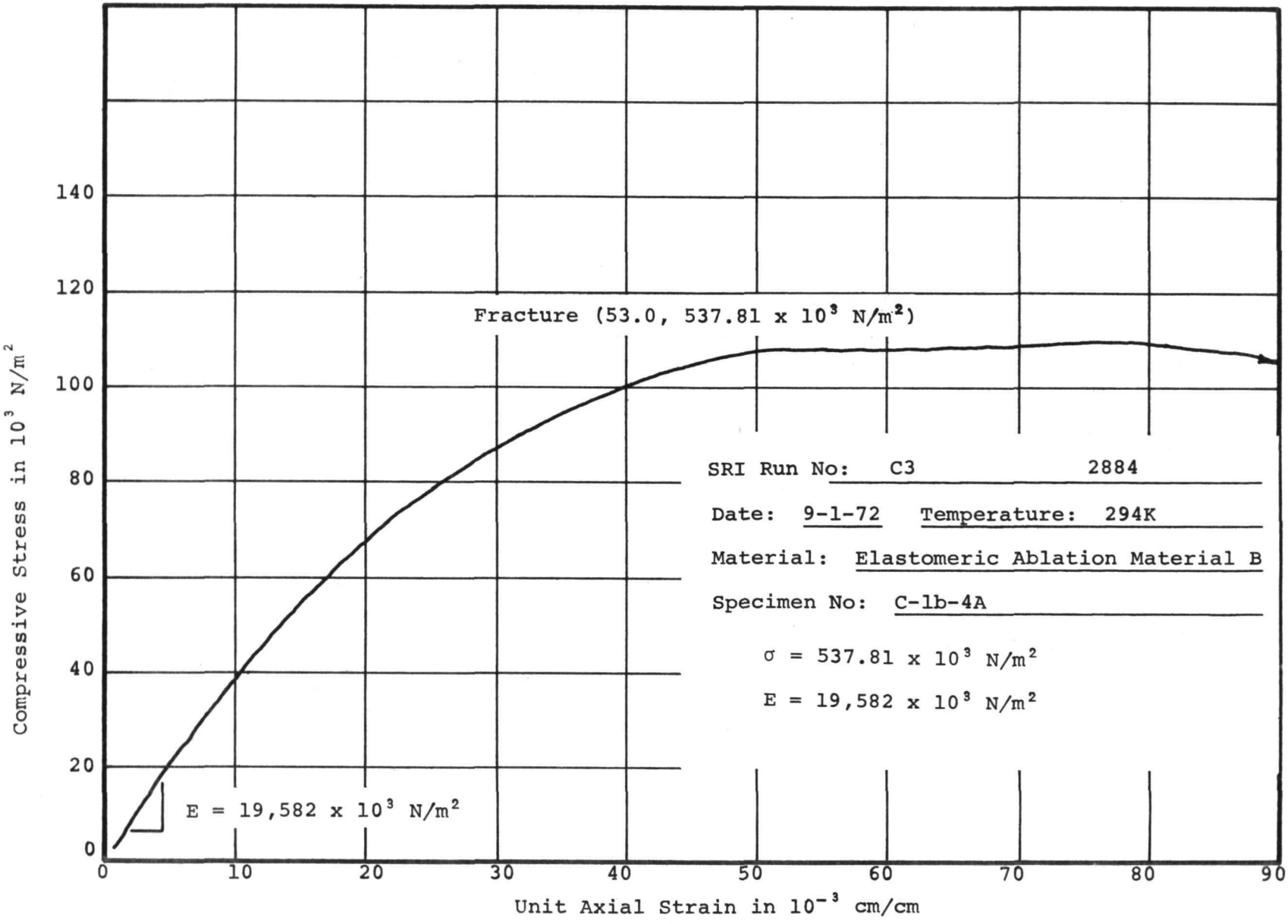

Figure 25. Compressive stress versus axial strain for specimen C-1b-4A at 294K

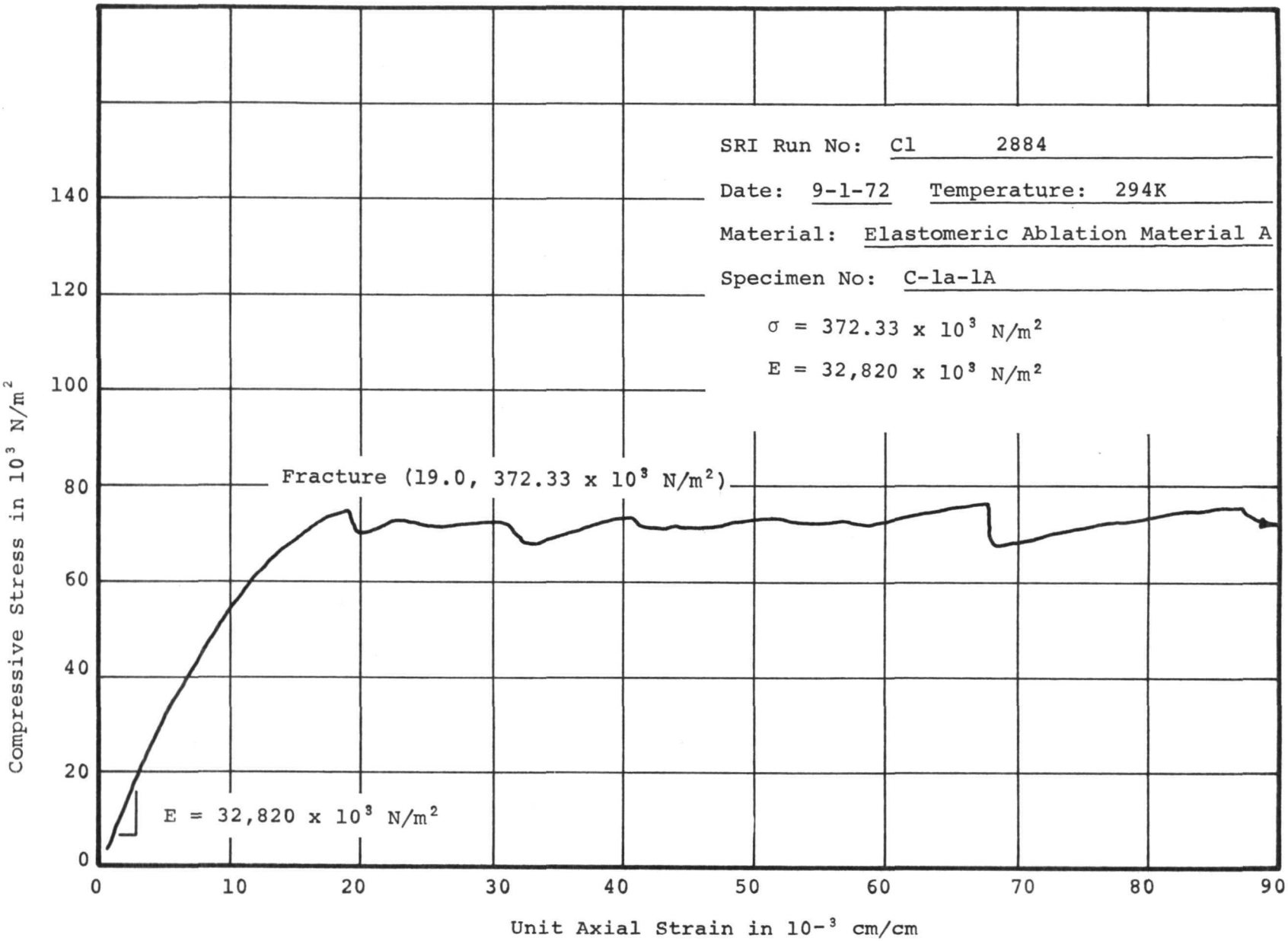

Figure 26. Compressive stress versus axial strain for specimen C-1a-1A at 294K

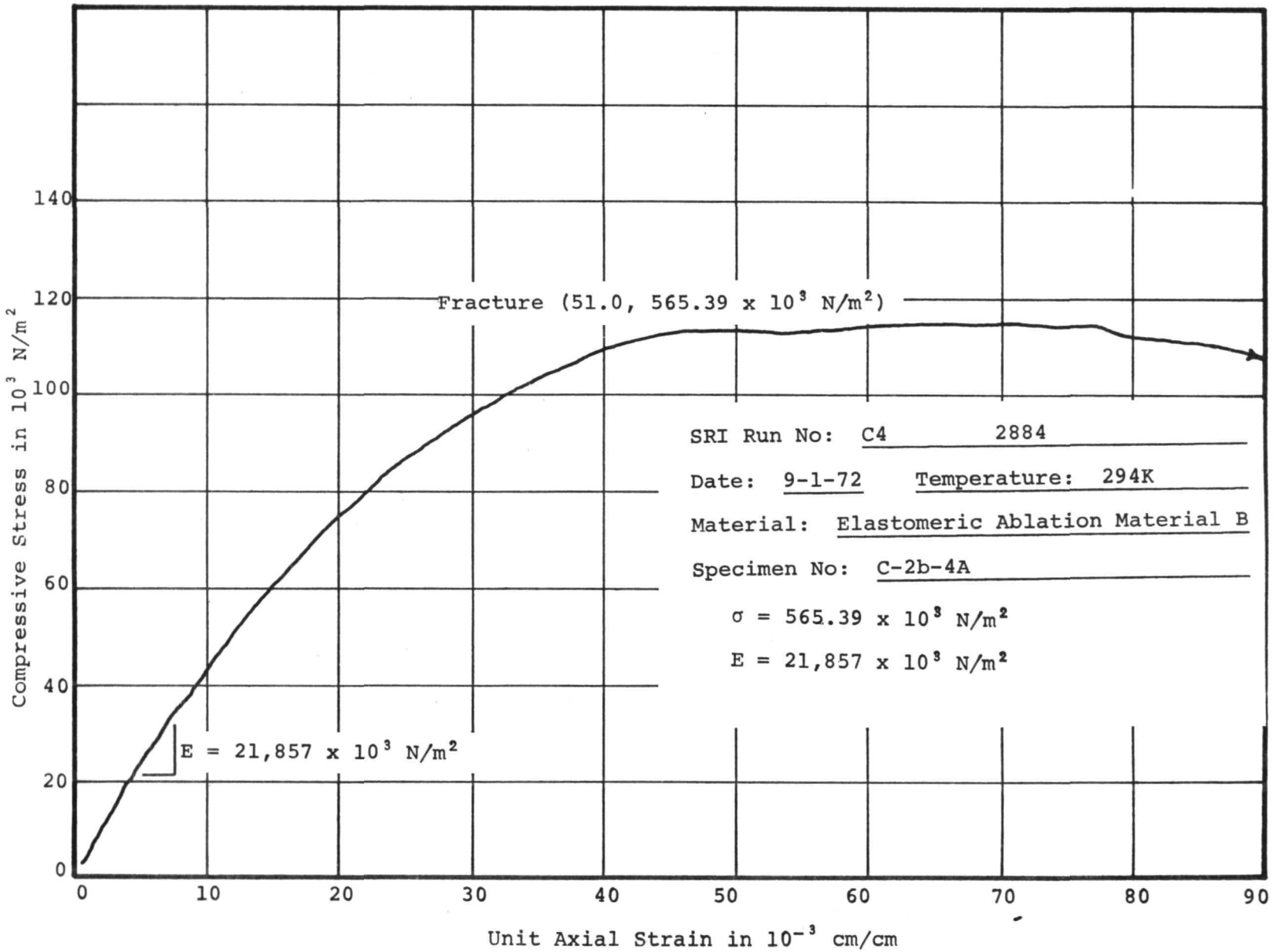

Figure 27. Compressive stress versus axial strain for specimen C-2b-4A at 70°F

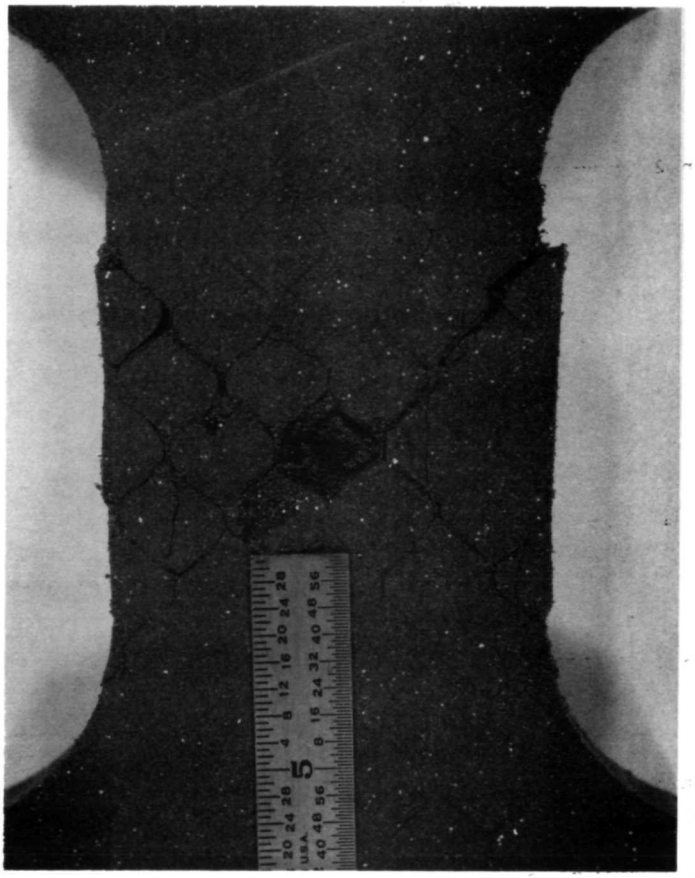

Figure 28. Typical fracture for compressive specimen

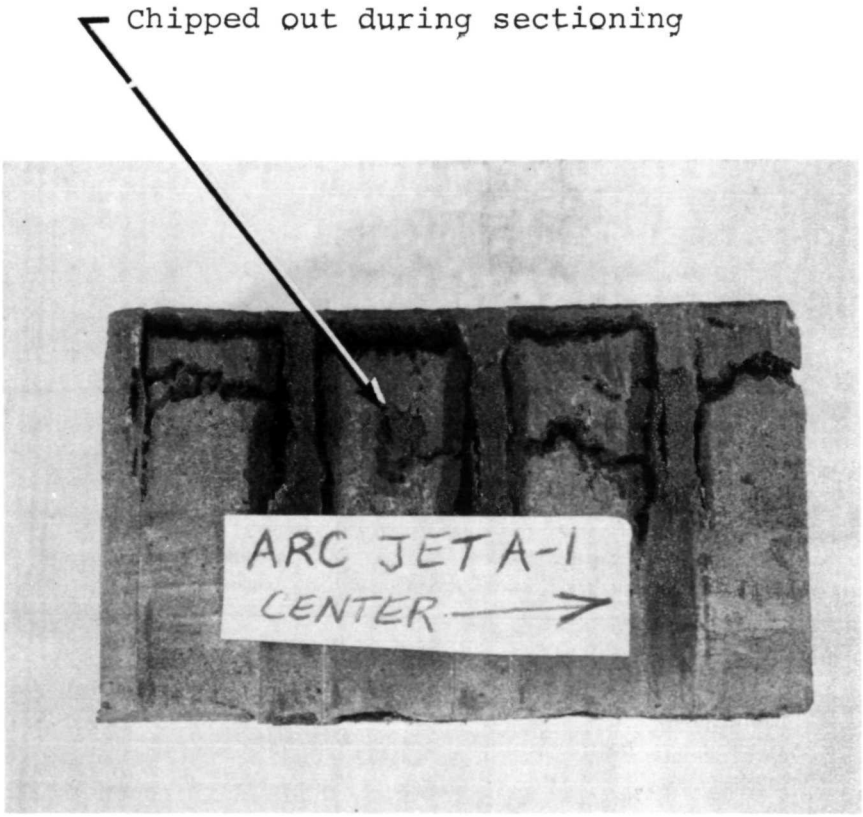

Specimen A, Section 1
(Section A-A from Figure 29)

Figure 30. Crossection of arc jet char illustrating the structure of the composite

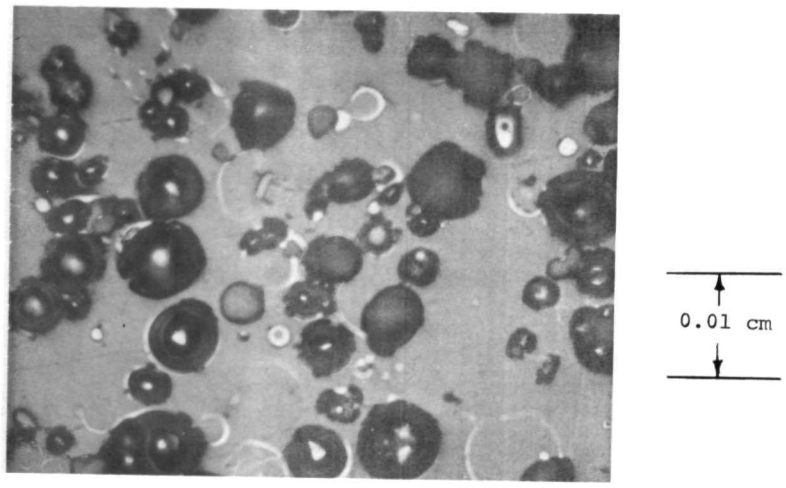

1644 K Rapid Heating by Immersion in Preheated Furnace

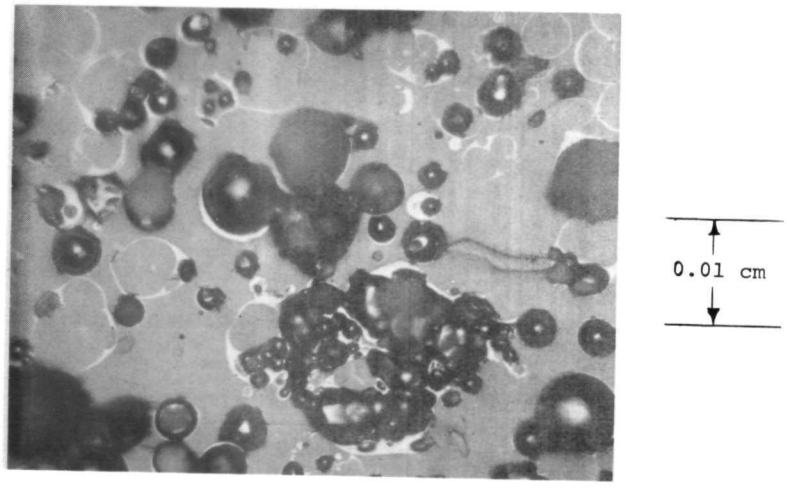

1644 K Slow Heating

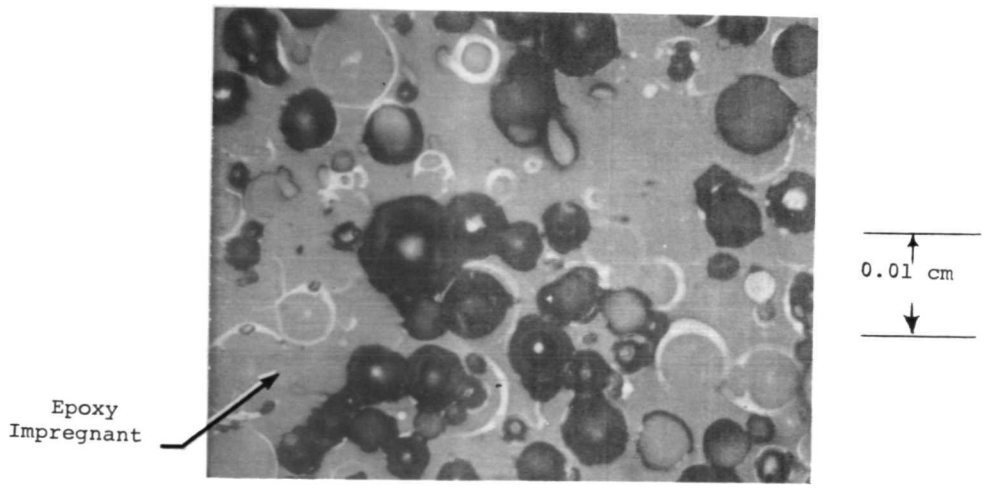

1373 K Slow Heating

Figure 32. Photomicrographs of chars prepared in furnace

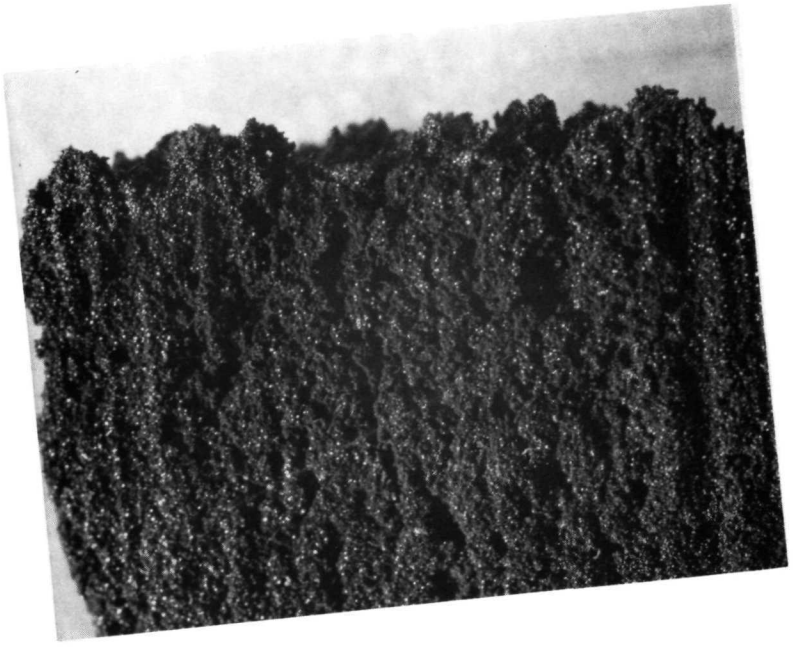

Arc Jet Char
(Zone 2)

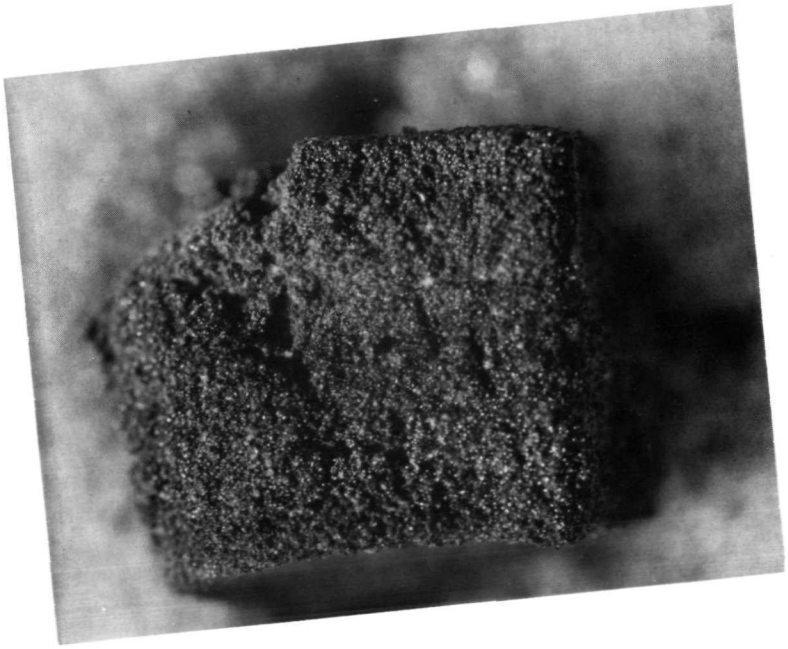

Furnace Char
(1380 K)

Figure 34. Photographs of the structure at 10X of a R1D furnace char and the arc jet char

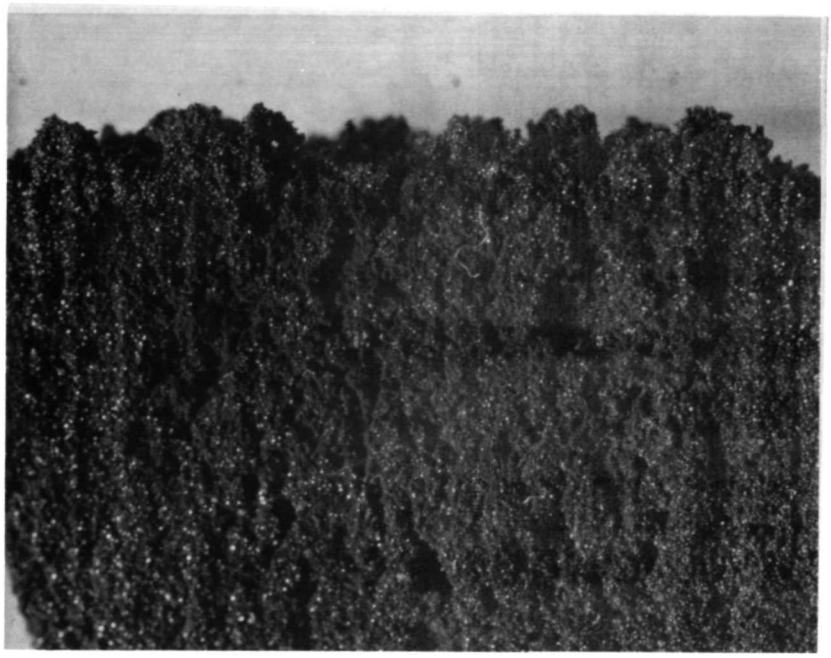

Arc Jet Char
(Zone 2)

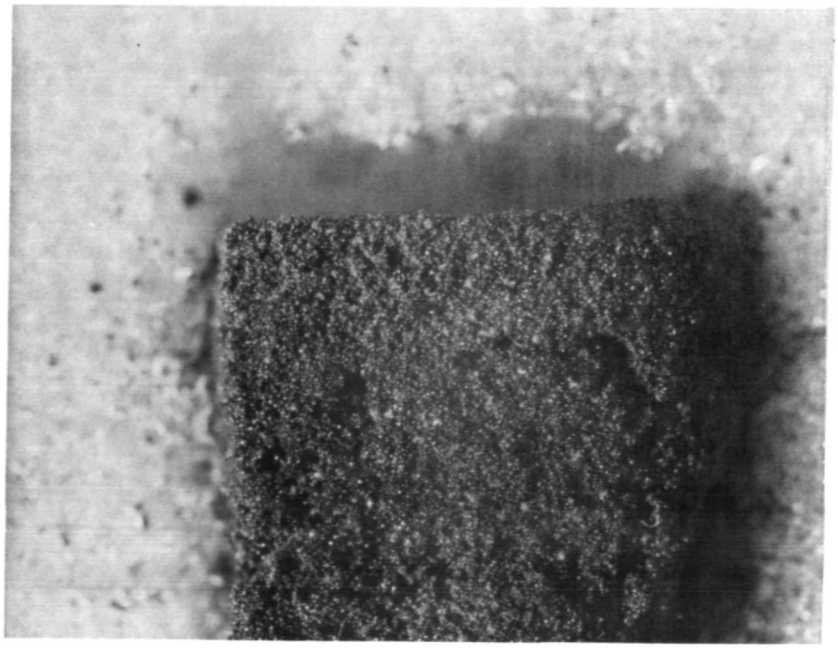

Furnace Char
(1380 K)

Figure 35. Photographs of the structure at 10X of a S1D furnace char and the arc jet char

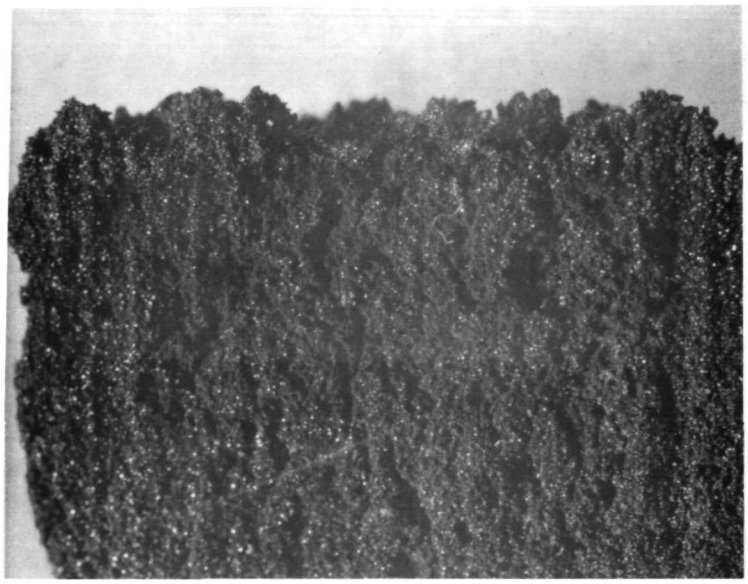

Arc Jet Char
(Zone 2)

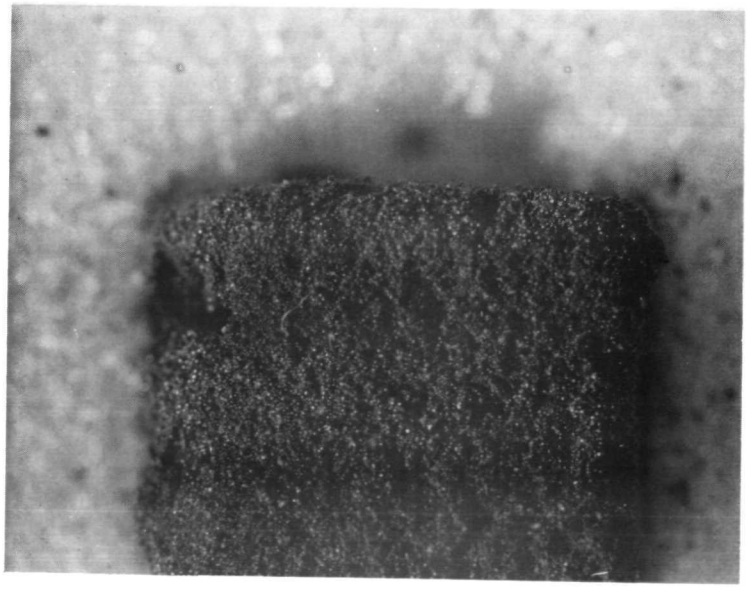

Furnace Char
(1380 K)

Figure 36. Photographs of the structure at 10X of a R2D furnace char and the arc jet char

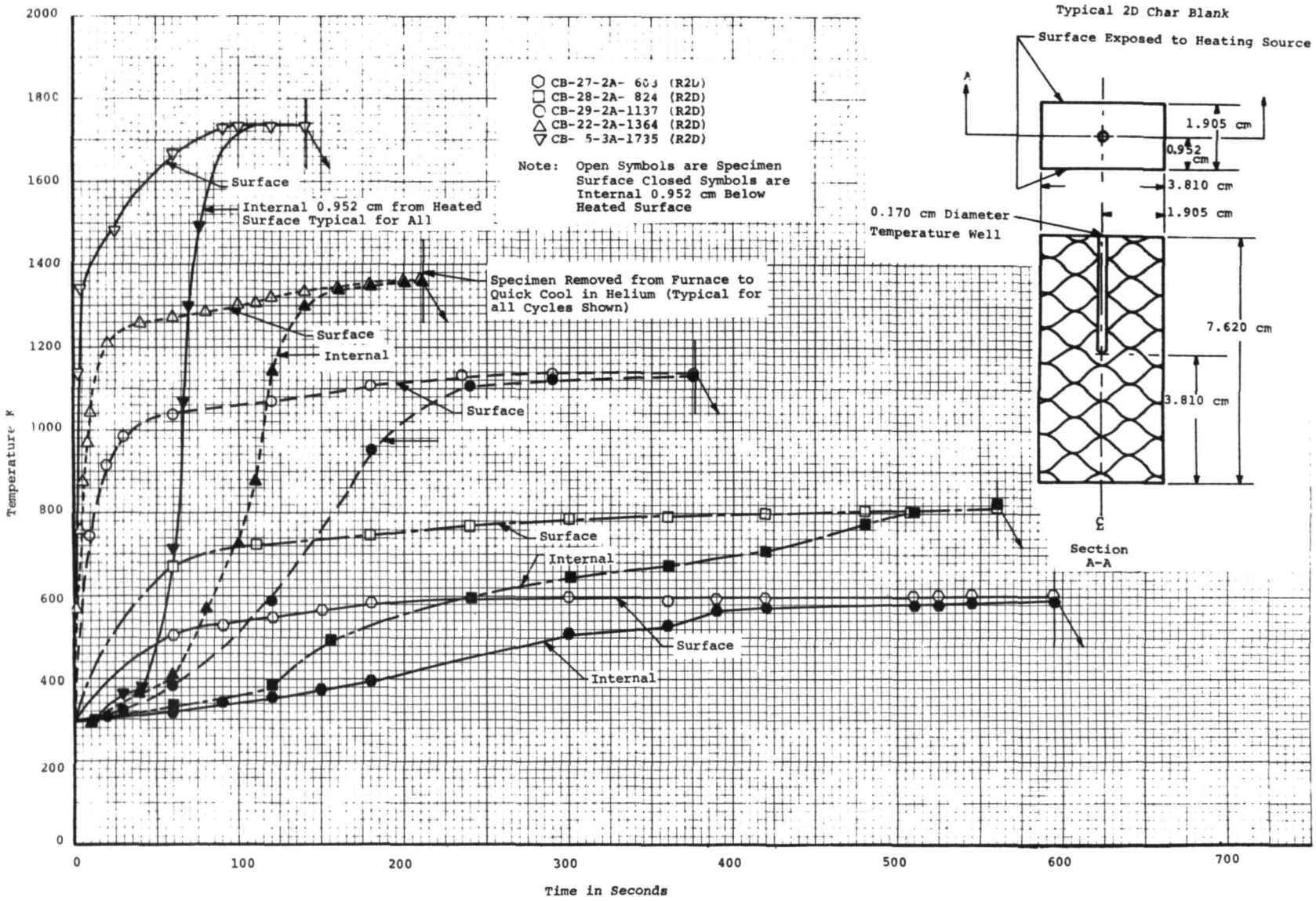

Figure 37. Typical Temperature Versus Time Curves for Furnace Char Prepared by Rapid 2D Heating

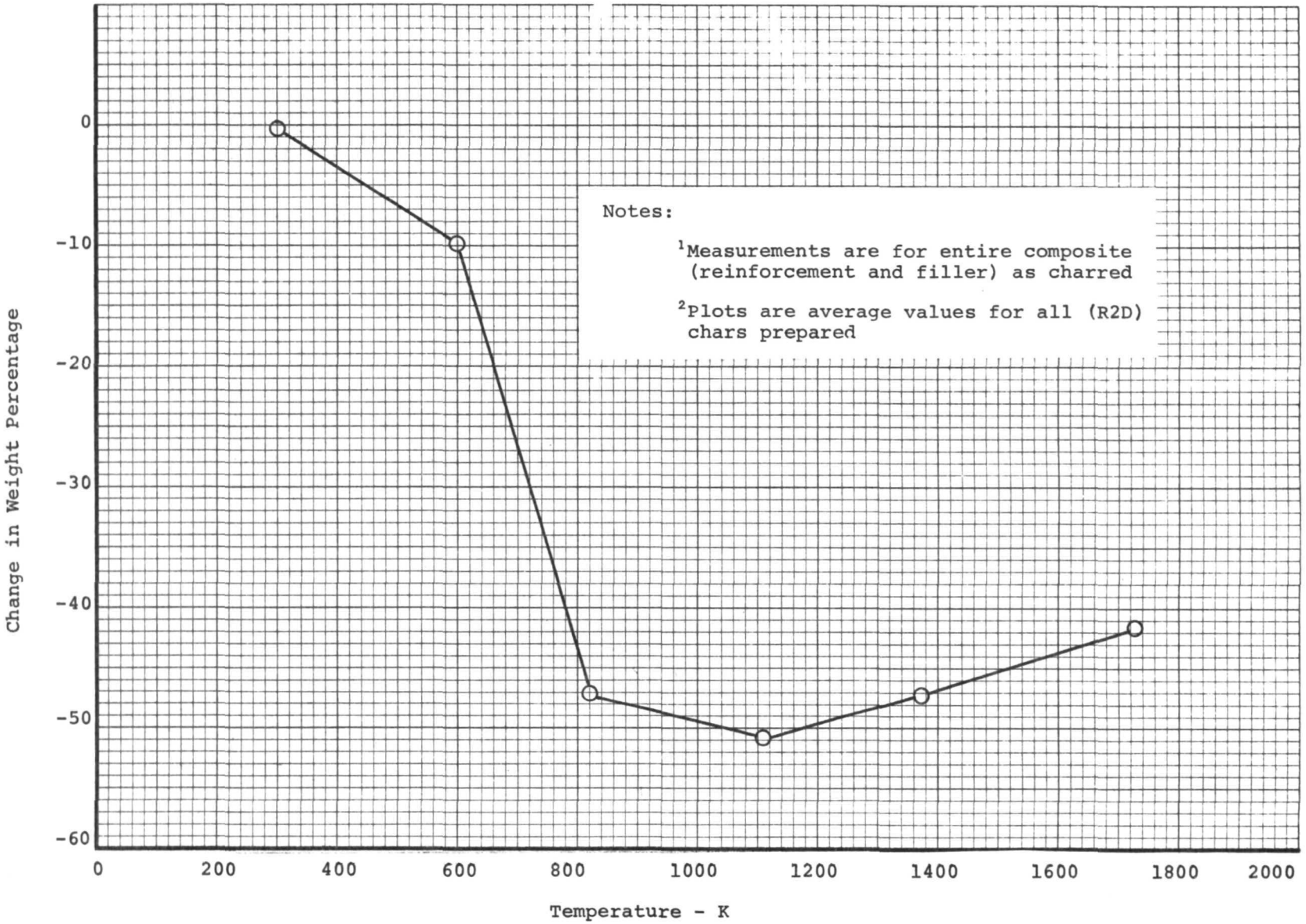

Figure 38. Effect of Char Temperature or Percentage Weight Loss for (R2D) Furnace Char Prepared from Material A

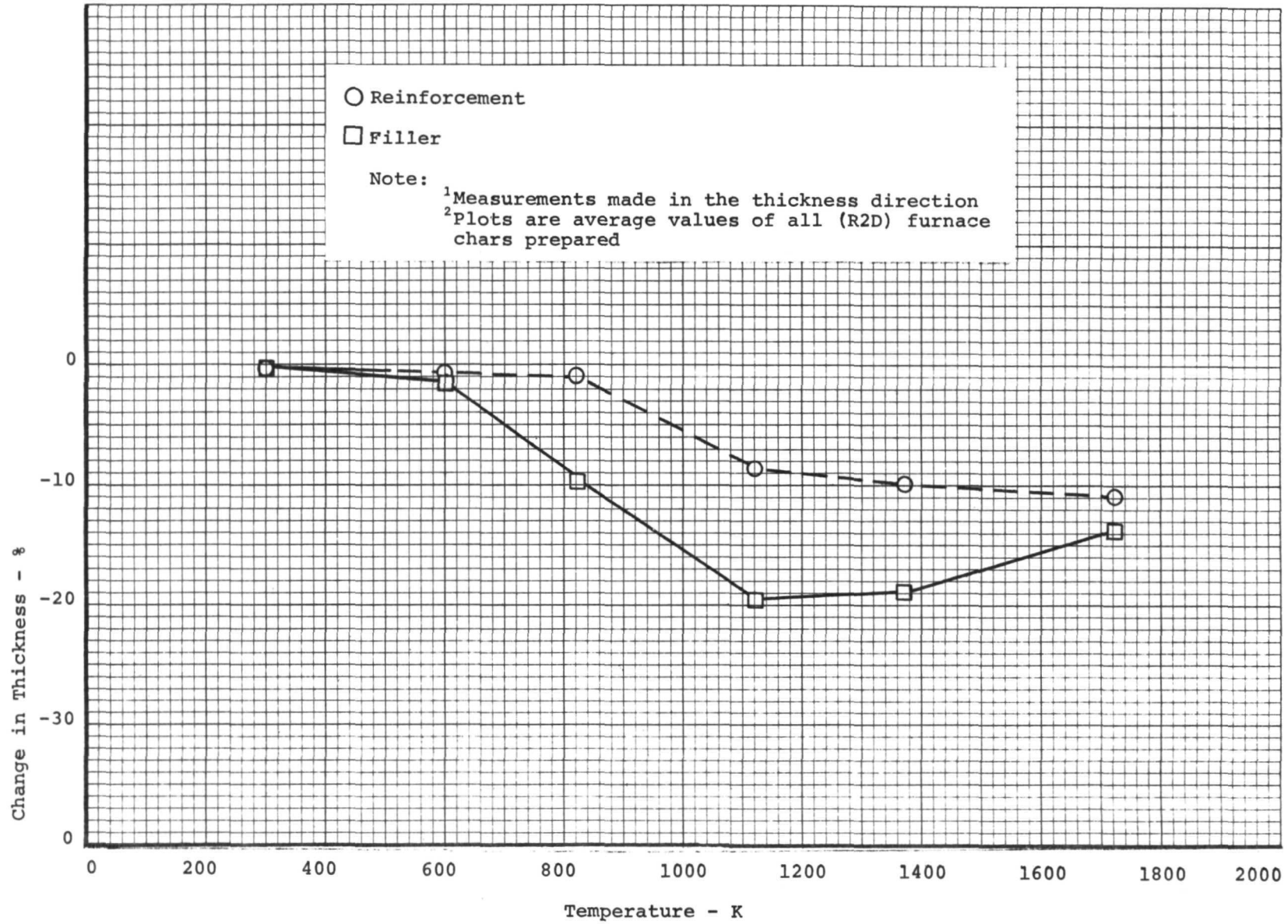

Figure 39. Effect of Char Temperature on Shrinkage for (R2D) Furnace Char Prepared from Material A

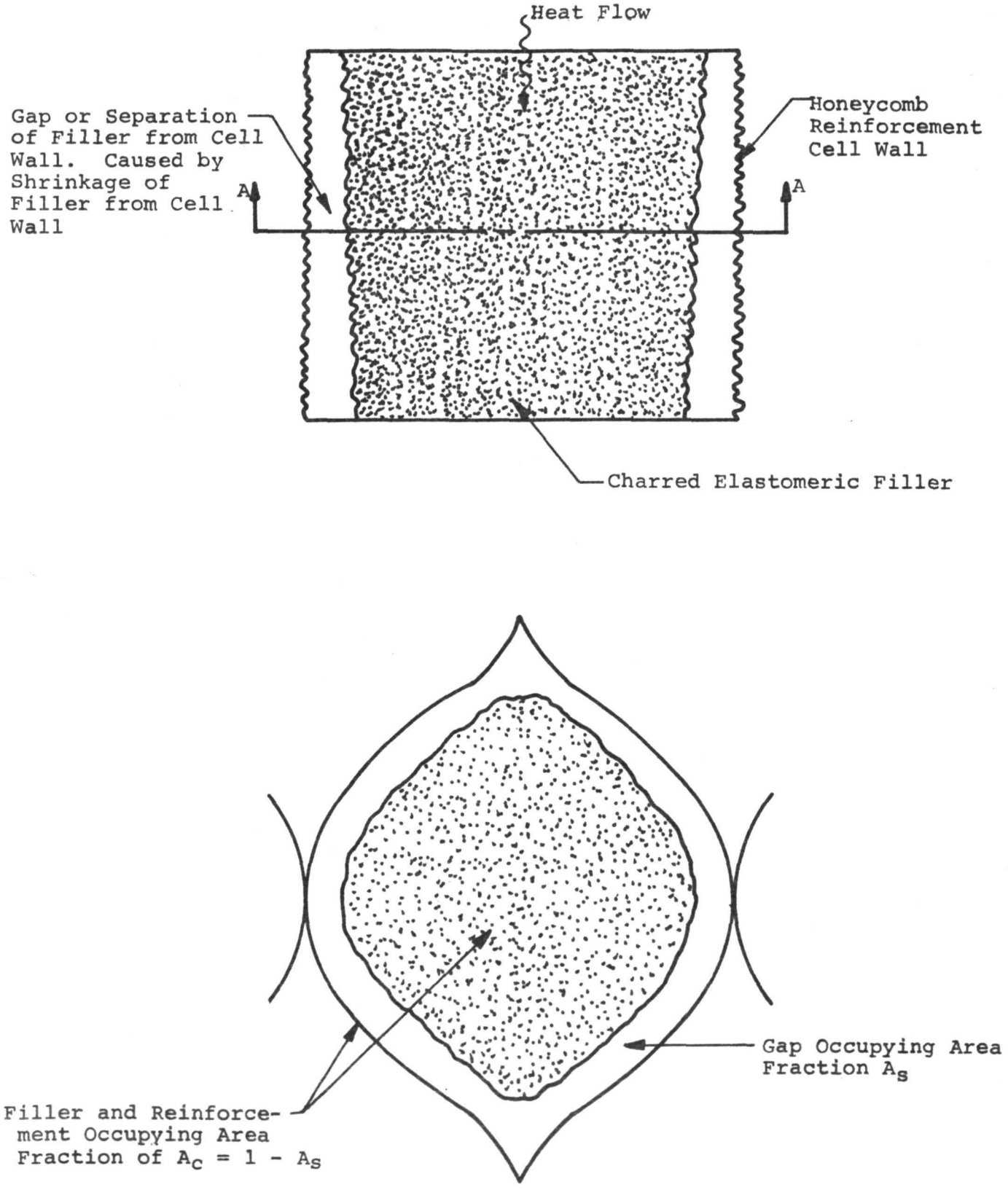

Figure 40. Model of Typical Furnace Char Cell

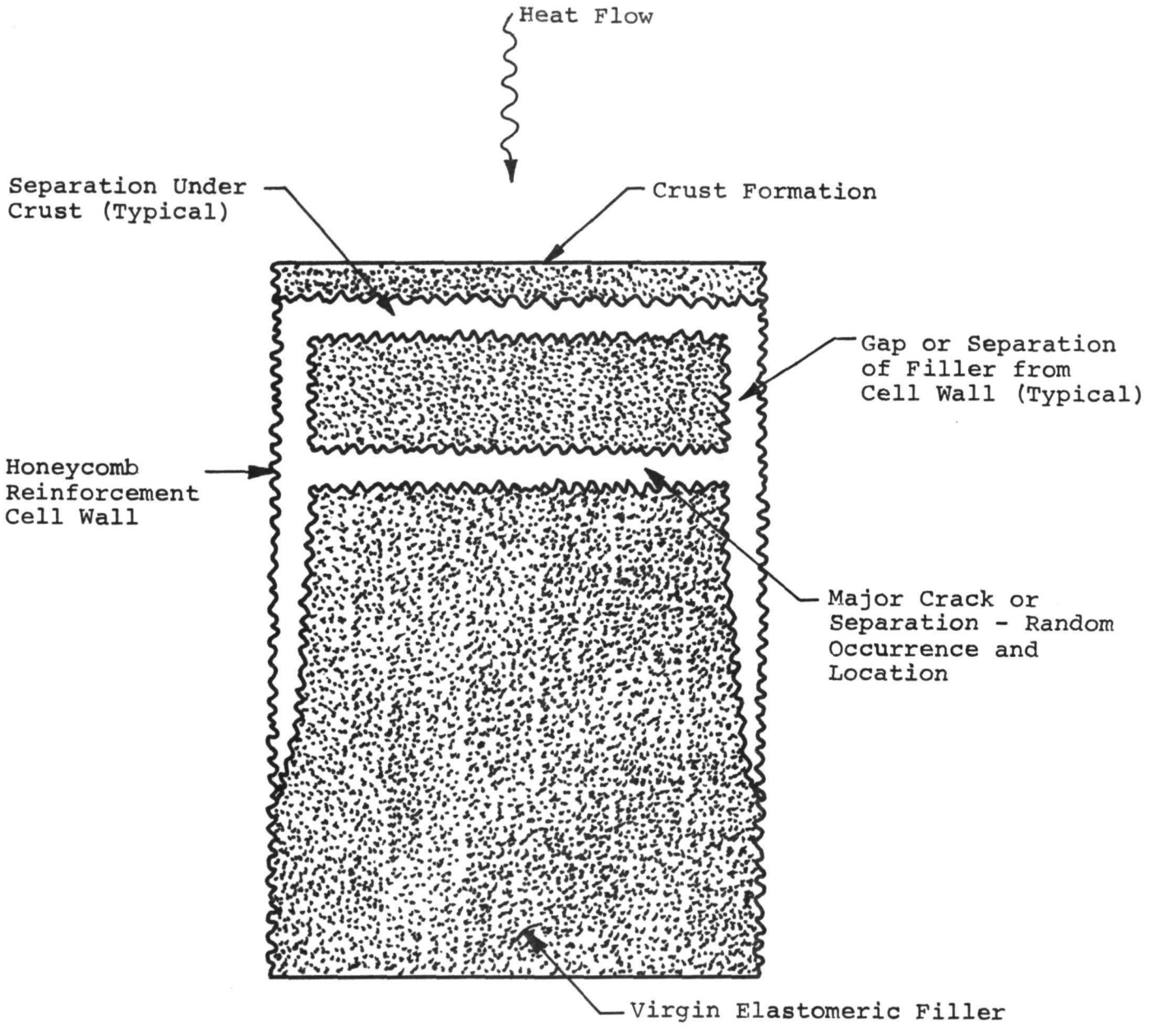

Figure 41. Model of Typical Arc Jet or Flight Char Cell

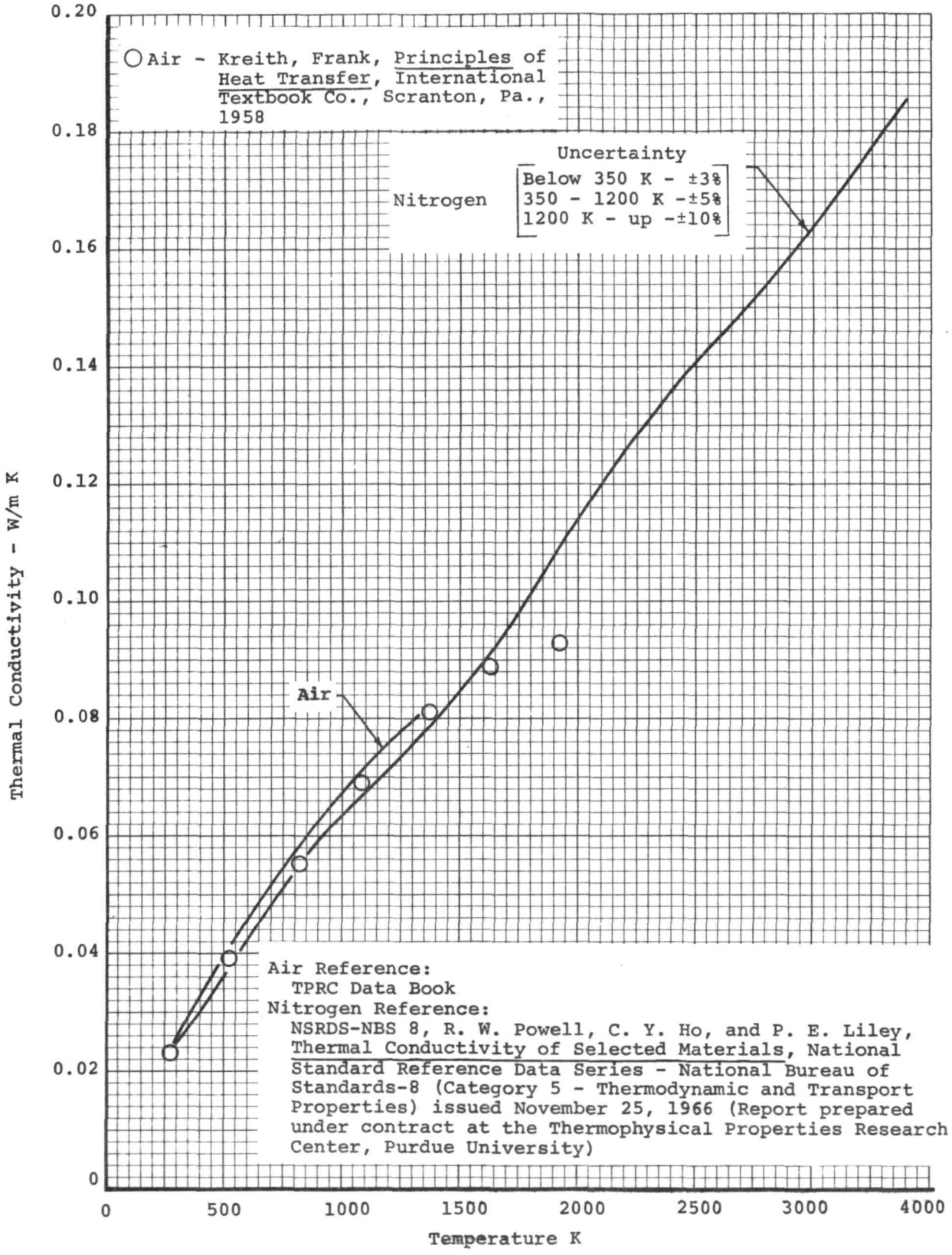

Figure 42. The thermal conductivities of gaseous nitrogen at pressure of 1 atmosphere

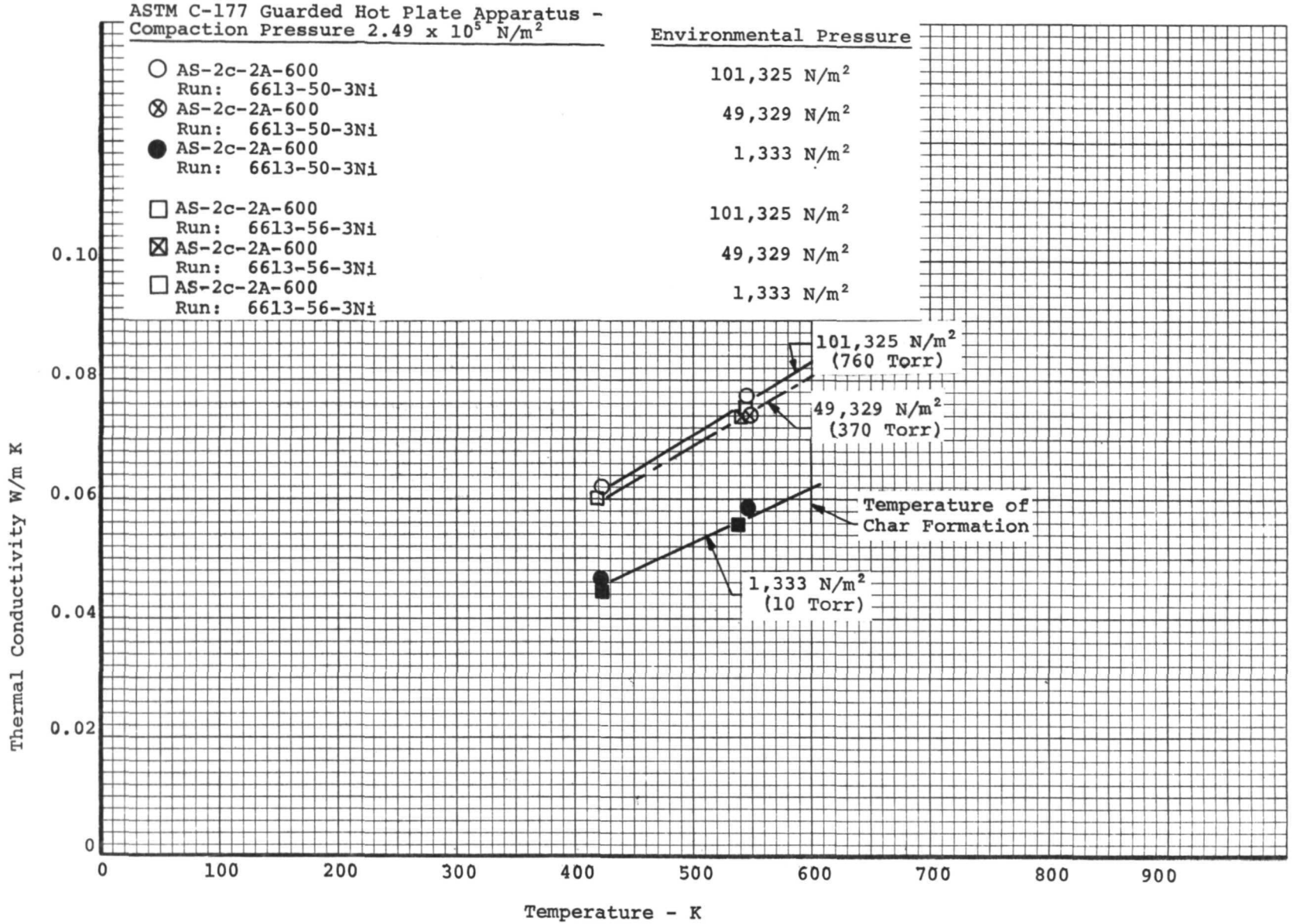

Figure 43. Effective Thermal Conductivity of the Furnace Char of Material A Formed at 600 K

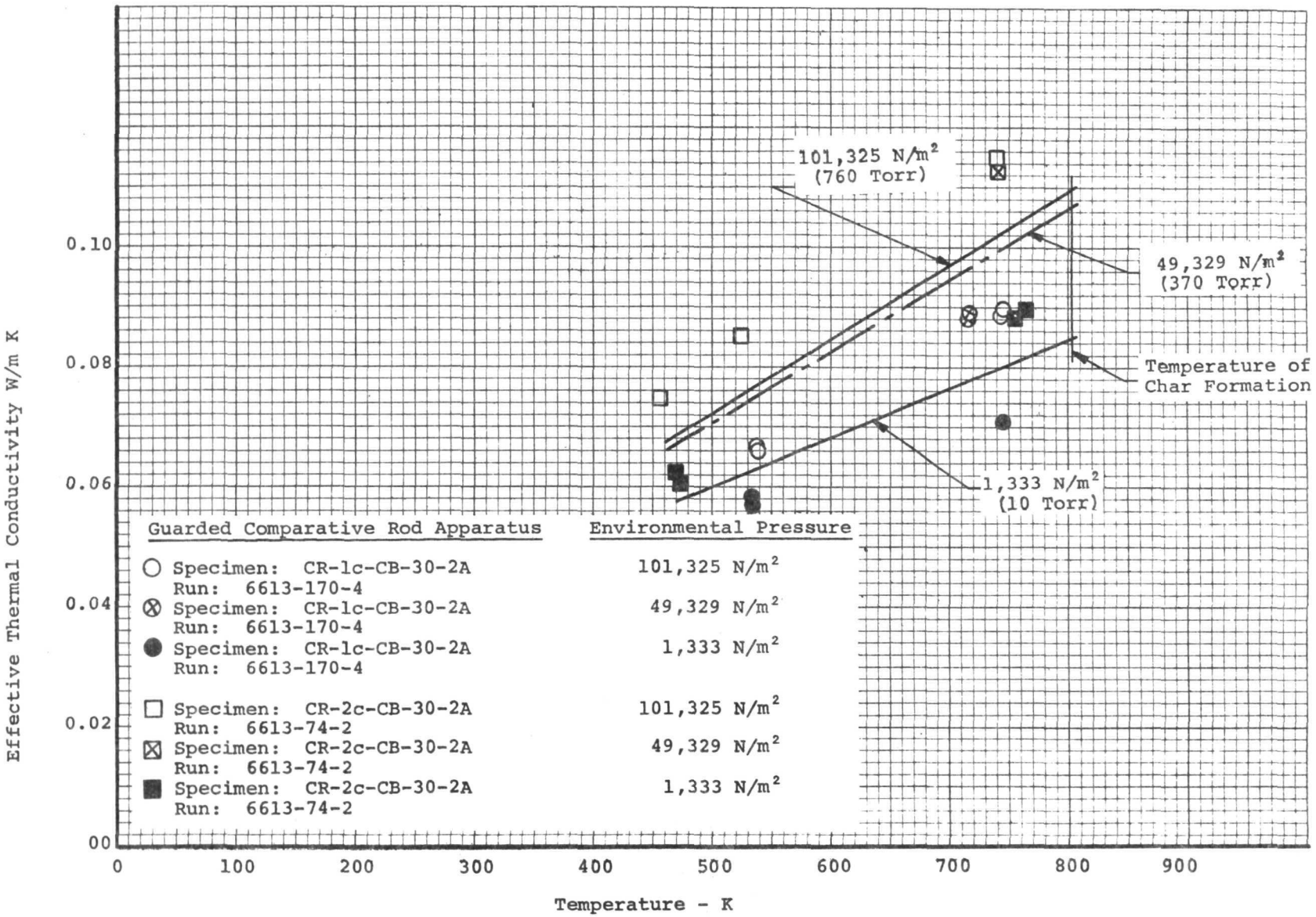

Figure 44. Effective Thermal Conductivity of Furnace Char of Material A Formed at 802K

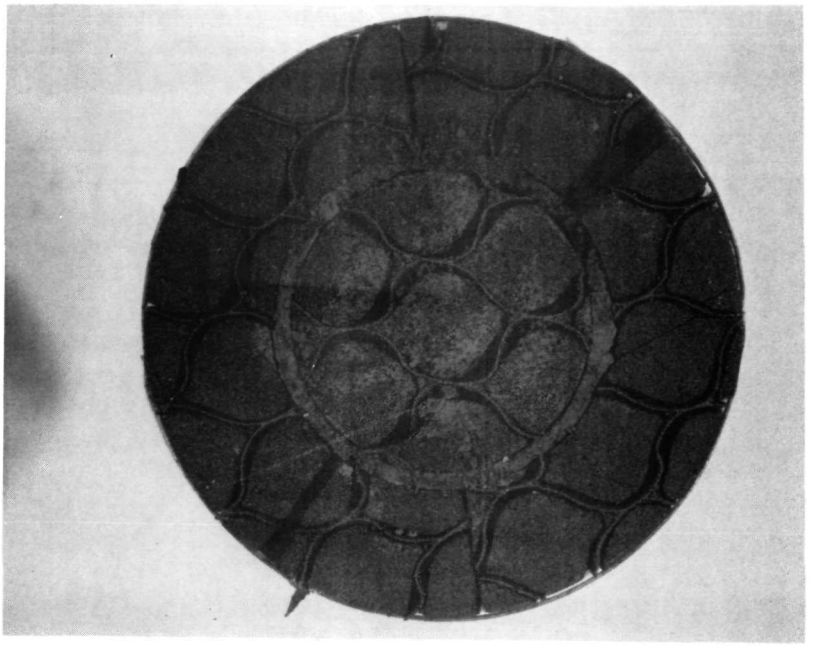

CR-1c-CB-30-2A
(Hot Face)

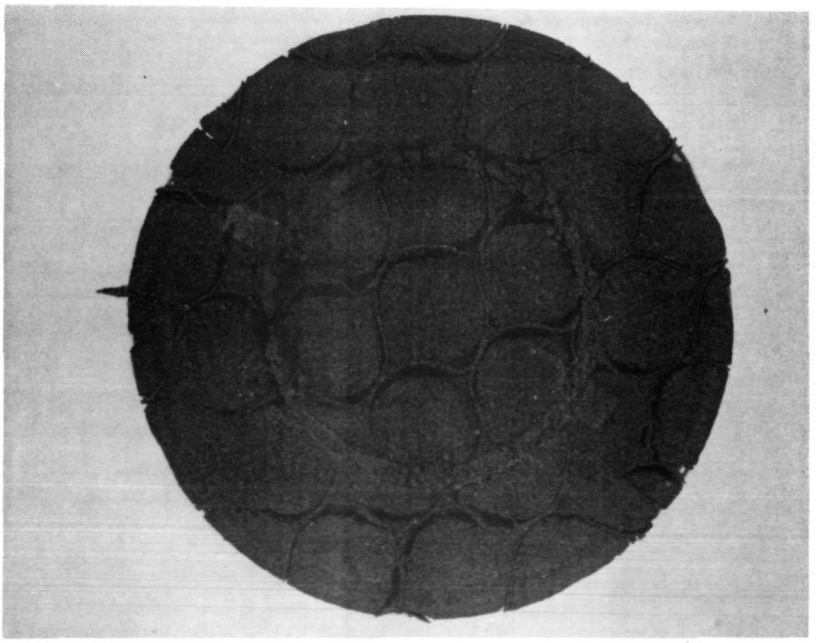

CR-1c-CB-30-2A
(Cold Face)

Figure 45. Photographs of the comparative rod specimen after the run, showing the structure of the furnace char of Material A formed at 800K

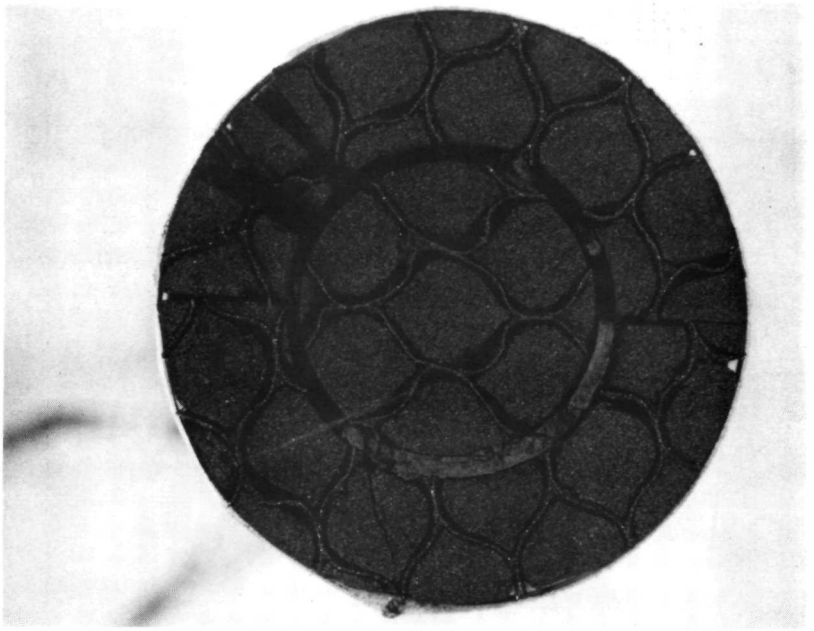

CR-2c-30-2A-802 R2D
(Hot Face)

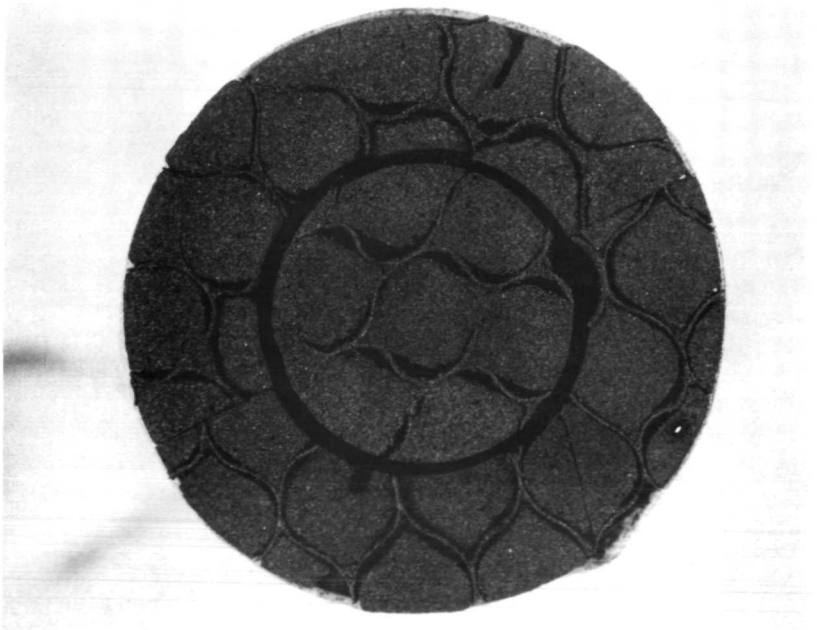

CR-2c-30-2A-802 R2D
(Cold Face)

Figure 46. Photographs of comparative rod specimen after the run showing the structure of the furnace char of Material A formed at 802K

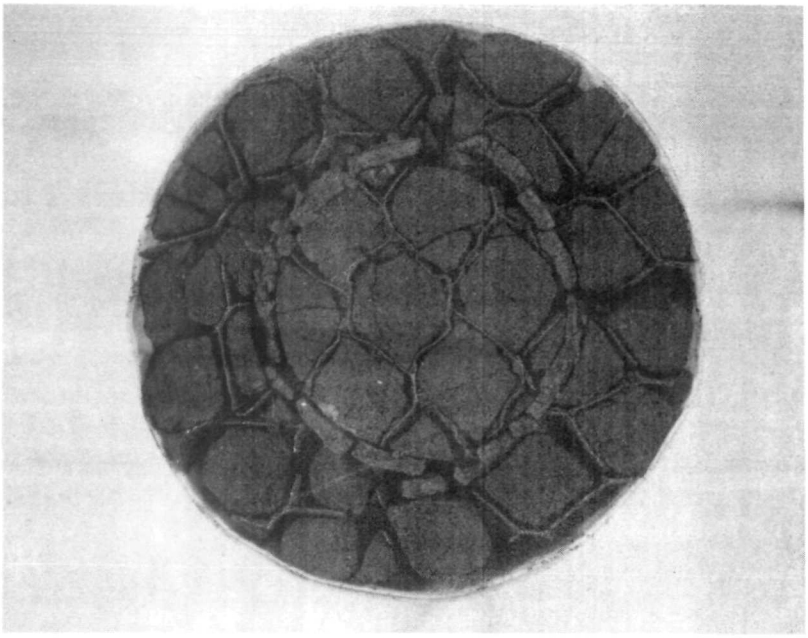

CR-1c-CB-27-3A
(Hot Side)

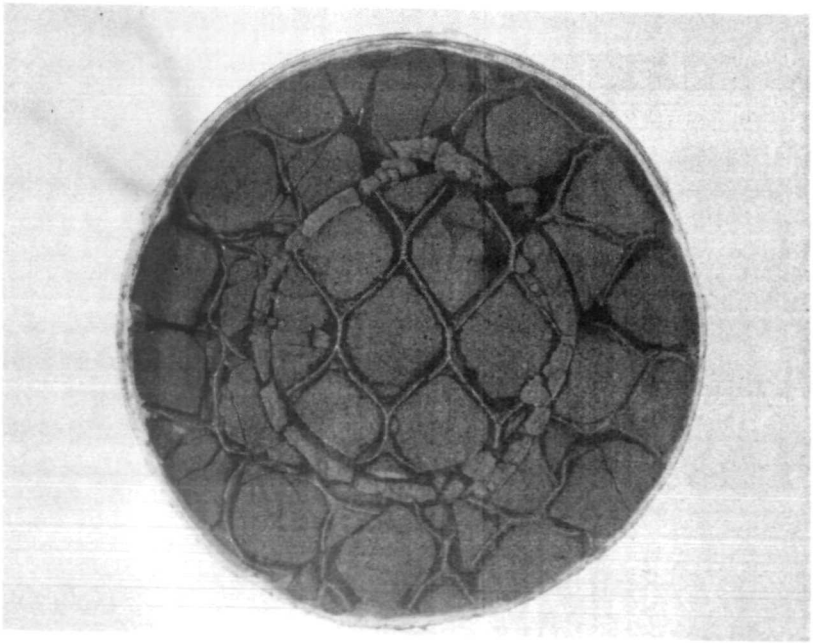

CR-1c-CB-27-3A
(Cold Side)

Figure 48. Photographs of the comparative rod specimen after the run showing the structure of the furnace char of Material A formed at 1127K

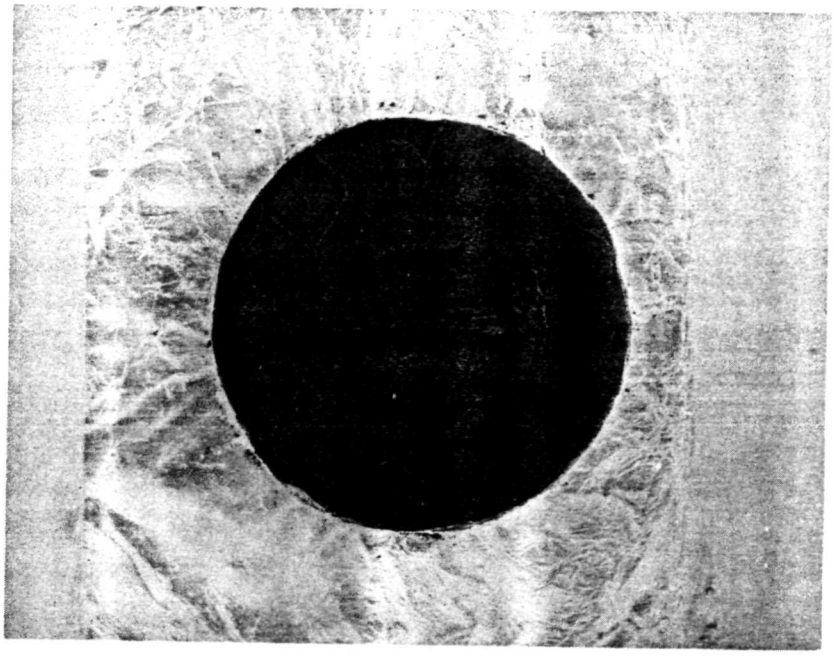

CR-1c-CB-6-3A
Hot Surface

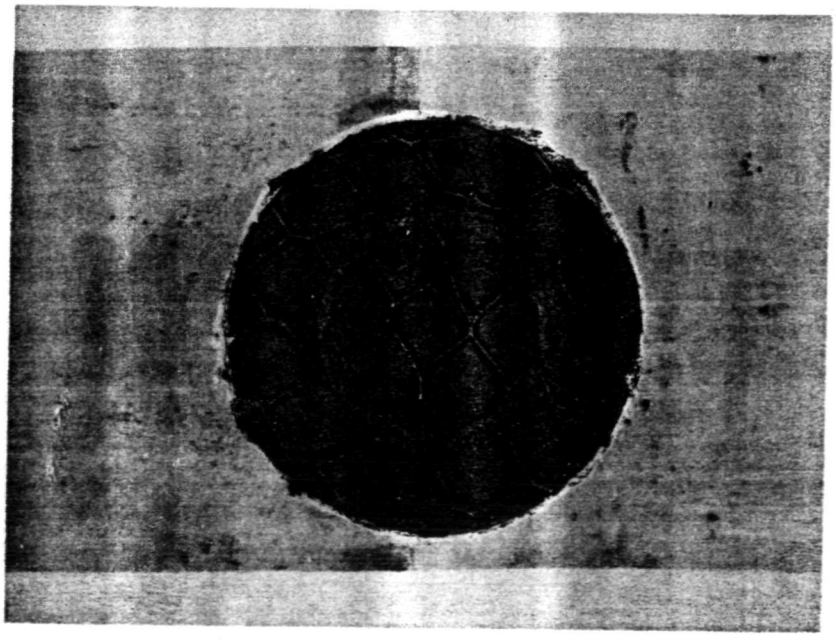

CR-1c-CB-6-3A
Cold Surface

Figure 50. Photographs of the comparative rod specimen after run showing structure of furnace char of Material A formed at 1372K

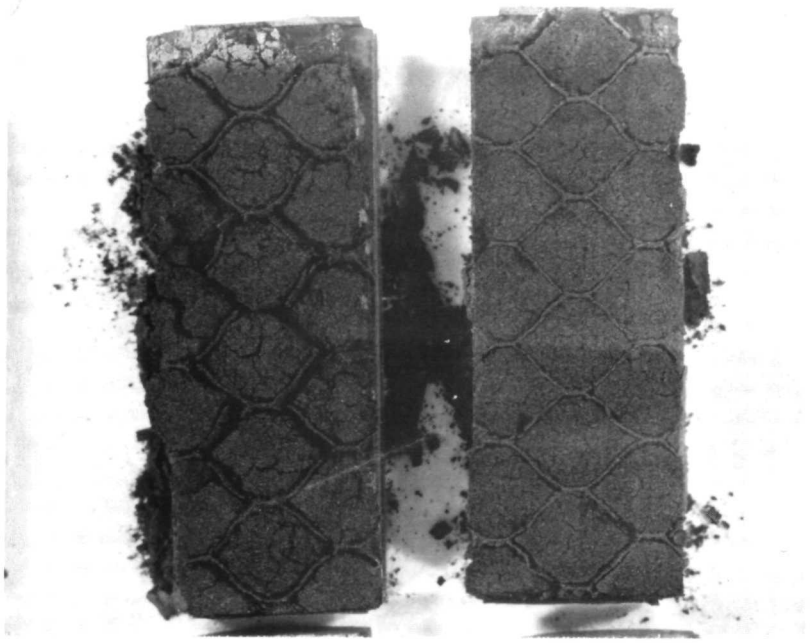

Specimen R1-1c-CB-9-3A Hot Face
(Front-Back Strips)

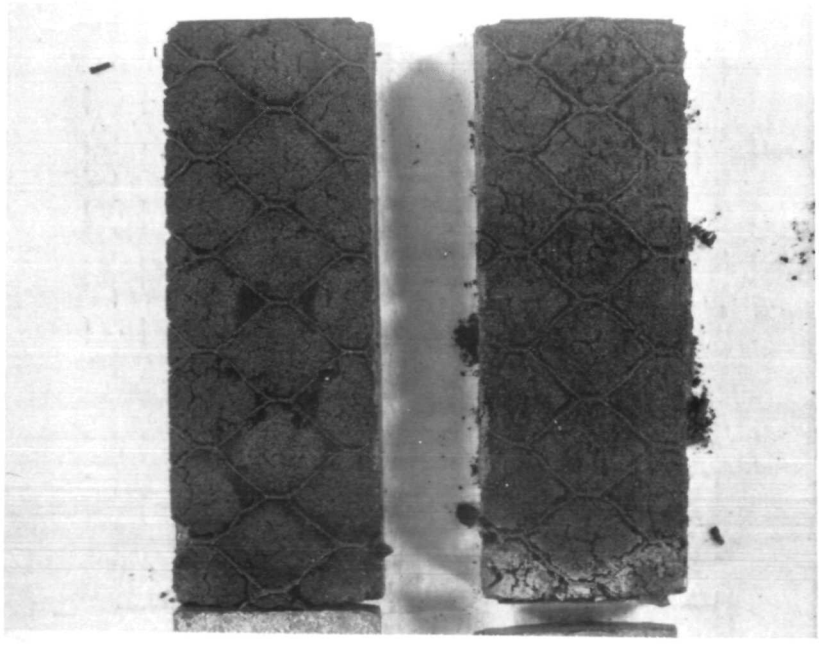

Specimen R1-1c-CB-8-3A Hot Face
(Side-Side Strips)

Figure 51. Photographs of radial inflow strips after run showing structure of furnace char of Material A formed at 1380K

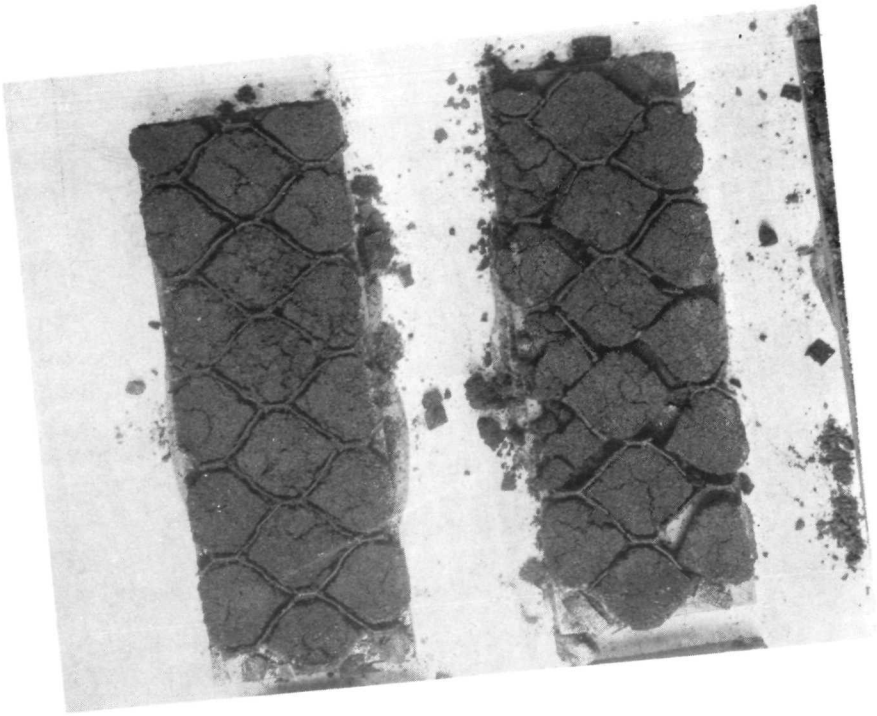

Specimen R1-1c-CB-9-3A Cold Face
(Front-Back Strips)

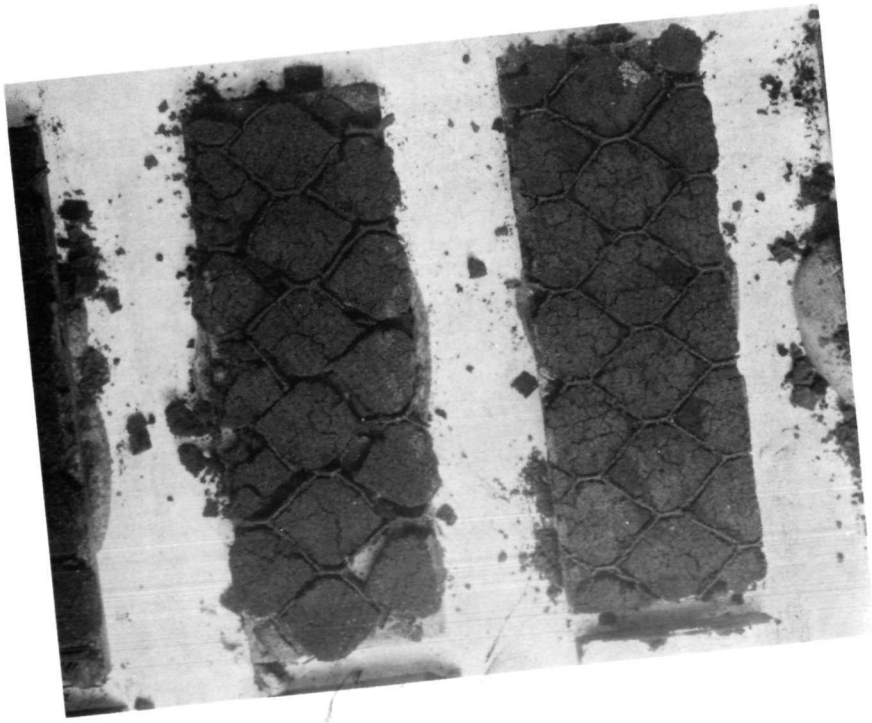

Specimen R1-1c-CB-8-3A Cold Face
(Side-Side Strips)

Figure 52. Photographs of radial inflow strips after run showing structure of furnace char of Material A formed at 1380K

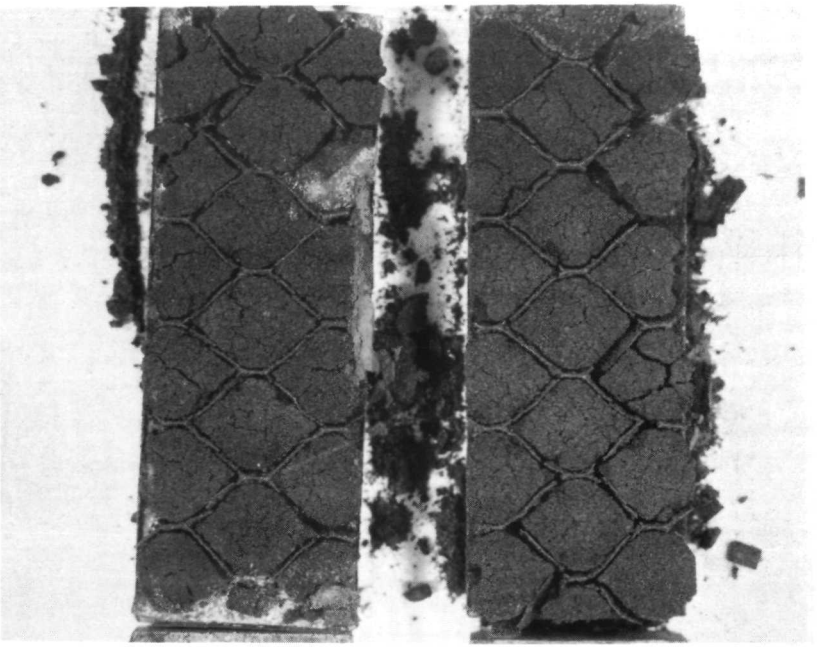

Specimen R1-2c-CB-10-3A Cold Face
(Front-Back Strips)

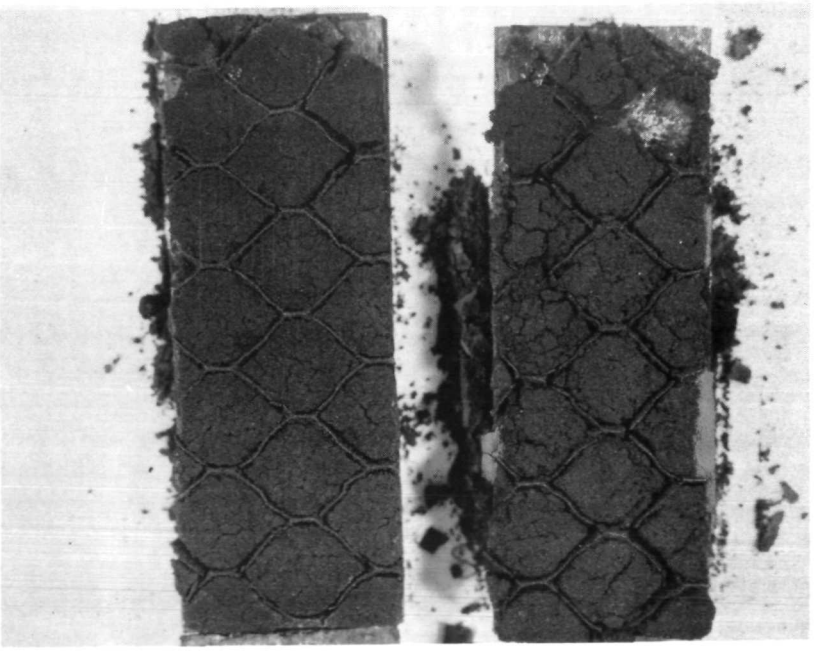

Specimen R1-2c-CB-11-3A Cold Face
(Side-Side Strips)

Figure 54. Photographs of radial inflow strips after run showing structure of furnace char of Material A formed at 1372K

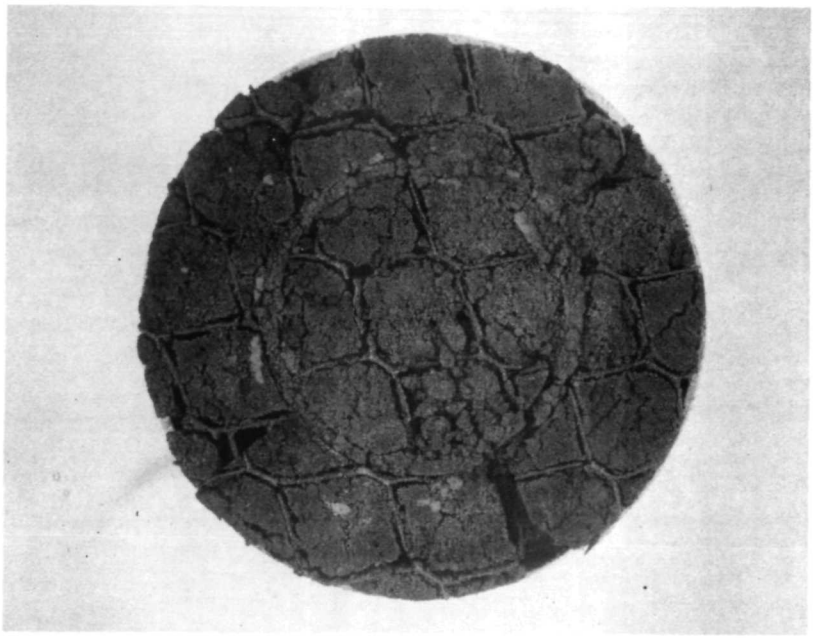

Specimen CR-1c-CB-17-3A Hot Face

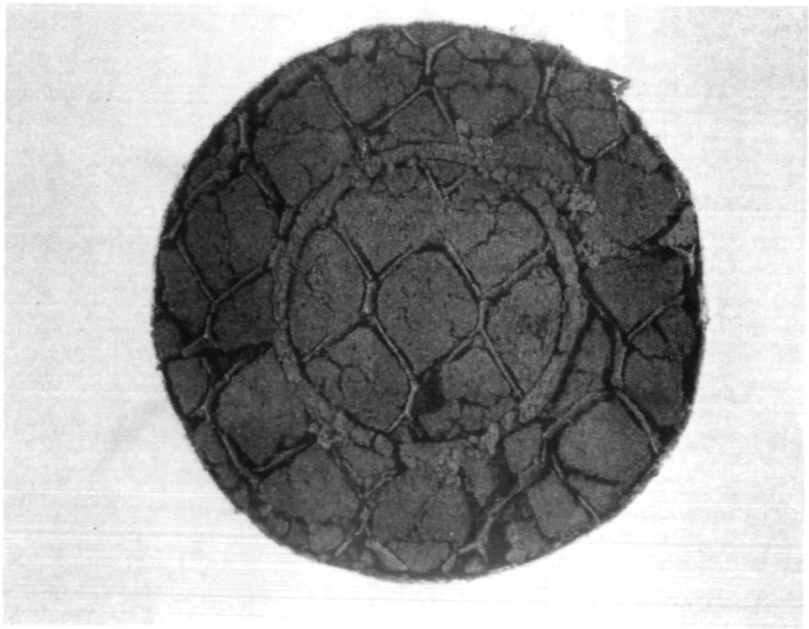

Specimen CR-1c-CB-17-3A Cold Face
Cold Face for Conductivity Run

Figure 56. Photographs of comparative rod specimen after run showing structure of furnace char of Material A formed at 1733K

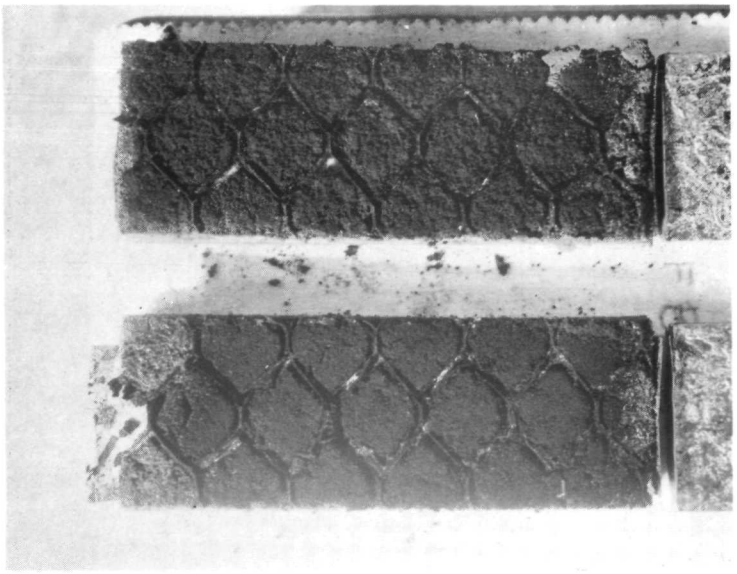

Specimen R1-2c-CB-14-3A Hot Face
(Front-Back Strips)

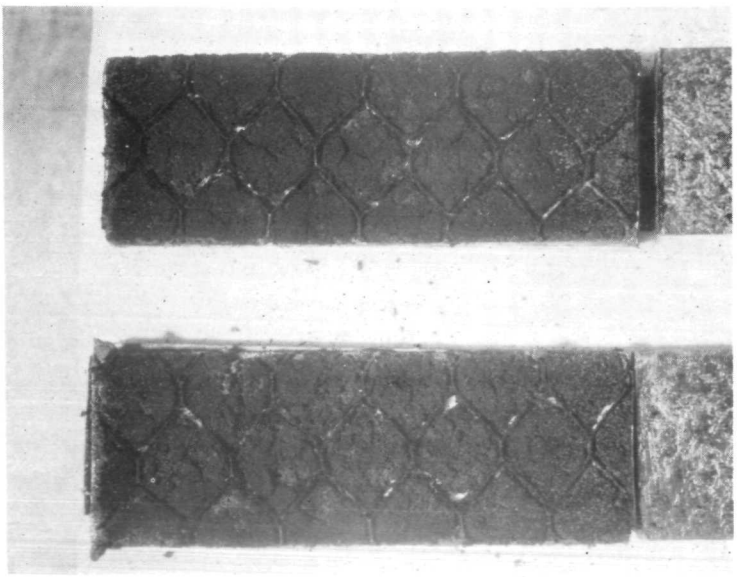

Specimen R1-2c-CB-15-3A Hot Face
(Side-Side Strips)

Figure 58. Photographs of radial inflow strips after run showing structure of furnace char of Material A formed at 1740K

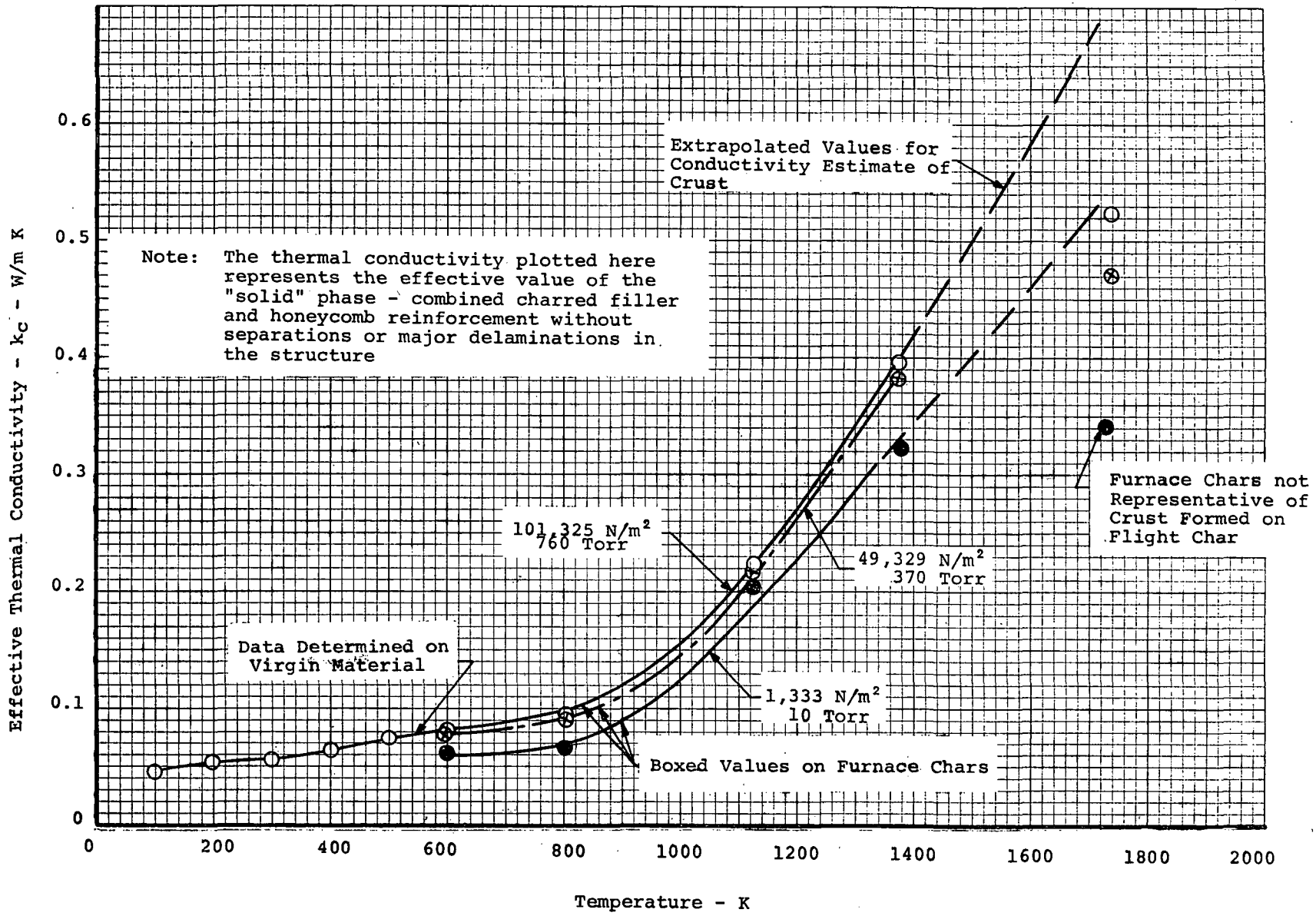

Figure 59. Effective Thermal Conductivity of Material A During Ablative Charring Using the Boxing Analysis

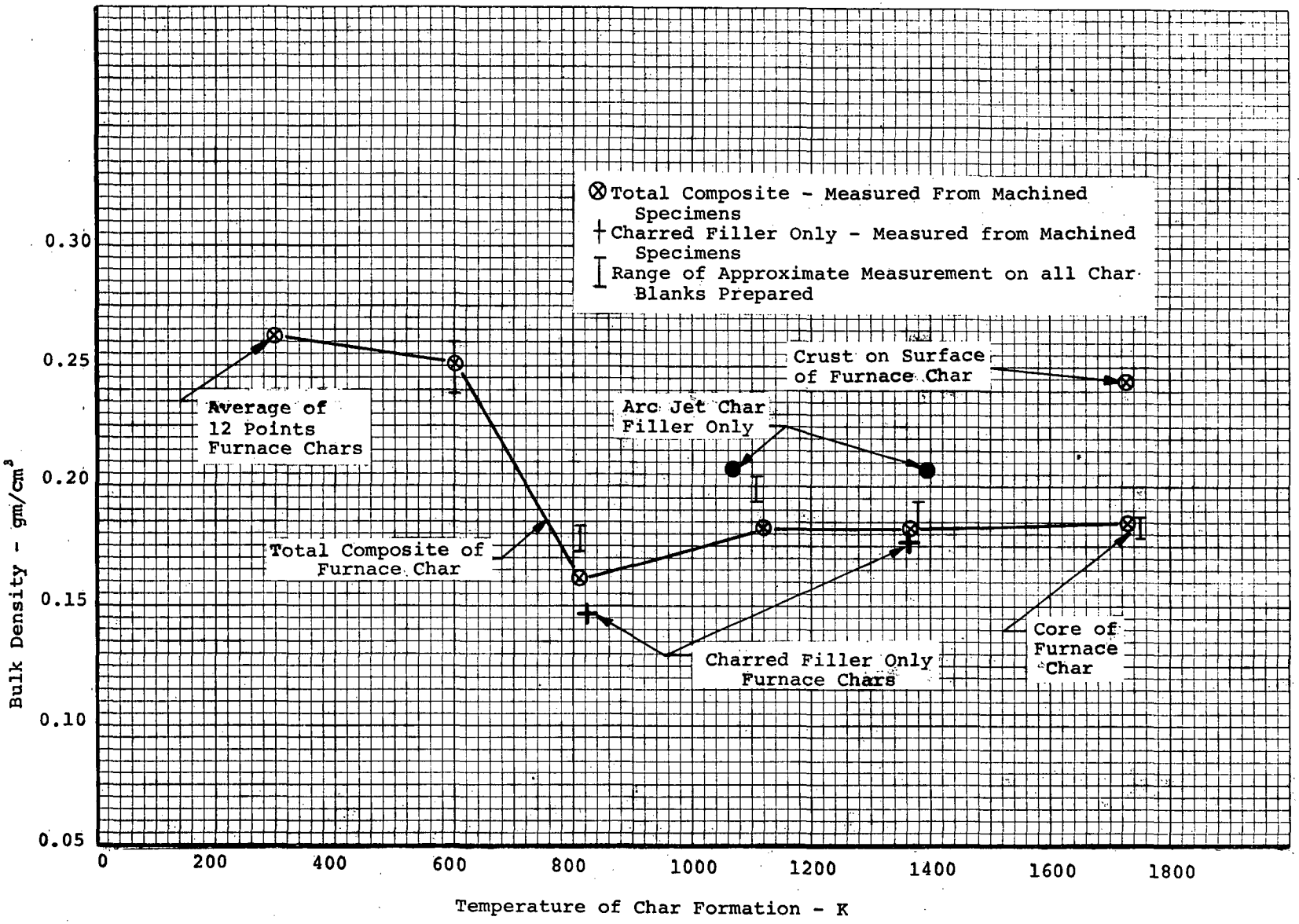

Figure 60. Bulk Density of Furnace and Arc Jet Chars of Material A

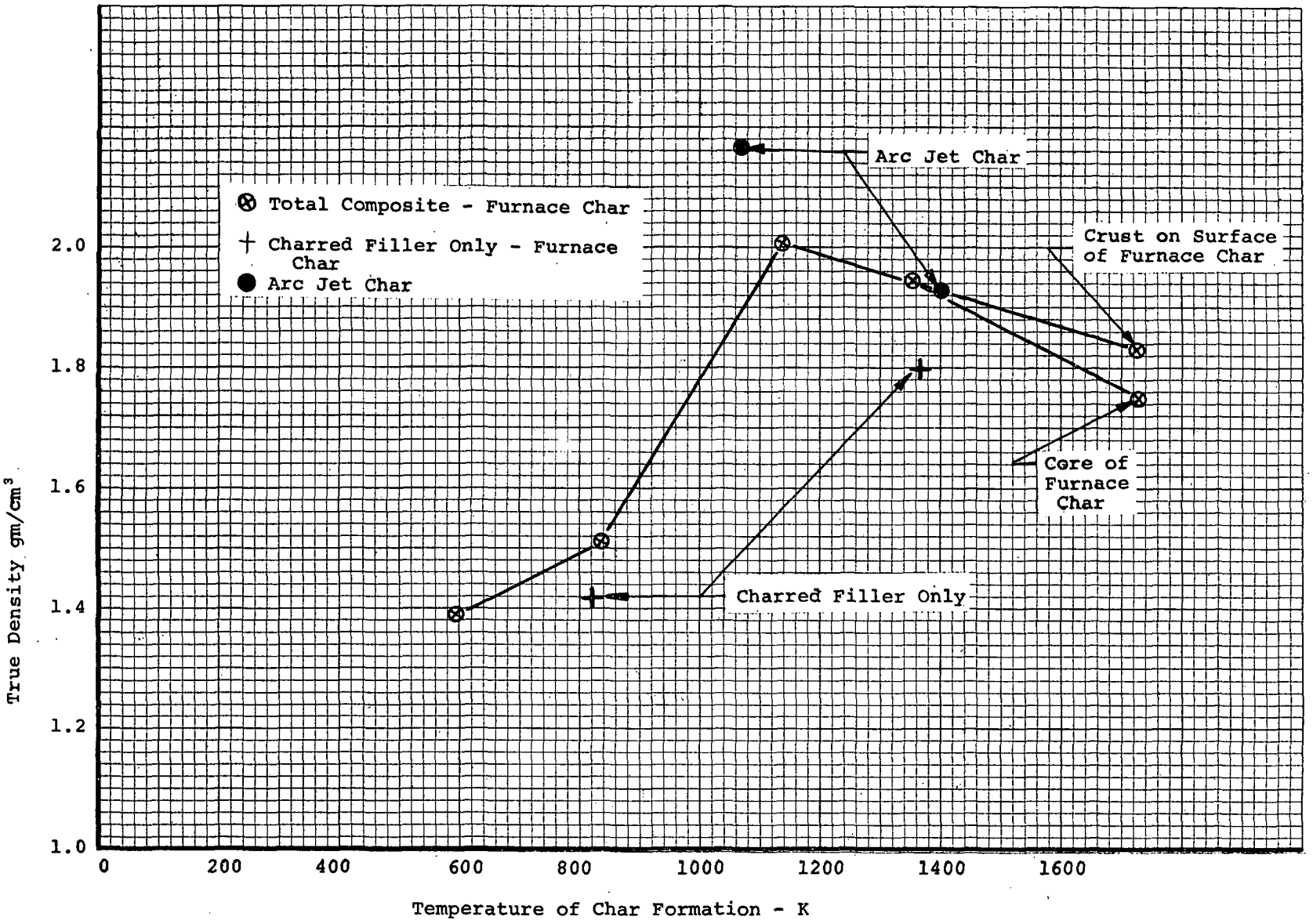

Figure 61. True Density of Furnace and Arc Jet Chars of Material A

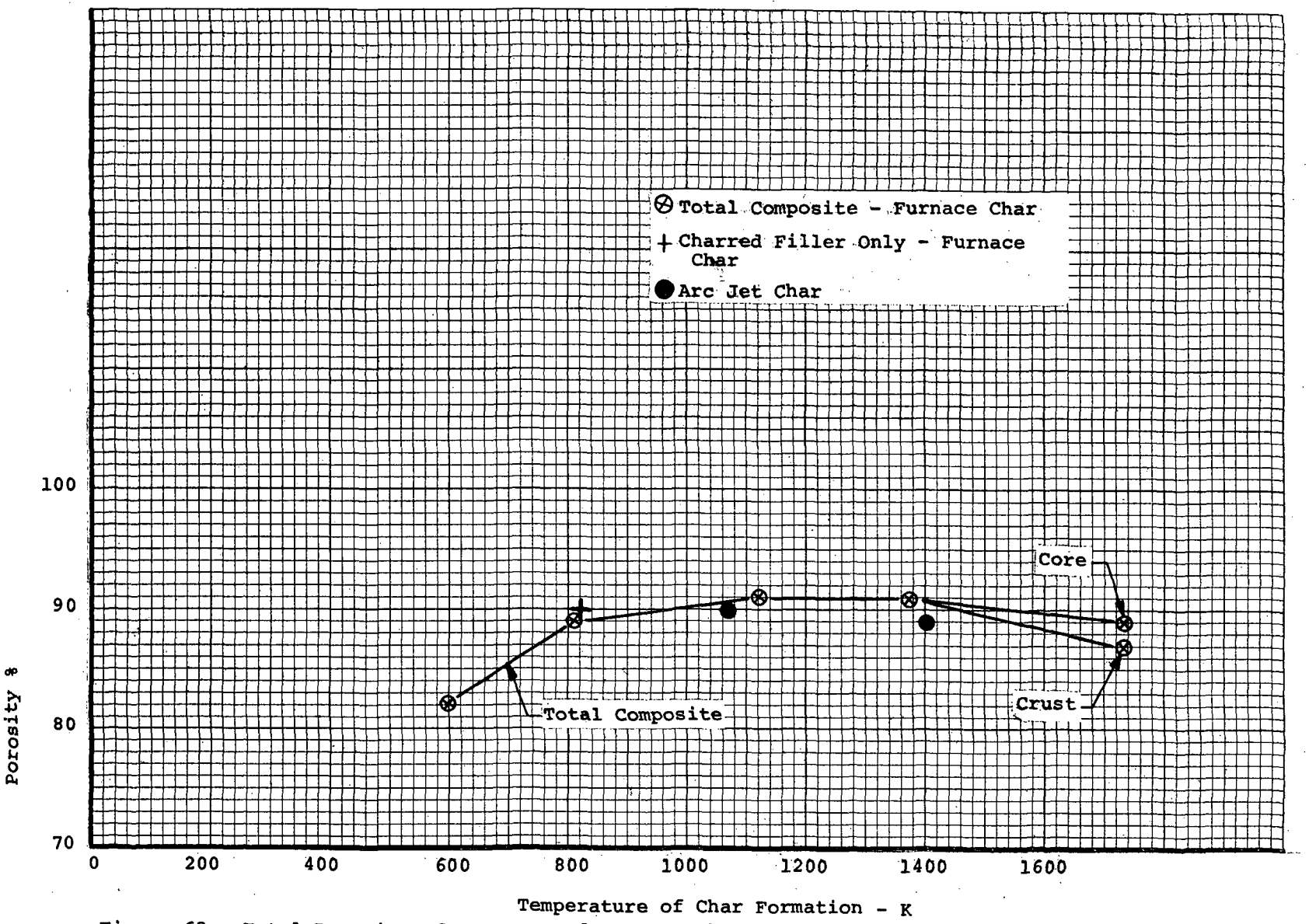

Figure 62. Total Porosity of Furnace and Arc Jet Chars of Material A

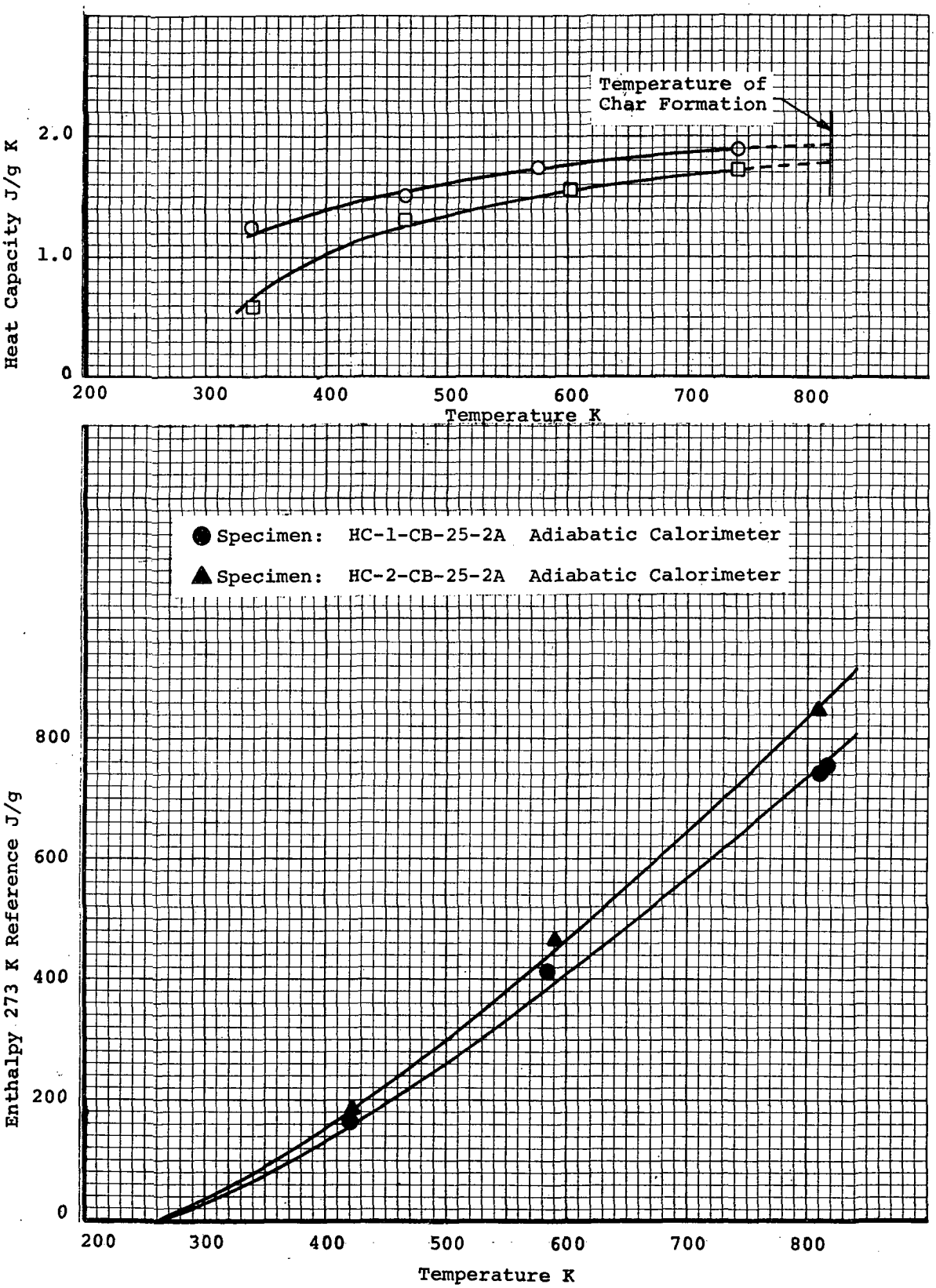

Figure 63. Enthalpy and Heat Capacity of Furnace Char of Material A Formed at 800 K

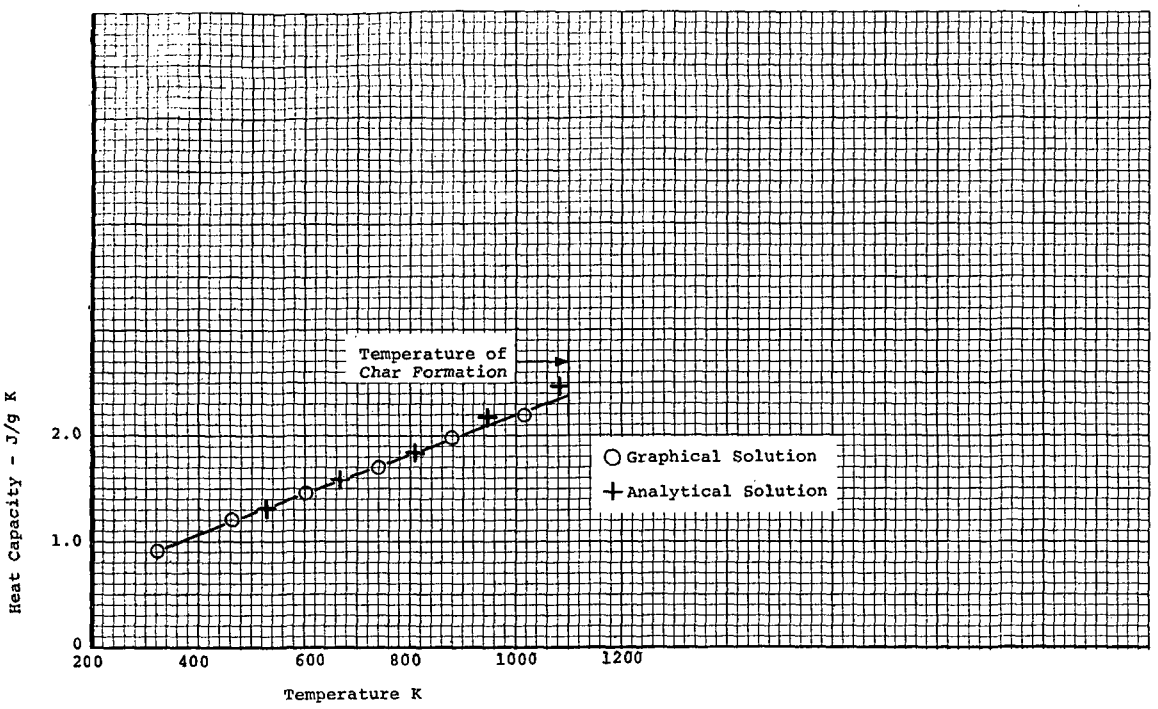

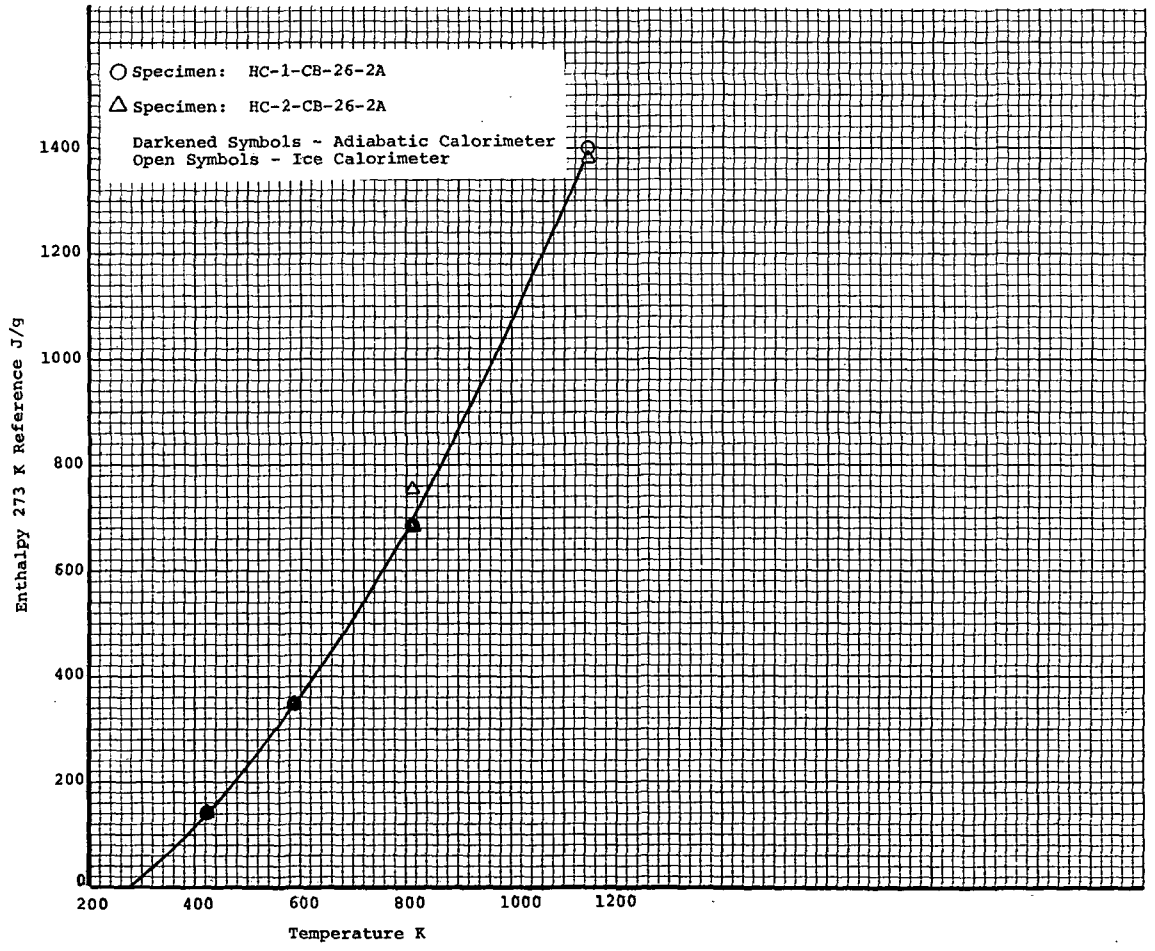

Figure 64. Enthalpy and Heat Capacity of Furnace Char of Material A Formed at 1100 K

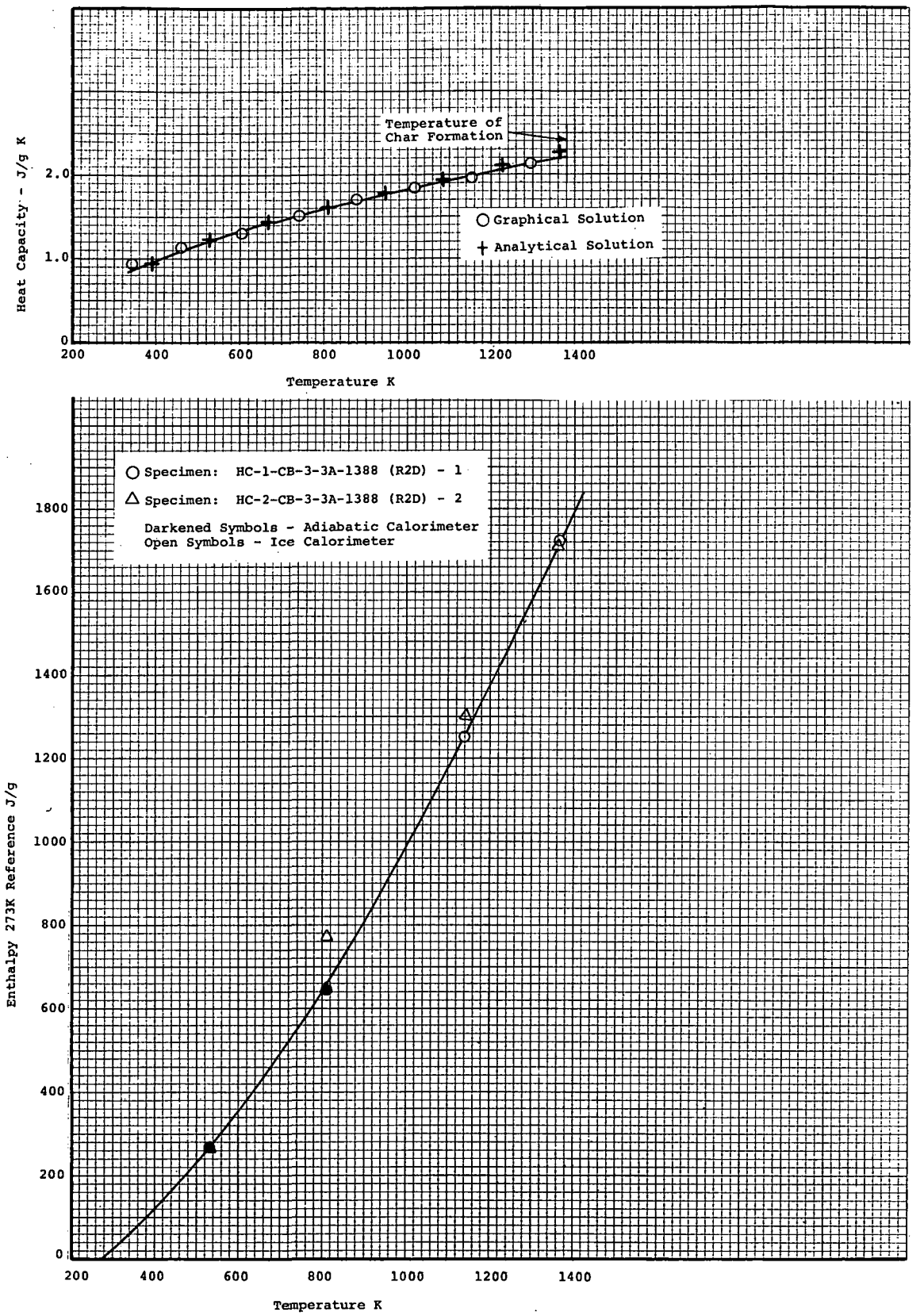

Figure 65. Enthalpy and Heat Capacity of Furnace Char of Material A Formed at 1388 K

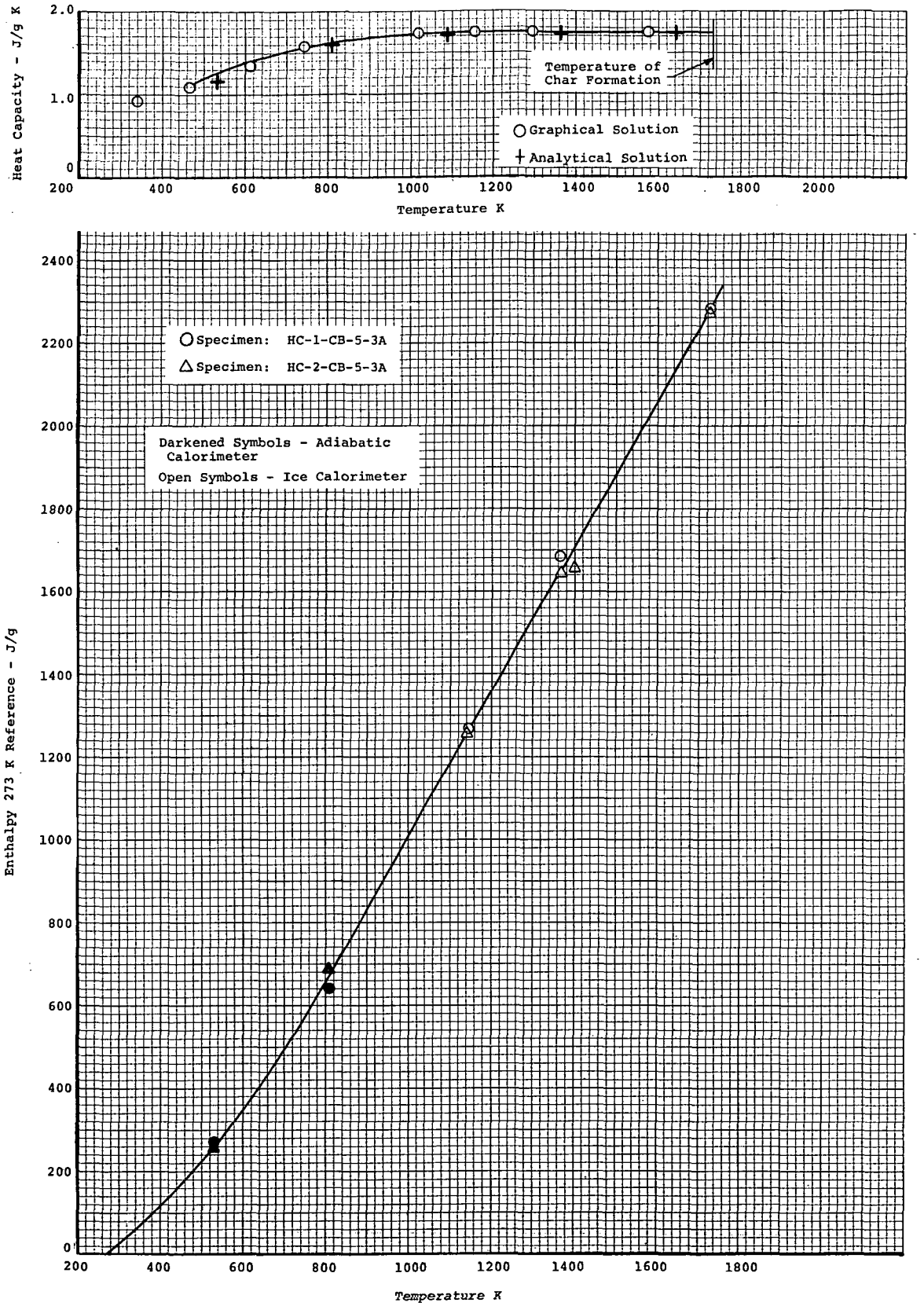

Figure 66. Enthalpy and Heat Capacity of Furnace Char of Material A Formed at 1735 K

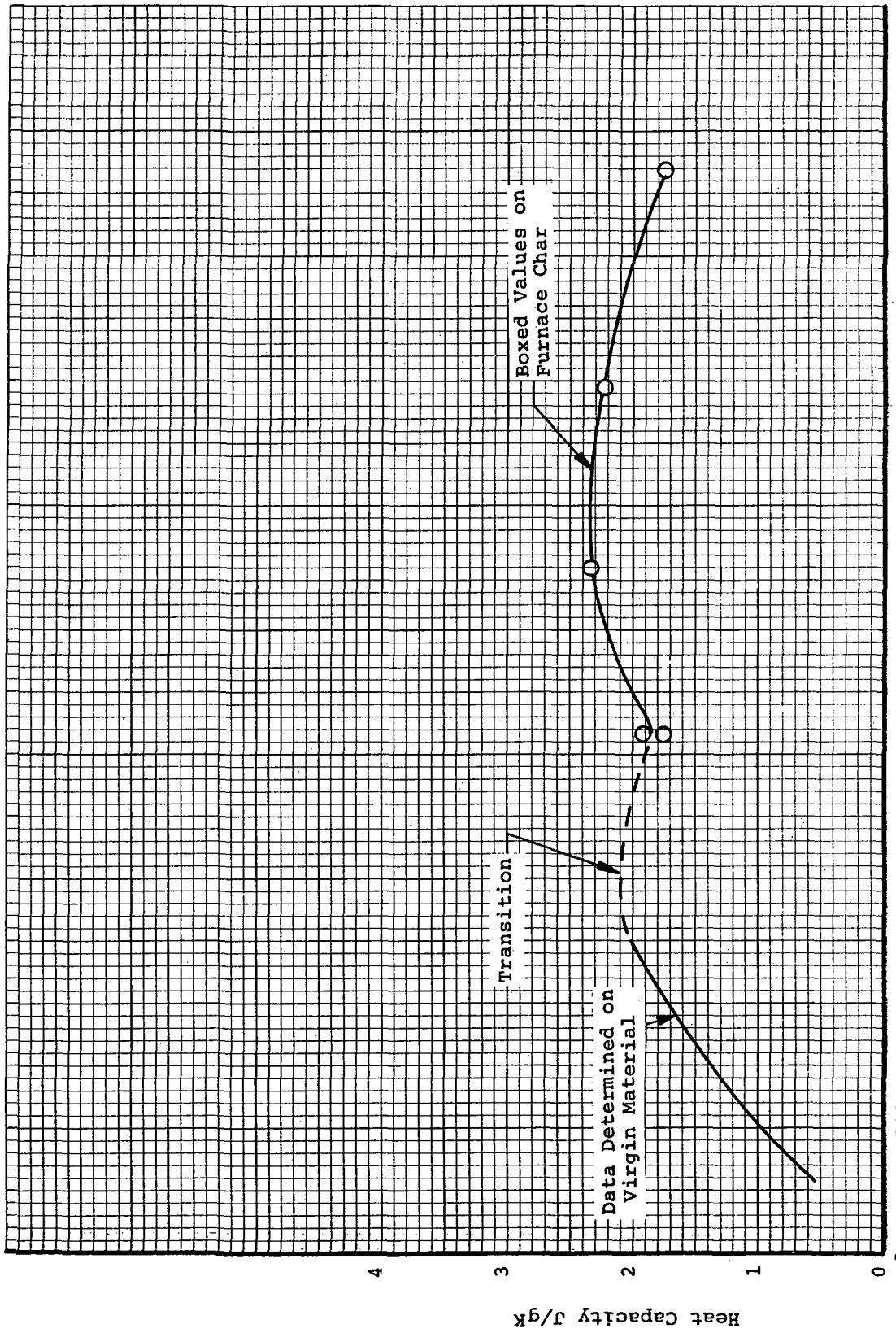

Figure 67. Heat Capacity of Material A During Ablative Charring Using the Boxing Analysis

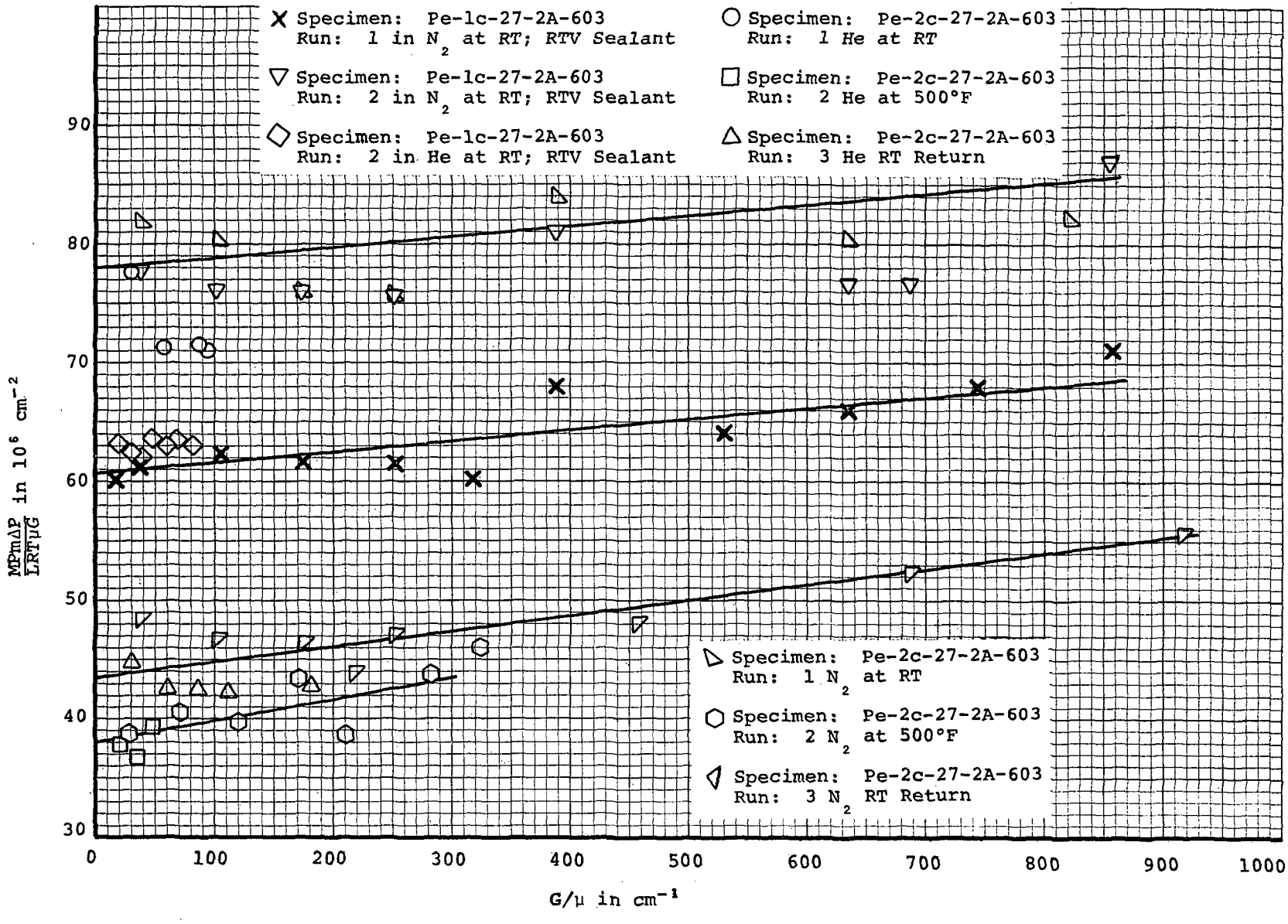

Figure 68. The Permeability of the Furnace Char of Material A Formed at 603 K

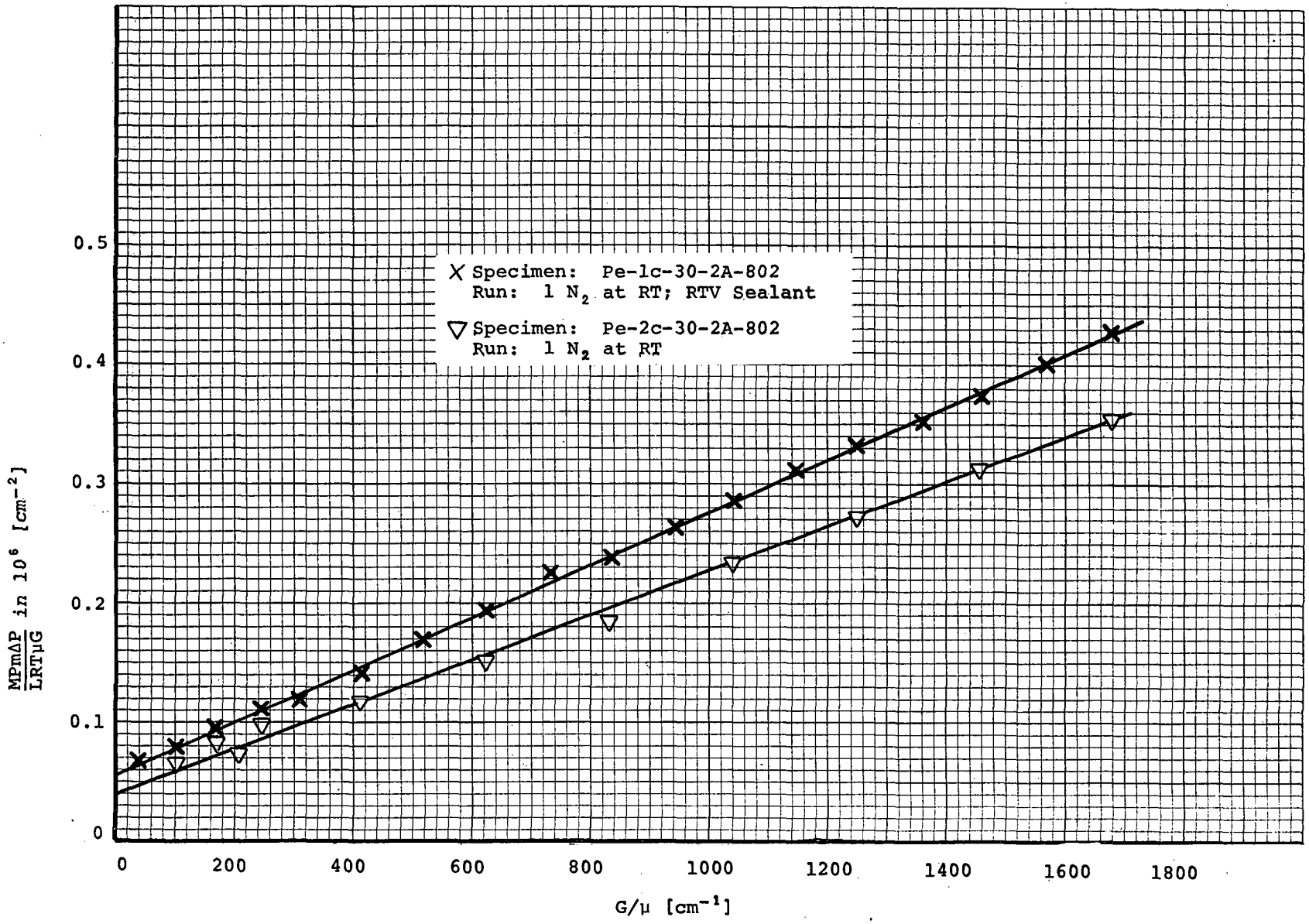

Figure 69. The Permeability of the Furnace Char of Material A Formed at 802 K

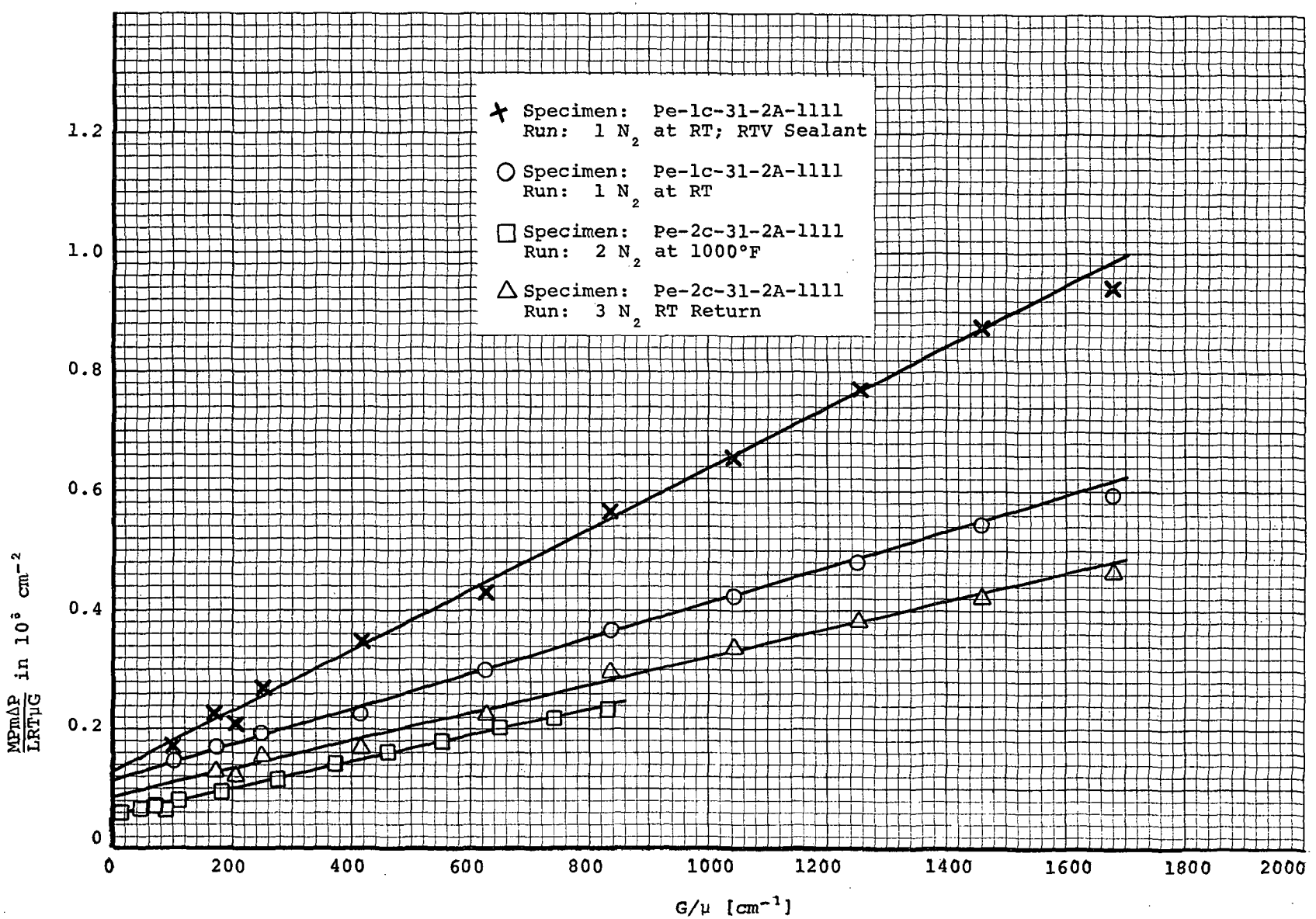

Figure 70. The Permeability of the Furnace Char of Material A Formed at 1111 K

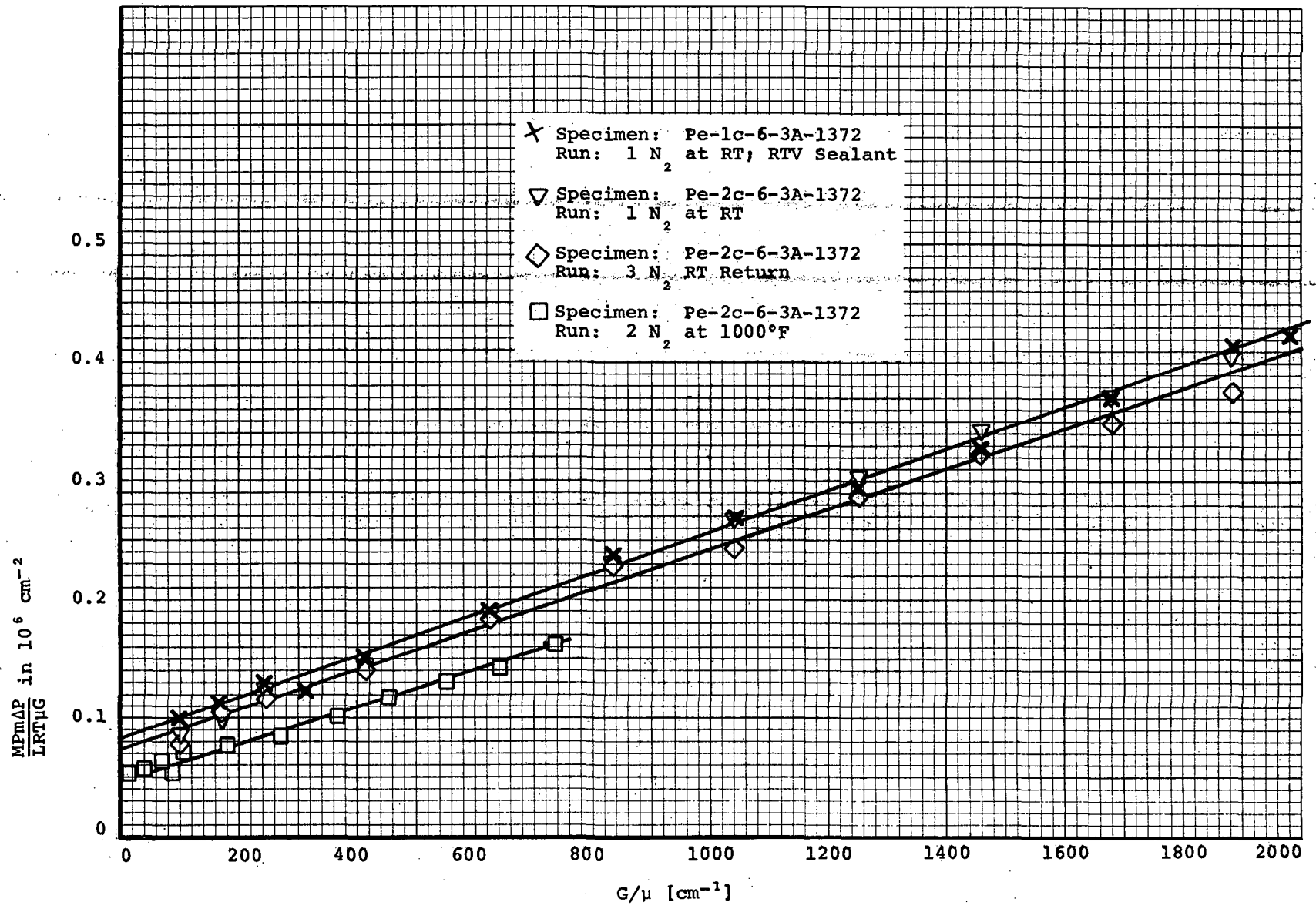

Figure 71. The Permeability of the Furnace Char of Material A Formed at 1372 K

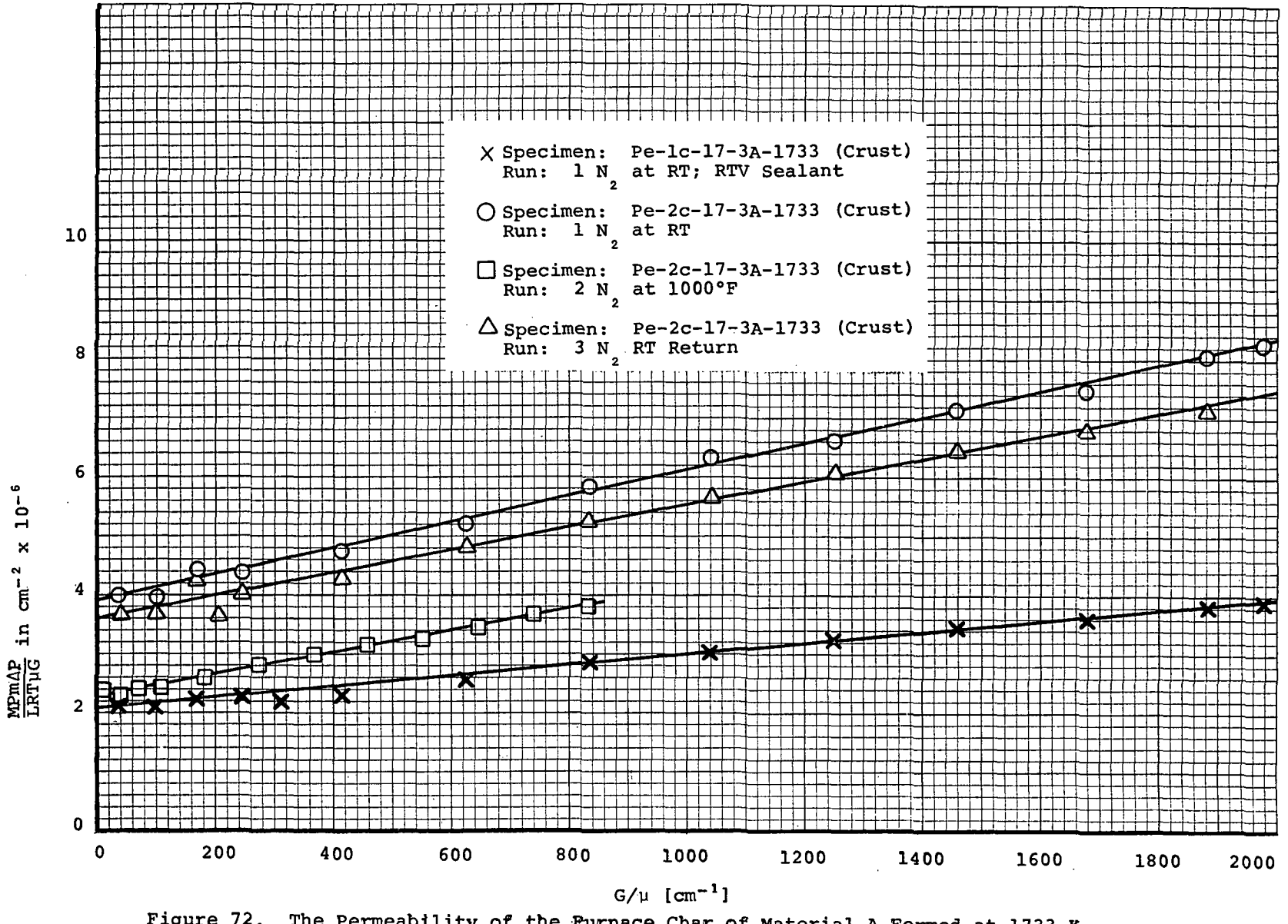

Figure 72. The Permeability of the Furnace Char of Material A Formed at 1733 K

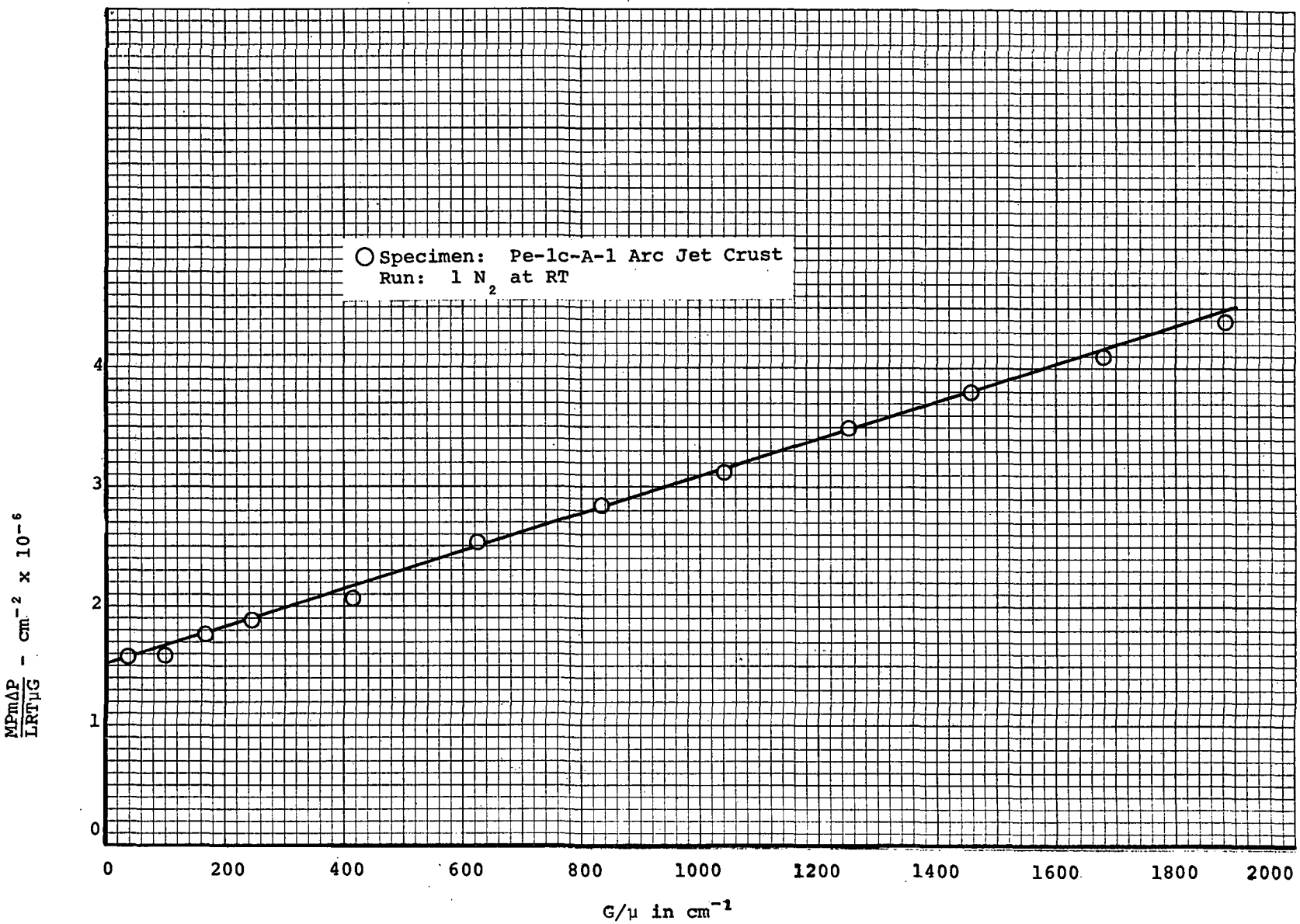

Figure 73. The Permeability of the Arc Jet Crust

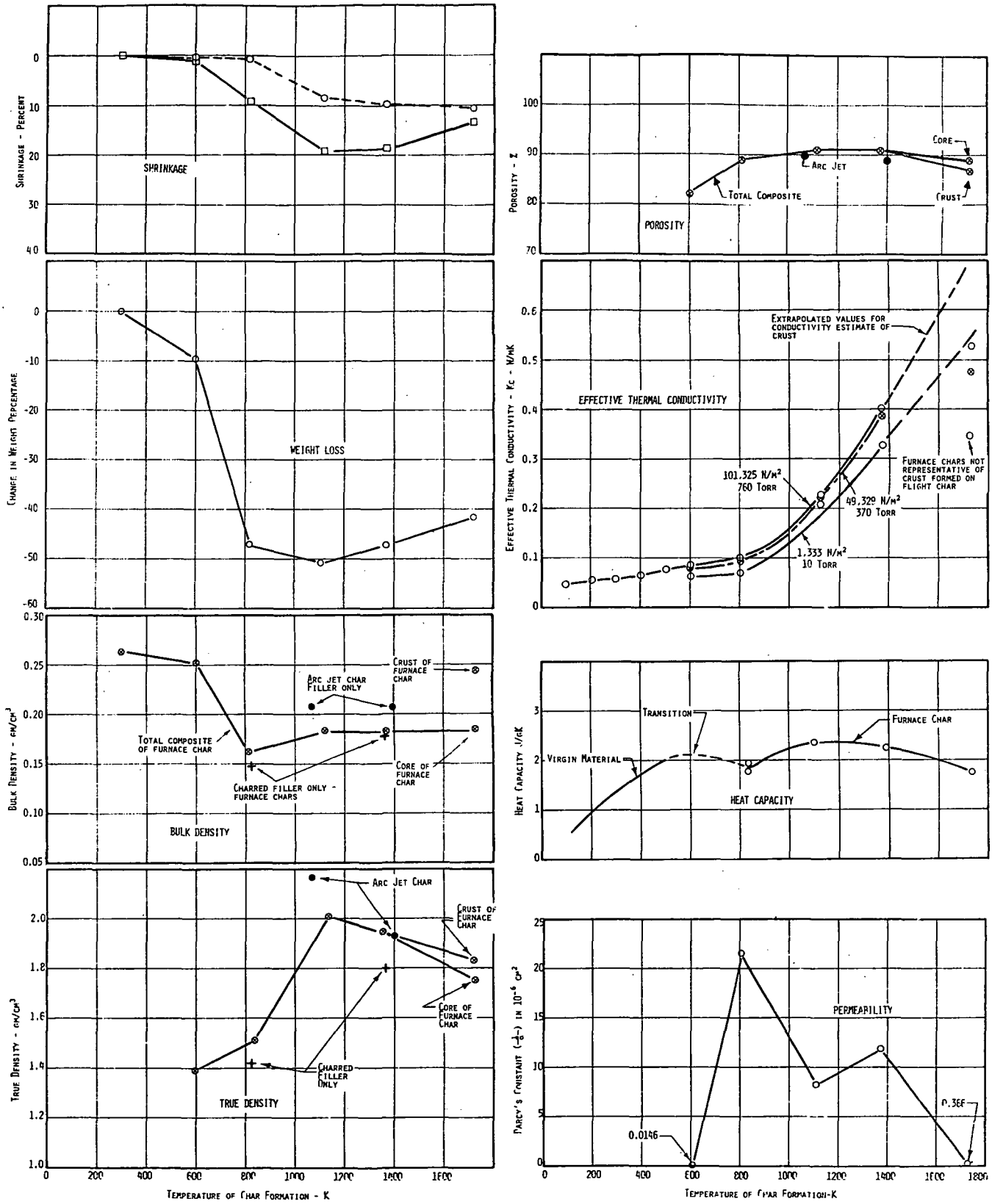

Figure 74. Composite of Properties Determined on Material A During Degradation and Char Formation

TABLE 1

COLD WALL HEAT FLUX
OF FURNACE CHARS

Furnace Preheat Temperature K	Approximate Cold Wall Heat Flux W/m-K
600	0.6×10^2
800	17.0×10^3
1100	65.0×10^3
1370	160.0×10^3
1730	400.0×10^3

Note: Cold wall heat fluxes are for immersion of specimen within preheated furnace. Emittance of surface assumed at 0.8.

TABLE 2

THERMAL CONDUCTIVITY OF A LOW-DENSITY ELASTOMERIC ABLATION MATERIAL (MATERIAL A) IN 1 ATMOSPHERE NITROGEN MEASURED IN THE ASTM C177 GUARDED HOT PLATE APPARATUS

Avg. Specimen Mean Temp. K	Total Heat Input Watts	Average Specimen ΔT K	Specimen Gage cm	Specimen Thermal Conductivity W/m- K	Time to Temperature[3] hr
Specimen AS-1c-2A Run: 6613-26-3 Ni					
Internal Gage					
121	1.365	41.47	0.5006	0.0465	7.0
124	1.401	45.28		0.0437	8.0
126	1.395	43.67		0.0451	9.0
232	0.727	18.50		0.0555	2.4
231	0.727	18.49		0.0555	3.0
335	1.440	34.05		0.0597	21.5
335	1.440	33.96		0.0599	22.0
421	2.893	59.24		0.0690	16.3
422	2.838	59.47		0.0674	16.8
499	4.868	86.97		0.0790	5.0
499	4.868	86.95		0.0791	5.5
Gage Over Total Thickness					
119	1.365	62.51	0.763	0.0453	7.0
124	1.401	63.40		0.0458	8.0
123	1.395	65.94		0.0453	9.0
230	0.727	26.72		0.0565	2.4
232	0.727	26.71		0.0565	3.0
334	1.440	48.60		0.0615	21.5
334	1.440	48.36		0.0618	22.0
417	2.893	85.08		0.0706	16.3
418	2.838	85.17		0.0692	16.8
493	4.868	125.38		0.0806	5.0
493	4.868	125.36		0.0806	5.5
Specimen AS-2c-2A Run: 6613-33-3 Ni - Internal Gage Only					
113	1.356	36.29	0.4872	0.0500	3.0
121	1.356	36.36		0.0505	3.5
192	4.092	100.46		0.0545	3.4
194	4.082	100.29		0.0544	4.2
282	2.712	64.66		0.0561	4.3
282	2.712	64.64		0.0561	5.1
377	1.796	38.28		0.0627	18.0
377	1.796	38.25		0.0628	18.5
490	4.488	80.96		0.0742	16.0
490	4.488	80.83		0.0743	18.0

Notes:

1. Diameter of central heater = 4.826 cm.
2. Thermal conductivity values based on measured gage at each temperature level.
3. Time to temperature implies the time elapsed between adjustment of power and obtaining data.

Bulk Density and Specimen Weights

AS-1C-2A Bottom Disc 0.261 gm/cm^3; Initial Weight, 3.6610 gm
Final Weight, 3.6605 gm

Top Disc 0.273 gm/cm^3; Initial Weight, 3.8399 gm
Final Weight, 3.7884 gm

AS-2C-2A Bottom Disc 0.271 gm/cm^3; Initial Weight, 3.8064 gm
Final Weight, 3.6927 gm

Top Disc 0.260 gm/cm^3; Initial Weight, 3.6523 gm
Final Weight, 3.5428 gm

TABLE 3

ENTHALPY OF A LOW DENSITY ELASTOMERIC ABLATION MATERIAL (MATERIAL A)
MEASURED IN THE ADIABATIC CALORIMETER

Specimen	Run	Initial Cup Temp °K	Final Cup Temp °K	Change in Cup Temp °K	Initial Sample Temp °K	Initial Wt of Sample gm	Final Wt of Sample °K	Enthalpy Joules/gm Above 303°K
HC-1-4A	1	296.288	296.994	0.706	393.48	2.6093	2.5035	133.48
HC-2-4A	1	297.069	297.777	0.708	394.96	2.5834	2.4976	135.55
HC-2-4A	2	299.578	301.167	0.589	518.84	2.4976	2.1563	367.76
HC-3-4A	1	301.087	302.617	1.530	501.99	2.3891	2.2404	343.85
HC-5-4A	1	297.617	296.876	-0.741	197.20	3.1103	3.0926	-127.94
HC-6-4A	1	298.694	297.786	-0.908	182.48	3.1691	3.1704	-150.67
HC-5-4A	2	296.416	295.273	-1.143	79.99	3.0926	3.0800	-193.62
HC-6-4A	2	296.749	295.516	-1.233	80.55	3.1704	3.1734	-202.69
HC-6-4A	3	296.473	295.781	-0.692	196.37	3.1734	3.1665	-117.85
HC-6-4A	4	296.126	298.050	1.924	499.39	3.1665	2.9771	318.08
HC-5-4A	3	297.938	300.096	2.158	499.95	3.0800	2.8918	370.83

TABLE 4

TENSILE STRENGTH PROPERTIES OF A LOW DENSITY ELASTOMERIC ABLATION MATERIAL (MATERIAL A)

Load Direction	Temp °F	Rate	Specimen Number	Bulk Density gm/cm^3	Ultimate Strength N/m^2	Initial Elastic Modulus N/m^2	Total Unit Axial Strain m/m	Sonic Velocity cm/μsec
A	70	-	T-1a-1A	0.274	3.48×10^5	31.37×10^5	0.0192	0.2916
		-	T-2a-1A	0.264	1.86×10^5	30.47×10^5	0.0106	0.3010
B	70	-	T-1b-4A	0.259	1.39×10^5	18.48×10^5	0.0201	0.3078
		-	T-2b-4A	0.257	1.68×10^5	13.38×10^5	0.0195	0.3317

TABLE 5

COMPRESSIVE STRENGTH PROPERTIES OF A LOW-DENSITY ELASTOMERIC ABLATION MATERIAL (MATERIAL A)

Load Direction	Temp °F	Rate	Specimen Number	Bulk Density gm/cm^3	Ultimate Strength N/m^2	Initial Elastic Modulus N/m^2	Total Unit Axial Strain m/m	Sonic Velocity cm/μsec
A	70	-	C-1a-1A	0.2361	3.72×10^3	32.82×10^3	0.0190	0.3117
		-	C-2a-1A	0.2761	4.69×10^3	46.61×10^3	0.0140	0.3208
B	70	-	C-1b-4A	0.2606	5.38×10^3	19.58×10^3	0.0530	0.3269
		-	C-2b-4A	0.2606	5.65×10^3	21.86×10^3	0.0510	0.3401

TABLE 6

SUMMARY OF CHAR BLANKS PREPARED DURING THE PRELIMINARY INVESTIGATION

Temp Category	Specimen No.[1]	Virgin Bulk Density gm/cm³	Max Temp K	Weight Loss %	Shrinkage[2] in Thickness Reinforce Cell %	Filler %	Char[3] Bulk Density of Entire Composite gm/cm³	Change in Bulk Density of Entire Composite %	Bulk[4] Density of Filler gm/cm³	Water Absorption Filler %	Bulk Density of Filler From Absorption gm/cm³	Effective Thermal Conductivity kJ/m-K at 533K	at 811K	X-Ray Diffraction Intensities at d=4.05	d=2485
800K	CB-1-2A-819 (R1D)	0.2721	819	41.98	0.54	11.42	0.1947	28.44						0	0
	*CB-25-2A-818 (R2D)	0.2634	818	43.96	0.26	8.66	0.1744	33.78	0.1723						
1100K	CB-8-2A-1056 (R1D)	0.2580	1056	51.27	6.37	22.07	0.2018	21.78		313.28	0.2475				
	CB-20-2A-1056 (R1D)	0.2703	1056	51.40	5.94	20.54	0.2197	18.71				0.095	0.11		
	*CB-26-2A-1100 (R2D)	0.2637	1100	51.74	8.66	16.80	0.1934	26.65							
1370K	CB-6-2A-1373 (S1D)	0.2698	1373	57.00	7.11	21.02	0.2005	25.68	0.1958					4500	500
	CB-17-2A-1369 (S1D)	0.2720	1369	54.09	7.78	21.46	0.2217	18.49				0.143	0.196		
	CB-7-2A-1369 (S1D)	0.2700	1369	54.38	7.41	22.36	0.2191	18.85		326.93	0.2315				
	CB-2-2A-1373 (R1D)	0.2593	1373	45.84	9.22	20.08	0.2192	15.46		324.74	0.2376			2000	200
	CB-18-2A-1383 (R1D)	0.2590	1383	47.48	9.87	22.37	0.2244	13.35	0.1961			0.143	0.196		
	CB-19-2A-1383 (R1D)	0.2721	1383	47.71	10.57	23.39	0.2370	12.89							
	CB-13-2A-1390 (R1D)	0.2538	1390	-	12.96	23.84	-	-							
	CB-14-2A 1390 (R1D)	0.2665	1390	-	8.00	22.62	-	-							
	CB-15-2A 1354 (R1D)	0.2720	1354	48.07	9.17	20.90	0.2302	15.36	0.2320						
	CB-16-2A 1378 (R1D)	0.2606	1378	49.78	9.94	21.98	0.2157	17.22							
	CB-9-2A-1355 (R2D)	0.2715	1355	50.41	10.70	23.32	0.2156	20.58	0.1915	337.80	0.2253	0.113	0.160		
	CB-10-2A-1371 (R2D)	0.2558	1371	51.53	9.57	23.66	0.2012	21.34	0.1936			0.113	0.160		
	CB-22-2A-1364 Total	0.2654	1364	48.41	8.00	19.09	0.1892	28.71	0.1966	332.79	0.2416				
	CB-22-2A-1364 (R2D) 1/4	0.2654	1364	-	-	-	-	-	0.1956	296.87	0.2530	0.101	0.147		
	CB-23-2A-1306 (R2D) 1 Second Soak	0.2658	1306	45.17	17.84	9.97	0.2039	23.28							
	CB-24-2A-1375 (R2D) 30 Min. Soak	0.2634	1375	45.46	17.28	9.79	0.1929	26.76							
1650K	CB-5-2A-1644 (S1D)	0.2585	1644	58.42	6.81	20.60	0.1781	31.10	0.1841					6000	1000
	CB-4-2A-1644 (R1D)	0.2571	1644	45.78	10.06	19.06	0.2239	12.91	0.2031					1700	300
	CB-21-2A-1635 (R2D)	0.2603	1635	47.95	10.23	19.60	0.1846	29.08							
1900K	CB-3-2A-1922 (R1D)	0.2734	1922	40.89	11.79	11.79	0.1617	40.85						0	0
Arc Jet Char	Zone 2[5] (1250-1550K)								0.2061	217.06	0.3044			500	0
	Zone 3[5] (900-1250K)								0.2070	276.09	0.2666	0.095	0.126		
	Zone 4[5]									366.18	0.2309			0	0

[1]Specimen number contains designation R1D, R2D, S1D which infer the following:

R1D - Rapid heating rate, immersed in preheated furnace at desired temperature and held at temperature for 50 seconds. One dimensional heating.

R2D - Same as R1D except two dimensional heating. All held at temperature 50 seconds except CB-23-2A-1306-R2D and CB-24-2A-1375-R2D which were held at temperature for 1 second and 30 minutes, respectively.

S1D - Slow heating at 18K per hour held at temperature 20 minutes. One dimensional heating.

[2]Shrinkage was measured in the thickness direction. Shrinkage in both the filler and honeycomb cell reinforcement was measured.

[3]Bulk density of char measured approximately after extraction from the furnace. Thickness of filler rather than reinforcing cell used in calculation.

[4]Bulk density of filler measured approximately by a gravimetric means of the filler portion only.

[5]Diagram of Arc Jet Char with Zones 1 through 4 indicated

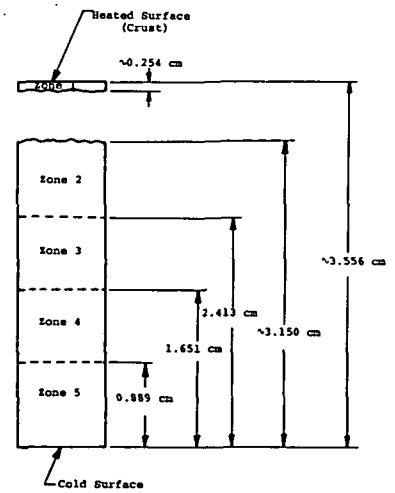

TABLE 7

SUMMARY OF CHAR BLANKS PREPARED (RAPID 2 DIMENSIONAL) FOR EVALUATION

Temperature Category	Specimen Blank Number	Virgin Bulk Density gm/cm³	Maximum Temp. K	Total Time in Furnace (Sec)	Weight Loss %	Shrinkage: Reinforcement %	Shrinkage: Cell Filler %	Char Bulk Density of Entire Composite gm/cm³	Change in Bulk Density of Entire Composite %	Specimen Prepared: Cp	Permeability	Density	CRA	RIA	Visual Inspection or Specimen Guards
600K	CB-27-2A-603 (R2D)	0.2663	603	595	5.43	0.04	0.14	0.2605	2.18		2				
	CB-24-3A-592 (R2D)	0.2648	592	600	13.61	0.40	2.01	0.2400	9.36			1			
	Average				9.51	0.22	1.08		5.77						
800K	CB-25-2A-818 (R2D)	0.2634	818	475	43.96	0.26	8.66	0.1744	33.78	2					
	CB-28-2A-824 (R2D)	0.2628	824	560	45.91	0.16	10.38	0.1841	29.94						1
	CB-30-2A-802 (R2D)	0.2624	802	560	50.09	0.17	11.20	0.1742	33.61		2		2		
	CB-22-3A-829 (R2D)	0.2623	829	475	47.94	0.86	10.41	0.1697	35.30			1			
	CB-23-3A-821 (R2D)	0.2589	821	475	47.21	0.94	7.31	0.1671	35.45			3			
	Average				47.02	0.48	9.59		33.62						
1100K	CB-26-2A-1100 (R2D)	0.2637	1100	375	51.74	8.66	16.80	0.1934	26.65	2					
	CB-27-3A-1127 (R2D)	0.2697	1127	300	51.17	7.69	18.89	0.2026	24.87				1		1
	CB-31-2A-1111 (R2D)	0.2626	1111	290	51.47	7.06	19.33	0.1985	24.40		2		2		
	CB- 4-3A-1072 (R2D)	0.2585	1072	270	49.57	7.68	20.66	0.1992	22.94			1			
	CB-29-2A-1137 (R2D)	0.2630	1137	290	50.42	9.95	19.95	0.2046	22.20			1			
	Average				50.87	8.21	19.13		24.21						
1370K	CB-26-3A-1354 (R2D)	0.2718	1354	210	48.59	9.81	17.97	0.1897	30.20			2			1
	CB-11-3A-1374 (R2D)	0.2591	1374	210	46.93	9.10	19.70	0.1839	29.02					2	
	CB-10-3A-1371 (R2D)	0.2598	1371	210	46.67	9.61	17.58	0.1863	28.29					2	
	CB- 9-3A-1377 (R2D)	0.2638	1377	210	46.72	9.93	19.20	0.1913	27.48					2	
	CB- 8-3A-1380 (R2D)	0.2616	1380	210	46.19	9.41	18.80	0.1937	25.95					2	
	CB-21-3A-1366 (R2D)	0.2587	1366	210	47.82	10.47	20.02	0.1865	27.90			3			
	CB-20-3A-1363 (R2D)	0.2628	1363	210	48.23	10.32	19.80	0.1893	27.96			1			
	CB- 7-3A-1377 (R2D)	0.2659	1377	210	46.20	9.13	17.21	0.1842	30.72						1
	CB- 6-3A-1372 (R2D)	0.2612	1372	200	46.00	9.24	18.41	0.1900	27.25		2		1		
	CB-22-2A-1364 (R2D)	0.2654	1364	212	48.41	8.00	19.09	0.1892	28.71				2		
	CB- 3-3A-1388 (R2D)	0.2585	1388	200	46.01	9.11	17.60	0.1874	27.50	2					1
	Average				47.07	9.47	18.67		28.27						
1730K	CB-25-3A-1729 (R2D)	0.2739	1729	140	41.54	10.82	13.71	0.1934	29.39			2			
	CB-19-3A-1724 (R2D)	0.2643	1724	140	41.55	11.17	14.36	0.1891	28.45			3			
	CB-13-3A-1708 (R2D)	0.2533	1708	140	42.01	9.82	13.01	0.1740	31.30						1
	CB-17-3A-1733 (R2D)	0.2695	1733	140	41.23	9.93	12.45	0.1887	30.09		2		1		
	CB-16-3A-1724 (R2D)	0.2636	1724	140	41.44	9.94	13.66	0.1862	29.36					2	
	CB-15-3A-1735 (R2D)	0.2649	1735	140	41.78	10.77	12.76	0.1856	29.93					2	
	CB-14-3A-1741 (R2D)	0.2627	1741	140	41.63	10.14	13.33	0.1847	29.69					2	
	CB-18-3A-1713 (R2D)	0.2667	1713	140	41.59	10.74	13.69	0.1894	28.98					2	
	CB-12-3A-1746 (R2D)	0.2521	1746	140	41.83	11.02	13.28	0.1791	28.95					2	1
	CB- 5-3A-1735 (R2D)	0.2617	1735	140	41.07	11.15	13.93	0.1870	28.54	2					
	Average				41.67	10.55	13.42		29.47						

TABLE 8

EFFECTIVE THERMAL CONDUCTIVITY OF FURNACE CHAR OF MATERIAL A FORMED AT 600K
MEASURED IN THE ASTM C177 GUARDED HOT PLATE

Average Specimen Mean Temperature K	Total Heat Input Watts	Average Specimen ΔT K	Specimen Gage cm	Specimen Thermal Conductivity $\frac{W}{m/K}$	Time to Temperature hr	Environmental Conditions Press Nitrogen N/M^2
Specimen: AS-2c-2A-600 Run: 6613-50-3Ni Bulk Density: Disc 3, Top: 0.2484 gm/cm³; Initial weight: 3.4719 gm; Final weight: 3.3700 gm Disc 4, Bottom: 0.2383 gm/cm³; Initial weight: 3.3345 gm; Final weight: 3.2340 gm						
422	1.670	47.62	0.483	0.0463	4.0	1333
422	1.680	47.542	0.483	0.0466	4.8	1333
422	2.212	47.328	0.483	0.0616	2.0	101325
422	2.219	47.153	0.483	0.0621	2.5	101325
547	3.220	72.589	0.483	0.0585	3.0	1333
547	3.229	72.783	0.483	0.0585	3.8	1333
548	4.134	73.083	0.483	0.0746	1.8	49329
548	4.124	73.089	0.483	0.0744	2.3	49329
547	4.439	75.750	0.483	0.0773	1.5	101325
547	4.439	75.125	0.483	0.0780	2.0	101325
423	1.673	49.54	0.483	0.0445	3.5	1333
424	1.650	49.37	0.483	0.0441	4.5	1333
420	2.197	48.17	0.483	0.0602	18.8	101325
420	2.235	48.10	0.483	0.0613	19.5	101325
540	3.202	75.48	0.483	0.0560	2.5	1333
540	3.206	75.50	0.483	0.0560	3.0	1333
543	4.072	72.10	0.483	0.0745	1.8	49329
542	4.061	72.20	0.483	0.0742	2.3	49329
545	4.417	75.75	0.483	0.0769	1.5	101325
545	4.417	75.80	0.483	0.0769	2.0	101325

Notes:

1. Diameter of central heater = 4.826 cm.

2. Thermal conductivity values based on measured gage at each temperature level.

3. Time to temperature implies the time elapsed between adjustment of power and obtaining data.

Bulk Density and Specimen Weights

AS-1C-2A Bottom Disc 0.261 gm/cm³; Initial Weight, 3.6610 gm
Final Weight, 3.6605 gm

Top Disc 0.273 gm/cm³; Initial Weight, 3.8399 gm
Final Weight, 3.7884 gm

AS-2C-2A Bottom Disc 0.271 gm/cm³; Initial Weight, 3.8064 gm
Final Weight, 3.6927 gm

Top Disc 0.260 gm/cm³; Initial Weight, 3.6523 gm
Final Weight, 3.5428 gm

TABLE 9

THERMAL CONDUCTIVITY OF FURNACE CHAR OF MATERIAL A FORMED AT 802K
MEASURED IN THE GUARDED COMPARATIVE ROD APPARATUS

Specimen	Measured Temperature K: Top Reference And Guard T1 K	T2 K	T3 K	Specimen And Guard T4 K	T5 K	T6 K	Bottom Reference And Guard T7 K	T8 K	T9 K	ΔT_1 Top Reference K	K_1 Top Reference W/m K	ΔT_2 Bottom Reference K	K_2 Bottom Reference W/m K	ΔT_s Specimen K	Environmental Pressure N/m^2	Mean Temperature Specimen K	Measured Thermal Conductivity W/m K	True Thermal Conductivity Corrected For Radial Heat Exchange and Axial Heat Shunting W/m K
CR-1c-CB-30-2A	629.94	620.11	638.00	583.88	537.82	482.54	442.81	441.31	433.92	8.056	1.1103	8.890	1.0382	101.34	1333	533	0.0623	0.0573
Run: 6613-120-4	629.94	620.16	637.94	583.88	537.82	482.60	442.87	441.48	433.98	8.001	1.1103	8.890	1.0382	101.28	1333	533	0.0622	0.0590
	624.77	613.05	615.94	582.10	544.38	495.93	461.70	459.37	452.03	8.834	1.1103	9.667	1.0527	86.17	101325	539	0.0805	0.0660
Gage Lengths	624.88	613.10	616.05	582.21	544.49	495.98	461.76	459.43	452.09	8.834	1.1103	9.667	1.0527	86.23	101325	539	0.0805	0.0662
Specimen:	871.46	853.96	858.63	808.56	754.23	680.88	623.11	619.49	608.78	12.834	1.1824	14.334	1.1103	127.68	1333	744	0.0842	0.0711
0.4394 cm	871.51	853.96	858.62	808.56	754.28	680.94	623.16	619.61	608.88	12.890	1.1824	14.279	1.1103	127.62	1333	744	0.0842	0.0711
Reference:	875.29	852.75	857.90	805.29	749.62	677.06	619.38	612.22	600.32	17.390	1.1824	19.057	1.1103	128.23	101325	741	0.1125	0.0900
0.6350	875.40	852.79	857.95	805.34	749.78	676.77	619.44	612.27	600.49	17.446	1.1824	18.946	1.1103	128.57	101325	741	0.1132	0.0892
	809.45	794.45	797.50	760.51	719.72	670.28	631.27	625.49	618.27	11.945	1.1536	13.001	1.1103	90.23	49329	715	0.1083	0.0894
	811.62	796.12	799.51	761.23	720.39	670.45	630.83	625.16	617.88	12.112	1.1536	12.945	1.1103	90.78	49329	715	0.1082	0.0885
	597.71	589.49	587.32	562.71	519.76	480.26	448.98	445.15	438.59	10.39	1.1103	10.39	1.0527	82.45	101325	521	0.0937	0.0855
CR-2c-CB-30-2A	597.82	589.71	587.54	562.93	519.99	480.48	449.09	445.31	438.70	10.28	1.1103	10.39	1.0527	82.45	101325	521	0.0936	0.0851
Run: 6613-74-2	519.43	513.65	512.14	491.71	457.65	426.09	401.20	398.53	393.53	7.29	1.0815	7.67	1.0094	65.62	101325	459	0.0828	0.0757
	519.37	513.65	512.04	491.59	457.48	426.08	401.25	398.59	393.53	7.33	1.0815	7.72	1.0094	65.51	101325	459	0.0829	0.0758
Gage Lengths	533.21	528.15	527.32	504.21	467.43	434.04	407.81	406.14	401.31	5.89	1.0959	6.50	1.0382	70.17	1333	469	0.0603	0.0627
Specimen:	535.43	530.38	529.65	506.48	469.65	436.47	410.31	408.64	403.92	5.78	1.0815	6.39	1.0094	70.01	1333	471	0.0630	0.0606
0.4394 cm	862.51	851.84	849.34	811.18	756.67	698.00	649.94	645.38	635.38	13.17	1.1824	14.56	1.1190	113.18	1333	754	0.0970	0.0883
Reference:	869.68	858.57	856.18	818.45	765.17	706.11	656.77	653.39	642.27	13.50	1.1824	14.50	1.1190	112.34	1333	762	0.0988	0.0900
0.6350 cm	841.90	828.84	825.06	791.00	740.17	687.83	643.11	636.44	626.28	16.84	1.1680	16.83	1.1190	103.17	101325	739	0.1285	0.1151
	842.73	829.68	825.84	791.56	740.50	687.89	642.77	636.16	625.82	16.89	1.1680	16.95	1.1190	103.67	101325	740	0.1288	0.1152
	850.46	837.07	833.29	797.73	745.28	690.78	644.00	637.44	626.83	17.17	1.1680	17.17	1.1190	106.95	49329	744	0.1268	0.1132
	853.85	840.51	836.52	800.79	748.00	693.17	646.00	639.22	628.83	17.33	1.1680	17.17	1.1190	107.62	49329	746	0.1269	0.1136

TABLE 10

THERMAL CONDUCTIVITY OF FURNACE CHAR OF MATERIAL A FORMED AT 1127 K
MEASURED IN THE GUARDED COMPARATIVE ROD APPARATUS

Specimen	Measured Temperature K									ΔT_1 Top Reference K	K_1 Top Reference W/m K	ΔT_2 Bottom Reference K	K_2 Bottom Reference W/m K	ΔT_s Specimen K	Environmental Pressure N/m^2	Mean Temperature Specimen K	Measured Thermal Conductivity W/m K	True Thermal Conductivity Corrected For Radial Heat Exchange and Axial Heat Shunting W/m K
	Top Reference And Guard			Specimen And Guard			Bottom Reference And Guard											
	T-1 K	T-2 K	T-3 K	T-4 K	T-5 K	T-6 K	T-7 K	T-8 K	T-9 K									
CR-1C-CB-27-3A Run: 6613-83-CR-2 Gage Lengths Specimen: 0.4064 cm Reference: 0.6350 cm	685.44	673.61	671.33	636.05	587.77	543.60	502.54	499.93	487.93	14.11	1.1248	14.61	1.0642	92.45	1333	590	0.1089	0.1031
	685.50	658.66	671.39	636.11	589.88	543.66	502.60	499.98	487.99	14.11	1.1248	14.61	1.0642	92.45	1333	590	0.1089	0.1037
	675.44	664.28	659.44	625.66	578.77	533.37	493.10	487.98	475.99	16.00	1.1276	17.11	1.0671	92.29	101325	579	0.1257	0.1155
	675.50	664.33	659.50	625.72	578.77	533.38	493.04	487.98	475.93	16.00	1.1276	17.11	1.0671	92.34	101325	579	0.1259	0.1155
	1155.31	1131.31	1124.20	1075.75	1031.30	965.19	908.91	904.07	875.69	31.11	1.2834	33.22	1.1868	110.56	1333	1020	0.2296	0.2029
	1155.42	1126.42	1124.31	1075.86	1031.42	965.35	909.07	904.13	875.85	31.11	1.2834	33.22	1.1868	110.51	1333	1020	0.2299	0.2035
	1140.81	1118.98	1111.31	1071.53	1030.86	974.97	928.02	919.52	896.96	29.50	1.2834	31.06	1.1839	96.56	49329	1023	0.2474	0.2150
	1140.87	1119.53	1111.37	1071.64	1030.97	975.08	928.19	919.68	897.13	29.50	1.2834	31.06	1.1839	96.56	49329	1023	0.2472	0.2157
	1140.31	1118.70	1111.20	1072.42	1031.92	978.58	932.69	923.80	901.69	29.11	1.2834	31.00	1.1839	93.84	101325	1025	0.2524	0.2210
	1140.15	1118.53	1110.93	1072.31	1031.69	978.36	932.52	923.63	901.52	29.22	1.2834	31.00	1.1839	93.95	101325	1025	0.2524	0.2210

TABLE 11

THERMAL CONDUCTIVITY OF FURNACE CHAR OF MATERIAL A FORMED AT 1372 K
MEASURED IN THE GUARDED COMPARATIVE ROD APPARATUS

Specimen	Measured Temperature K									ΔT_1 Top Reference K	K_1 Top Reference W/m K	ΔT_2 Bottom Reference k	K_2 Bottom Reference W/m K	ΔT_2 Specimen K	Environmental Pressure N/m^2	Mean Temperature Specimen K	Measured Thermal Conductivity W/m K	True Thermal Conductivity Corrected For Radial Heat Exchange and Axial Heat Shunting W/m K
	Top Reference And Guard			Specimen And Guard			Bottom Reference And Guard											
	T-1 K	T-2 K	T-3 K	T-4 K	T-5 K	T-6 K	T-7 K	T-8 K	T-9 K									
CR-1C-CB-6-3A Run: 6613-77-2 Gage Lengths	861.24	845.57	838.24	802.95	757.00	719.61	675.61	665.78	650.72	23.00	1.1680	24.89	1.1248	83.34	101325	761	0.1915	0.1774
	861.24	845.62	838.24	803.01	757.23	719.67	675.61	665.78	650.72	23.00	1.1680	24.89	1.1248	83.34	101325	761	0.1915	0.1774
Specimen: 0.3696 cm Reference: 0.6350 cm	861.35	848.35	842.29	803.68	755.56	715.90	664.94	658.00	644.61	19.06	1.1680	20.33	1.1248	87.78	1333	760	0.1495	0.1417
	861.51	848.46	842.40	803.73	755.62	715.95	665.00	658.11	644.78	19.11	1.1680	20.22	1.1248	87.78	1333	760	0.1497	0.1420
	568.27	560.99	556.55	532.49	504.76	470.43	440.81	436.53	426.81	11.72	1.0959	14.00	1.0382	62.06	101325	501	0.1285	0.1203
	568.49	561.16	556.77	532.65	504.98	470.59	440.98	436.76	426.92	11.72	1.0959	14.06	1.0382	62.06	101325	501	0.1288	0.1206
	563.93	557.10	552.54	529.76	504.48	471.59	443.87	440.59	431.04	11.39	1.0959	12.83	1.0382	58.17	49329	500	0.1330	0.1213
	562.38	557.16	550.99	529.82	504.60	471.59	443.92	440.70	431.14	11.39	1.0959	12.78	1.0382	58.23	49329	500	0.1289	0.1128
	559.04	555.32	551.37	529.10	505.71	475.82	447.42	445.92	437.97	7.67	1.0959	9.45	1.0382	53.28	1333	502	0.0994	0.0970
	559.10	555.38	551.43	529.15	-	475.81	447.42	445.92	437.97	7.67	1.0959	9.45	1.0382	53.34	1333	502	0.0995	0.0969

TABLE 12

THERMAL CONDUCTIVITY OF FURNACE CHAR OF MATERIAL A FORMED AT 1375K
MEASURED IN THE RADIAL INFLOW APPARATUS

	Time	Outer Face Temperature K	Average ΔT of Each Strip K	Heat Flow to Calorimeter Watts	Average Mean Temperature of Specimen K	Average Thermal Conductivity $\frac{W}{mK}$	Environmental Pressure $\frac{N}{m^2}$
Specimen No. R1-1c-CB-8 & 9-3A	On 11:00		188				
			-				
Run: 6228-100-69-3-GFE	Read 12:30		183 192				
Initial Thickness 0.254 cm	Avg.		188	12	838	0.136	1333
			197				
Final Thickness 0.248 cm			-				
			187				
	1:30		198				
	Avg.		195	18	831	0.187	101325
			210				
			-				
			210				
	2:55		217				
	Avg.		212	27	1240	0.265	1333
			236				
			-				
			230				
	3:25		241				
	Avg.		236	38	1243	0.329	49329
			238				
			-				
			231				
	3:40		242				
	Avg.		237	39	1237	0.335	101325
Specimen No. R1-2c-CB-10 & 11-3A	On 8:00		151 151 146				
			150				
Run: 6228-110-69-3-GFE	9:20 Avg.		149	13	833	0.174	1333
			163				
Initial Thickness 0.254 cm			161 153				
Final Thickness 0.246 cm			158				
	10:10						
	Avg.		159	18	808	0.235	101325
			174				
			173				
			167				
			168				
	11:25						
	Avg.	1339	170	24	1267	0.288	1333
			202				
			192				
			190				
			192				
	12:00						
	Avg.	1334	195	31	1249	0.327	49329
			206				
			202				
			193				
			196				
	12:45						
	Avg.	1340	199	34	1250	0.345	101325

TABLE 13

THERMAL CONDUCTIVITY OF FURNACE CHAR OF MATERIAL A FORMED AT 1733 K
MEASURED IN THE GUARDED COMPARATIVE ROD APPARATUS

Specimen	Measured Temperature K									ΔT_1 Top Reference K	K_1 Top Reference W/m K	ΔT_2 Bottom Reference K	K_2 Bottom Reference W/m K	ΔT_2 Specimen K	Environmental Pressure N/m^2	Mean Temperature Specimen K	Measured Thermal Conductivity W/m K	True Thermal Conductivity Corrected For Radial Heat Exchange and Axial Heat Shunting W/m K
	Top Reference And Guard			Specimen And Guard			Bottom Reference And Guard											
	T-1 K	T-2 K	T-3 K	T-4 K	T-5 K	T-6 K	T-7 K	T-8 K	T-9 K									
CR-1c-CB-17-3A Run: 6613-80-2 Specimen: 0.3810 cm Reference: 0.6350 cm	813.68	798.45	788.79	744.95	703.11	651.55	610.72	601.05	584.61	24.89	1.1536	26.11	1.1103	93.40	101325	698	0.1846	0.1736
	813.84	798.62	788.89	745.06	703.22	651.72	610.85	601.16	584.68	24.95	1.1536	26.17	1.1103	93.34	101325	698	0.1846	0.1739
	822.29	806.73	801.45	755.12	711.17	658.33	615.38	610.22	593.21	20.84	1.1536	22.17	1.1103	96.79	1333	706	0.1514	0.1429
	822.57	806.90	801.68	755.17	711.00	658.44	615.60	610.38	593.43	20.89	1.1536	22.17	1.1103	96.73	1333	702	0.1514	0.1429
	713.39	699.83	692.94	654.16	615.22	570.43	535.21	526.65	513.65	20.45	1.1248	21.56	1.0815	83.73	101325	612	0.1658	0.1554
	1142.59	1124.59	1113.14	1074.64	1033.86	989.19	947.41	934.24	914.96	29.45	1.2834	32.45	1.1969	85.45	101325	1031	0.2682	0.2479
	1142.76	1124.70	1113.31	1074.70	1033.92	989.25	947.46	934.35	915.07	29.45	1.2834	32.39	1.1969	85.45	101325	1031	0.2682	0.2477
	1172.87	1158.04	1144.92	1105.59	-	1015.47	970.47	955.52	935.69	27.95	1.3122	34.78	1.1969	90.12	49329	1060	0.2567	0.2465
	1156.31	1138.15	1129.64	1094.36	1058.75	1012.35	969.74	963.69	940.90	26.67	1.2978	28.84	1.1969	82.01	1333	1053	0.2538	0.2310
	1151.81	-	1125.70	1092.31	1056.64	1010.75	968.36	962.19	940.25	26.11	1.2978	28.11	1.1969	81.56	1333	1051	0.2480	0.2245

TABLE 14

THERMAL CONDUCTIVITY OF FURNACE CHAR OF MATERIAL A FORMED AT 1728K
MEASURED IN THE RADIAL INFLOW APPARATUS

	Time	Outer Face Temperature K	Average ΔT of Each Strip K	Heat Flow to Calorimeter Watts	Average Mean Temperature of Specimen K	Average Thermal Conductivity $\frac{W}{mK}$	Environmental Pressure $\frac{N}{m^2}$
Specimen No.	On		109				
R1-1c-CB-16	7:30		109				
& 18-3A			107				
Run: 6228-120-			106				
69-3-GFE	8:30						
Initial Thickness	Avg.		107	8	825	0.167	1333
0.254 cm							
Final Thickness			132				
0.245 cm			128				
			125				
			128				
	9:00						
	Avg.		128	13	803	0.218	101325
			127				
			125				
			119				
			117				
	10:10						
	Avg.	1418	122	19	1375	0.319	1333
			168				
			164				
			162				
			158				
	10:50						
	Avg.	1416	163	34	1353	0.424	101325
			133				
			133				
			134				
			129				
	12:25						
	Avg.	1729	132	27	1628	0.411	1333
			159				
			157				
			161				
			155				
	1:30						
	Avg.	1722	158	42	1625	0.542	49329
			166				
			157				
			168				
			165				
	2:15						
	Avg.	1729	164	45	1614	0.551	101325
Specimen No.	On						
R1-2c-CB-14	7:20		134				
& 15-3A			141				
Run: 6228-134-			134				
69-3-GFE			139				
Initial Thickness	8:40						
0.254 cm	Avg.		137	7	798	0.110	1333
Final Thickness			156				
0.242 cm			159				
			151				
			158				
	9:20						
	Avg.		156	13	801	0.169	101325
			161				
			176				
			163				
			170				
	10:20						
	Avg.	1418	168	19	1327	0.231	1333
			200				
			210				
			198				
			203				
	11:10						
	Avg.	1424	203	31	1323	0.301	101325
			192				
			204				
			199				
			202				
	12:15						
	Avg.	1722	199	48	1601	0.483	101325
			198				
			198				
			188				
			205				
	1:25						
	Avg.	1716	197	42	1589	0.425	49329
			172				
			183				
			168				
			175				
	2:10						
	Avg.	1724	174	30	1613	0.336	1333

Mean temperature below 2000°F calculated as the average of thermocouple readings.
Mean temperature above 2000°F is the average of hot and cold hole temperatures.

$$K = \frac{\ln (R_o/R_i)}{2\pi L} \frac{Q}{\Delta T}$$

where

K = thermal conductivity
R_o = outside radius = 0.437 in.
R_i = inside radius = 0.233 in.
Q = heat to calorimeter
ΔT = temperature drop from hot to cold hole on the outside and inside radius, respectively
L = gage length of calorimeter = 0.500 in.

TABLE 15

QUANTITATIVE EXAMINATION OF STRUCTURES OF FURNACE CHARS OF MATERIAL A FORMED AT TEMPERATURES FROM 800K to 1700K

	Maximum Temp K	Photo of Structure Figure Nos.	Avg Gap Width cm	Gap Length cm	Gap Area Per Cell cm^2	Total Area Per Cell cm^2	Gap Area Per Cell %
Comparative Rod Specimens							
CR-1C-CB-30-2A	802	45	0.0432	3.7236	0.1609	1.1055	14.55
CR-2C-CB-30-2A	802	46	0.0706	3.6424	0.2578	1.0570	24.38
	Average	-	0.0569	3.6830	0.2093	1.0816	19.46
CR-1C-CB-27-3A	1127	48	0.0467	3.4290	0.1602	0.9368	17.10
CR-1C-CB-6-3A	1372	50	0.0424	3.4849	0.1480	0.9678	15.28
CR-1C-CB-17-3A	1733	56	0.0340	3.5408	0.1208	0.9989	12.09
Radial Inflow Specimens							
R1-1C-CB- 8 & 9-3A	1380	51-52	0.0203	3.4087	0.0692	0.9259	8.70
R1-1C-CB-10 & 11-3A	1370	53-54	0.0279	3.566	0.0995	0.9995	9.95
	Average	-	0.0241	3.4874	0.0840	0.9627	8.70
R1-1C-CB-16 & 18-3A	1720	57	0.0643	3.5814	0.2303	1.0208	22.59
R1-2C-CB-14 & 15-3A	1740	58	0.0564	3.6881	0.2080	1.0850	19.16
	Average	-	0.0602	3.6347	0.2188	1.0531	20.88

TABLE 16

BOXING ANALYSIS OF THERMAL CONDUCTIVITY DATA
MEASURED ON FURNACE CHARS

Temperature of Char Formation K	Environmental Pressure N/m^2	k_m W/m K	A_s %	k_{cd} W/m K	k_r W/m K	k_c W/m K	$\frac{k_m - k_c}{KM}$ %
600	101325	0.0830	0	-	-	0.0830	
	49329	0.0805	0	-	-	0.0805	
	1333	0.0620	0	-	-	0.0620	
802	101325	0.110	19.5	0.055	0.11	0.099	10%
	49329	0.107	19.5	0.055	0.11	0.095	12%
	1333	0.085	19.5	0.055	0.11	0.068	20%
1127	101325	0.245	17.1	0.068	0.27	0.225	10%
	49329	0.240	17.1	0.068	0.27	0.219	10%
	1333	0.230	17.1	0.068	0.27	0.208	10%
1375	101325	0.390	8.7	0.078	0.22	0.399	10%
	49329	0.375	8.7	0.078	0.22	0.382	10%
	1333	0.320	8.7	0.078	0.22	0.322	10%
1728	101325	0.575	20.8	0.097	0.68	0.524	10%
	49329	0.535	20.8	0.097	0.68	0.473	12%
	1333	0.430	20.8	0.097	0.68	0.342	20%

k_m - Effective thermal conductivity as measured

A_s - Area fraction of gap or separation between honeycomb and filler

k_{cd} - Effective thermal conductivity of the gas within the gap

k_r - Effective thermal conductivity through the gap due to thermal radiation

k_c - Effective thermal conductivity of the "solid" phase. Contribution to heat transfer by the gap is removed

Equation for calculation

$$k_c = \frac{k_m - A_s (k_{cd} + k_r)}{1 - A_s}$$

TABLE 17

BULK DENSITY OF FURNACE CHAR OF MATERIAL A FORMED
AT TEMPERATURES FROM 600K TO 1700K
(MEASUREMENTS MADE ON MACHINED SPECIMENS)

Specimen No	Maximum Temperature K	Length cm	Width cm	Thickness cm	Weight gm	Bulk Density gm/cm^3	Remarks
Total Composite							
Pe-1c-CB-27-2A	603	0.8166	*2.5146	-	0.9925	0.2447	
Pe-2c-CB-27-2A	603	0.8166	*2.5146	-	1.0447	0.2576	
AS-2c-2A (3)[1]	600	0.7427	*4.7940	-	3.4719	0.2589	
AS-2c-2A (4)[1]	600	0.7412	*4.8000	-	3.335	0.2486	
BD-1-CB-24-3A	592	7.1770	3.2370	1.6840	9.4394	0.2412	
Average = 600					Average =	0.2502	
Pe-1c-CB-30-2A	802	0.6617	*2.5400	-	0.5613	0.1674	
Pe-2c-CB-30-2A	802	0.6617	*2.5400	-	0.4842	0.1444	
CR-1c-CB-30-2A	802	0.4394	*2.5400	-	0.5895	0.1676	
CR-2c-CB-30-2A	802	0.4394	*2.5400	-	0.6021	0.1713	
BD-1-CB-22-3A	829	6.9253	3.2205	1.5423	5.5075	0.1601	
Average = 807					Average =	0.1621	
Pe-1c-CB-31-2A	1111	0.5850	*2.5400	-	0.5506	0.1857	
Pe-2c-CB-31-2A	1111	0.6248	*2.5400	-	0.5291	0.1671	
BD-1-CB-29-2A	1137	4.5791	2.9007	1.3797	3.5925	0.1960	
Average =1120					Average =	0.1829	
Pe-1c-CB-6-3A	1372	0.6223	*2.5400	-	0.5272	0.1671	
Pe-2c-CB-6-3A	1372	0.6223	*2.5400	-	0.5446	0.1727	
BD-1-CB-26-3A	1354	7.2941	3.3025	1.4409	6.4812	0.1867	
R1-1c-CB-8 & 9-3A	1380	6.3500	2.2606	0.2540	0.7507	0.2058	
R1-2c-CB-10 &11-3A	1370	6.3500	2.2606	0.2540	0.6674	0.1830	
Average =1370					Average =	0.1830	
BD-1-CB-25-3A	1729	4.2113	3.6932	0.8821	2.5365	0.1848	Core
BD-1-CB-12-3A	1746	6.3630	4.5301	0.1314	0.8475	0.2237	Crust
BD-1-CB-19-3A	1724	5.7404	3.1570	0.1041	0.4994	0.2489	Crust
BD-2-CB-19-3A	1724	5.3365	3.1547	0.141	0.4365	0.2646	Crust
Pe-1c-CB-17-3A	1733	0.1524	*2.5400	-	0.1810	0.2343	Crust
Pe-2c-CB-17-3A	1733	0.1524	*2.5400	-	0.1945	0.2518	Crust
Average =1732					Average =	0.2446	Crust
BDF-1-CB-23-3A	821	1.6109	0.7005	0.6993	0.1191	0.1509	
BDF-2-CB-23-3A	821	1.6358	0.7269	0.7140	0.1214	0.1430	No Impregnant Used
BDF-3-CB-23-3A	821	1.6261	0.7180	0.7086	0.1251	0.1511	
					Average =	0.1483	
BDF-1-CB-21-3A	1366	1.3487	(0.6350)	-	0.0738	0.1728	
BDF-2-CB-21-3A	1366	1.2700	(0.6350)	-	0.0708	0.1760	
BDF-3-CB-21-3A	1366	1.0958	(0.6350)	-	0.0642	0.1850	
BDF-4-CB-21-3A	1366	1.2065	(0.6358)	-	0.0800	0.1795	
					Average =	0.1783	

*Diameter

[1]Density determined on specimen AS-2c-2A (3) & (4) after charring at 600K prior to Thermal Conductivity run

TABLE 18

TRUE DENSITY OF THE FURNACE CHARS
OF MATERIAL A FORMED AT TEMPERATURES
FROM 600 to 1700K

Specimen No.	Maximum Temperature of Formation K	True Density at 299 K gm/cm^3	Remarks
TD-CB-24-3A	592	1.39	
TD-CB-22-3A	829	1.51	
TDF-CB-23-3A	821	1.42	Filler only
TD-CB-29-2A	1137	2.01	
TD-CB-26-3A	1354	1.95	
TDF-CB-21-3A	1366	1.80	Filler only
TD-CB-25-3A	1729	1.75	Core
TD-CB-19-3A	1724	1.83	Crust

TABLE 19

TOTAL POROSITY OF THE FURNACE
AND ARC JET CHARS OF MATERIAL A

Temperature of Char Formation K	True Density gm/cm^3	Bulk Density gm/cm^3	Total Porosity %
Total Composite			
600	1.39	0.2502	82
807	1.51	0.1621	89
1120	2.01	0.1829	91
1370	1.95	0.1830	91
1732 (Crust)	1.83	0.2446	87
1729 (Core)	1.75	0.1848	89
Filler Only			
821	1.42	0.1483	90
1366	1.80	0.1783	90
Arc Jet Filler			
Zone 2 (1250-1550)	1.93	0.2061	89
Zone 3 (900-1250)	2.16	0.2070	90

TABLE 20

ENTHALPY OF THE FURNACE CHAR OF MATERIAL A FORMED AT 800K
MEASURED IN THE ADIABATIC CALORIMETER

Specimen and Run Number	Initial Cup Temp. K	Final Cup Temp. K	Change in Cup Temp. K	Initial Sample Temp. K	Time at Temp. Min	Initial Wt. of Sample g	Final Wt. of Sample g	Enthalpy 303 K Reference J/g	Enthalpy 273K Reference J/g
CB-25-2A-818 (R2D) - 1									
Run No. 1	296.376	297.103	0.727	422.26	20	2.2600	2.2106	135.59	163.50
Run No. 2	297.954	299.880	1.926	587.82	20	2.2106	2.1682	386.78	414.69
Run No. 3	298.492	301.784	3.292	813.40	20	2.1682	1.9927	715.65	743.56
Run No. 4 6613-108	295.857	299.122	3.265	819.51	20	1.9927	1.9288	727.68	754.49
CB-25-2A-818 (R2D) - 2									
Run No. 1	297.136	297.907	0.770	424.48	20	2.3696	2.1505	159.78	187.69
Run No. 2	298.761	300.741	1.980	592.10	20	2.1505	2.0997	437.25	465.16
Run No. 3 6613-108	299.519	302.939	3.420	811.18	20	2.0997	1.9279	824.26	852.17

TABLE 21

ENTHALPY OF THE FURNACE CHAR OF MATERIAL A FORMED AT 1100K
MEASURED IN THE ADIABATIC CALORIMETER

Specimen and Run Number	Initial Cup Temp. K	Final Cup Temp. K	Change in Cup Temp. K	Initial Sample Temp. K	Time at Temp. Min	Initial Wt. of Sample g	Final Wt. of Sample g	Enthalpy 303 K Reference J/g	Enthalpy 273K Reference J/g
CB-26-2A-1100 (R2D) - 1									
Run No. 1	296.733	297.649	0.916	423.09	20	3.5170	3.4258	122.10	147.69
Run No. 2	298.686	300.983	2.297	588.55	20	3.4258	3.3790	320.96	348.40
Run No. 3 6613-110	299.544	304.058	4.514	812.54	20	3.3790	3.2910	659.13	684.72
CB-26-2A-1100 (R2D) - 2									
Run No. 1	297.624	298.660	1.036	420.59	20	4.0225	3.9199	119.08	144.66
Run No. 2	300.169	302.810	2.641	587.10	20	3.9199	3.8625	320.50	348.40
Run No. 3 6613-110	299.001	304.042	5.041	818.12	20	3.7773	3.6389	658.43	684.02

TABLE 22

ENTHALPY OF THE FURNACE CHAR OF MATERIAL A FORMED AT 1100K MEASURED IN THE ICE CALORIMETER

Specimen Number	SRI Log Number	Drop Temperature K	Initial Weight Grams	Final Weight Grams	Enthalpy 273K Reference J/g
CB-26-2A-1100 (R2D)-1	6613-124 Run #1	1142	3.3261	3.2113	1397.11
CB-26-2A-1100 (R2D)-2	6613-117 Run #1	810	3.4647	3.3509	757.28
	Run #2	1142	3.3509	3.2746	1381.29

TABLE 23

ENTHALPY OF FURNACE CHAR OF MATERIAL A FORMED AT 1390K
MEASURED IN THE ADIABATIC CALORIMETER

Specimen and Run Number	Initial Cup Temp. K	Final Cup Temp. K	Change in Cup Temp. K	Initial Sample Temp. K	Time at Temp. Min	Initial Wt. of Sample g	Final Wt. of Sample g	Enthalpy 303 K Reference J/g	Enthalpy 273K Reference J/g
CB-3-3A-1388 (R2D)-1									
Run #1	297.019	299.010	1.991	531.99	20	3.8305	3.7784	242.81	268.40
Run #2 6613-113	298.686	303.543	4.857	812.01	20	3.7784	3.7271	614.48	640.06
CB-3-3A-1388 (R2D)-2									
Run #1	298.953	300.805	1.852	531.99	20	3.6287	3.5789	237.23	262.82
Run #2 6613-113	300.732	305.266	4.534	815.34	20	3.5415	3.3919	625.87	651.46

TABLE 24

ENTHALPY OF THE FURNACE CHAR OF MATERIAL A FORMED AT 1390K MEASURED IN THE ICE CALORIMETER

Specimen Number	SRI Log Number	Drop Temperature K	Initial Weight Grams	Final Weight Grams	Enthalpy 273K Reference J/g
CB-3-3A-1388 (R2D) -1	6613-124 Run #1	1141	3.4184	3.3573	1248.72
	Run #2	1367	3.3573	3.2871	1722.95
CB-3-3A-1388 (R2D) -2	6613-117 Run #1	815	3.1081	3.0501	771.70
	Run #2	1143	3.0501	3.0265	1300.12
	Run #3	1361	3.0265	2.9671	1710.39

TABLE 25

ENTHALPY OF THE FURNACE CHAR OF MATERIAL A FORMED AT 1735K
MEASURED IN THE ADIABATIC CALORIMETER

Specimen and Run Number	Initial Cup Temp. K	Final Cup Temp. K	Change in Cup Temp. K	Initial Sample Temp. K	Time at Temp. Min	Initial Wt. of Sample g	Final Wt. of Sample g	Enthalpy 303 K Reference J/g	Enthalpy 273K Reference J/g
HC-1-CB-5-3A Run #1	298.124	300.145	2.021	536.15	20	3.9199	3.8704	242.35	267.93
Run #2 6613-115	298.483	303.472	4.989	811.73	20	3.8704	3.8274	615.87	641.46
HC-2-CB-5-3A Run #1	300.048	302.230	2.182	536.43	20	4.5472	4.4901	229.56	255.14
Run #2 6613-115	300.411	305.894	5.483	809.51	20	3.9269	3.8699	664.48	690.06

TABLE 26

ENTHALPY OF THE FURNACE CHAR FORMED AT 1740K OF MATERIAL A MEASURED IN THE ICE CALORIMETER

Specimen Number	SRI Log Number	Drop Temperature K	Initial Weight Grams	Final Weight Grams	Enthalpy 273K Reference J/g
CB-5-3A-1735 (R2D)-1	6613-125 Run #1	1146	2.7734	2.7268	1267.79
	Run #2	1367	2.7268	2.6998	1689.23
	Run #3	1727	2.6998	2.2671	2287.19
CB-5-3A-1735 (R2D)-2	6613-123 Run #1	1142	3.0512	3.0361	1259.65
	Run #2	1369	3.0361	3.0067	1651.32
	Run #3	1401	3.0067	2.9434	1661.78
	Run #4	1727	2.9434	2.5031	2277.42

TABLE 27

THE PERMEABILITY OF THE FURNACE CHAR OF MATERIAL A FORMED AT 603 K

Permeating Gas	Gage Pressure at Flowmeter (N/m^2)	Pressure Drop through Specimen (P_2-P_1) ΔP (N/m^2)	Downstream Gage Pressure P_1 (N/m^2)	Absolute Mean Specimen Pressure P_m (N/m^2)	Downstream Gas Temperature K	Volumetric Flow Rate Corrected to Standard Conditions Q_{stp} (cm^3/sec)	(1) $\frac{MP_m\Delta P}{LTR\mu G}$ (cm^{-2})	(1) $\frac{G}{\mu}$ (cm^{-1})
Specimen: Pe-1c-27-2A; A = 4.98 cm^2; L = 0.816 cm; Density = 0.2447 gm/cm^3								
Run: 1								
Nitrogen	41300	5090	1.74	103847	295	30	61.2×10^6	40
	41300	13030	4.98	107820	295	78	62.3	104
	41300	21050	7.47	111832	295	132	61.7	176
	41300	29300	12.4	115962	295	191	61.8	253
	79300	35100	16.2	118866	295	240	60.3	318
	79300	46300	24.9	124475	295	294	68.1	389
	79300	57000	37.4	129837	295	400	64.2	531
	79300	67800	49.8	135250	295	480	66.2	636
	79300	78300	69.8	140520	295	562	68.1	744
Nitrogen	89600	90700	92.2	146742	295	647	71.3	857
Run 2								
Nitrogen	41300	6430	-0-	104515	295	30	77.8	40
	41300	15730	2.49	109167	295	78	76.2	104
	41300	25550	6.72	114082	295	132	76.3	176
	41300	35100	12.5	118862	295	191	75.8	253
	79300	53600	28.6	128129	295	294	81.1	389
	79300	76300	59.8	139510	295	480	76.9	636
	79300	81200	69.8	141970	295	520	76.7	689
	103300	105200	114.0	154014	295	647	87.0	857
Helium	75800	24100	1.99	113352	295	131	63.3	22
	75800	32700	3.74	117654	295	187	62.4	32
	75800	40500	5.73	121556	295	241	62.0	41
	75800	49300	8.72	125959	295	296	63.7	50
	75800	57500	11.2	130061	295	359	63.2	60
	75800	64700	14.2	133664	295	412	63.7	69
Helium	75800	73300	18.2	137968	295	485	63.2	82

TABLE 27 (CONTINUED)

Permeating Gas	Gage Pressure at Flowmeter (N/m^2)	Pressure Drop through Specimen (P_2-P_1) ΔP (N/m^2)	Downstream Gage Pressure P_1 (N/m^2)	Absolute Mean Specimen Pressure P_m (N/m^2)	Downstream Gas Temperature K	Volumetric Flow Rate Corrected to Standard Conditions Q_{stp} (cm^3/sec)	(1) $\frac{MP_m\Delta P}{LTR\mu G}$ (cm^{-2})	(1) $\frac{G}{\mu}$ (cm^{-1})
Specimen: Pe-2c-27-2A; A = 4.98 cm^2; L = 0.816 cm; Density = 0.2576 gm/cm^3								
Run: 1								
Nitrogen	41300	6780	0.75	104691	295	30	82.0×10^6	40
	41300	16600	3.24	109603	295	78	80.6	104
	41300	25500	6.23	114056	295	132	76.2	176
	41300	35400	10.5	119010	295	191	76.6	253
	82800	55300	24.9	128975	295	294	84.1	389
	82800	79100	54.8	140905	295	480	80.6	636
Nitrogen	103300	97900	88.4	150338	295	619	82.3	822
Helium	103300	39300	6.25	120956	295	206	77.7	31
	103300	63200	12.4	132912	295	358	71.3	60
	103300	85800	19.9	144220	295	525	71.7	88
Helium	103300	96500	24.9	149575	295	614	71.3	97
Run: 2	68900	10770	1.99	106687	539	34	38.5	28
Nitrogen	68900	26950	8.72	114784	539	88	40.5	73
	68900	41200	20.4	121920	539	146	39.7	121
	68900	60400	39.3	131539	544	210	43.5	174
	103300	64700	46.8	133722	539	258	38.7	213
	103300	89300	80.7	146031	544	344	43.8	284
Nitrogen	103300	103200	99.6	153000	544	396	46.1	326
Helium	103300	49250	12.9	125938	525	21	37.9	21
Helium	103300	75100	24.4	138874	524	322	36.7	36
Helium	103300	102100	44.3	152394	524	449	39.4	50
Run: 3	41300	4070	2.00	103337	295	30	48.6	40
Nitrogen	41300	9930	4.98	106270	295	78	46.8	104
	41300	16200	11.2	109411	295	132	46.5	176
	41300	23050	17.9	112843	295	191	47.2	253
	103300	19040	13.7	110834	295	174	44.0	220
	103300	39700	44.3	121194	295	345	48.3	458
	103300	59700	85.8	131236	295	518	52.5	687
	103300	79000	138.0	140938	295	691	55.8	918
Nitrogen	103300	97800	207.0	150407	295	863	59.1	1145
Helium	103300	24160	8.22	113388	295	206	44.8	31

TABLE 27 (CONTINUED)

Permeating Gas	Gage Pressure at Flowmeter (N/m^2)	Pressure Drop through Specimen (P_2-P_1) ΔP (N/m^2)	Downstream Gage Pressure P_1 (N/m^2)	Absolute Mean Specimen Pressure P_m (N/m^2)	Downstream Gas Temperature K	Volumetric Flow Rate Corrected to Standard Conditions Q_{stp} (cm^3/sec)	(1) $\frac{MP_m\Delta P}{LTR\mu G}$ (cm^{-2})	(1) $\frac{G}{\mu}$ (cm^{-1})
Helium	103300	41200	17.4	121917	295	358	42.6	60
	103300	56800	32.4	129732	295	525	42.6	88
	103300	69000	47.8	135848	295	672	42.3	113
	103300	100300	89.7	151540	295	1078	42.8	181

TABLE 28

THE PERMEABILITY OF THE FURNACE CHAR OF MATERIAL A FORMED AT 802 K

Permeating Gas	Gage Pressure at Flowmeter (N/m^2)	Pressure Drop through Specimen (P_2-P_1) ΔP (N/m^2)	Downstream Gage Pressure P_1 (N/m^2)	Absolute Mean Specimen Pressure P_m (N/m^2)	Downstream Gas Temperature K	Volumetric Flow Rate Corrected to Standard Conditions Q_{stp} (cm^3/sec)	(1) $\frac{MP_m\Delta P}{LTR\mu G}$ (cm^{-2})	(1) $\frac{G}{\mu}$ (cm^{-1})
Specimen: Pe-1c-30-2A; A = 5.08 cm^2; L = 0.652 cm; Density = 0.1674 gm/cm^3								
Run: 1								
Nitrogen	41300	4.98	-0-	101302	295	31	0.0688 x 10^6	40
	41300	14.9	-0-	101308		80	0.0792	104
	41300	29.9	4.98	101318		132	0.0951	172
	41300	49.8	9.96	101330		192	0.1104	249
	79300	67.2	14.9	101341		240	0.119	312
	79300	107	24.9	101369		321	0.142	418
	79300	159	37.4	101403		401	0.169	521
	79300	219	52.3	101443		481	0.194	627
	79300	299	72.3	101494		565	0.226	735
	79300	361	89.7	101537		642	0.239	838
	79300	448	112	101595		727	0.263	946
	79300	538	137	101655		802	0.286	1043
	79300	643	162	101722		883	0.311	1150
	79300	749	190	101794		965	0.332	1253
	79300	866	222	101872		1046	0.353	1362
	79300	991	254	101955		1127	0.376	1460
	79300	1133	289	102048		1210	0.402	1570
Nitrogen	79300	1287	329	102149	295	1286	0.428	1680
Specimen: Pe-2c-30-2A; A = 5.08 cm^2; L = 0.652 cm; Density = 0.1444 gm/cm^3								
Run: 1								
Nitrogen	41300	12.4	2.49	101308	295	80	0.0658 x 10^6	104
	41300	24.9	7.47	101320	295	132	0.801	172
	41300	44.3	12.4	101334	295	192	0.0983	249
	79300	27.4	8.72	101322	295	160	0.0727	208
	79300	89.2	24.9	101374	295	321	0.118	418
	79300	172	49.8	101444	295	481	0.152	627
	79300	280	84.7	101536	295	642	0.185	838
	79300	443	136	101675	295	802	0.236	1043
	79300	615	192	101823	295	965	0.273	1253
	79300	822	259	102002	295	1127	0.313	1460
Nitrogen	79300	1063	338	102211	295	1286	0.354	1680

TABLE 29

THE PERMEABILITY OF THE FURNACE CHAR OF MATERIAL A FORMED AT 1111K

Permeating Gas	Gage Pressure at Flowmeter (N/m^2)	Pressure Drop through Specimen (P_2-P_1) ΔP (N/m^2)	Downstream Gage Pressure P_1 (N/m^2)	Absolute Mean Specimen Pressure P_m (N/m^2)	Downstream Gas Temperature K	Volumetric Flow Rate Corrected to Standard Conditions Q_{stp} (cm^3/sec)	(1) $\frac{MP_m\Delta P}{LTR\mu G}$ (cm^{-2})	(1) $\frac{G}{\mu}$ (cm^{-1})
Specimen: Pe-1c-31-2A; A = 5.08 cm^2; L = 0.586 cm; Density = 0.1857 gm/cm^3								
Run: 1								
Nitrogen	41300	28.6	4.98	101320	295	80	0.176×10^6	104
	41300	61.1	8.72	101340	295	132	0.228	172
	41300	106	13.7	101367		192	0.273	249
	79300	68.4	4.98	101339		160	0.210	208
	79300	227	24.9	101432		321	0.349	418
	79300	433	52.3	101576		481	0.434	627
	79300	734	99.6	101778		642	0.565	838
	79300	1085	149	102010		802	0.658	1043
	79300	1500	207	102279		965	0.774	1253
	79300	1980	276	102598		1127	0.878	1460
Nitrogen	79300	2430	346	102906	295	1286	0.945	1680
Specimen: Pe-2c-31-2A; A = 5.08 cm^2; L = 0.625 cm; Density = 0.1671 gm/cm^3								
Run: 1								
Nitrogen	41300	24.9	3.74	101316	295	80	0.144×10^6	104
	41300	48.6	7.47	101332	295	132	0.170	172
	41300	79.7	12.4	101352	295	192	0.193	249
Nitrogen	82800	158	27.9	101411	295	321	0.228	418
	82800	311	58.5	101521	295	481	0.300	627
	82800	513	104	101672		642	0.370	838
	82800	737	158	101844		802	0.428	1043
	82800	998	218	102040		965	0.483	1253
	82800	1316	286	102276		1127	0.547	1460
Nitrogen	82800	1647	366	102531	295	1286	0.598	1680

TABLE 29 (CONTINUED)

Permeating Gas	Gage Pressure at Flowmeter (N/m^2)	Pressure Drop through Specimen (P_2-P_1) ΔP (N/m^2)	Downstream Gage Pressure P_1 (N/m^2)	Absolute Mean Specimen Pressure P_m (N/m^2)	Downstream Gas Temperature K	Volumetric Flow Rate Corrected to Standard Conditions Q_{stp} (cm^3/sec)	(1) $\frac{MP_m\Delta P}{LTR\mu G}$ (cm^{-2})	(1) $\frac{G}{\mu}$ (cm^{-1})
Run: 2								
Nitrogen	41300	24.9	3.74	101316	805	31	0.0607	18
	41300	66.0	9.46	101342	797	80	0.0645	46
	41300	127.0	18.7	101382	792	132	0.0722	76
	41300	205	31.9	101434	793	192	0.0803	110
	82800	137	18.7	101388	797	160	0.0642	92
	82800	406	74.7	101582	798	321	0.0949	185
	82800	757	167	101853	805	481	0.118	278
	82800	1220	278	102200	809	642	0.143	371
	82800	1710	413	102584	805	802	0.162	461
	82800	2290	697	103167	808	965	0.182	555
	82800	3000	922	103754	811	1127	0.204	648
	82800	3675	1207	104387	811	1286	0.220	742
Nitrogen	82800	4400	1482	105037	811	1450	0.236	834
Run: 3								
Nitrogen	41300	37.4	7.47	101326	295	132	0.131	172
	41300	64.8	12.4	101344		192	0.157	249
	82800	42.3	8.72	101330		160	0.122	208
	82800	119	27.4	101390		321	0.172	418
	82800	236	58.6	101485		481	0.227	627
	82800	416	94.7	101614		642	0.300	838
	82800	588	144	101755		802	0.341	1043
	82800	798	199	101922		965	0.386	1253
	82800	1026	266	102111		1127	0.426	1460
Nitrogen	82800	1287	344	102329	295	1286	0.468	1680

TABLE 30

THE PERMEABILITY OF THE FURNACE CHAR OF MATERIAL A FORMED AT 1372 K

Permeating Gas	Gage Pressure at Flowmeter (N/m^2)	Pressure Drop through Specimen (P_2-P_1) ΔP (N/m^2)	Downstream Gage Pressure P_1 (N/m^2)	Absolute Mean Specimen Pressure P_m (N/m^2)	Downstream Gas Temperature K	Volumetric Flow Rate Corrected to Standard Conditions Q_{stp} (cm^3/sec)	(1) $\frac{MP_m\Delta P}{LTR\mu G}$ (cm^{-2})	(1) $\frac{G}{\mu}$ (cm^{-1})
Specimen: Pe-1c-6-3A; A = 5.08 cm^2; L = 0.623 cm; Density = 0.1671 gm/cm^3								
Run: 1								
Nitrogen	41300	17.4	2.49	101310	295	80	0.101×10^6	104
	41300	32.4	4.98	101318		132	0.114	172
	41300	53.6	9.96	101332		192	0.130	249
	79300	64.7	14.9	101350		243	0.124	315
	79300	105	23.7	101380		321	0.151	418
	79300	199	51.1	101458		481	0.192	627
	79300	329	89.7	101566		642	0.238	838
	79300	463	134	101683		802	0.270	1043
	79300	615	189	101820		965	0.298	1253
	79300	792	249	101978		1127	0.329	1460
	79300	1023	329	102182		1286	0.372	1680
	79300	1287	413	102410		1450	0.417	1885
Nitrogen	79300	1374	456	102503	295	1520	0.426	1980
Specimen: Pe-2c-6-3A; A = 5.08 cm^2; L = 0.623 cm; Density = 0.1727 gm/cm^3								
Run: 1								
Nitrogen	41300	15.0	3.73	101312	295	80	0.0871×10^6	104
Nitrogen	41300	30.0	7.47	101322	295	132	0.101	172
Nitrogen	41300	52.3	14.9	101341	295	192	0.127	249
	79300	101	33.6	101388		321	0.146	418
	79300	196	67.2	101472		481	0.189	627
	79300	319.0	111	101582		642	0.231	838
	79300	463	162	101711		802	0.270	1043
	79300	630	227	101866		965	0.306	1253
	79300	827	304	102050		1127	0.346	1460
	79300	1028	388	102244		1286	0.374	1680
Nitrogen	79300	1253	483	102464	295	1450	0.407	1885

TABLE 30 (CONTINUED)

Permeating Gas	Gage Pressure at Flowmeter (N/m^2)	Pressure Drop through Specimen (P_2-P_1) ΔP (N/m^2)	Downstream Gage Pressure P_1 (N/m^2)	Absolute Mean Specimen Pressure P_m (N/m^2)	Downstream Gas Temperature K	Volumetric Flow Rate Corrected to Standard Conditions Q_{stp} (cm^3/sec)	(1) $\frac{MP_m\Delta P}{LTR\mu G}$ (cm^{-2})	(1) $\frac{G}{\mu}$ (cm^{-1})
Run: 2								
Nitrogen	41300	22.4	3.74	101315	823	31	0.0542	18
	41300	62.3	9.97	101341	817	80	0.0580	46
	41300	115	19.9	101378	805	132	0.0646	76
	41300	189	34.9	101430	811	192	0.0735	110
	79300	117	22.4	101380	805	160	0.0544	92
	79300	339	82.2	101555	807	321	0.0787	184
	79300	553	174	101758	803	481	0.0856	276
	79300	888	296	102052	797	642	0.103	368
	79300	1271	408	102360	792	802	0.119	459
	79300	1705	598	102774	788	965	0.133	551
Nitrogen	79300	2165	822	103237	788	1127	0.146	643
Nitrogen	79300	2770	1096	103921	797	1286	0.164	740
Run: 3								
Nitrogen	41300	13.7	3.74	101311	295	80	0.0795	104
	41300	29.4	7.47	101322		132	0.103	172
	41300	48.6	12.4	101336		192	0.118	249
	79300	98.8	27.4	101377		321	0.143	418
	79300	193	54.8	101452		481	0.187	627
	79300	318	94.7	101555		642	0.230	838
	79300	423	144	101673		802	0.246	1043
	79300	596	204	101826		965	0.289	1253
	79300	782	277	102000		1127	0.325	1460
	79300	964	354	102176		1286	0.351	1680
Nitrogen	79300	1163	433	102368	295	1450	0.377	1885

TABLE 31

THE PERMEABILITY OF THE FURNACE CHAR OF MATERIAL A FORMED AT 1733 K

Permeating Gas	Gage Pressure at Flowmeter (N/m^2)	Pressure Drop through Specimen (P_2-P_1) ΔP (N/m^2)	Downstream Gage Pressure P_1 (N/m^2)	Absolute Mean Specimen Pressure P_m (N/m^2)	Downstream Gas Temperature K	Volumetric Flow Rate Corrected to Standard Conditions Q_{stp} (cm^3/sec)	(1) $\frac{MP_m\Delta P}{LTR\mu G}$ (cm^{-2})	(1) $\frac{G}{\mu}$ (cm^{-1})
Specimen: Pe-1c-17-3A; A = 5.08 cm^2; L = 0.152 cm; Density = 0.2343 gm/cm^3								
Run: 1								
Nitrogen	41300	34.9	-0-	101318	295	31	2.16×10^6	40
	41300	89.6	1.24	101346		80	2.12	104
	41300	157	4.98	101384		132	2.26	172
	41300	233	9.96	101426		192	2.31	249
	79300	279	13.7	101456		243	2.19	315
	79300	391	22.4	101521		321	2.32	418
	79300	658	47.3	101684		481	2.60	627
	79300	973	84.7	101883		642	2.88	838
	79300	1286	130	102090		802	3.07	1043
	79300	1636	182	102324		965	3.26	1253
	79300	2025	246	102591		1127	3.46	1460
	79300	2410	314	102859		1286	3.61	1680
	79300	2845	390	103665		1450	3.82	1885
	79300	3070	435	103330	295	1520	3.92	1980
Specimen: Pe-2c-17-3A; A = 5.08 cm^2; L = 0.152 cm; Density = 0.2518 gm/cm^3								
Run: 1								
Nitrogen	41300	64.7	1.25	101334	295	31	4.00×10^6	40
Nitrogen	41300	168	3.74	101388		80	3.99	104
	41300	296	6.97	101455		132	4.26	172
	41300	443	12.4	101534		192	4.40	249
	82800	807	26.2	101732		321	4.79	418
	82800	1320	57.3	102024		481	5.24	627
	82800	1970	101	102398		642	5.88	838
	82800	2650	154	102794		802	6.37	1043
	82800	3310	209	103184		965	6.64	1253
	82800	4170	285	103700		1127	7.19	1460
	82800	4960	360	104175		1286	7.52	1680
	82800	5960	443	104773		1450	8.07	1885
Nitrogen	82800	6400	493	105053	295	1520	8.28	1980

TABLE 31 (CONTINUED)

Permeating Gas	Gage Pressure at Flowmeter (N/m^2)	Pressure Drop through Specimen (P_2-P_1) ΔP (N/m^2)	Downstream Gage Pressure P_1 (N/m^2)	Absolute Mean Specimen Pressure P_m (N/m^2)	Downstream Gas Temperature K	Volumetric Flow Rate Corrected to Standard Conditions Q_{stp} (cm^3/sec)	(1) $\frac{MP_m\Delta P}{LTR\mu G}$ (cm^{-2})	(1) $\frac{G}{\mu}$ (cm^{-1})
Run: 2								
Nitrogen	41300	239	2.99	101422	806	31	2.39	18
	41300	598	9.47	101608	802	80	2.30	46
	41300	1027	17.9	101832	793	132	2.40	76
	41300	1523	32.4	102094	798	192	2.46	110
	82800	2680	72.2	102717	810	321	2.61	185
	82800	4340	157	103637	810	481	2.83	278
	82800	6080	279	104629	803	642	3.00	371
Nitrogen	82800	7930	436	105721	807	802	3.18	461
Nitrogen	82800	9800	548	106763	802	965	3.30	553
	82800	11970	673	107988	803	1127	3.48	648
	82800	14330	946	109956	810	1286	3.72	742
Nitrogen	82800	16520	1172	110782	812	1450	3.84	835
Run: 3								
Nitrogen	41300	59.8	1.99	101332	295	31	3.69	40
	41300	157	4.48	101382		80	3.72	104
	41300	299	7.47	101456		132	4.30	172
	41300	408	12.4	101516		192	4.05	249
	82800	311	8.72	101464		160	3.69	208
	82800	727	25.4	101692		321	4.31	418
	82800	1217	58.5	101974		481	4.83	627
	82800	1783	99.7	102302		642	5.31	838
	82800	2367	152	102654		802	5.69	1043
	82800	3040	212	103057		965	6.10	1253
	82800	3750	284	103489		1127	6.46	1460
	82800	4500	361	103951		1286	6.81	1680
	82800	5300	453	104458	295	1450	7.16	1885

TABLE 32

THE PERMEABILITY OF THE ARC JET

Permeating Gas	Gage Pressure at Flowmeter (N/m^2)	Pressure Drop through Specimen (P_2-P_1) ΔP (N/m^2)	Downstream Gage Pressure P_1 (N/m^2)	Absolute Mean Specimen Pressure P_m (N/m^2)	Downstream Gas Temperature K	Volumetric Flow Rate Corrected to Standard Conditions Q_{stp} (cm^3/sec)	(1) $\frac{MP_m\Delta P}{LTR\mu G}$ (cm^{-2})	(1) $\frac{G}{\mu}$ (cm^{-1})
Specimen: Pe-1c-A-1; A = 5.08 cm^2; L = 0.111 cm; Density = 0.2518 gm/cm^3								
Run: 1								
Nitrogen	41300	18.7	1.99	101312	295	31	1.58×10^6	40
	41300	49.2	4.73	101330		80	1.60	104
	41300	89.7	7.97	101353		132	1.77	172
	41300	141	12.9	101384		192	1.91	249
	82800	257	29.9	101462		321	2.08	418
	82800	473	61.7	101606		481	2.56	627
	82800	707	105	101769		642	2.87	838
	82800	968	157	101958		802	3.16	1043
	82800	1293	222	102191		965	3.52	1253
	82800	1634	299	102448		1127	3.82	1460
	82800	2010	376	102721		1286	4.12	1680
Nitrogen	82800	2415	463	103026	295	1450	4.41	1885

TABLE 33

SUMMARY OF PERMEABILITY COEFFICIENTS

Specimen	Temperature of Char Formation	Temperature [°F]	α [cm^{-2}]	$k = \frac{1}{\alpha}$ [cm^{-2}]	β [cm^{-1}]	ρ [gm/cm^3]
Pe-1c-27-2A	603	RT	60.6×10^6	0.0165×10^{-6}	9.5×10^3	0.2447
Pe-2c-27-2A	(Furnace Char)	RT	78.0	0.0128	9.5×10^3	0.2576
Pe-2c-27-2A		500	38.0	0.0263	18.5×10^3	
Pe-2c-27-2A		RT Return	43.5	0.0230	13.0	
Pe-1c-30-2A	802	RT	0.055×10^6	18.2×10^{-6}	0.22×10^3	0.1674
Pe-2c-30-2A	(Furnace Char)	RT	0.040	25.0	0.185	0.1444
Pe-1c-31-2A	1111	RT	0.130×10^6	7.68×10^{-6}	0.508×10^3	0.1857
Pe-2c-31-2A	(Furnace Char)	RT	0.113	8.84	0.305	0.1671
Pe-2c-31-2A		1000	0.056	17.8	0.228	
Pe-2c-31-2A		RT Return	0.087	11.5	0.238	
Pe-1c- 6-3A	1372	RT	0.084×10^6	11.9×10^{-6}	0.172×10^3	0.1671
Pe-2c- 6-3A	(Furnace Char)	RT	0.084	11.9	0.172	0.1727
Pe-2c- 6-3A		1000	0.047	21.3	0.158	
Pe-2c- 6-3A		RT Return	0.074	13.5	0.172	
Pe-1c-17-3A	1733	RT	2.10×10^6	0.477×10^{-6}	0.925×10^3	0.2343
Pe-2c-17-3A	(Furnace Char)	RT	3.92	0.255	2.28	0.2518
Pe-2c-17-3A		1000	2.28	0.438	1.92	
Pe-2c-17-3A		RT Return	3.60	0.278	1.50	
Pe-1c- A-1	Arc Jet Crust	RT	1.53×10^6	0.653×10^{-6}	1.57×10^3	0.2558

REFERENCES

[1] Pears, C. D., and Schoffner, J. E.: "The Thermal Response of Ablative Materials". Presented at VIII National Symposium of SAMPLE, San Francisco, California, May 25-28, 1965.

[2] Smyly, E. D., and Pears, C. D.: The Effects of the Conditions of Char Formation on the Physical Properties of a Charred Phenolic-Nylon, NASA Contractor Report, NASA CR-112 136, July, 1972.

[3] Flynn, D. R., "Thermal Guarding of Cut-Bar Apparatus", Conference on Thermal Conductivity Methods, Batelle Memorial Institute, 1961.

[4] Robinson, H. E., "Thermal Conductivity Reference Standards", Proceedings of the Second Conference on Thermal Conductivity, 1962.

[5] Flynn, D. R., "Thermal Conductivity of Ceramics", Mechanical and Thermal Properties of Ceramics, edited by J. B. Wachtman, Jr., NBS Special Publication 303, Washington, D. C., May, 1969, pp. 63-123.

[6] Jakob, Max: Heat Transfer, Vol. II, Wiley and Sons, 1957, p. 62.

[7] Smyly, E. D., et al: "Thermal and Mechanical Properties of a Low-Density Phenolic-Nylon and Silicone-Phenolic Ablators", Vol. III, NASA Contractor Report, NASA CR 111909, June, 1971.

APPENDICES

Appendix A	Thermal Conductivity to 1000°F
Appendix B	A Comparative Rod Apparatus for Measuring Thermal Conductivity to 2000°F
Appendix C	Guarded Comparative Rod Apparatus
Appendix D	Heat Capacity to 1000°F
Appendix E	Heat Capacity to 5000°F
Appendix F	Permeability to 1000°F
Appendix G	Liquid Absorption (In Monitor Laboratory)

APPENDIX A

THERMAL CONDUCTIVITY TO 1000°F

Apparatus and Procedure

Thermal conductivity runs can be made with any of the three guarded hot plate apparatuses which are slightly modified from the standard ASTM C177-45 design. All three are identical in operating procedure and design except in size and are classified as either the 14", 7", or 3" apparatus depending on the diameter of the specimen used. Actually the diameters for the 7" and 3" apparatuses are 7-3/8" and 3-1/4", respectively. Specimen thicknesses are from 1/8" to 3" and duplicate specimens are required per run. Figure 1 is a schematic of a typical assembly used for all three apparatuses.

The apparatus consists of a central heater plate surrounded by a guard heater, each separately controlled. The guard ring is maintained at the same temperature as the central heater so that all of the heat flow is normal to the specimen surfaces. The temperature differences between the guard and central sections are measured by means of differential-thermocouple junctions connected in series. The 14" and 7" apparatuses contain eight differential junctions, whereas the 3" apparatus contains four. The heater plate is sandwiched between layers of filler material, the hot-face thermocouples, the specimen, cold-face thermocouples, filler material, a copper plate, and finally a cold source to dissipate the heat. The cold source consists of a copper coil enclosed in an aluminum box on the 14" apparatus, a copper coil soldered to a copper plate on the 7" apparatus, and a spiral baffled copper container on the 3" apparatus. In addition to the thermocouples in contact with the specimen, thermocouples are located in the central heater and the outer copper cold plates.

To provide intimate contact at all interfaces, the entire sandwich assembly is pressed firmly together by spring loading with the total load application desired, which is usually 600 pounds.

Normally for the determinations between -50°F to 150°F, a filler material of gum rubber is used. From 150°F to 1000°F Fiberfrax paper is used as a filler. The overlapping data at 150°F provides a check on any possible uncertainty due to poor intimate contact resulting from either specimen or filler surface irregularities. If the data agree within approximately 5%, the run is continued; however, if the agreement is not within 5%, the thermocouples are replaced, the specimen is removed, surfaces are resanded, and the run is repeated.

The thermocouples used on the hot and cold side of the specimen are made from 0.005" diameter chromel-alumel wire electrically insulated with 0.003" teflon tape. The junction is made by soldering the wires to a small square of 0.002" thick brass shim stock called a "getter". The teflon insulated leads are sandwiched between the specimen and filler material to assure isothermal conditions along the length of the wire. This arrangement insures that there is no air film between the specimen and the thermocouples, and that good, intimate contact exists at all interfaces.

Single thermocouples in the center of the heater plate and cold plate monitor the temperatures of the heater and cold plates in order to obtain the over-all temperature drop through the assembly.

The assembly is arranged to operate with the specimen placed in the apparatus horizontally, as shown in Figure 1. The specimen required are flat panels sized to fit the apparatus. The assembly is insulated around the edges by either Fiberfrax or glass wool batt.

A constant voltage transformer is used in conjunction with variable voltage transformers to assure a constant power supply at each setting. The central heater and guard heater are controlled individually by the variable voltage transformers. The voltage and current to the central heater are monitored by means of a voltmeter and an ammeter which are switched out of the circuit except when actually being read. The voltage to the guard heater is monitored constantly by a voltmeter.

All of the thermocouple readings are taken on a Leeds and Northrup K-3 potentiometer in conjunction with a galvanometer of 0.43 microvolts per mm deflection sensitivity.

To obtain mean sample temperatures above room temperature, water is circulated through the cooling section. For mean sample temperatures below room temperature, cold trichloroethylene is pumped through the cooling section. This coolant is chilled by circulating it through copper coils in a trichloroethylene dry-ice bath. Equilibrium conditions are certified before readings are taken.

Coefficients of thermal conductivity are calculated from the expression:

$$k_s = \frac{Ql_s}{A\Delta t}$$

Improvement and Calibrations on the ASTM C177-5 Technique

The ASTM C177-45 guarded hot plate apparatus is only recommended for determining values below 5 Btu in./hr ft^2°F. Due to the higher conductivities of many of the new reinforced plastics such as the phenolic graphites and carbons, considerable work was necessary before the above procedures were incorporated, which provides accurate data between 5 and 10 Btu in./hr ft^2°F. The following is a resume of the work and analysis performed which extended the range to 10 Btu in./hr ft^2°F.

It was decided at the beginning of the investigation that data from -50°F to 150°F would be determined using a filler of gum rubber and determining the conductivity of the specimen by both "direct" measurement of the temperature drop across the specimen and a "series-resistance" or "composite" method, as explained. From 150°F to the maximum temperature, the data would be obtained by using an asbestos filler and determining the conductivity by a "direct" calculation from the measured face temperatures of the specimen. Both methods were used at the 150°F to determine if any uncertainty existed due to poor intimate contact resulting from either specimen or filler surface irregularities.

Considerable deviation of approximately 20 percent to 30 percent occurred between the values obtained for the "composite" method and the "direct" method for the higher conductivity materials. The evaluations with plexiglas and pyrex at that time indicated the following (see Table 1):

1. The "composite" method, when calibrated with pyrex and plexiglas, exhibited somewhat high values of 8 Btu in./hr ft^2°F at 150°F and +1.23 Btu in./hr ft^2°F at 150°F, respectively. The major difficulty was the great scatter between different data.

2. The "direct" method, when calibrated with pyrex, was in error by exhibiting values averaging about 20 percent low. However, the plexiglas calibration indicated excellent agreement.

The above results indicated that the conductivity data for values above 5 Btu in./hr ft^2°F should be determined using the composite method, with the direct method employed for the lower values. However, the composite method is much too critical under certain conditions, and data scatter was as high as 30 percent. By considering equation 2 in close detail, it was found that normal experimental error in determining (l_F/k_F) can result in a magnified error of k_S if (l_F/k_F) is critically close to (l_T/k_T). With certain conditions,

Q = total heat flow - Btu/hr

l_s = average thickness of specimens - inches

A = area of central heater section - square feet

Δt = sum of temperature drop across each sample - °F

Theoretically, Q, the heat input, should split, with exactly half of the input flowing through each sample. The temperature drops indicate that this condition rarely exists. Instead, there is a slight unbalance in the heat flow. The above formula then permits a calculation of the arithmetic average for the two panels. In this calculation the temperatures are measured directly at the faces of the specimen by the "getters", resulting in a "direct" method.

As a check, the thermal conductivity is calculated for the specimen with a "series-resistance" or "composite" expression. This method utilizes the same run data, except that the temperature difference between the heater plate and the cold plate is utilized and, since the resistance of the filler is measured separately in the same apparatus, the following series-resistance equation can be used to determine the thermal conductivity of the specimen:

$$k_s = \frac{l_s}{(l_T/k_T) - (l_F/k_F)} \qquad (2)$$

l_s = thickness of the specimen - inches

k_s = thermal conductivity of the specimen - Btu in./hr ft^2 °F

(l_T/k_T) = thermal resistance of the total composite of filler and specimen, calculated from the temperature difference between the hot and cold plate

(l_F/k_F) = thermal resistance of the filler alone, determined under the same conditions that exist for (l_T/k_T)

The (l_F/k_F) term for the gum rubber filler is determined both with and without copper plates inserted between the rubber pads to simulate interface resistance that is present during the evaluation of the specimen.

an error of 3 percent in (l_F/k_F) can result in a 10 percent to 50 percent error in k_S. Therefore, it was mandatory that the direct method be improved for use over the entire range of values, and that the composite be used only as a check.

It was determined that a majority of the error obtained with the direct method was due to the lack of intimate contact at the interfaces of the specimens when the load and fillers were improperly selected. This error was magnified (even percentagewise) when the conductivities were about 5 Btu in./hr ft^2°F. In order to obtain intimate contact at the interfaces, proper selection of compaction load and filler material for each test material is required. An extensive evaluation was performed on the effect of measured conductivity of increased compaction loading using either no filler material or fillers of gum rubber, Fiberfrax, or asbestos. The specimens used in this evaluation were plexiglas, pyrex, and other plastic materials, which represented a range of conditions including different surface finish, flatness, flexibility, and conductivity. Table 1 presents the calibration data obtained for pyrex and plexiglas in the 3" and 7" diameter and 14" square ASTM C177-45 guarded hot plate apparatuses.

Under the normal compaction load of approximately 600 pounds, the 3" diameter apparatus provided reliable data for plexiglas using either filler or no filler, and for pyrex using the filler only. Under the normal load the 14" apparatus provided accurate data for plexiglas; however, the values were occasionally low on the pyrex using the direct method of calculation. The 7" diameter apparatus provided data about 8 percent low for pyrex under normal load with a gum rubber filler. For plexiglas, the 7" diameter apparatus provided accurate data under normal compaction loads with no filler and gum rubber of Fiberfrax filler; however, the data were 7 percent low using an asbestos filler. Subsequent work indicated that the 7" apparatus was somewhat erratic, so the heater was rebuilt and the agreement with standards improved even more to within about 5 percent, although the trend remained similar. Such extensive data were not reobtained.

Under varying load, the 7" diameter apparatus with gum rubber filler provided values for pyrex that increased 7.5 percent as the load was increased from 100 pounds to 600 pounds and only increased 3 percent more from 600 pounds to 4000 pounds. The excessively high compaction pressures provided values on plexiglas with a gum rubber filler that were not orderly and were noticeably higher than reported in the literature for this material, regardless of the technique.

The data obtained with increasing load on the other plastic materials (not standards) demonstrated in most cases that an increase in compaction load from the normal 600 pounds did not increase the values insignificantly but did introduce unorderly changes. It was apparent, therefore, that excessively high loadings were neither required nor desirable. As a matter of fact, the bonds between the resin and reinforcement on some materials could be influenced, thermally, by such high pressures. Further, stress fields are created and data obtained here have indicated an influence of stress on the conductivity of the structures involved for a material such as plexiglas. The mechanism is probably one of the induced alignment of the chains.

The major requirements was to provide intimate thermal contact on all faces, which could be done by the proper selection of compaction load and filler, depending on the properties of the particular specimen. The actual load on the sandwich was more important than the pressure since it is the load and not the pressure that best correlates with flattening a curved plate or specimen. For example, it requires more load to flatten a 7" plate than it does a 14" plate. So, if the same pressure were maintained on the two apparatuses, the lower compaction force on the smaller one would not flatten the bow. The pressure would be important in providing deformations, locally, of the filler and/or specimen where a low or high spot may exist; however, the data on plexiglas and pyrex with rubber and Fiberfrax, particularly, clearly demonstrated that small compaction loads were sufficient to provide enough pressure to deform the filler into local areas. The compaction load needed was not as excessive as had been suggested in some literature in which the pressure was considered of major importance. An indication of the importance of the load-filler combination rather than pressure was apparent from the data, which provided higher conductivities on the 7" rig with the rubber filler and 600 pound load than on the same rig with no filler at 3000 pound load. Higher conductivities were obtained with the lower pressure by substituting the proper combination of load-filler.

From the above, it has been decided that the higher thermal conductivity materials can be evaluated accurately by the direct measurement method using a filler if the flat surfaces are held flat, and the compaction loads are held at a nominal level sufficient to provide intimate contact at the interfaces. The amount of loading depends on the flatness, the flexibility of the specimen, and the type of filler used. For very rigid materials like pyrex, it is doubtful if enough pressure could be applied when run without filler without breaking the specimen. No one technique is adequate for the determination of the conductivity of all specimens over the full temperature range. Careful judgement is required by the investigator in each case to select the compaction load, the filler (or no filler), the heat flow level, and to evaluate the condition of the apparatus.

The above analysis led to the modifications and improvements which have been made on the ASTM apparatuses beyond those normally employed to assure better accuracy of the data. The screw loading device on the 14" apparatus has been modified to incorporate spring loading at the center and edge clamps to insure more uniform loading, and thus provide flatter surfaces and more intimate contact. The edges are monitored with 1 mil pull-out tabs to insure that no gaps existed in the plates. The thermocouple wires are more carefully placed along the isothermal surface of the specimen. The Fiberfrax paper has been adopted as a high temperature filler, since it conformed to any irregularities on the surface exceptionally well allowing the placement of the small thermocouple wires, electrically insulated with 0.003" teflon tape, without disrupting the intimate contact required. It has also been noted that increasing the heat level, and thus the temperature difference, across the specimen provides less deviation at the 150°F overlap temperature. The minimum heat flow level depends on the conductivity of the material and cannot be defined at a given temperature drop. The random deviation between values on the same specimen as evaluated with rubber filler from -50°F to 150°F, and with Fiberfrax filler from 150°F to 1000°F, has been reduced to a maximum of about 5 percent. Past experience has shown that the Fiberfrax filler provides slightly higher data on ~30 percent of the runs and slightly lower data on the remaining runs at the change-over temperature (from one filler to the other) at about 150°F.

Table 1 presents the many calibrations performed on the apparatuses for both before and after the above improvements were incorporated.

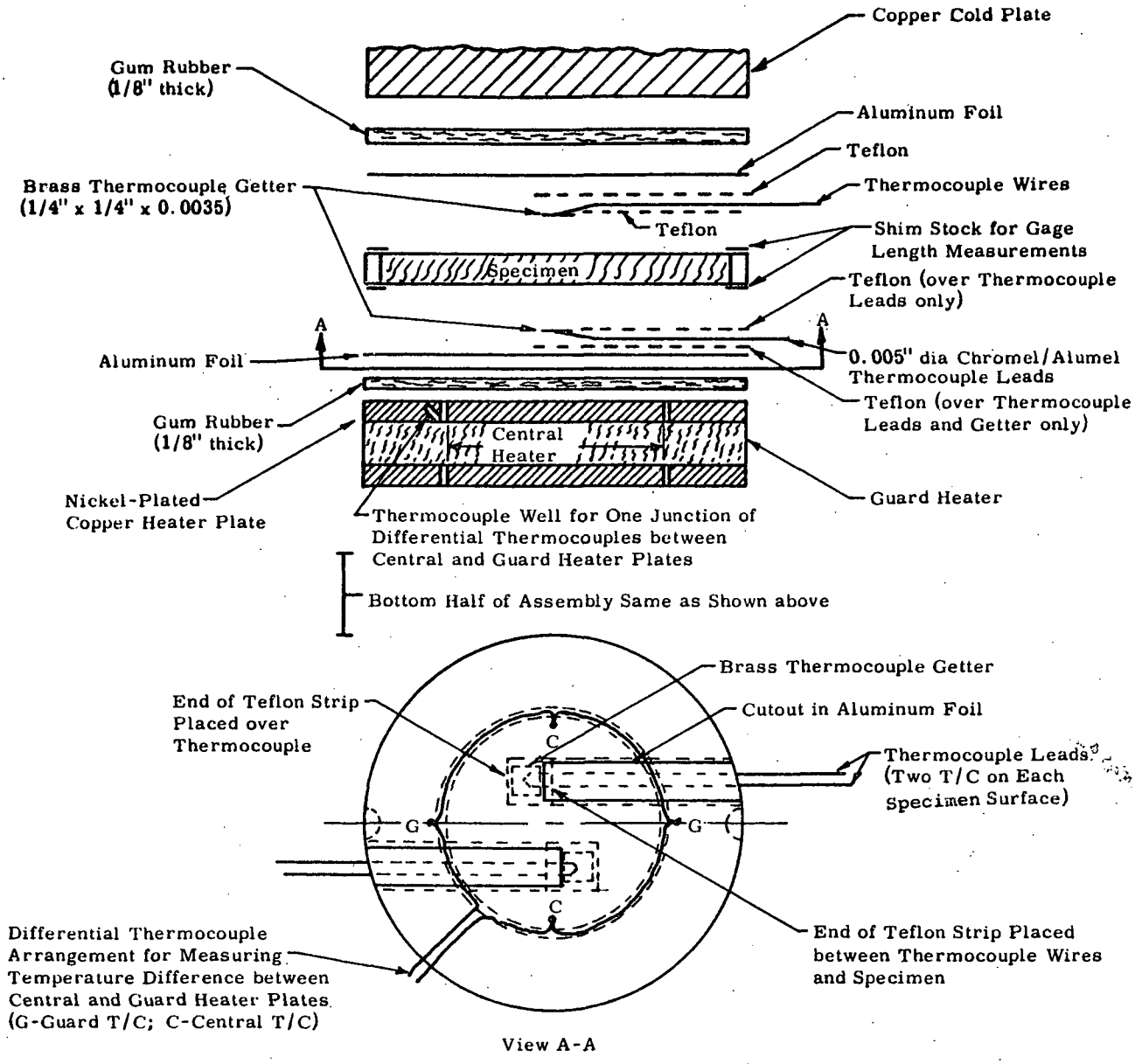

Notes:

1. Buildup shown is used up to 150°F.
2. Above 150°F, gum rubber on hot surface of specimen is replaced by two Fiberfrax discs each 1/8 inch thick and a Fiberfrax disc of the same thickness is placed between the gum rubber and the specimen on the cold surface.
3. At elevated temperatures, an asbestos disc can be placed between the gum rubber and Fiberfrax at the cold surfaces to control temperature drop across the specimen.

Figure 1. Schematic of buildup used for ASTM C177 guarded hot plate thermal conductivity apparatus

Table 1

CALIBRATIONS OF ASTM C 177 APPARATUSES AND PROCEDURES WITH PLEXIGLAS AND PYREX 7740 STANDARDS AT ABOUT 150°F to 200°F (DIRECT METHOD UNLESS OTHERWISE NOTED)

Apparatus	Plexiglas Thermal Conductivity Btu/hr/ft²/°F/in.	Pyrex Thermal Conductivity Btu/hr/ft²/°F/in.
14" rig with asbestos or rubber filler, composite method and 600 pounds	1.33 to 1.39	7.1 to 8.9
14" rig with asbestos filler and 600 pounds	1.17 to 1.20	5.96
14" rig and rubber filler and 600 pounds	1.19 to 1.22 to 1.30	7.35 to 7.39
14" rig with Fiberfrax filler and 600 pounds after improvements made	1.34	7.64 to 7.83
7" diameter rig with rubber filler and compaction of:		
100 pounds	1.25	-7.3%
600 pounds	1.26 to 1.09 with Q	0%, 7.74
1000 pounds	1.25	0%
3000 pounds	-	+2.0%
4000 pounds	1.14 to 1.33 with Q	+2.1%
7" diameter rig with asbestos filler and compaction of:		
100 pounds	-	
600 pounds	1.11 to 1.17	5.0
1000 pounds	1.11	
3000 pounds	-	
4000 pounds	1.16	
7" diameter rig with no filler with compaction loads of:		
100 pounds	1.12	
600 pounds	1.21	4.0
1000 pounds	1.23	
3000 pounds	1.27	
4000 pounds	1.29	
7" diameter rig with Fiberfrax and 600 pounds after improvements made	1.14	7.13 to 8.1
3" diameter rig with rubber filler and 600 pounds	1.17	7.34 to 7.6
3" diameter rig with Fiberfrax filler and 600 pounds	1.15, 1.18, 1.19, 1.41 to 1.19	7.4 to 7.6
3" diameter rig with asbestos filler and 600 pounds	1.16, 1.16, 1.16	7.28
3" diameter rig without filler and 600 pounds	1.18 to 1.19	6.70 to 6.79

1. Literature and previous work reports the thermal conductivity of plexiglas to be 1.19.

2. Literature reports the thermal conductivity of 7740 pyrex to be from 7.1 to 8.1 at about 200°F by Knapp, American Ceramic Society, 1942, and the NBS, respectively. The NBS data are by the series resistance or composite technique. Prior values by the NBS using direct method were about 7.4 to 7.5.

3. Thicknesses of specimens vary with investigator.

APPENDIX B

A COMPARATIVE ROD APPARATUS FOR MEASURING THERMAL CONDUCTIVITY TO 2000°F

Southern Research Institute's comparative rod apparatus is used to measure thermal conductivities of a wide variety of materials from -300°F to 2000°F. This apparatus, shown schematically in Figure 1, consists basically of two cylindrical reference pieces of known thermal conductivity stacked in series with the cylindrical specimen. Heat is introduced to one end of the rod, composed of the references and specimen, by a small electrical heater. A cold sink or heater is employed at the opposite end of the rod as required to maintain the temperature drop through the specimen at the preferred level. Cylinders of zirconia may be inserted in the rod assembly to assist in controlling the temperature drop. Radial losses are minimized by means of radial guard heaters surrounding the rod and consisting of three separate coils of 16, 18 or 20-gage Kanthal wire wound on a 2 or 4- inch diameter alumina core. The annulus between the rod and the guard heaters is filled with diatomaceous earth, thermatomic carbon, bubbled alumina or zirconia powder. Surrounding the guard is an annulus of diatomaceous earth enclosed in an aluminum or transite shell.

The specimens and references (see Figure 2) are normally 1-inch diameter by 1-inch long. Thermocouples located 3/4 inch apart in radially drilled holes measure the axial temperature gradients. Thermocouples located at matching points in each guard heater are used to monitor guard temperatures, which are adjusted to match those at corresponding locations in the test section.

In operation, the apparatus is turned on and allowed to reach steady state. The guard and rod heaters are adjusted to minimize radial temperature gradients between the rod and guard sections consistent with maintaining equal heat flows in the references. Temperatures are measured on a Leeds and Northrup Type K-3 potentiometer, and the temperature gradients calculated. A typical temperature profile in the test section is shown in Figure 3.

The thermal conductivity of the specimen is calculated from the relation

$$K_s = \frac{K_1 \Delta T + K_2 \Delta T}{2\Delta T_s} \quad \frac{\Delta X_s}{\Delta X_r}$$

where K_1 and K_2 are the thermal conductivities of the upper and lower references; ΔT_1, ΔT_2 and ΔT_s are the temperature differences in the upper and lower references and specimen, respectively; ΔX_s and ΔX_r are the distances between thermocouples in the specimen and references.

Note that for purely axial heat flow, the products $K_1\Delta T_1$ and $K_2\Delta T_2$ should be equal. Due to imperfectly matched guarding and other factors, this condition is seldom attained in practice; therefore, the average of the two values is used in the calculations. Their difference is maintained as small as possible, usually within 5% of the smaller.

For identical specimens, the ratio $\Delta X_s/\Delta X_r$ should be unity but may vary due to the uncertainty in hole locations. To prevent introducing an additional error in calculations, ΔX is determined as follows: the depth of the hole is measured by inserting a snugly fitting drill rod in the hole, measuring the projecting length and subtracting it from the total length of the rod. The slope, or angle the hole makes with the perpendicular to the specimen axis, is determined by making measurements to the face of the hole and the outer end of the drill rod with respect to a datum plane, using a dial gage. From these measurements, the location of the bottom of the hole can be calculated.

Generally, measurements with the comparative rod apparatus are performed in an inert helium environment. The apparatus can also be operated in vacuum and at gas pressures of up to 100 psig. We have had experience operating under all conditions.

The primary reference materials which we use are Code 9606 Pyroceram and Armco iron for measurements on materials with low and high thermal conductivities, respectively. Primary standard reference sets are kept and are used to calibrate other references made from the same materials. The standards of Code 9606 Pyroceram were made from a batch of material which NBS purchased shortly after their measurements on a sample of Code 9606 Pyroceram. The curve which Flynn presented for the thermal conductivity of the Pyroceram is given in Figure 4.[1] Note that the curve is in good agreement

---

[1] Robinson, H.E. and Flynn, D. R., Proceedings of Third Conference on Thermal Conductivity, pages 308-321, 1963 (with author's permission)

with the recommended values from NSRDS-NBS 8[2]. The standards of Armco iron were made from the stock which was used in the round-robin investigations from which Powell[3] developed the most probable values for Armco iron. The curve used for the Armco iron standards is shown in Figure 5. Powell estimated the uncertainty to be within ±2 percent over the temperature range from 0° to 1000°C. Note in Figure 5 that numerous evaluations of Armco iron from other batches of material have agreed within ±3 percent (coefficient of variation about curve) with Powell's original data.

In addition to Code 9606 Pyroceram and Armco iron several other materials have been used as references. These include copper for high conductivity specimens, 316 stainless steel for specimens of intermediate thermal conductivity and Teflon or Pyrex for low conductivity materials.

Copper references have been calibrated against Armco iron and excellent agreement with literature data has been obtained. Thermal conductivity values obtained from calibrations of 316 stainless steel against Pyroceram, Armco iron and a set of 316 stainless steel standards are presented in Figure 6. Note the consistency of the data obtained with the three different sets of references. The coefficient of variation of the data shown in Figure 6, about the curve value, was ±3.3%. These data indicate the internal consistency of the stainless steel and the reference materials. Note that the thermal conductivity values for 316 stainless steel presented in Figure 6 lie between values reported by several steel manufacturers and Lucks and Deem.[4]

The calibrations indicate that for materials with moderate to high thermal conductivities the apparatus operates with a precision of about ±3 percent and a total uncertainty of about ±5 percent at temperatures above 0°F if temperatures between the guard and test section are closely matched. Below 0°F, the precision achieved to date has been about ±7 percent with a total uncertainty of about ±10 percent. We anticipate that the precision and uncertainty at cryogenic temperatures can be improved by additional calibrations.

---

[2] Powell, R. W., C. Y. Ho and P. E. Liley, Thermal Conductivity of Selected Materials, NSRDS-NBS 8, Department of Commerce, November 25, 1966

[3] Powell, R. W., Proceedings of Third Conference on Thermal Conductivity, pages 322-341, 1963

[4] WADC TR58-476, "The Thermophysical Properties of Solid Materials," Armour Research Foundation, November, 1960.

Some additional data obtained on the comparative rod apparatus are shown in Figure 7 and 8. Figure 7 shows thermal conductivity data for ATJ graphite, with grain, using Armco iron as the reference material. These data show excellent agreement with earlier data obtained here and by other sources[5] [7]. The maximum scatter of the comparative rod points was about 5 percent.

Figure 8 shows data for thermocouple grade constantan obtained on the comparative rod apparatus using Armco iron references, and on Southern Research Institute's high temperature radial inflow apparatus. Note the excellent agreement. These data also show close agreement with data obtained by Silverman[4] on an alloy of very similar composition.

---

[5] ASD-TDR-62-765, "The Thermal Properties of Twenty-Six Solid Materials to 5000°F or Their Destruction Temperatures," Southern Research Institute, August, 1962

[6] Pears, C. D., Proceedings of Third Conference on Thermal Conductivity, 453-479 (1963)

[7] NSRDS-NBS 16, "Thermal Conductivity of Selected Materials", Part 2, by C. Y. Ho, R. W. Powell and P. E. Liley, National Bureau of Standards, 1968.

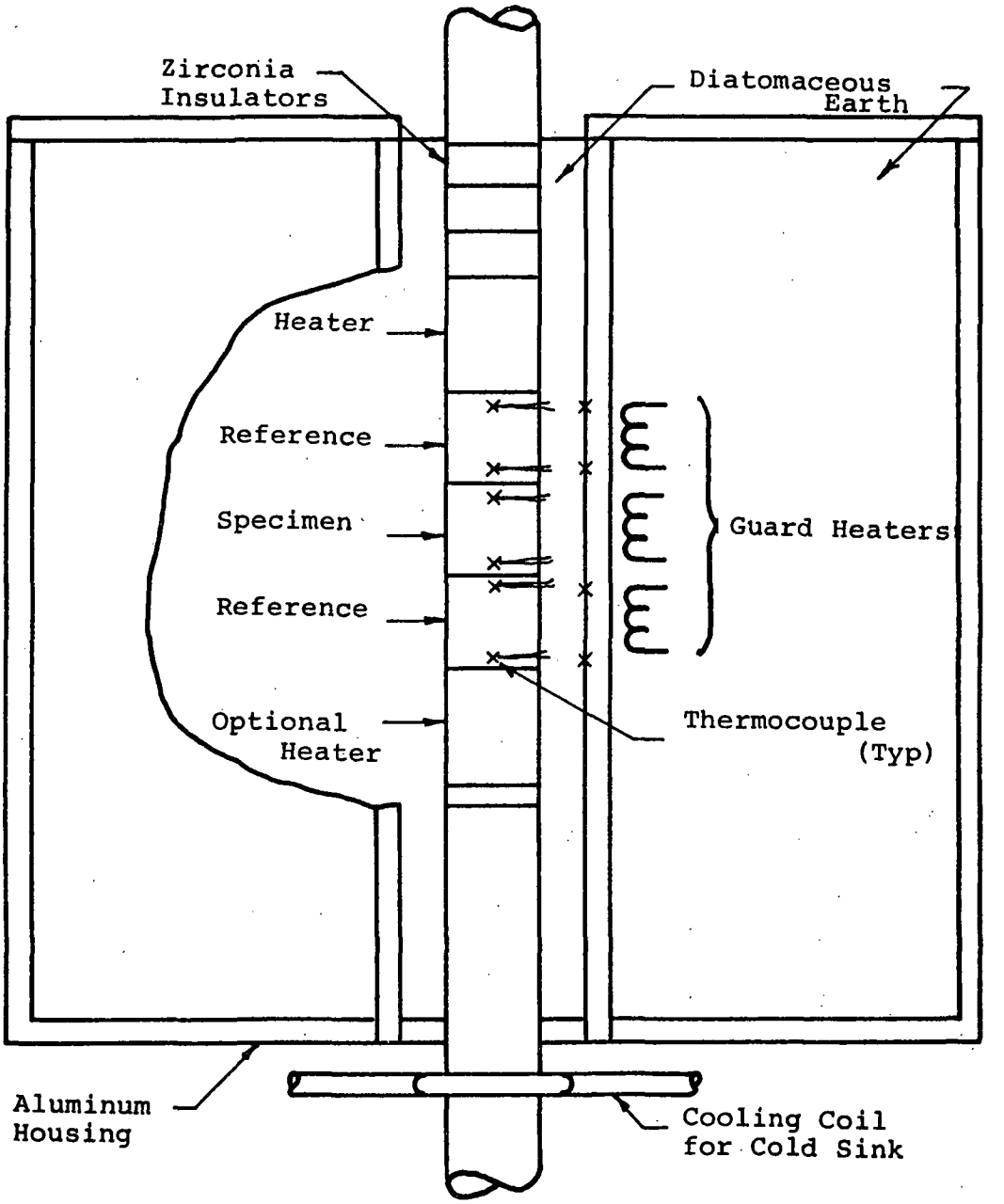

Figure 1. Schematic of Comparative Rod Thermal Conductivity Apparatus

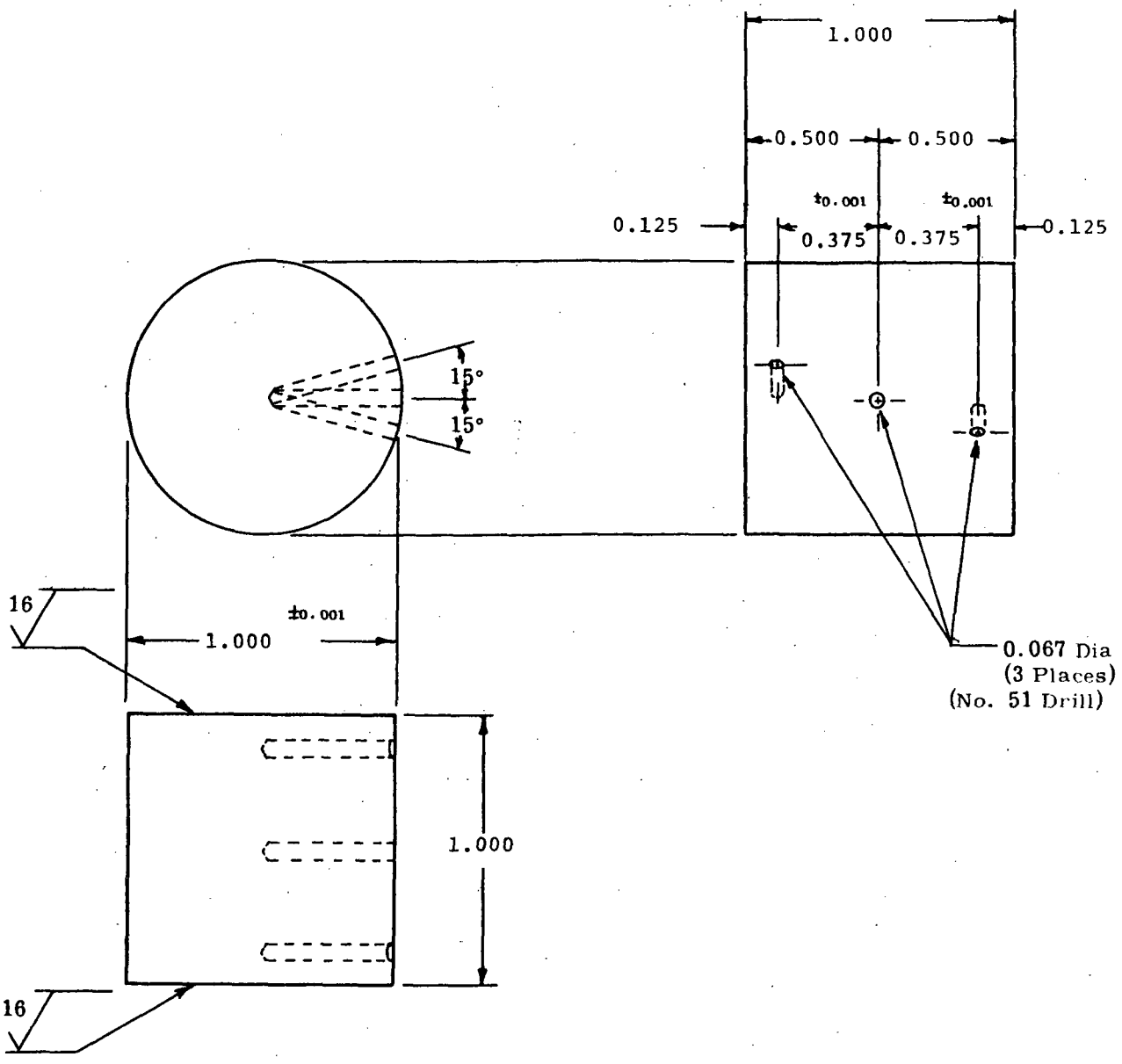

Note: All dimensions ±0.005 except where noted

Figure 2. Drawing of Specimen for Thermal Conductivity Measurements in Comparative Rod Apparatus to 1800°F

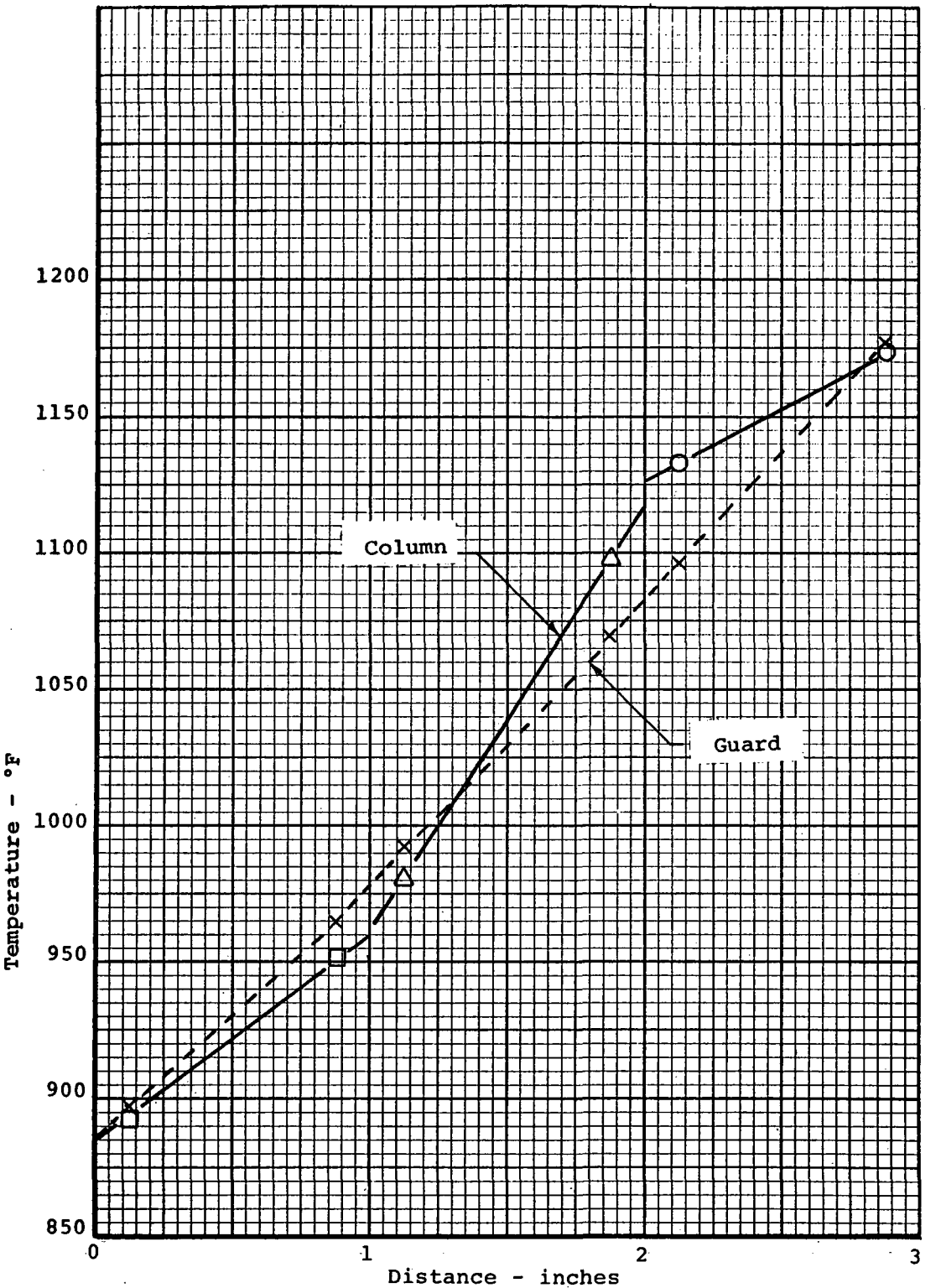

Figure 3. Typical Temperature Profile in Test Section

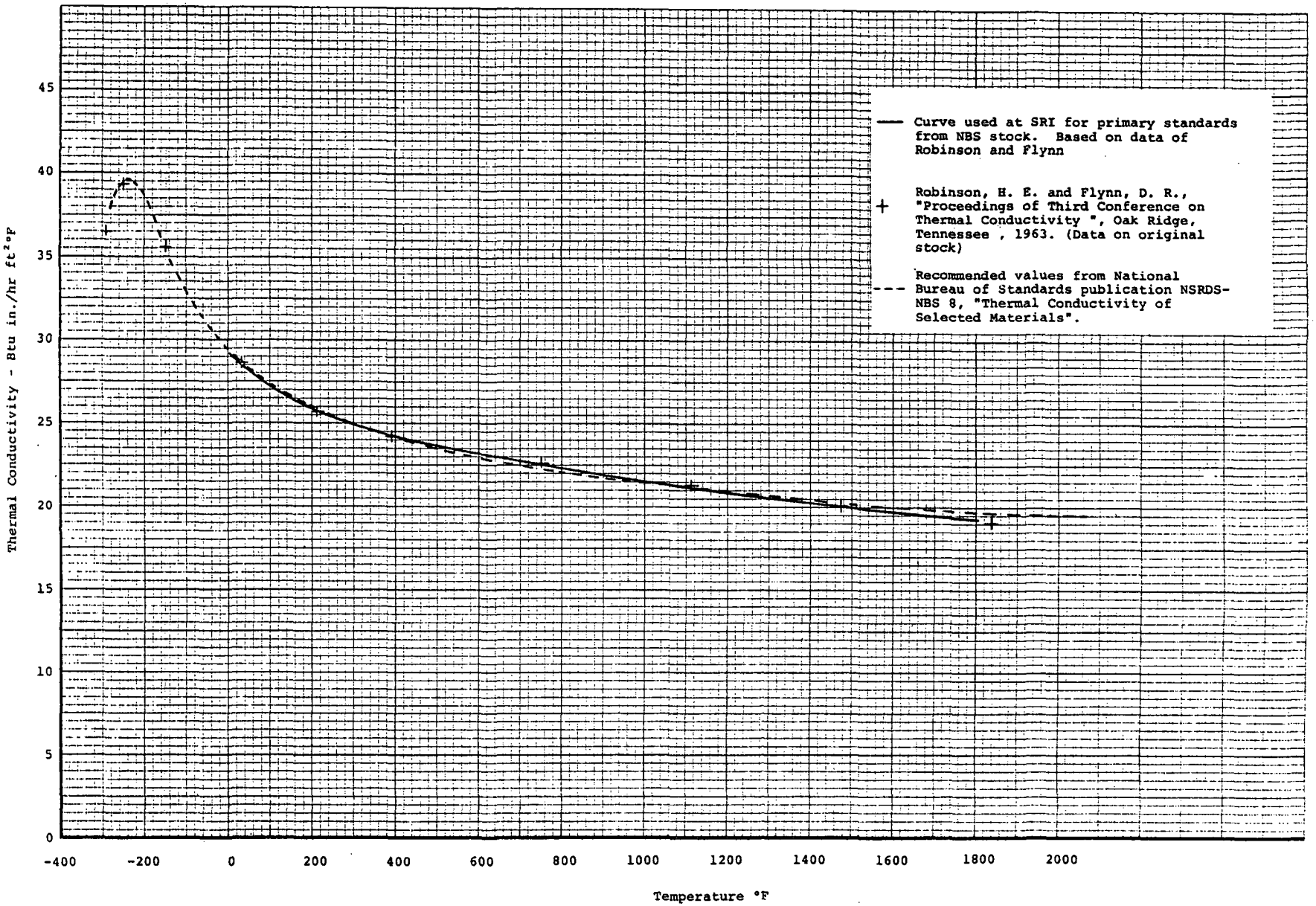

Figure 4. The Thermal Conductivity of Primary SRI Standards from NBS Stock of Code 9606 Pyroceram

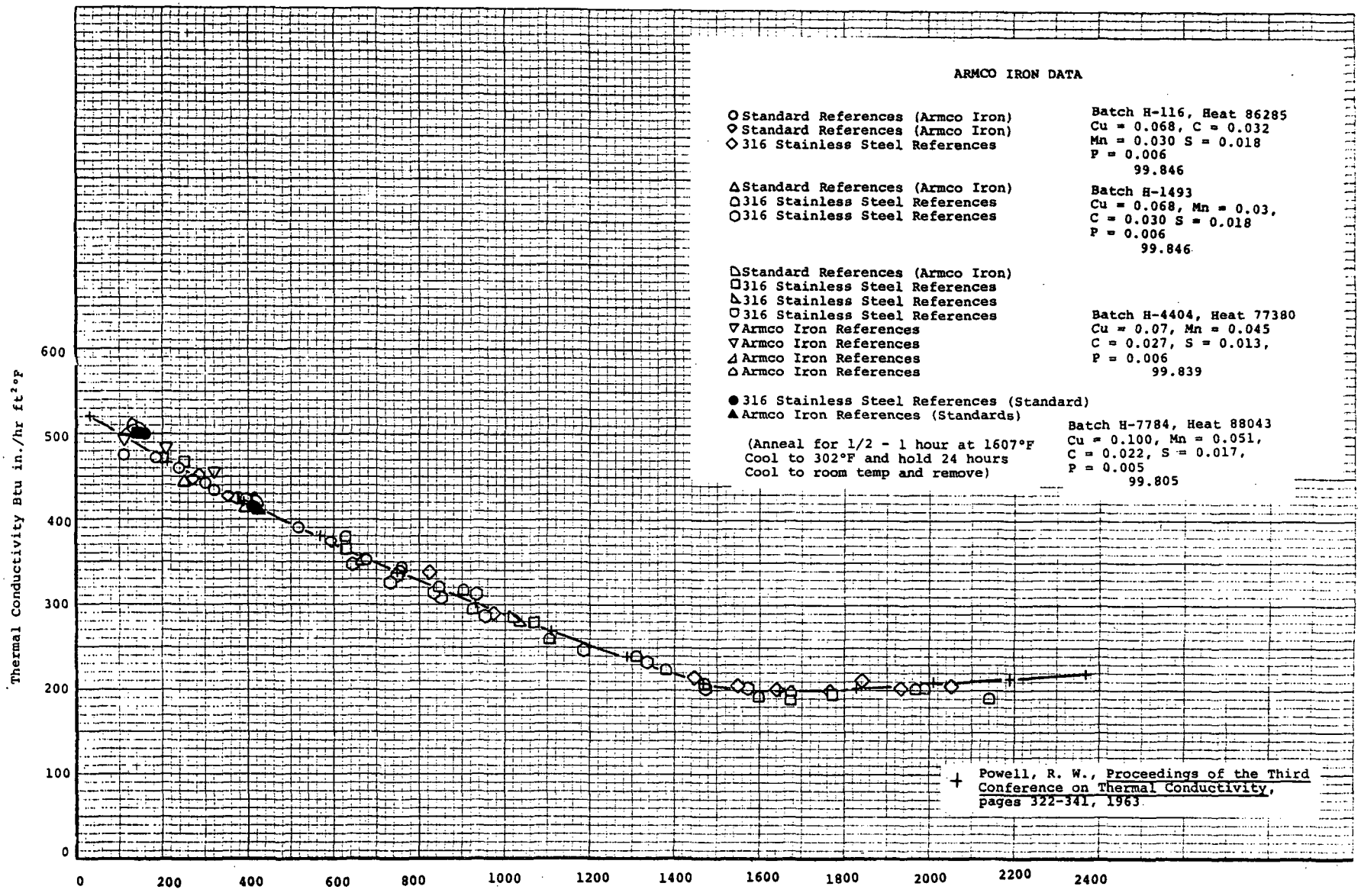

Figure 5. The Thermal Conductivity of Armco Iron

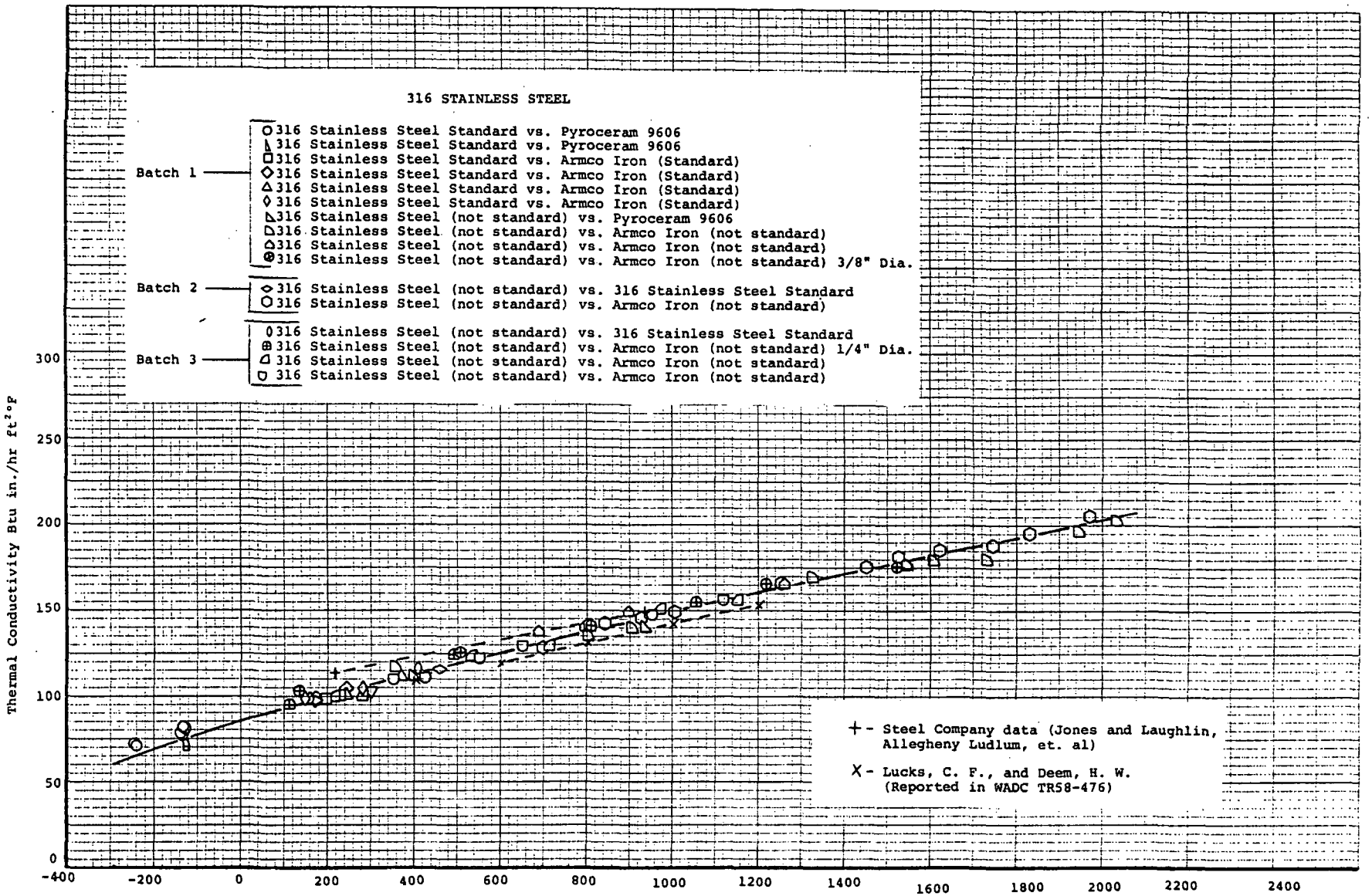

Figure 6. The Thermal Conductivity of 316 Stainless Steel

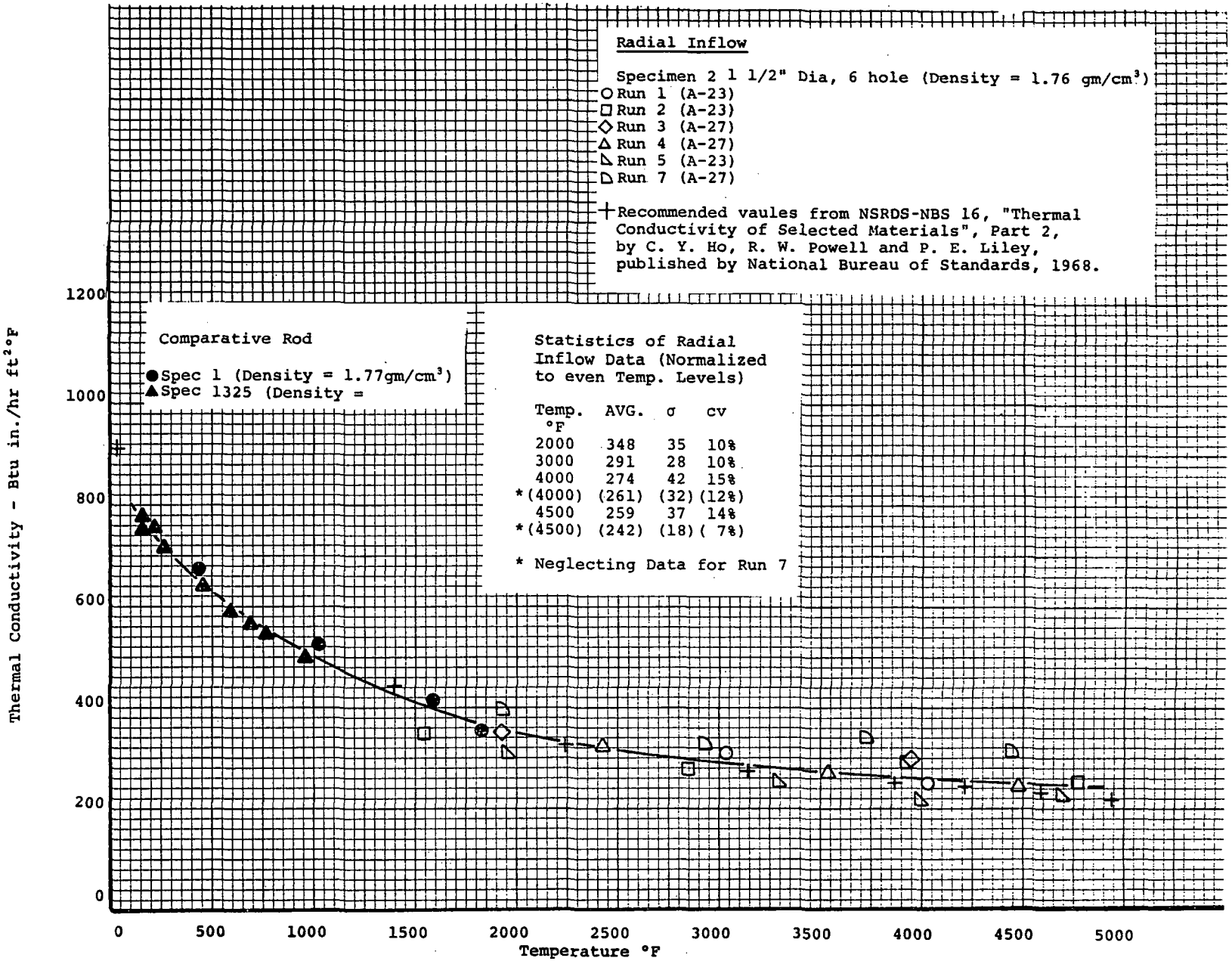

Figure 7. The Thermal Conductivity of ATJ Graphite, With Grain

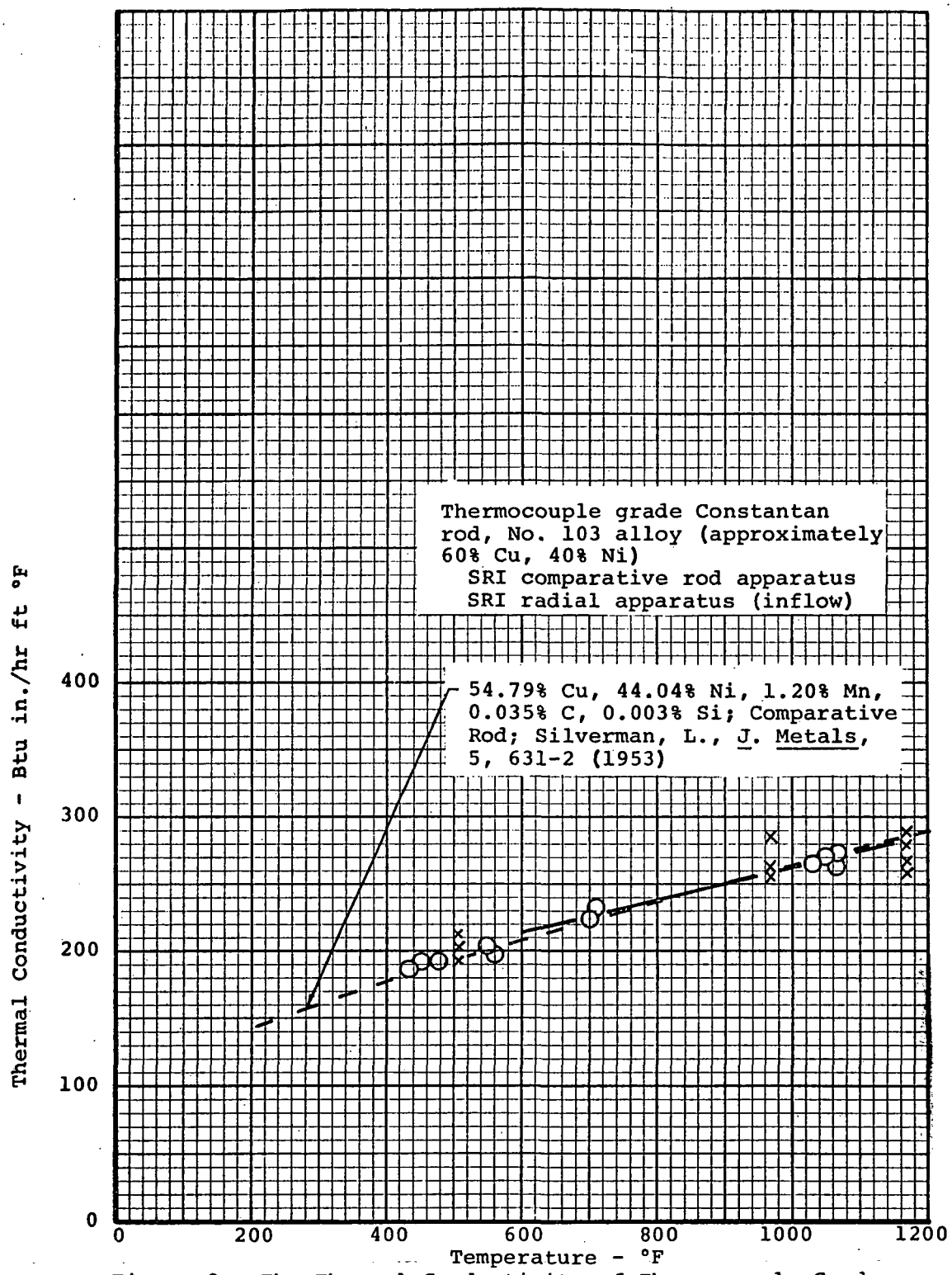

Figure 8. The Thermal Conductivity of Thermocouple Grade Constantan Rod

APPENDIX C

GUARDED COMPARATIVE ROD APPARATUS

The guarded comparative rod apparatus is a modified assembly of the basic comparative rod apparatus and is employed for samples with thermal conductivities less than 10 Btu in./hr ft^2 °F.

The reason for this is that analyses [1, 2][1] have shown that heat can shunt the specimen [through the insulation] when the thermal conductivity of the specimen is not an order-of-magnitude or more than that of the insulation and the guard heater is, say, twice the diameter of the specimen or more. Note that the shunting effectively gives a larger specimen area and results in an erroneously low temperature difference in the specimen relative to the reference (assuming that the references have a higher thermal conductivity than the specimen). This yields erroneously high values of thermal conductivity. With certain values for the thermal conductivities of the references, specimen and insulation, guard heater to specimen diameter ratio and guard to specimen temperature profile, these errors can easily reach 100 percent.

Analyses [1, 2[have shown that the heat shunting problem can be overcome if the following conditions are satisfied:

1. The guard profile matches the specimen profile.

2. The ratio of guard diameter to specimen diameter is as near one as possible.

These concepts are applied to the modified technique described here.

The experimental configuration used for the measurements is shown in Figure 1. The assembly consists of a central column comprised of a 1 inch diameter specimen sandwiched between two references of known thermal conductivity. Guard rings made of the same materials as the specimen and references surrounded the central column. The guard rings were constructed to match the specimen and reference lengthwise. The annulus between the central column and guard ring was 1/16 inch wide which gave a guard diameter to specimen diameter of 1.125. A drawing of the specimen and guard ring is given in Figure 2.

---

[1]Bracketed numbers denote references given at end of text.

The references used are slip cast fused silica, the conductivity of which has been defined with the ASTM C 177 guarded hot plate apparatus. The thermal conductivity for the references are shown in Figure 3.

Heaters made of Armco iron are placed on either end of the column to control heat flow and mean temperature. Armco iron is used because its thermal conductivity is about 200 times that of the specimen and; hence, the temperature gradient along a radial line at the top of the build-up was estimated to be no more than one or two degrees. Thus, the guard and central temperatures are matched at the ends. The entire assembly is surrounded by diatomaceous earth or thermatomic carbon insulation depending on the specimen insulation contained inside a 4 inch diameter guard heater.

Temperatures are measured at two axial locations in each reference and in the specimen. A beaded chromel/alumel thermocouple is inserted into the drilled holes in a 1/32 inch double bore alumina insulator. The insulator is broken about every 1/8 inch to minimize conduction losses. The thermocouples in the specimen are potted in place at the bead with Silastic RTV-731, silicone rubber.

Specimen gage lengths are determined from post-run radiographs or X-rays. The X-rays are examined at 10 x magnification to determine the gage distance relative to the overall thickness. Then the relative distances were converted to true distances from the actual thickness of the specimens.

The idea for the assembly shown in Figure 1 is to use identical materials for a guard ring and thus create as closely as possible a matched guard condition to minimize radial heat exchange and heat shunting. Further, the annulus is kept small to minimize heat shunting which occurs even with matched guarding.

In practice, perfect matching of the guard and central columns is not achieved. Hence, corrections for radial heat exchange are made to the measured data based on the measured temperature profiles. Further, corrections are made for the heat shunting through the annulus. The following paragraphs discuss these corrections.

Note in Figure 1 that guard temperatures are measured at the center of each of the three guard sections. These temperatures are used in the analysis of radial heat exchange. For the analysis a one-dimensional fin-type heat transfer analysis is used. The analysis is applied to determine the actual heat flux density into and out of the specimen based on the measured temperatures in the references and under the assumption of a linear temperature profile

in the guard. Consider the following sketch for the top reference and guard (see Figure 1 for identification of thermocouples):

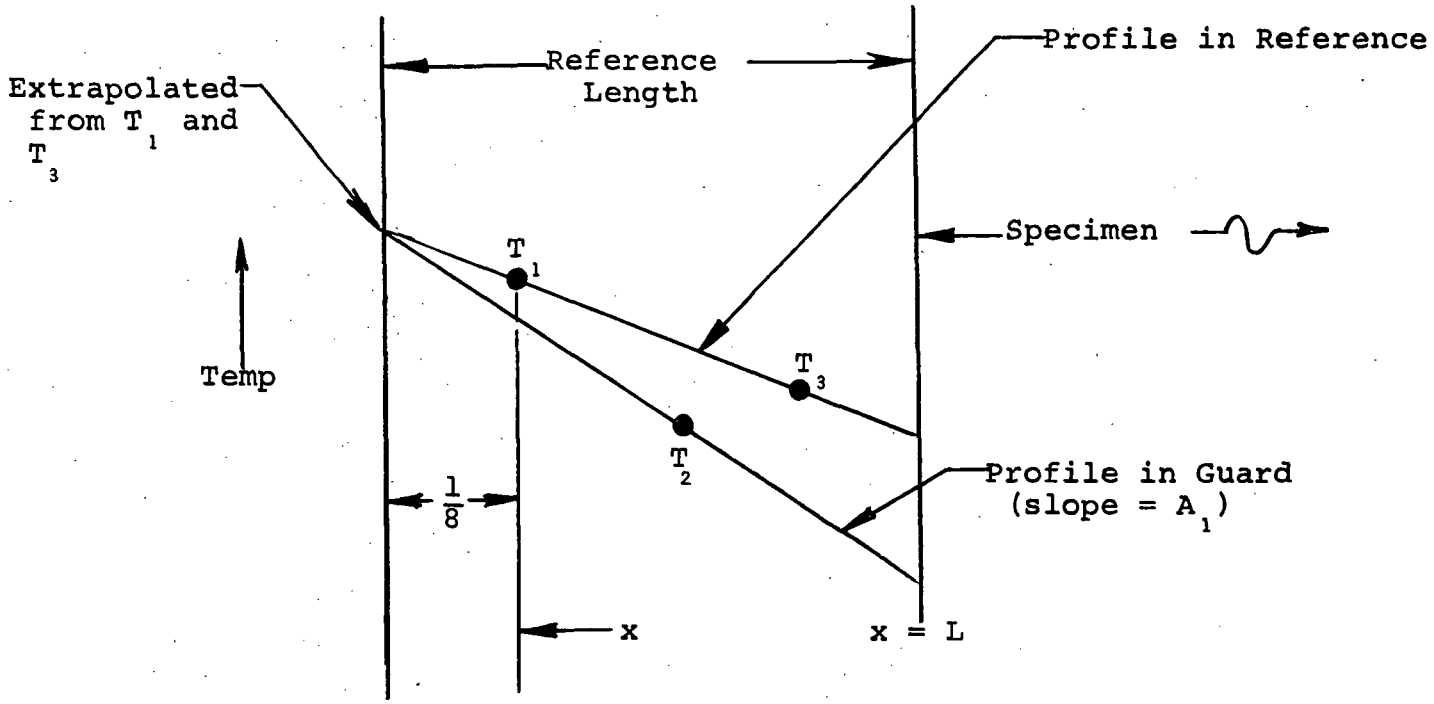

The temperature profile in the reference is given by

$$t = C_1 e^{Nx} + C_2 e^{-Nx} + T_2 + A_1 \left(\frac{1}{8} - x\right) \qquad (1)$$

where

t = temperature

C_1, C_2 = constants of integration

$$N = \sqrt{\frac{hp}{k}}$$

h = effective heat transfer coefficient between two points of radial temperature measurement

p = perimeter of reference

k = thermal conductivity of reference

To solve for Q_S, the heat flux density into the specimen at X = L, equation (1) is subjected to the following boundary conditions:

$$t = T_1 \quad @ \; x = o \tag{2}$$

$$k = \frac{dt}{dx} = -Q_S \quad @ \; X = L \tag{3}$$

A solution is obtained from equation (1) and boundary conditions (2) and (3). There are two unknowns in the resulting equation; namely, Q_S and t. Q_S is determined from the known temperature, T_3, at x = 0.25 inch. Note that the interface temperature at the heater is determined from a linear extrapolation of the reference temperatures. The interface temperature at the heater is assumed to be the same for the central and guard columns and is used along with T_2, the guard temperature, to calculate the temperature gradient in the guard, A_1.

The same type of analysis is used to calculate the actual heat flux into the surface of the bottom reference.

The radial heat loss along the specimen is calculated by assuming a linear temperature profile through the specimen and through the guard. The actual heat flux into the top of the specimen is used and heat fluxes are calculated at each thermocouple location, at the midpoint of the specimen and at the bottom of the specimen. If the heat flux calculated at the bottom of the specimen differed from that calculated from the measurements at the bottom reference, the difference is halved and the heat flux at the top of the specimen is adjusted by that amount. The calculations for the heat flux profile through the specimen are then repeated with the adjusted value. Then, the average heat flux between the points of temperature measurement in the specimen is calculated from

$$Q_{sp} = \frac{Q_{s1} + 2\,Q_{s2} + Q_{s3}}{4} \tag{4}$$

where

Q_{sp} = average heat flux through specimen

Q_{s1} = heat flux at thermocouple No. 4

Q_{s2} = heat flux at midpoint of specimen

Q_{s3} = heat flux at thermocouple No. 6

Now, the measured thermal conductivity is based on the average heat fluxes through the top and bottom references as calculated under the assumption of a linear temperature gradient and no heat losses. The measured thermal conductivity is converted to the corrected value by the equation

$$k_{cr} = \frac{Q_{sp}\ k_m}{Q_m} \tag{5}$$

where

k_{cr} = effective thermal conductivity of specimen corrected for radial heat exchange

Q_{sp} = average heat flow through specimen calculated from analysis

Q_m = average heat flow in references under assumption of no heat loss

k_m = measured thermal conductivity of sample

Next, the method of obtaining the heat transfer coefficients for use in the analysis of radial heat exchange will be considered. Note in Figure 1 that the space between points of radial temperature measurements is filled with either the fused silica or the specimen and the insulation in the annulus between the central column and guard. The thermal conductivities of these elements and the radial thicknesses are used to compute an effective heat transfer coefficient for the analysis. For example, the heat transfer coefficient across the 1/16 inch gap between the central column and guard column is calculated from the equation

$$h = \frac{k}{R_s \ln (R_2/R_1)} \tag{6}$$

where

k = thermal conductivity of material between R_1 and R_2

R_s = radius of central column

R_2 = outer radius

R_1 = inner radius

The thermal resistances of the slip cast fused silica and the specimen between the points of radial temperature measurement are also included in the effective heat transfer coefficients. For the central column the effective heat transfer coefficient is calculated assuming radii (for Equation 6) of 0.25 and 0.5 inch.

For the guard ring, the radii used in Equation 6 are 0.562 and 0.781 inch. Of course, for this analysis the thermal conductivity used in Equation 6 is that of the slip cast fused silica or the specimen.

The overall heat transfer coefficient used in the analysis of radial heat exchange is calculated from the equation

$$h = \frac{h_s\, h_a\, h_g}{h_s\, h_g + h_a\, h_s + h_a\, h_g} \qquad (7)$$

where

h = overall heat transfer coefficient used in Equation 1 $\left[N = \sqrt{\frac{hp}{k}}\right]$

h_s = effective heat transfer coefficient due to radial thermal resistance of central column

h_a = effective heat transfer coefficient of annulus between central and guard sections

h_g = effective heat transfer coefficient of guard ring from inner radius to thermocouple location

The heat transfer coefficients are calculated as a function of temperature. In the analysis of radial heat losses, different values of the heat transfer coefficient are used for the top reference, specimen and bottom reference based on the mean temperatures at those locations.

The thermal conductivity values for the slip cast fused silica which are used to calculate the heat transfer coefficients are presented in Figure 3. The thermal conductivity values which are used for the calculation of the effective heat transfer coefficient of the insulations of diatomaceous earth or thermatomic carbon in nitrogen at 760mm and vacuum are presented in Figure 4, 5 and 6. Also shown in Figure 4 are thermal conductivity values for nitrogen. Literature values for the thermal conductivity of the diatomaceous earth in air (nitrogen) were found to a temperature of 800°F and were extrapolated to 2000°F. Values for the thermatomic carbon were obtained from previous measurements made in our radial inflow apparatus.

With the above information and the measured thermal conductivity of the specimen, the heat transfer coefficients in Equation 7 are calculated.

In addition to the errors associated with radial heat exchange, there are errors due to the shunting heat flow around the specimen through the insulation. This error occurs even with perfect temperature matching of the central and guard columns. This error has been defined analytically by Flynn [3] as

$$\alpha = k_i \left[\frac{1}{k_r} - \frac{1}{k_{cr}} \right] F_g \tag{8}$$

$$k_c = \frac{k_{cr}}{1-\alpha} \tag{9}$$

where

k_c = final corrected thermal conductivity

k_{cr} = measured thermal conductivity corrected for radial heat exchange

k_i = thermal conductivity of insulation

k_r = thermal conductivity of references

F_g = a geometrical factor

Flynn [3] gives the following equation for the maximum value of F_g

$$F_g \leq \left[\frac{(b^2/a^2) - 1}{2 \ln (b/a)} \right] - 1 \tag{10}$$

where

a = radius of specimen
b = inner radius of guard cylinder

Equations 8, 9 and 10 are used to correct for the shunting heat flow. The value used for F_g is 0.116 which is calculated from Equation (10) for the geometry of our system.

Note that two different corrections are applied to the experimental data. However, lest one should become overly concerned with this it should be considered that the maximum value for both corrections is about 10 percent. Hence, sizeable uncertainties in the correction procedures do not lend large

uncertainties to the final data. The several sources of uncertainty and the estimated values are summarized below:

1. Uncertainty in final data due to uncertainty in correction analysis, property data used in analysis and radial temperature differences = 5 percent (maximum).

2. Uncertainty in thermal conductivity of fused silica references = 5 percent to 500°F, 7 percent to 1800°F

3. Uncertainty in gage length = 2 percent.

4. Uncertainty in temperature difference measurements = 2 percent.

The combined uncertainty for the several sources of uncertainty listed above is ±8 percent to 500°F and ±10 percent to 1800°F.

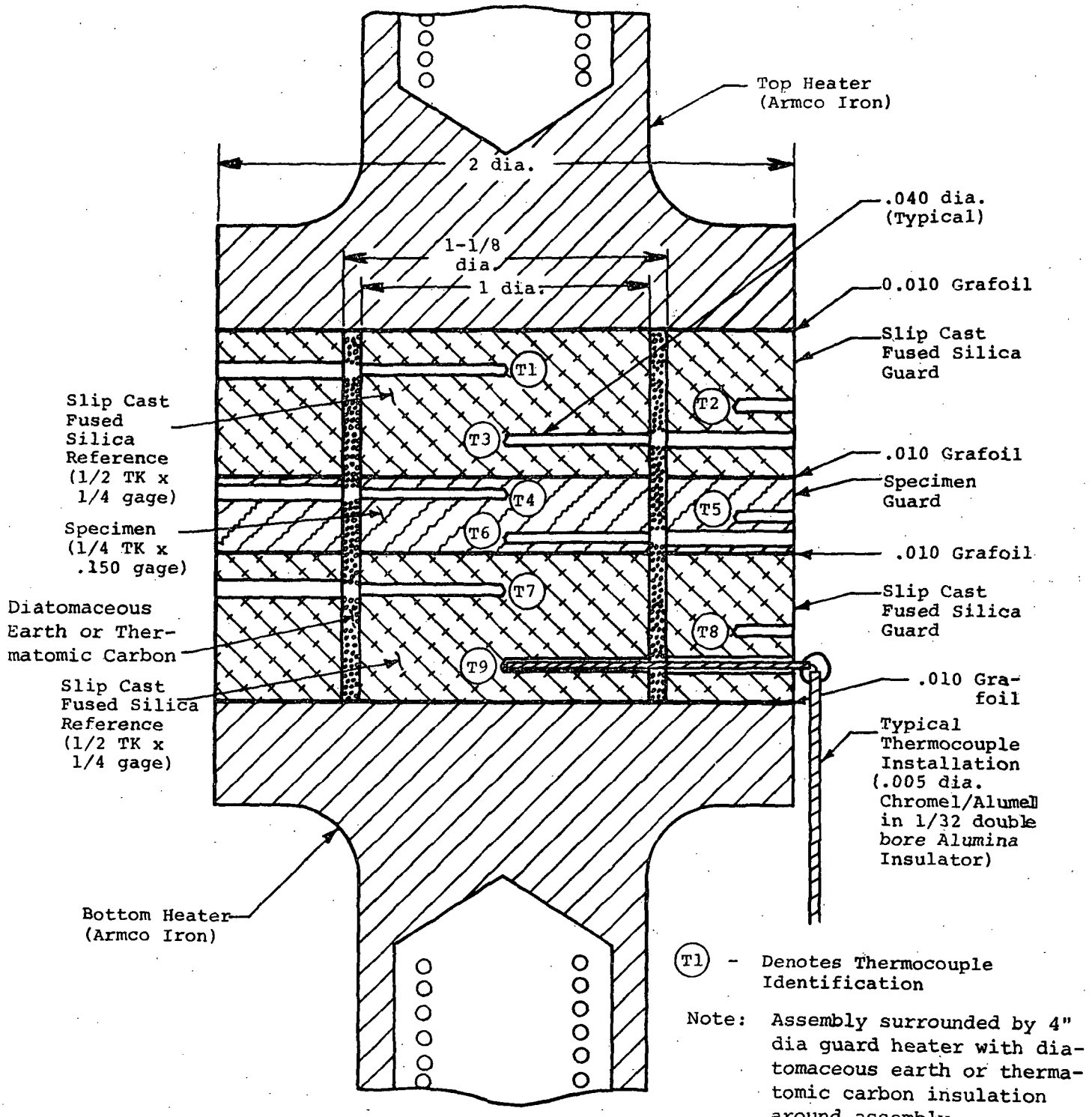

Figure 1. Assembly of Guarded Comparative Rod Apparatus

Note: Size thickness of specimen and guard ring at same time for thickness match.

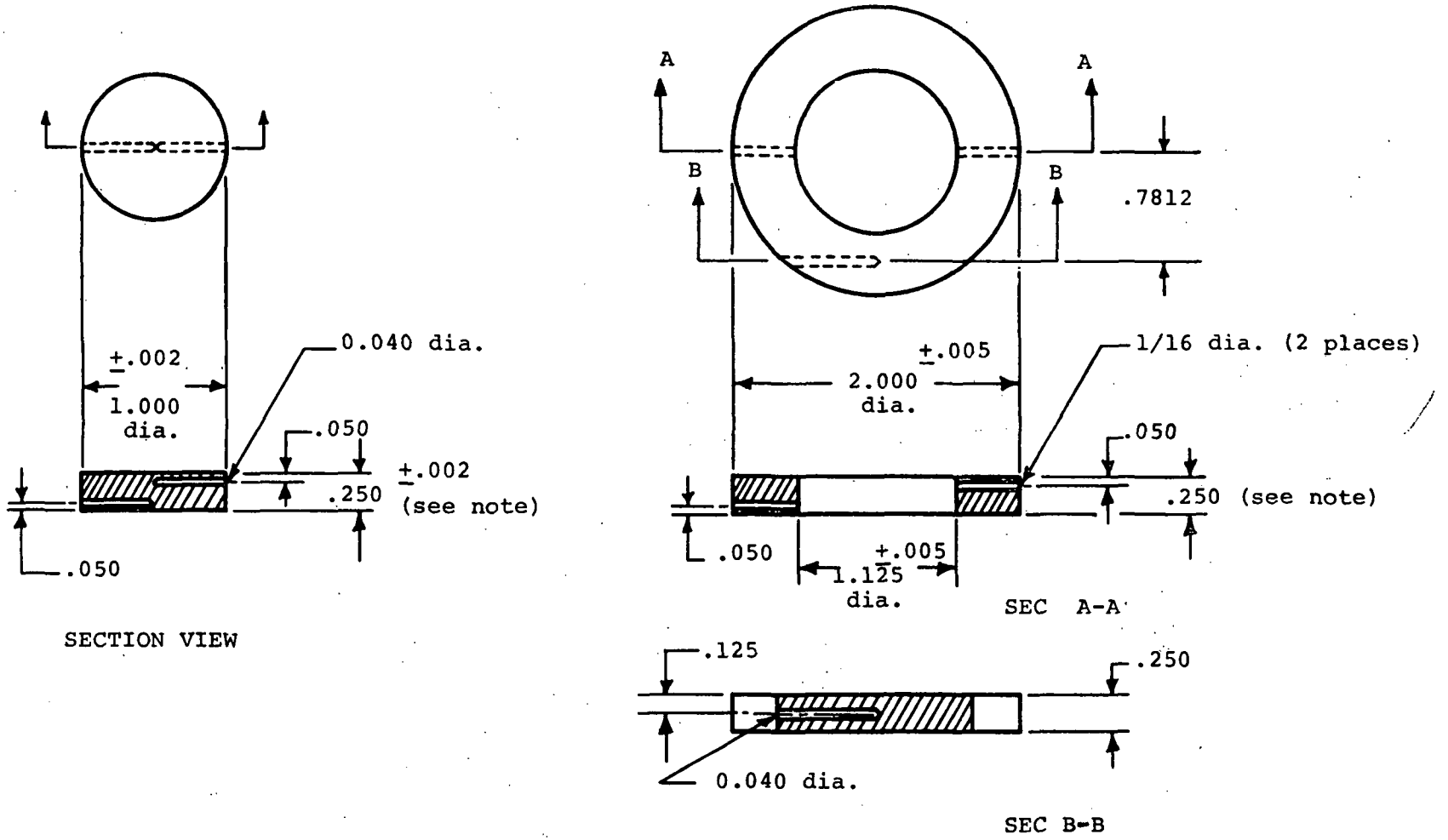

Figure 2. Specimen and Guard Ring for Measurements in Guarded CRA.

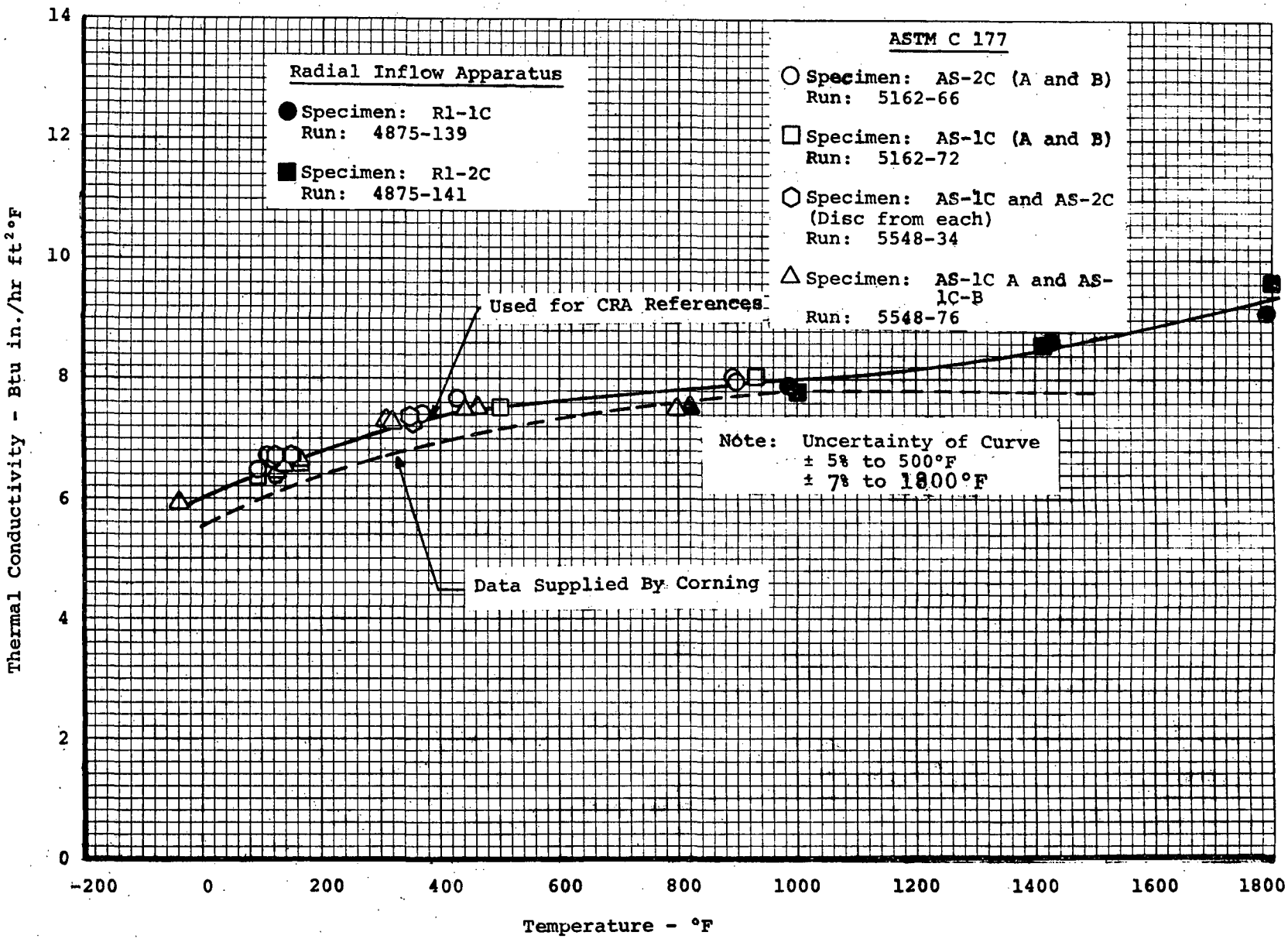

Figure 3. Thermal Conductivity of the Slip Cast Fused Silica References Used in the Comparative Rod Apparatus

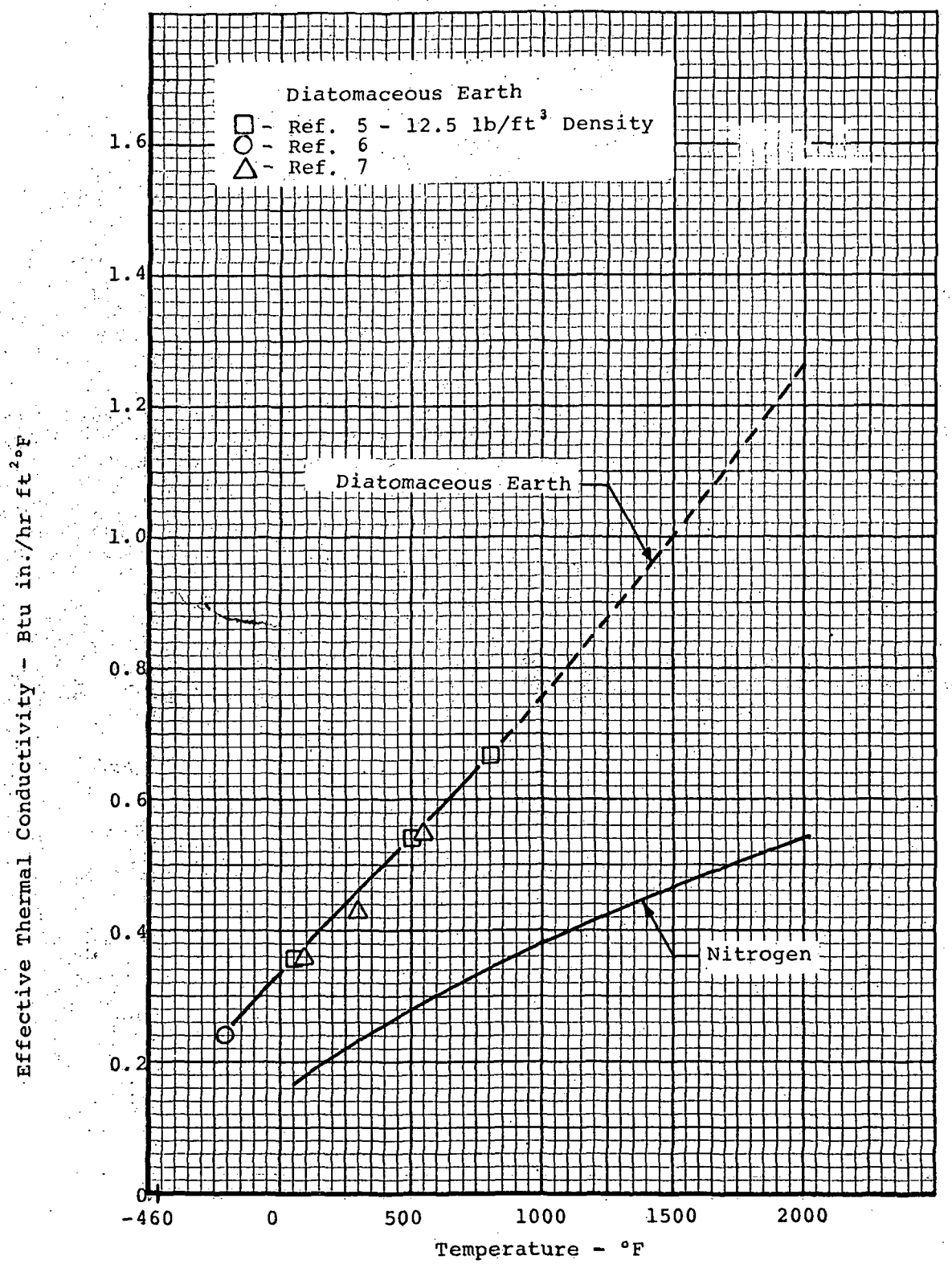

Figure 4. Thermal Conductivity of Diatomaceous Earth in Air (Nitrogen).

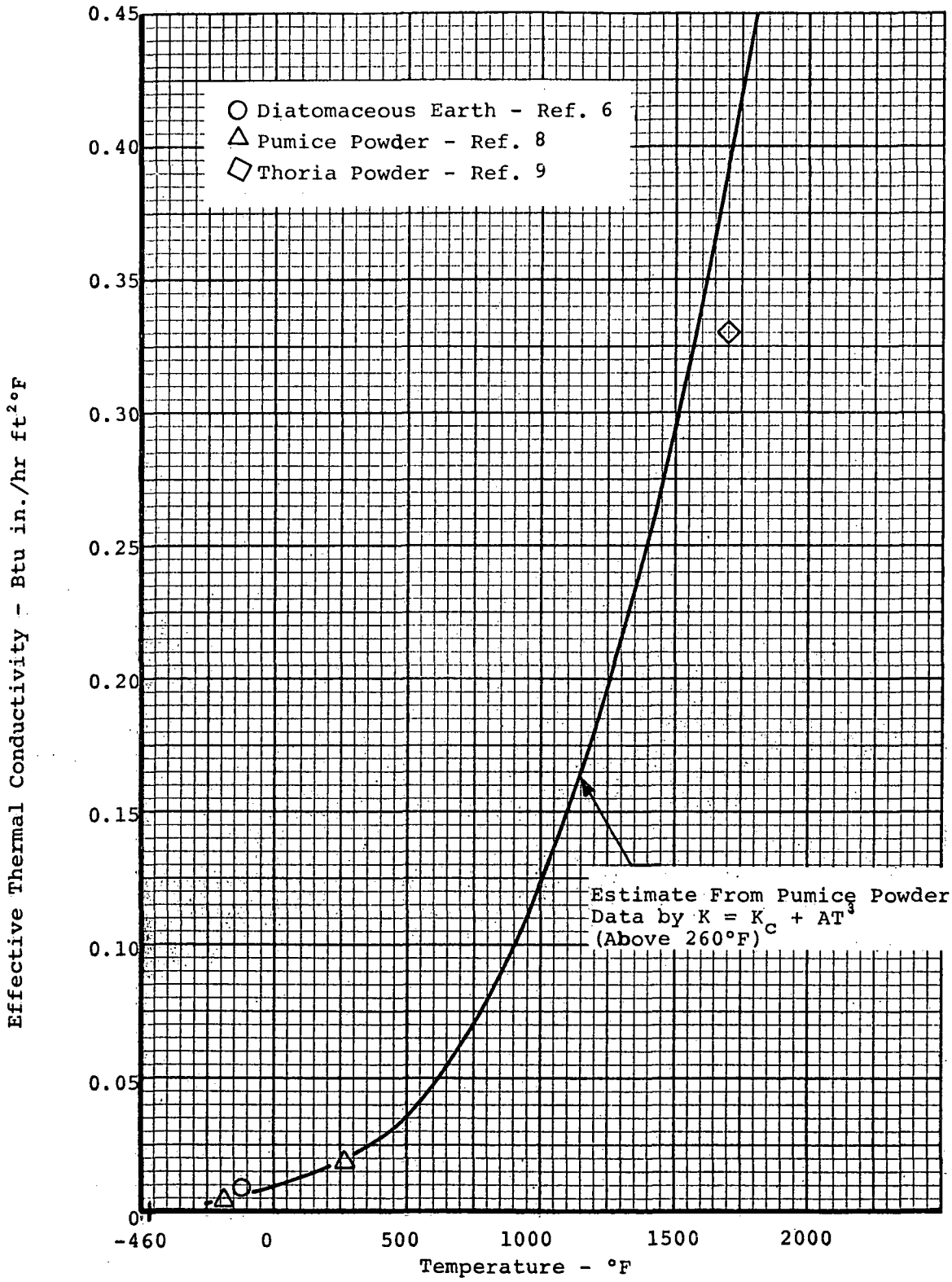

Figure 5. Estimated Thermal Conductivity of Diatomaceous Earth in Vacuum.

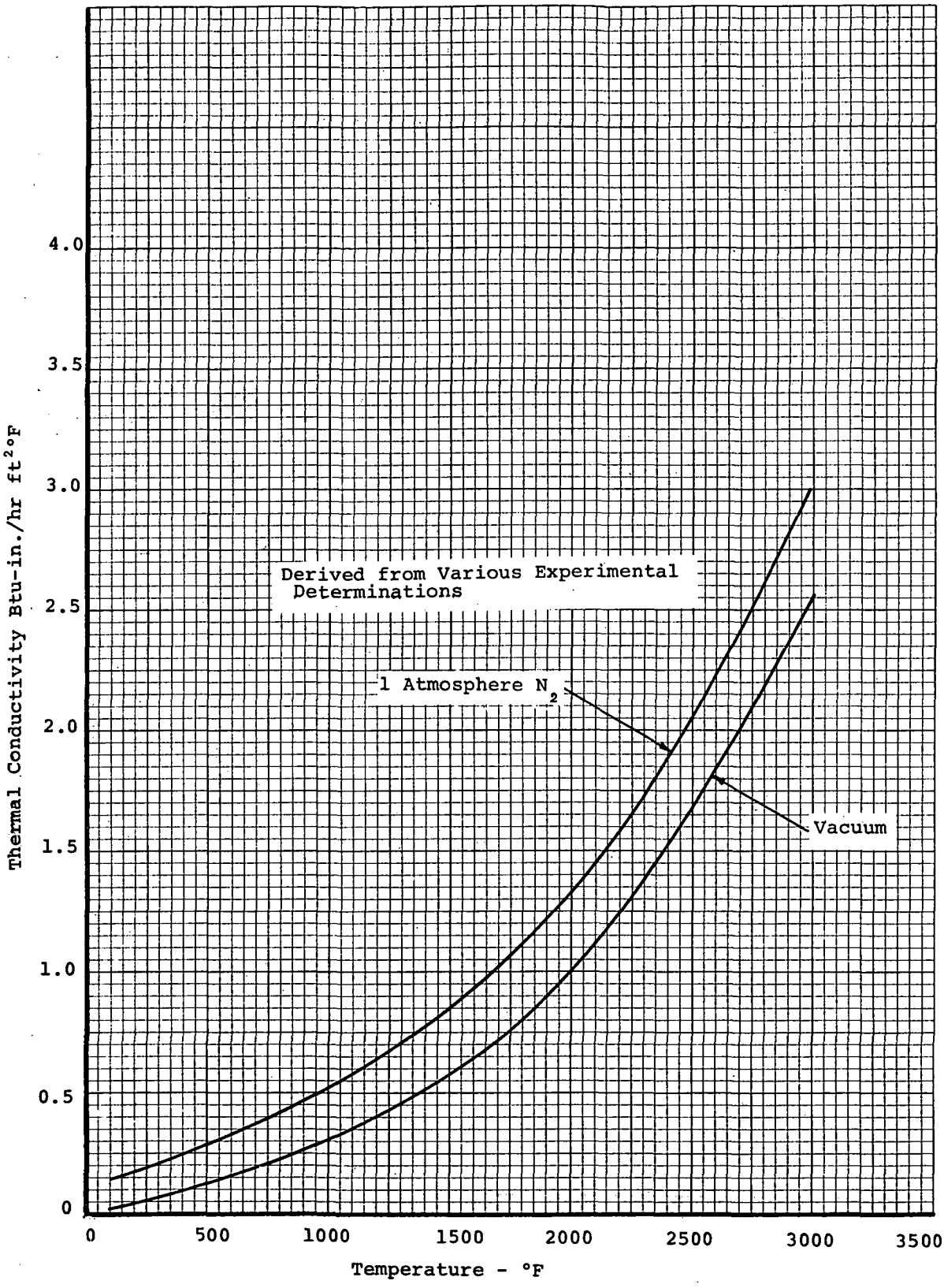

Figure 6. Thermal conductivity of thermatomic carbon in nitrogen and vacuum

APPENDIX D

HEAT CAPACITY TO 1000°F

The heat capacity to 1000°F is determined from data obtained in an adiabatic calorimeter. In this apparatus the heated specimen is dropped into a thermally guarded, calibrated cup, and the enthalpy is measured as a function of the increase in temperature of the cup. The heat capacity is the slope of the enthalpy versus temperature curve. A picture of the apparatus is shown in Figure 1.

A tubular furnace and a cold box are used to bring the specimens to temperature. By pivoting this equipment on a common post near the calorimeter, the samples are transferred to a position directly over the calorimeter cup. At this position the specimen is released from a suspension assembly that is triggered externally. Thermocouples located near the specimen are used to measure specimen temperature. The normal specimen size is about 1" x 1" x 1".

Elevated specimen temperatures are maintained by a manual setting of a variable voltage transformer, which controls the power input to the furnace. Cold sample temperatures are obtained by filling the cold box with dry ice and, when required, injecting liquid nitrogen vapors. The cold box consists of two concentric cylinders enclosed in a housing. The smaller cylinder (3" diameter by 16" high) is constructed of 1/4" mesh hardware cloth. The larger cylinder is made of galvanized sheet metal (15" diameter and 16" high). The annulus is partially filled with dry ice.

Specimens of the materials are heated or cooled to the desired temperature, and following a stabilization period, are dropped into the calorimeter cup. Adiabatic conditions are maintained during each run by manually adjusting cup guard bath temperature.

The covered cup of the drop-type adiabatic calorimeter is approximately 2-1/2" diameter by 2" deep. Three thermocouple wells are located in the bottom wall of the cup. The cup is mounted on cork supports, which rest in a silver-plated copper jacket. The jacket is immersed in a bath of ethylene glycol which is maintained at the temperature of the cup by means of a heater and copper cooling coils immersed in the liquid. Chilled trichloroethylene is circulated through the coils to cool the bath below ambient temperature when cold enthalpy measurements are made. A double-bladed stirrer maintains uniform bath temperature.

The enthalpy-temperature curve established is used to determine heat capacity (specific heat) by measuring its slope at different temperatures. This is done both graphically and by analytical methods which first fit the enthalpy data to an equation of the following type:

$$h_{85} = aT + bT^2 + cT^{-1} + d \qquad (3)$$

The temperature (T) employed usually is in degrees Rankine. While this equation may not provide the best definition of the enthalpy data over the entire temperature range, it does anticipate the theoretical behavior and is consistent with methods recommended in WADC TR 57-308 and by K. K. Kelley.[1] The derivative of this equation, the heat capacity, is used with the constant "c" adjusted so that the analytical solution agrees with the value determined graphically at 150°F. This technique is similar to that of Kelley in forcing the heat capacity equation through a known value. The equations are developed using a digital computer.

The accuracy of the apparatus has been confirmed by measuring the enthalpy of sapphire (SRM 734 from NBS) and other standard specimens. The results of the comparison on sapphire and other data indicate that the overall uncertainty of the apparatus is at ±3 percent.

---

1. Kelley, K. K., "Contributions to Data on Theoretical Metallurgy," Vol. XIII High Temperature Heat Content, Heat Capacity, and Enthalpy Data for Elements and Inorganic Compounds, Bulletin 584, U.S. Bureau of Mines, Nov. 1958.

The enthalpy-temperature curve established is used to determine heat capacity (specific heat) by measuring its slope at different temperatures. This is done both graphically and by analytical methods which first fit the enthalpy data to an equation of the following type:

$$h_{85} = aT + bT^2 + cT^{-1} + d \qquad (3)$$

The temperature (T) employed usually is in degrees Rankine. While this equation may not provide the best definition of the enthalpy data over the entire temperature range, it does anticipate the theoretical behavior and is consistent with methods recommended in WADC TR 57-308 and by K. K. Kelley.[1] The derivative of this equation, the heat capacity, is used with the constant "c" adjusted so that the analytical solution agrees with the value determined graphically at 150°F. This technique is similar to that of Kelley in forcing the heat capacity equation through a known value. The equations are developed using a digital computer.

The accuracy of the apparatus has been confirmed by measuring the enthalpy of sapphire (SRM 734 from NBS) and other standard specimens. The results of the comparison on sapphire and other data indicate that the overall uncertainty of the apparatus is at ±3 percent.

---

1. Kelley, K. K., "Contributions to Data on Theoretical Metallurgy," Vol. XIII High Temperature Heat Content, Heat Capacity, and Enthalpy Data for Elements and Inorganic Compounds, Bulletin 584, U.S. Bureau of Mines, Nov. 1958.

Table 1

Comparison of the Specific Heat of Sapphire Obtained by the Adiabatic Calorimeter to Several Other Sources

SRI Adiabatic Calorimeter		SRI Ice Calorimeter		Armour Research Foundation		Linde Company		International Critical Tables	
Temp. °F	Specific Heat Btu/lb °F	Temp. °F	Specific Heat Btu/lb °F	Approx. Temp. °F	Specific Heat Btu/lb °F	Approx. Temp. °F	Specific Heat Btu/lb °F	Temp. °F	Specific Heat Btu/lb °F
490	0.233	497	0.210	500	0.263	500	0.2125		
996	0.240	1008	0.241	1000	0.280	1000	0.2265	922	0.239

APPENDIX E

HEAT CAPACITY TO 5500°F

The apparatus used for heat capacity employs the drop technique in which the specimen is heated in a furnace and then dropped into an ice calorimeter. The calorimeter contains a cup surrounded by a frozen ice mantle. Water at an inlet temperature of 32°F is circulated through an annulus surrounding the mantle in order to absorb heat leak from the surroundings. The entire system is insulated with glass wool. The enthalpy of the specimen is sensed as a change in volume of the water-ice system of the calorimeter as the ice melts. The annulus containing the flooded ice mantle communicates with the atmosphere through a mercury column in order that the change in volume can be read directly in a burette. An assembly drawing of the calorimeter is shown in Figure 1 and a picture of the calorimeter is shown in Figure 2. A picture of the ice mantle is shown in Figure 3. The specimen nominally is 3/4 inch diameter x 3/4 inch long.

The specimen is placed in either a graphite or stainless steel basket and heated in the furnace in a controlled atmosphere such as helium. The specimen and basket are dropped into the calorimeter and the volume change due to the resultant melting of ice is measured. The flutter valve immediately above the cup and the diaphragm valve immediately below the furnace are major features of the apparatus since the first blocks off radiation losses from the specimen up to the drop tube, and the second blocks radiation gains from the furnace down the drop tube just prior to dropping. The volume changes due to the baskets are measured and correction curves are established. Separate basket calibration minimizes the radiation error accompanying drop techniques. These errors are reported to be only about 0.5 percent[1]. Our theoretical calculations indicate even smaller errors from this source.

The heat necessary to melt enough ice to cause a volume change of 1 cc has been established by the U.S. National Bureau of Standards[2] at 3.487 Btu. This value is reported as the theoretical one for any ice calorimeter. Figure 4 shows a typical curve of mercury

---

[1] Furukawa, G.T., Douglas, McCoskey, and Ginnings, "Thermal Properties of Aluminum Oxide from 0° to 1200°K".

[2] Ginnings, D.C. and R. J. Corruccini, "An Improved Ice Calorimeter", NBS Research Journal, Volume 38, 1947, p583.

displacement versus time for one drop using a synthetic sapphire specimen. The correction for the stainless steel basket is subtracted from the measured mercury displacement and the result used to calculate specimen enthalpy above 32°F. The heat capacity, which is by definition the slope of the enthalpy versus temperature curve, is determined both graphically and analytically. The analytical approach is to fit the enthalpy data to an equation of the form

$$h_{32} = aT + bT^2 + cT^{-1} + d \qquad (1)$$

using a least squares technique. The derivative of this equation, the heat capacity, is computed with the constant "c" adjusted so that the analytical solution agrees with the graphical solution at 5000°F.[3] This technique is similar to that of Kelley in forcing the heat capacity equation through a known value[4]. The equations are developed using a digital computer.

A compilation of all errors has indicated that the apparatus is accurate to well within 5 percent uncertainty over the entire temperature range. Comparison of Southern Research Institute data on copper, Linde synthetic sapphire, and ATJ graphite all have confirmed this value.

---

[3] Pears, C.D., and J. G. Allen, "The Thermal Properties of Twenty-six Solid Materials to 5000°F or Their Destruction Temperatures", ASD-TDR-62-765.

[4] Kelley, K.K., "Contributions to Data on Theoretical Metallurgy", Volume XIII, High Temperature Heat Content, Heat Capacity and Enthalpy Data for the Elements and Inorganic Compounds, USBM 584, November, 1958.

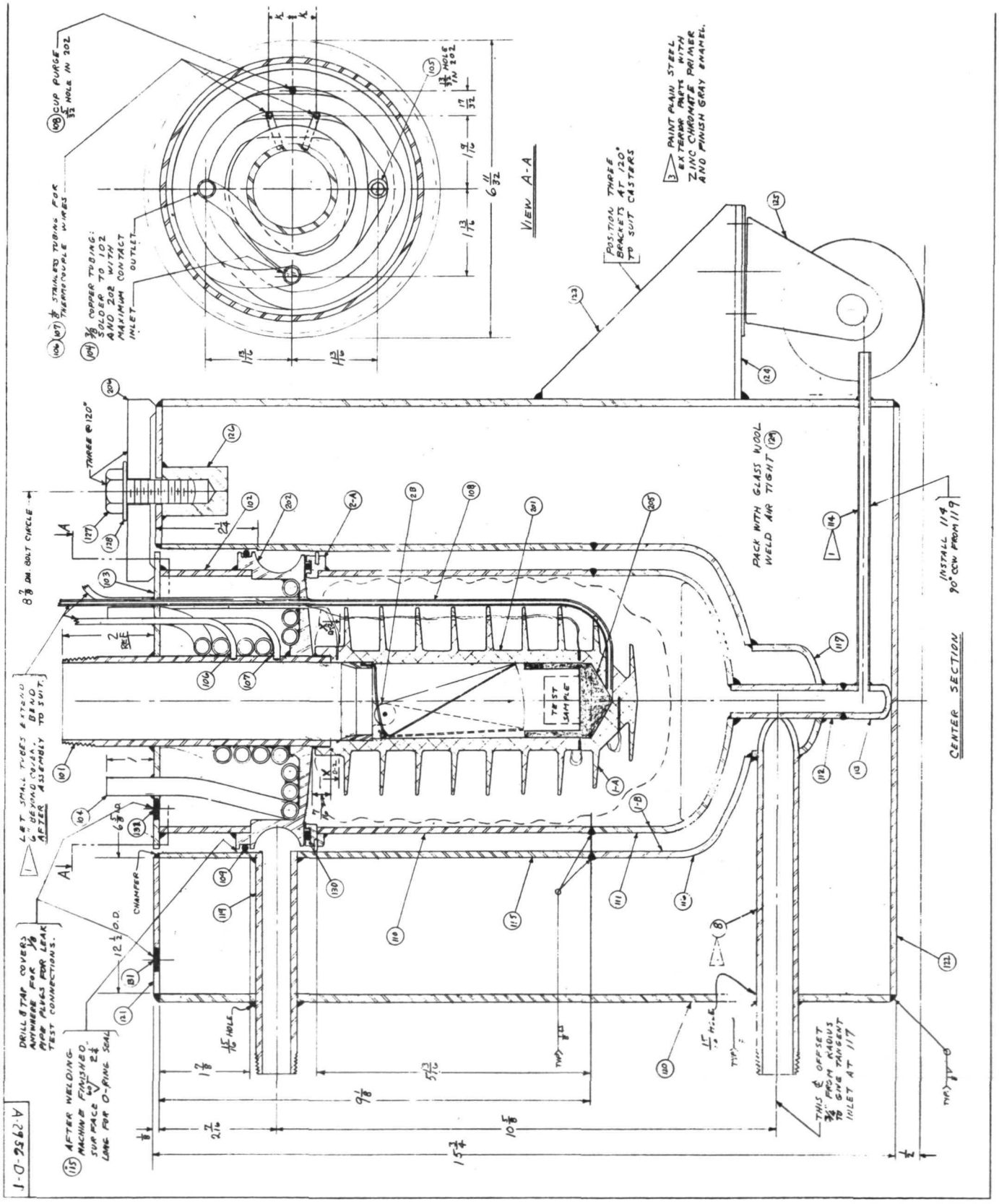

Figure 1. Ice Calorimeter, Drop Type - Specimens to 5500°F

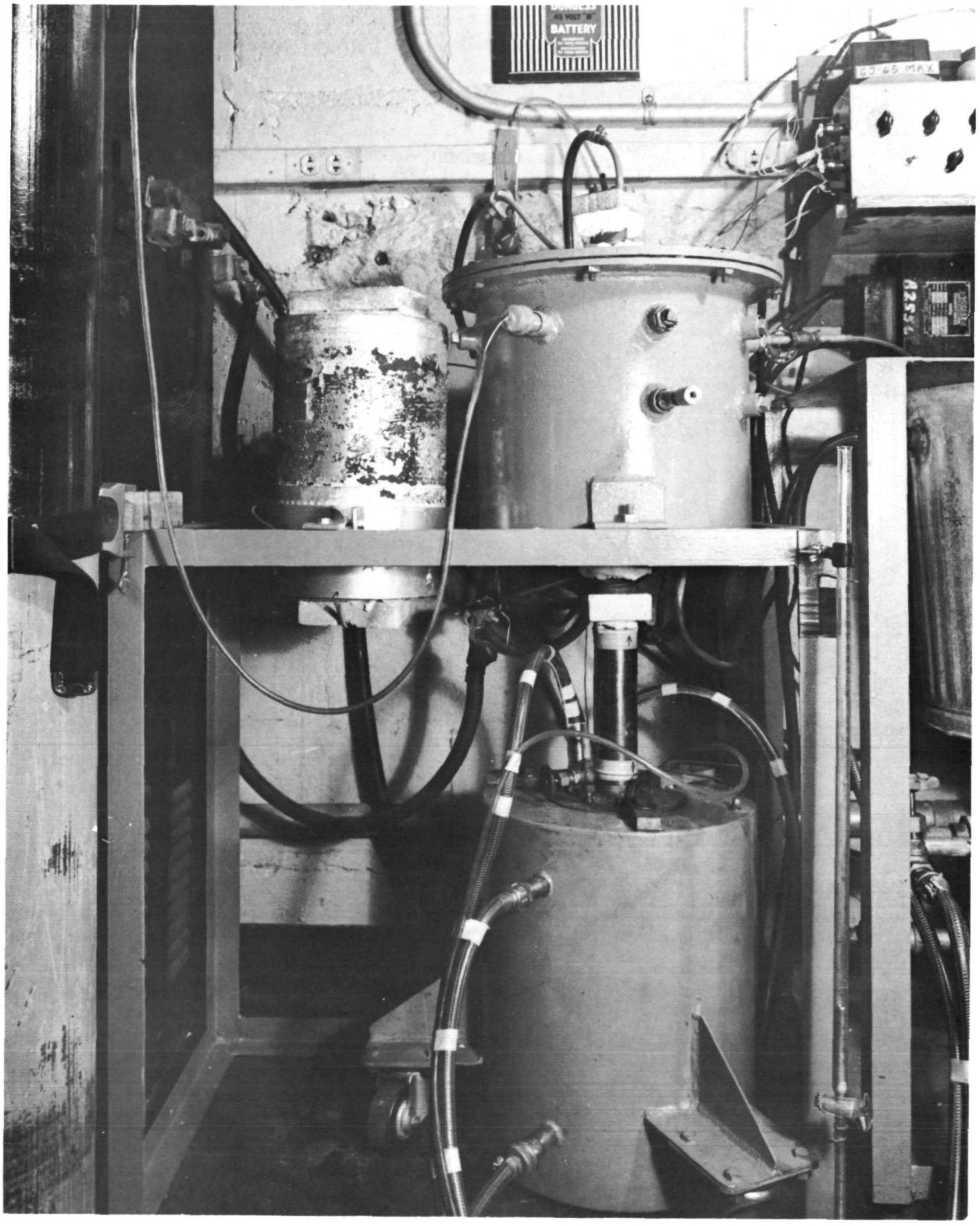

Figure 2. Picture of Heat Capacity Equipment with Drop Shield Tube in Place

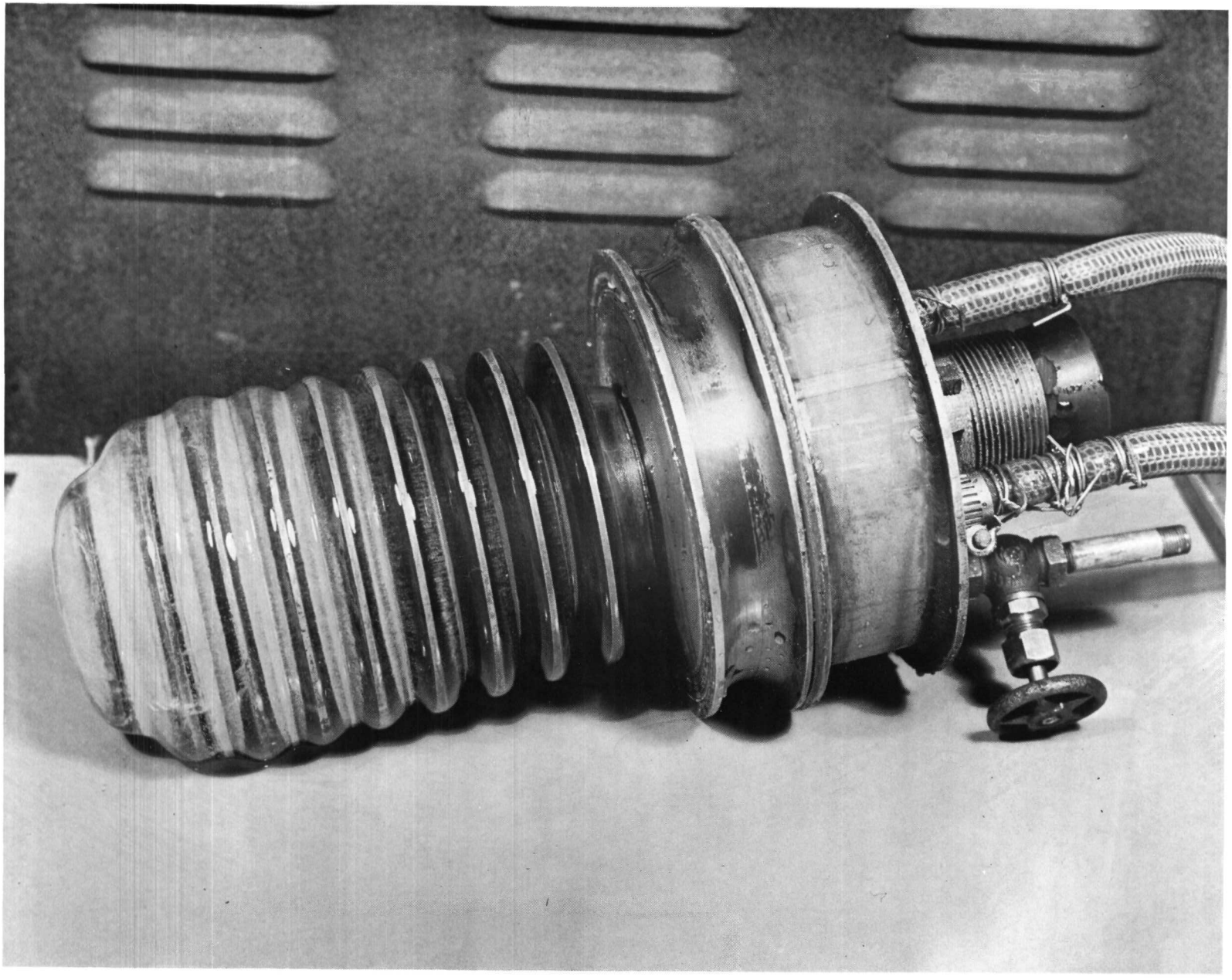

Figure 3. Picture of Ice Mantle in Heat Capacity Ice Calorimeter

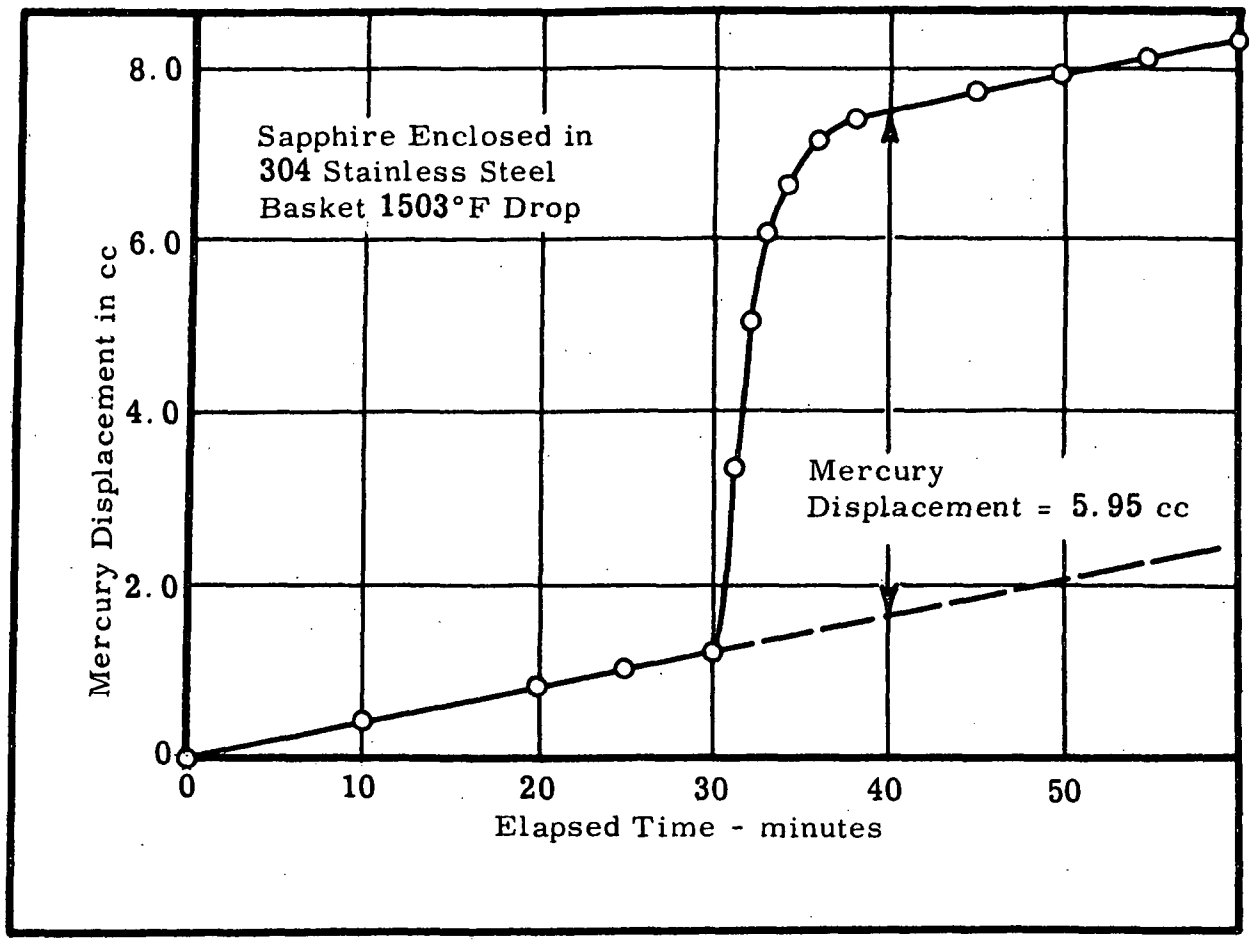

Figure 4. Mercury Displacement Due to Sapphire and 304 Stainless Steel Basket

APPENDIX F

PERMEABILITY TO 1000°F

We have two apparatus in which to make permeability measurements. One apparatus is designed for operation to 1000°F and the other is designed for room temperature measurements. These apparatus are basically the same in principle, except for the method in which pressure measurements are made. Static pressures across the specimen are measured with the room temperature apparatus, whereas the total pressure is measured in the 1000°F apparatus.

Room Temperature Apparatus

This apparatus is shown schematically in Figure 1. It consists of a copper housing and a copper specimen holder. An O-ring is used as a seal between the housing and the specimen holder. Gas is supplied to the specimen from a commercial gas cylinder. Static pressures are measured at the inlet and exit points to the housing. Flow rates are measured with either a bubble type flowmeter, a variable area flowmeter or a wet test meter; the type of instrument used to measure the flow rate depending upon the magnitude of the flow.

The specimen, which is 1 inch in diameter by 1/2 inch thick, is mounted in the housing as shown in Figure 2. The specimen is mounted on a shoulder approximately 1/64 inch wide and 1/64 inch deep. On the upstream side the specimen holder is bored out to a diameter of 1.5 inches and the annulus between the specimen and the holder is filled with silicone rubber (Dow Corning RTV-731 Silastic). This silicone rubber has been employed successfully as a sealant in prior permeability measurements.

High Temperature Apparatus

This apparatus is shown schematically in Figure 2. A detail cutaway view of the housing and specimen holder is shown in Figure 3. The apparatus as shown in these figures was designed for operation to 1000°F. Gas is supplied to the apparatus from a commercial gas cylinder. The volumetric flow rate is measured with a variable area flowmeter. The inlet pressure to the flowmeter is read with a mercury filled U-tube manometer. This pressure measurement is used to correct the indicated flowmeter reading to the volumetric flow rate at standard pressure. Between the flowmeter and the specimen housing, the gas passes through a preheater section. This consists of thin-walled stainless steel tubing which is resistively heated using low voltage and high current. Power is supplied

from a 25 KV step-down transformer, the input of which is regulated by a 220 V Powerstat. The gas then passes through the specimen and is exhausted to the atmosphere.

The pressures upstream and downstream of the specimen are measured with total pressure probes. These pressure monitors are connected to U-tube manometers such that the manometers read the pressure difference across the specimen and the gage pressure on the downstream side of the specimen.

Temperatures are measured with two chromel alumel thermocouples. One thermocouple is mounted in the stainless steel specimen holder. The other thermocouple is used to monitor the temperature of the gas leaving the downstream side of the specimen. The exposed junction of the gas thermocouple is placed so that the hot gas leaving the specimen impinges directly upon it.

Knife edges are machined on the faces of the housing and specimen holder. A copper gasket is used between these knife edges to provide a leak tight seal.

The specimen is mounted in a stainless steel housing as shown in Figure 4. The specimen rests in a recess approximately 1/64 inch wide by 1/32 inch deep. Above this recess the holder is bored out to a diameter of 1.5 inches. Normally, specimens used for the measurements are 1 inch in diameter by 1/2 inch thick. Smaller specimens may also be accommodated. The annulus between the specimen and the housing is filled with a sealing compound. A silicone rubber (Dow Corning RTV-731 Silastic) is used as the sealing compound for low temperature measurements. For high temperature runs, Sauereisen 31 cement is used as a sealant. Both of these sealing compounds have been used successfully in prior evaluations. A stainless steel washer is mounted on the exposed surface of the Sauereisen cement while it is still wet. This washer reduces the exposed area of the cement and serves as a secondary seal.

The procedure for setting up the specimen using the Sauereisen cement is as follows. The annulus is filled about 3/4 full with a fairly dry mix of the cement and then cured for about four hours at 250°F. Next, a wet wash is applied and the washer placed on top. The assembly is then cured for about four hours at 700°F.

Procedure

Ambient Temperature Runs - The procedure in making the runs at ambient temperature is as follows: when the wet test meter is used, the system is purged for about 30 minutes to remove residual gases from the meter. The pressure regulator is adjusted to give the desired pressure difference across the specimen. Several minutes are allowed for the system to stabilize. Then the measurements are made.

Elevated Temperature Runs - The procedure in making the runs at elevated temperatures is as follows: the housing is brought up to temperature with no gas flow through the apparatus. After the housing temperature stabilizes, the gas flow is turned on and the pressure regulator is set to give the desired pressure drop across the specimen. The gas preheater is then turned on and the input power is increased until the gas reaches the same temperature as the housing. At least two data points are taken at each pressure level to monitor that the two temperatures are in equilibrium and to reduce the risk of obtaining spurious readings.

General

During the runs the following data are recorded:

1. Atmospheric pressure.
2. Differential pressure across specimen.
3. Downstream gage pressure.
4. Pressure at flow instrument (at inlet to wet test meter or flowmeter; when flowmeter is used on the downstream side of housing no readings are taken because of the small pressure drop through the flowmeter venting to atmosphere).
5. Flowmeter readings.
6. Housing temperature.
7. Gas temperature.
8. Temperature at wet test meter (when used).

All flowmeter readings are converted to the volumetric flow rate at standard pressure.

DATA CORRELATION

Theory

Greenberg and Weger[1] concluded from a review of some of the literature on permeability that most of the data could be correlated with an equation of the type:

$$-\frac{dP}{dx} = \alpha \mu V + \beta \rho V^n \qquad (1)$$

where

$\frac{dP}{dx}$ = pressure gradient in the direction of flow

α = viscous flow coefficient (reciprocal of Darcy's constant, k)

V = instantaneous gas velocity

β = inertial flow coefficient

ρ = instantaneous gas density

μ = absolute viscosity

and where n is some number between 1 and 2.

Carman[2] selected the value of n as 2 to account for turbulent flow. Greenberg and Weger[1] also state that correlations of the data of Cornell and Katz indicate that the value of n should be 2 to account for inertial flow through consolidated media.

In equation (1), the first term on the right-hand side represents the resistance due to viscous flow. The second term on the right-hand side represents the resistance due to inertial flow. Inertial flow results from turbulence induced by the tortuous path the gas must follow through the porous material and also by high velocities. Both of these phenomena depend upon the kinetic energy of the fluid per unit volume, ρV^2. Thus, in developing equation (1) it was assumed that the expression for the inertial resistance could be superimposed upon the expression for the viscous resistance.

---

[1]See Refererences

Under steady-state conditions, the mass velocity of gas (for one-dimensional flow) through a porous media must be constant. By letting $\rho V = G$ and $n = 2$, equation (1) becomes

$$-\rho \frac{dP}{dx} = \alpha \mu G + \beta G^2 \tag{2}$$

where G = mass velocity.

Now, for an ideal gas

$$\rho = \frac{PM}{RT} \tag{3}$$

where

P = absolute pressure

M = molecular weight of gas

R = universal gas constant

T = absolute temperature

Substituting equation (3) into equation (2) and rearranging yields

$$-\frac{PM}{RT\mu G}\frac{dP}{dx} = \alpha + \frac{\beta G}{\mu} \tag{4}$$

or

$$-\frac{M}{RT\mu G}\int_{P_1}^{P_2} PdP = \left(\alpha + \frac{\beta G}{\mu}\right)\int_0^L dx$$

Integrating and rearranging equation (4) yields

$$\frac{MP_m\Delta P}{LRT\mu G} = \alpha + \beta\left(\frac{G}{\mu}\right) \tag{5}$$

where

$P_m = \frac{1}{2}(P_1 + P_2)$ = mean specimen pressure

$\Delta P = (P_1 - P_2)$ = differential pressure

L = thickness of specimen

Since G is a constant, one may write

$$G = \frac{Q_{STP}\,\rho_{STP}}{A} \tag{6}$$

where

Q_{STP} = volumetric flow rate at standard conditions

ρ_{STP} = gas density at standard conditions

A = total cross section of porous media normal to flow

Data Reduction

The dependent and independent variables in equation (5) are calculated for each data point. Then a plot of $MP_m\Delta P/LRT\mu G$ versus G/μ is made. Such a presentation is known as a Cornell and Katz plot. A straight line is drawn through the points thus plotted and the viscous and inertial coefficients obtained from the intercept and slope of the curve, respectively. Thus, for each specimen evaluated one viscous and one inertial coefficient are calculated at a given temperature level. Data are obtained over a sufficient range of the parameter (G/μ) to allow a good correlation and reduce the effects of spurious readings. The uncertainty in the reduced data is estimated to be ± 5 percent.

Some reduced data for a low-density phenolic-nylon char are presented in Figure 3. This figure shows typical data scatter about a straight line plotted through the data points. It has been our experience that the equation shown plotted in Figure 3, equation (5), correlates the data for porous materials which we have evaluated.

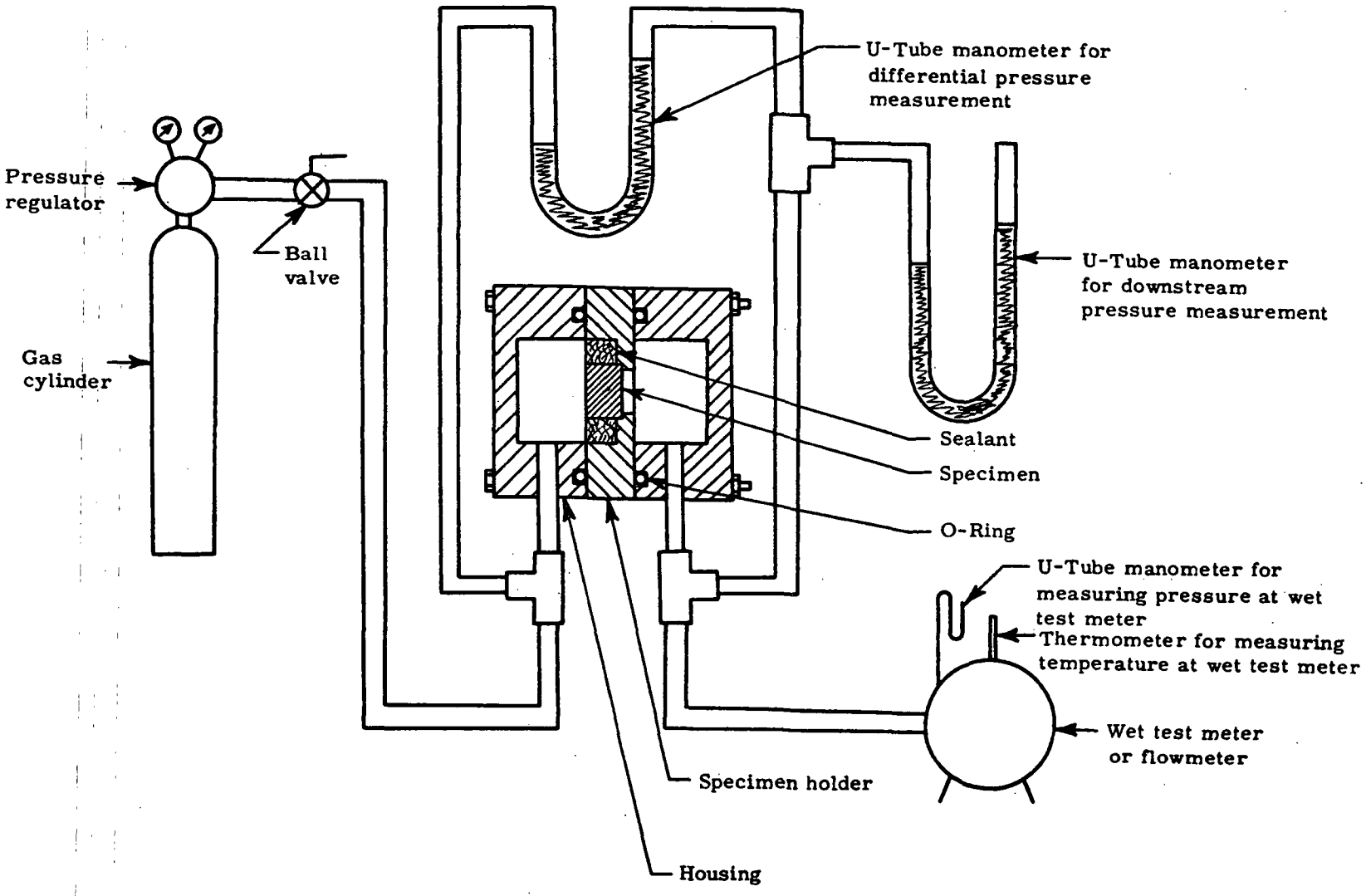

Figure 1. Permeability apparatus for room temperature permeability measurements

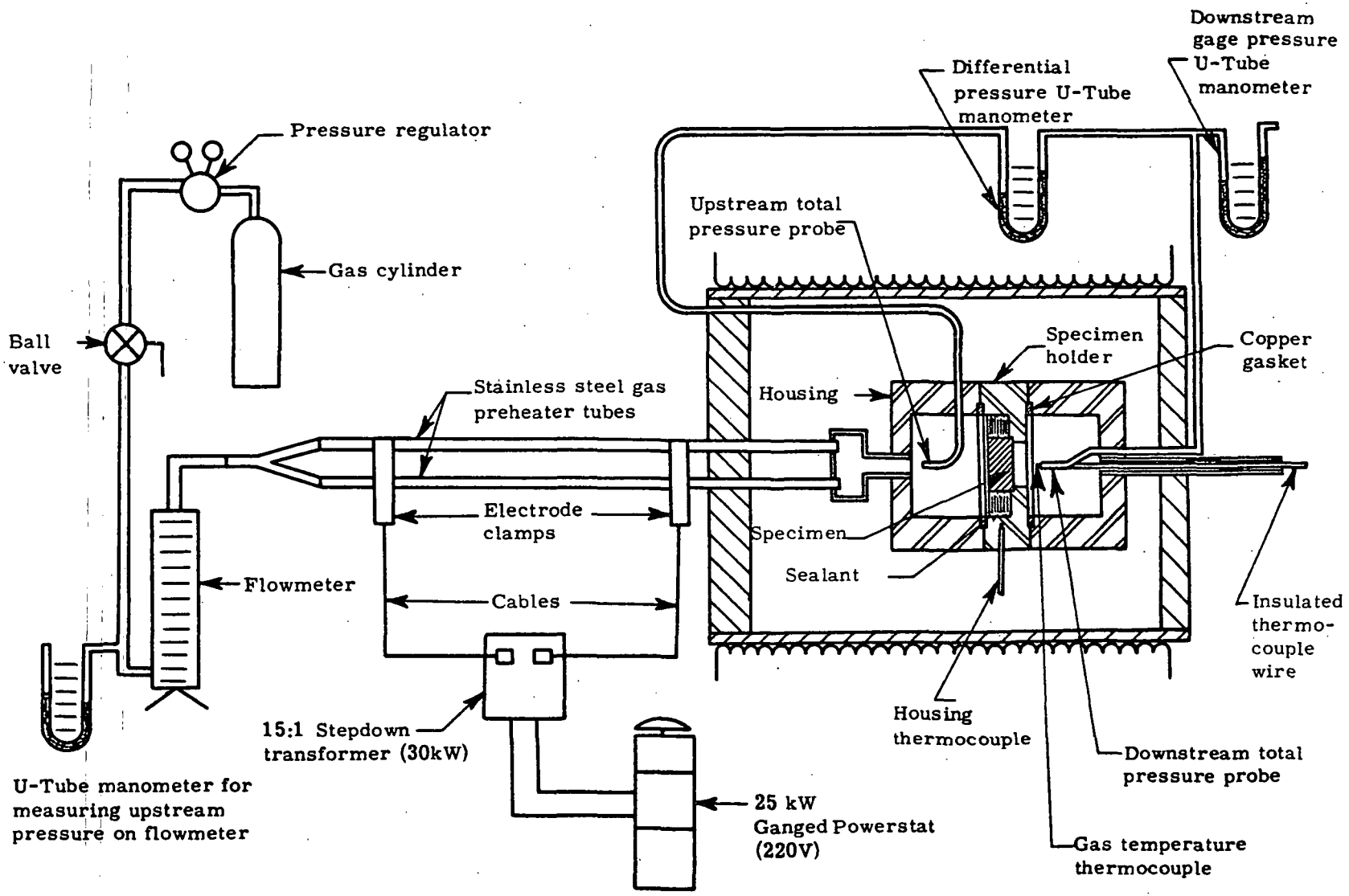

Figure 2. Permeability apparatus for measurements to 1000°F

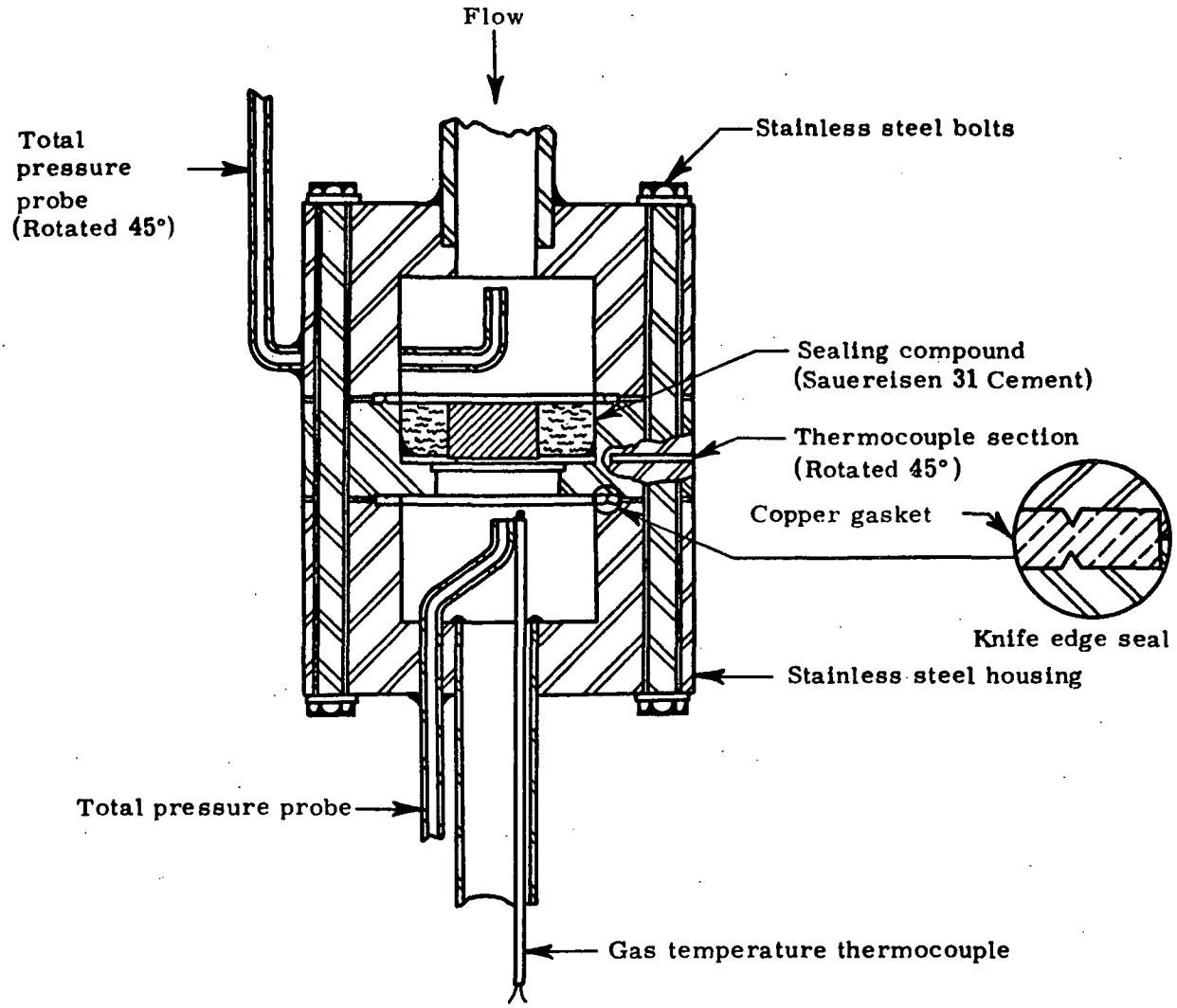

Figure 3. Details of specimen holder for high temperature permeability measurements

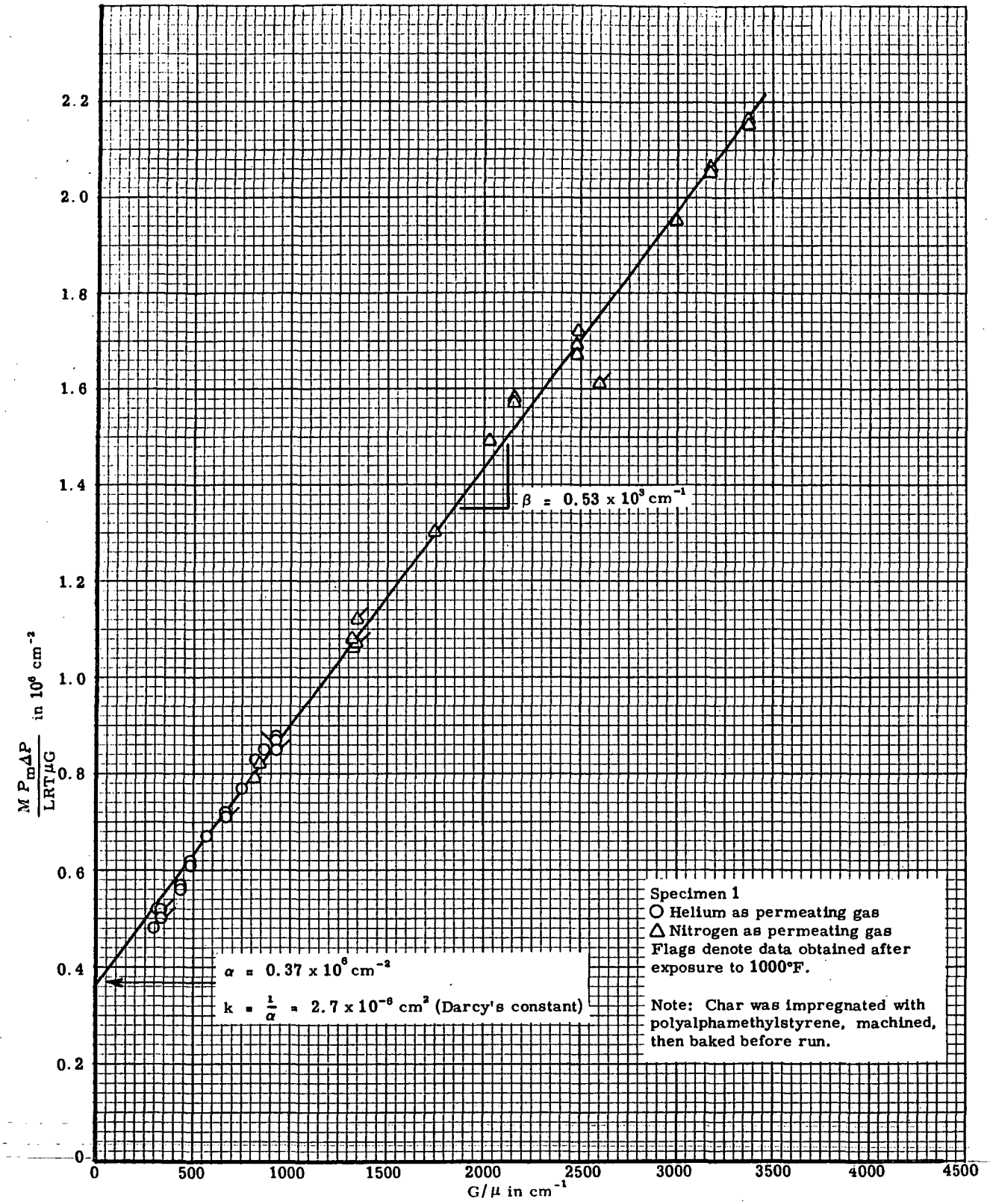

Figure 4. Cornell and Katz plot for low-density phenolic-nylon char perpendicular to the charring direction at room temperature

REFERENCES

1. Greenberg, D. B. and E. Weger, "An Investigation of the Viscous and Inertial Coefficients for the Flow of Gases through Porous Sintered Metals with High Pressure Gradients," Chemical Engineering Science 12, Pergamon Press Ltd., London, pp 8-19, 1960.

2. Carman, P. C., Flow of Gases through Porous Media, Academic Press, Inc., New York, 1956.

APPENDIX G

LIQUID ABSORPTION
(In Monitor Laboratory)

Liquid absorption measurements are made to determine open and closed porosity, bulk density and apparent density. These measurements are made by vacuum impregnating specimens with mineral spirits. Primary apparatuses used in this test are:

1. Mechanical vacuum pump (capability, 50 microns Hg)
2. Oven, thermostatically controlled
3. Balance, accurate chemical

Samples to be tested are dried at 300°F for four hours. After removal from oven, they are immediately weighed for dry weight. Then each dried specimen is placed in a small beaker. The end of the beaker is closed off with gauze. The small beakers are then placed on their side in the bottom of a desiccator with their open ends aligned toward the center of the desiccator. The desiccator is then closed off and evacuated to about 50 microns of Hg. After holding this vacuum for about two hours, the desiccator is purged with mineral spirits. After about 15 minutes, the mineral spirits is introduced more rapidly until the beakers are covered. Then the desiccator is vented, and the samples are allowed to soak for 20 minutes to allow any vapor inside the samples to condense. Upon completion of impregnation the samples are weighed (immersed in mineral spirits and in air). When specimens are removed from mineral spirits, they are carefully wiped to remove any excess liquid from the surface and weighed immediately.

From the measurements taken (dry weight, saturated weight, and suspended weight), the percent water absorption, open porosity, closed porosity, bulk density and apparent density can be determined directly. The total porosity of the sample can be derived from the measurements if the true density of the material is known. These values are calculated as follows:

$$W_a = \left(\frac{W_{sa} - W_d}{W_d}\right) \left(\frac{\rho_w}{\rho_m}\right) \times 100 \text{ percent}$$

$$P_o = \left(\frac{W_{sa} - W_d}{W_{sa} - W_{su}}\right) \times 100 \text{ percent}$$

$$\rho_b = \left(\frac{W_d}{W_{sa} - W_{su}}\right) \times \rho_m$$

$$\rho_a = \left(\frac{W_d}{W_d - W_{su}}\right) \times \rho_m$$

$$P_t = \frac{\left(\frac{W_{sa} - W_{su}}{\rho_m} - \frac{W_d}{\rho_t}\right)}{\left(\frac{W_{sa} - W_{su}}{\rho_m}\right)}$$

where:

W_a = water absorption
W_{sa} = weight of sample when saturated with liquid m
W_d = dry weight of sample
W_{su} = weight of sample when suspended in liquid m
ρ_m = density of liquid m (0.774 g/cm^3 for mineral spirits)
ρ_w = density of liquid water
ρ_t = true density of sample
ρ_b = bulk density of sample
ρ_a = apparent density of sample
P_o = open porosity
P_t = total porosity